INVESTIGATION ON DETECTION, CLASSIFICATION, AND LOCATION OF FAULTS IN TRANSMISSION LINES FOR IMPROVED TRANSFER CAPABILITY

Ph.D. Thesis

JAY PRAKASH KESHRI

ID: 2014REE9538

DEPARTMENT OF ELECTRICAL ENGINEERING

MALAVIYA NATIONAL INSTITUTE OF TECHNOLOGY JAIPUR

January 2020

INVESTIGATION ON DETECTION, CLASSIFICATION, AND LOCATION OF FAULTS IN TRANSMISSION LINES FOR IMPROVED TRANSFER CAPABILITY

Submitted in

fulfillment of the requirements for the degree of

Doctor of Philosophy

by

Jay Prakash Keshri

ID: 2014REE9538

Under the Supervision of

Prof. Harpal Tiwari

DEPARTMENT OF ELECTRICAL ENGINEERING

MALAVIYA NATIONAL INSTITUTE OF TECHNOLOGY JAIPUR

January 2020

Departement of Electrical Engineering
Malaviya National Institute of Technology Jaipur

Candidate's Declaration

I, **Jay Prakash Keshri** (Enroll. ID: 2014REE9538) declare that this thesis titled, ***"Investigation on Detection, Classification, and Location of Faults in Transmission Lines for Improved Transfer Capability"*** and work presented in it, is my own, under the supervision of Dr. Harpal Tiwari, Department of Electrical Engineering, Malaviya National Institute of Technology, Jaipur (Rajasthan), India. I confirm that:

- This work was done wholly or mainly while in candidature for Ph.D degree at MNIT.
- No any part of this thesis has been submitted for a degree or any other qualification at MNIT or any other institution.
- Where I have consulted the published work of others, this is clearly attributed.
- Where I have quoted from the work of others, the source is always given. With the exception of such quotations, this thesis is entirely my own work.
- I have acknowledged all main sources of help.
- Where the thesis is based on work done by myself.

Date: 10 January 2020

Jay Prakash Keshri

(2014REE9538)

Departement of Electrical Engineering
Malaviya National Institute of Technology Jaipur

Certificate

This is to certify that the thesis entitled ***"Investigation on Detection, Classification, and Location of Faults in Transmission Lines for Improved Transfer Capability"*** submitted by **Jay Prakash Keshri** (Enroll. ID: 2014REE9538) to Malaviya National Institute of Technology Jaipur for the award of the degree of **Doctor of Philosophy** in Electrical Engineering is a bonafide record of original research work carried out by him under my supervision.

It is further certified that:

i. The results contained in this thesis have not been submitted in part or in full, to any other University or Institute for the award of any degree or diploma.

ii. Mr. Jay Prakash Keshri has fulfilled the requirements for the submission of this thesis.

Prof. Harpal Tiwari

Professor
Department of Electrical Engineering
Malaviya National Institute of Technology Jaipur

Place: Jaipur
Date: 10 January 2020

"Dedicated to my lovable parents & family"

Acknowledgements

This doctoral thesis would only be possible with magnificent people who not only helped but also inspired me throughout my journey. I sincerely acknowledge my vote of thanks, from my core of heart, to a number of individuals who supported me during my Ph.D work.

First and foremost, I wish to express my sincere gratitude and thanks to my supervisor, ***Prof. Harpal Tiwari***, for his valuable guidance, scholarly inputs and consistent encouragement during my research work. This feat is possible only because of the unconditional moral support provided by him. A man with an amicable and positive disposition, he has always made himself available to clarify my doubts despite his busy schedule and it was a great opportunity to do Ph.D under his supervision and to learn from him. I had great freedom to play and execute my ideas in research without any pressure. This made me identify my own strength and drawbacks, and particularly boosted my self-confidence. I thank him again for all his help and support.

I own my sincere gratitude to ***Prof. Udaykumar R. Yaragatti***, Director, MNIT, for extending all kinds of infrastructural facilities required for pursuing my Ph.D. I would like to thank ***Prof. Rajesh Kumar***, Head of the Department and ***Prof. Manoj Fozdar***, Convener, DPGC for encouraging me in all possible manners during the course of my Ph.D. I would like to extend my special gratitude towards ***Prof. Vikas Gupta***, ***Prof. Rajive Tiwari***, and ***Dr. Satyanarayana Neeli***, the member of DREC committee and advisors for their valuable comments and suggestions to give the required direction during my Ph.D work.

I am deeply grateful to ***Prof. K. R. Niazi*** for his constant support, inspiration and motivation to carry out this challenging work to its logical end. I will forever be obliged for the immense moral support given by him when I was facing tough times in my life. He sets an example of a world-class teacher as well as a wonderful human being with his positive disposition.

My special thanks to my wonderful friends Dr. Nand Kishor Meena, Dr. Saurabh Ratra, Dr. Ajit Singh, Dr. Pradeep Singh, Mr. Pranda Prasant Gupta, Mr. Bhanu Pratap Soni, Mr. Ajay Kumar, and all others fellow researcher for revitalizing each day. I cherish the prayers and support extended by them during low phases. I treasure the shared precious moments. I am also very grateful to all faculty members, non-teaching

staff, undergraduate and postgraduate students of Electrical Engineering Department for their moral support who were associated with me.

My heartfelt thanks goes to my marvellous friends Dr. Pankaj Kumar, Dr. Rajvir Kaur, Mr. Saurabh Kumar, Mr. Rayees Ahmad Thokar, Ms. Jyotsna Singh, Mr. Tanuj Rawat, and Mr. Vipin Panday for reviewing my research articles and spending time for reading my thesis. They all provide much support for me during my needs.

My heartily thanks goes to my lifelong friends Mr. Abhishek Mankar, Mr. Shashi Bhushan, Mr. Raghwendra Narayan Raghav and Mr. Sachin Sharma for their friendship and unconditional moral support.

Finally, I would like to express profound heartily gratitude to my family members for all they have undergone to bring me up to this stage. My family has always been supportive and encouraging. I will be forever indebted to mother ***Mrs. Radha Devi*** and my father ***Mr. Ram Krishna Prasad Keshri***,for being a pillar of support and whose prayer has showered the blessings of the Almighty God.

At the end of the thesis, it is a pleasant task to express my thanks to all those who contributed directly or indirectly in many ways to the success of this study and made an unforgettable experience for me.

For any glitches or inadequacies that may remain in this work, the responsibility is entirely my own.

(Jay Prakash Keshri)

Abstract

THE power system is one of the largest interconnected dynamic involving thousands of electrical sources, loads, transmission and distribution lines, power and distribution transformers, relays, circuit breakers etc. to maintain continuous reliability and quality of systems. Transmission systems of electric power system are the veins that pump life into the modern world, supplying electricity to customers in their homes, offices, commercial areas and industries. Therefore, protection of transmission systems becomes the first and foremost job for the transmission system operators for assuring the smooth operation of transmission lines to provide an un-interrupted power supply for operating electrical power system with high reliability. As an effect of continuous exposure to irregular atmospheric and non-natural conditions, the occurrence of faults on transmission systems is a common problem. Fault estimation methods is an efficient way to detect fault and to accelerate repairs after a transmission system fault occurs. Therefore, there is a pressing need of fault detection, location and classification methods, collectively called as fault estimation methods. These methods find a very prominent place in transmission systems for secure, efficient and reliable operation. This thesis mainly focus on fault and aftermath in transmission system security.

To ensure the security of the transmission systems, highly precise and efficient assessment methods of faults must be developed. This becomes even a huge task for long transmission line through inaccessible areas where patrolling is difficult and time consuming. Also, visual inspection is difficult during adverse weather conditions. Fault detection, location and classification methods provide an estimation for both sustained and transient faults. Transient faults generally cause minor damage that is not readily noticeable on inspection. A lot of studies has been performed over the years on the multiple methods for precise fault assessment. Many techniques use line information from one or more terminals to access the faults. However, these methods lose out on the ease of detection, location and classification for providing a high degree of precision due to line parameters which are sometimes hard to evaluate. To overcome these issues, some fault estimation and analysis methods are developed created on the grounds of accessible voltage and present measurements across fault line terminals. These methods minimize the impacts of parameters owing to uncertain weather and load variations. This thesis presents two distinct approaches for fault detection, location, and classification without consideration transmission line parameters. These two methods are impedance and supervised machine learning based approach.

This work proposes a multi-objective parameter-less fault estimation (PLFE) method for fault estimation in HVAC transmission systems. This method is used for simultaneous detection, location, and classification of symmetrical, as well as, asymmetrical faults in HVAC transmission systems. This method overcomes the limitations of established impedance-based methods by developing independent system parameter. This proposed fault estimation method renders the prior awareness of line parameters as obsolete, which is of excellent support to grid engineers and technicians. Kirchhoff's Voltage Law and Least Error Square Principal are suggested in a different way to determine fault estimation using impedance approach. The Least Error Square Principle is used on positive and negative sequence equivalent circuits to calculate the fault estimation from the reference bus. PLFE method is simple to understand and implement. Moreover, it can be applied to both lumped and distributed transmission systems and requires less measured data with the non-iterative process. The efficacy of proposed method is thoroughly investigated on the standard and realistic HVAC transmission test systems and the results obtained are within the prescribe limits of IEEE standards. The results obtained for fault detection, location, and classification schemes using PLFE method are compared with other available methods for the HVAC transmission systems and are found quite acceptable. The modeling and designing of HVAC transmission test system with the consideration of frequency dependent model is performed using PSCAD software for validation of proposed method. PLFE method takes half cycle data for providing results after fault initiation in few milliseconds with acceptable accuracy. PLFA method is simple, non-iterative and effective for the HVAC transmission system protection. This method provides flexibility to the transmission system operators to accelerate the system rest-rotation process as quick as possible with less effort.

In the above context, a supervised machine learning based fault estimation method is proposed for HVDC transmission systems. For this a feature selected support vector machine (F-SVM) multi-objective method for fault estimation is developed to detect, to locate, and to classify the faults in HVDC transmission systems. It overcomes the limitations of established impedance-based methods for being system specific and low accurate detection of wave front in traveling wave-based methods bydeveloping a computational intelligence-based method. For doing this, support vector machine (SVM) is utilized by modifying with feature selection scheme and Taguchi optimization approaches to determine fault estimation. In F-SVM method feature extraction is accomplished with fourteen defined feature functions. Along with, F-scorebased feature selection scheme is designed to reduce the dimension of feature space vector according to the dominating feature. It is well known that SVM does not depend on a number of features. However, it depends

on dominating features. Feature selection based F-SVM requires a half cycle of data for detection, classification,and location of the different types of faults. The method is thoroughly investigated on the standard and realistic HVDC as well as hybrid HVAC and HVDC transmission test systems. Test cases of different configurations of transmission systems are developed in EMTP/PSCAD. The result obtained and compared with existing methods in reported literature. F-SVM method is simple, fast, accurate non-iterative, and effective for transmission system protection and provides resilience to the transmission system operator to speed up the rest-rotation process in minimum span of time. The test findings are then related to the evaluation of the efficacy and precision of these methods. In future, the proposed fault estimation methods can be improved by incorporating advanced data management approaches. The designing of different disturbance scenarios prevailing in the power systems and incorporating in the proposed methods with some improvement can also be the major extension of this work.

Contents

Certificate **vii**

Acknowledgements **xi**

Abstract **xiii**

Contents **xvi**

List of Tables **xix**

List of Figures **xxi**

Abbreviations **xxiii**

Symbols **xxv**

1 Introduction **1**
1.1 Introduction 1
1.2 Motivation for the Presented Work 4
1.3 Contributions of the Presented work 6
1.4 Organization of the Thesis 7

2 Literature Review **11**
2.1 Introduction 11
2.1.1 Fault Estimation for HVAC Transmission System 12
2.1.2 Fault Estimation for HVDC Transmission System 15
2.2 Critical Review 17
2.3 Research Objectives 18
2.4 Selection of Tools for System Modeling 18

3 Fault Protection Strategies for HVAC Transmission Systems **21**
3.1 Introduction 21
3.2 Proposed PLFE Fault Estimation Method 23

3.2.1 PLFE Fault Detection Scheme 30
3.2.2 PLFE Fault Location Scheme 30
3.2.3 PLFE Fault Classification Scheme 31
3.3 Test System for Simulation 32
3.3.1 Case-1: Two-terminal HVAC Transmission Test System 32
3.3.2 Case-2: Two-terminal Double Circuit HVAC Transmission Test System 35
3.3.3 Case-3: IEEE 39-Bus New England Transmission Test System . . . 40
3.4 Results and Discussions 43
3.4.1 Case-1: Two-terminal HVAC Transmission Test System 43
3.4.1.1 Outcomes with PLFE Fault Detection Scheme 43
3.4.1.2 Outcomes with PLFE Fault Location Scheme 44
3.4.1.3 Outcomes with PLFE Fault Classification Scheme 47
3.4.2 Case-2: Two-terminal HVAC Double Circuit Transmission Test System 48
3.4.2.1 Outcomes with PLFE Fault Detection Scheme 49
3.4.2.2 Outcomes with PLFE Fault Location Scheme 49
3.4.2.3 Outcomes with PLFE Fault Classification Scheme 51
3.4.3 Case-3: New England IEEE 39-Bus Transmission Test System . . . 52
3.4.3.1 Outcomes with PLFE Fault Detection Scheme 53
3.4.3.2 Outcomes with PLFE Fault Location Scheme 54
3.4.3.3 Outcomes with PLFE Fault Classification Scheme 56
3.5 Summary of the Chapter 57

4 Fault Protection Strategies for HVDC Transmission Systems 59
4.1 Introduction 59
4.2 Proposed F-SVM Fault Estimation Method 61
4.2.1 SVM as Binary Classifier 62
4.2.2 SVM as Multi-class Classifier 64
4.2.3 Feature Extraction Scheme 65
4.2.4 Feature Selection with Modified F-Score 67
4.2.5 F-SVM Fault Detection Scheme 71
4.2.6 F-SVM Fault Location Scheme 71
4.2.7 F-SVM Classification Scheme 73
4.3 Test System for Simulation 74
4.3.1 Case-1: Two-terminal HVDC Transmission Test System 75
4.3.2 Case-2: Multi-terminal HVDC Transmission Test System 80
4.4 Results and Discussions 86
4.4.1 Case-1: Two-terminal HVDC Transmission Test System 86
4.4.1.1 Outcomes with F-SVM Fault Detection Scheme 87
4.4.1.2 Outcomes with F-SVM Fault Location Scheme 88
4.4.1.3 Outcomes with F-SVM Classification Scheme 90
4.4.2 Case-2: Multi-terminal HVDC Transmission Test System 93
4.4.2.1 Outcomes with F-SVM Fault Detection Scheme 93

4.4.2.2 Outcomes with F-SVM Fault Location Scheme 94
4.4.2.3 Outcomes with F-SVM Classification Scheme 96
4.5 Summary of the Chapter 100

5 Fault Protection Strategies for Hybrid Transmission Systems 101
5.1 Introduction 101
5.2 Proposed F-SVM Fault Estimation Method 102
5.3 DC Grid Control Strategies 106
5.3.1 DC Voltage Control in DC System 106
5.3.2 Droop Control at VSC Converter 106
5.3.3 3-Level Cascaded Control at VSC Terminal 107
5.3.4 Dispatcher Center Controller 108
5.3.5 DC/DC Converter Control 108
5.3.6 Wind Farm VSC Converter Control 108
5.4 Test System for Simulation 109
5.4.1 Case-1: Two Terminal Hybrid Transmission Test System 110
5.4.2 Case-2: CIGRE (B4.57 and B4.58) Hybrid Transmission Test System 115
5.4.3 Case-3: IEEE 30-Bus Transmission Test System 119
5.5 Results and Discussions 122
5.5.1 Case-1: Two-terminal Hybrid Transmission Test System 123
5.5.1.1 Outcomes with F-SVM Fault Detection Scheme 123
5.5.1.2 Outcomes with F-SVM Fault Location Scheme 125
5.5.1.3 Outcomes with F-SVM Fault Classification Scheme 127
5.5.2 Case-2: CIGRE (B4.57 and B4.58) Hybrid Transmission Test System 131
5.5.2.1 Outcomes with F-SVM Fault Detection Scheme 131
5.5.2.2 Outcomes with F-SVM Fault Location Scheme 133
5.5.2.3 Outcomes with F-SVM Fault Classification Scheme 136
5.5.3 Case-3: IEEE 30-Bus HVAC Transmission Test System 140
5.5.3.1 Outcomes with F-SVM Fault Detection Scheme 141
5.5.3.2 Outcomes with F-SVM Fault Location Scheme 141
5.5.3.3 Outcomes with F-SVM Fault Classification Scheme 142
5.6 Summary of the Chapter 146

6 Conclusions and Future Scope 149
6.1 General 149
6.2 Summary of the Significant Findings 150
6.3 Future Scope for Research 151

A Transmission Test Systems 155
A.1 Study System–1 (IEEE 30-Bus Data) 155
A.2 Study System–2 (IEEE 39-Bus Data) 158
A.3 Study System–3 (CIGRE (B4.57 and B4.58) Hybrid Transmission System Data) 162

A.3.1 **Basic System Data for DC Grid** 164

B Commercial and Technical Information **167**
B.1 Indian Scenario of Power Transmission System 167

Bibliography **173**

Biography **189**

List of Tables

2.1 Comparison of existing power system software package for fault studies . . . 19

3.1 Definition of class with respect to different types of fault 35
3.2 Result obtained with PLFE fault detector scheme (case-1) 44
3.3 Result obtained with PLFE fault location scheme using synchronized bus voltage and current data (case-1) 45
3.4 Result obtained with PLFE fault location scheme using un-synchronized bus voltage and current data (case-1) 46
3.5 Result obtained with PLFE fault classification scheme in sample wise (case-1) 47
3.6 Result obtained with PLFE fault classification scheme in % wise (case-1) . 47
3.7 Result obtained with PLFE fault detector scheme (case-2) 48
3.8 Result obtained with PLFE fault location scheme in line-1 (case-2) 50
3.9 Result obtained with PLFE fault location scheme in line-2 (case-2) 51
3.10 Result obtained with PLFE fault classification scheme in sample wise (case-2) 52
3.11 Result obtained with PLFE fault classification scheme in % wise (case-2) . 52
3.12 Result obtained with PLFE fault detector scheme (case-3) 53
3.13 Result obtained with PLFE fault location scheme (case-3) 54
3.14 PLFE fault location scheme comparison with some existing methods 55
3.15 Result obtained with PLFE fault classification scheme in sample wise (case-3) 56
3.16 Result obtained with PLFE fault classification scheme in % wise (case-3) . 56

4.1 Result obtained with F-SVM fault detector scheme (case-1) 88
4.2 Result obtained with F-SVM fault location scheme (case-1) 89
4.3 Comparison between with or without using F-score based multi-class F-SVM classifier outcomes (case-1) 93
4.4 Result obtained with F-SVM fault detector scheme (case-2) 94
4.5 Result obtained with F-SVM fault location scheme (case-2) 96
4.6 F-SVM fault location scheme comparison with some existing methods . . . 96
4.7 Comparison between with or without using F-score based multi-class F-SVM classifier outcomes (case-2) 97

5.1 Definition of class with respect to different types of fault 115
5.2 Result obtained with F-SVM fault detector scheme in AC section (case-1) . 123
5.3 Result obtained with F-SVM fault detector scheme in DC section (case-1) . 124
5.4 Result obtained with F-SVM fault location scheme in AC section (case-1) . 125
5.5 Result obtained with F-SVM fault location scheme in DC section (case-1) . 126

5.6 Comparison between with or without using F-score based multi-class F-SVM classifier outcomes (case-1) . . . 130
5.7 Result obtained with F-SVM fault detector scheme in AC section for (case-2) 132
5.8 Result obtained with F-SVM fault detector scheme in DC section for (case-2) 133
5.9 Result obtained with F-SVM fault location scheme in AC section (case-2) . 134
5.10 Result obtained with F-SVM fault location scheme in DC section (case-2) . 135
5.11 Comparison between with or without using F-score based multi-class F-SVM classifier outcomes (case-2) . . . 137
5.12 Result obtained with F-SVM fault detector scheme (case-3) . . . 140
5.13 Result obtained with F-SVM fault location scheme (case-3) . . . 142
5.14 F-SVM fault location scheme comparison with some existing methods . . . 143
5.15 Comparison between with or without using F-score based multi-class F-SVM classifier outcomes (case-3) . . . 146

A.1 Terminal conditions of IEEE 30-bus system . . . 156
A.2 Transmission line characteristics of IEEE 30-bus system . . . 156
A.3 Approximate line lengths based on typical line reactance values of IEEE 30-bus system . . . 157
A.4 Load characteristics of IEEE 30-bus system . . . 158
A.5 Typical line reactance values of IEEE 30-bus system . . . 158
A.6 Terminal conditions of IEEE 39-bus system . . . 159
A.7 Transmission line characteristics of IEEE 39-bus system . . . 160
A.8 Typical line reactance values of IEEE 39-bus system . . . 160
A.9 Approximate line lengths based on typical line reactance values of IEEE 39-bus system . . . 161
A.10 Load characteristics of IEEE 39-bus system . . . 162
A.11 System data . . . 164
A.12 AC bus data . . . 164
A.13 DCS1 data . . . 164
A.14 DCS2 data . . . 164
A.15 DCS3 data . . . 165
A.16 AC-DC converter pole data . . . 165
A.17 DC-DC converter station data . . . 165
A.18 Line data for average value model simulation . . . 165
A.19 Slack bus data . . . 166
A.20 DCS1 control data . . . 166
A.21 DCS2 control data . . . 166
A.22 DCS3 control data . . . 166
A.23 DC-DC converter control data . . . 166

B.1 HVDC transmission system: Indian scenario . . . 171
B.2 Transmission system projection during 12^{th} plan in India . . . 172

List of Figures

1.1 Thesis structure 8

3.1 Schematic diagram of two terminal transmission test system 23
3.2 The equivalent circuit at the time of fault 24
3.3 Flowchart for the proposed PLFE method 29
3.4 Schematic diagram of two terminal transmission test system 32
3.5 Tower configuration of two terminal transmission Line 33
3.6 Voltage at terminal-1 (case-1) 33
3.7 Current at terminal-1 (case-1) 34
3.8 Voltage at terminal-2 (case-1) 34
3.9 Current at terminal-2 (case-1) 34
3.10 Active and reactive power at both ends (case-1) 35
3.11 Schematic diagram of two terminal double circuit transmission test system 36
3.12 Tower configuration of double circuit transmission line 36
3.13 Voltage at terminal-1 in line-1 (case-2) 37
3.14 Current at terminal-1 in line-1 (case-2) 37
3.15 Voltage at terminal-2 in line-1 (case-2) 37
3.16 Current at terminal-2 in line-1 (case-2) 38
3.17 Voltage at terminal-1 in line-2 (case-2) 38
3.18 Current at terminal-1 in line-2 (case-2) 38
3.19 Voltage at terminal-2 in line-2 (case-2) 39
3.20 Current at terminal-2 in line-2 (case-2) 39
3.21 Active and reactive power at both ends in line-1 (case-2) 39
3.22 Active and reactive power at both ends in line-2 (case-2) 40
3.23 Schematic diagram of new England 39-bus IEEE dynamic transmission test system 40
3.24 Voltage at bus-26 (case-3) 41
3.25 Current in section (26-29) at bus-26 (case-3) 41
3.26 Voltage at bus-29 (case-3) 42
3.27 Current in section (26-29) at bus-29 (case-3) 42
3.28 Active and reactive power flow in section (26-29) (case-3) 42
3.29 Performance of PLFE fault location scheme with synchronized bus data (case-1) 45
3.30 Performance of PLFE fault location scheme with un-synchronized bus data (case-1) 46

3.31 Performance of PLFE fault location scheme in line-1 (case-2) 49
3.32 Performance of PLFE fault location scheme in line-2 (case-2) 49
3.33 Performance of PLFE fault location scheme (case-3) 55

4.1 Working steps for proposed F-SVM method 62
4.2 SVM classification 63
4.3 Flowchart for feature extraction approach 67
4.4 Feature extraction using time and frequency domain descriptors 68
4.5 Different class distribution in feature space (a) Uneven distribution of features (b) Even distribution of features 70
4.6 Flowchart for the proposed F-SVM method 72
4.7 A VSC-HVDC system controller 75
4.8 Schematic diagram of two-terminal HVDC transmission test system 75
4.9 Tower configuration of HVDC transmission line 76
4.10 AC voltage at rectifier end (case-1) 77
4.11 AC current at rectifier end (case-1) 77
4.12 AC voltage at inverter end (case-1) 77
4.13 AC current at inverter end (case-1) 78
4.14 DC voltage at rectifier and inverter end (case-1) 78
4.15 DC current at rectifier and inverter end (case-1) 78
4.16 DC RMS voltage at rectifier and inverter end (case-1) 79
4.17 DC current at rectifier and inverter end (case-1) 79
4.18 DC RMS voltage at rectifier and inverter end (case-1) 79
4.19 Schematic diagram of multi-terminal HVDC transmission test system . . . 80
4.20 Tower configuration of HVDC transmission cable 81
4.21 Zoomed signal of voltage in AC side at the time of fault (case-2) 82
4.22 Zoomed signal of current in AC side at the time of fault (case-2) 83
4.23 Zoomed signal of DC side voltage at the time of fault (case-2) 83
4.24 Zoomed signal of DC side current at the time of fault (case-2) 84
4.25 Zoomed signal of Rms voltage and current at terminal-1 (case-2) 84
4.26 Zoomed signal of Rms voltage and current at terminal-2 (case-2) 85
4.27 Zoomed signal of Rms voltage and current at terminal-2 (case-2) 86
4.28 Response signal of fault detection scheme (case-1) 87
4.29 Performance of F-SVM fault location scheme (case-1) 89
4.30 Confusion matrix for F-SVM classifier without using F-score (case-1) 91
4.31 Confusion Matrix for F-SVM classifier with using F-score (case-1) 92
4.32 Response signal of fault detection scheme (case-2) 95
4.33 Performance of F-SVM fault location scheme (case-2) 95
4.34 Confusion matrix for F-SVM classifier without using F-score (case-2) 98
4.35 Confusion Matrix for F-SVM classifier with using F-score (case-2) 99

5.1 Working steps of the proposed F-SVM fault estimation method 105
5.2 Schematic diagram of the VSC controller with typical droop DC voltage feedback 107
5.3 Schematic diagram of the control structure of 3-LCC for d-axis of VSCs . . 107

5.4 Schematic diagram of the control structure dispatcher center 108
5.5 Schematic diagram of the control structure of the DC/DC converter 109
5.6 Schematic diagram of the control structure of the wind farm VSC converter 109
5.7 Schematic diagram of two terminal hybrid transmission test system 110
5.8 Tower configuration of hybrid transmission Line 111
5.9 Voltage at bus-3 at time of fault (case-1) 111
5.10 Current at bus-3 at time of fault (case-1) 112
5.11 Voltage at bus-4 at time of fault (case-1) 112
5.12 Current at bus-4 at time of fault (case-1) 113
5.13 Active and reactive power at bus-3 and bus-4 at time of fault (case-1) . . . 113
5.14 Dc Voltage at bus-2 and bus-3 at time of fault (case-1) 114
5.15 Current at bus-2 and bus-3 at time of fault (case-1) 114
5.16 Schematic diagram of CIGRE (B4.57 and B4.58) hybrid transmission test system 116
5.17 Voltage at bus (Ba-B0) at the time of fault (case-2) 117
5.18 Current at bus (Ba-B0-Ba-b1) at bus (Ba-B0) at the time of fault (case-2) 117
5.19 Voltage at bus (Ba-B1) at the time of fault (case-2) 118
5.20 Current at bus (Ba-b0-Ba-B1) at bus (Ba-B1) at the time of fault (case-2) 118
5.21 Schematic diagram of IEEE 30-bus dynamic transmission test system . . . 119
5.22 Voltage at bus-27 at the time of fault (case-3) 120
5.23 Current in section(27-30) at bus-27 at time of fault (case-3) 120
5.24 Voltage at bus-30 at the time of fault (case-3) 121
5.25 Current in section(27-30) at bus-30 at time of fault (case-3) 121
5.26 Power of both the buses at the time of fault (case-3) 122
5.27 Performance of F-SVM fault location scheme in AC section (case-1) 126
5.28 Performance of F-SVM fault location scheme in DC section (case-1) 127
5.29 Confusion matrix for F-SVM classifier without using F-score (Case-1) . . . 128
5.30 Confusion matrix for F-SVM classifier with using F-score (Case-1) 129
5.31 Performance of F-SVM fault location scheme in AC section (case-2) 134
5.32 Performance of F-SVM fault location scheme in DC section (Case-2) 136
5.33 Confusion matrix for F-SVM classifier without using F-score (Case-2) . . . 138
5.34 Confusion matrix for F-SVM classifier with using F-score (Case-2) 139
5.35 Performance of F-SVM fault location scheme (Case-3) 141
5.36 Confusion matrix for F-SVM classifier without using F-score (Case-3) . . . 144
5.37 Confusion Matrix for F-SVM classifier with using F-score (Case-3) 145

A.1 Single line diagram of IEEE-39 Bus transmission system 155
A.2 Single line diagram of IEEE-39 Bus transmission system 159
A.3 Schematic diagram of CIGRE (B4.57 and B4.58) hybrid HVAC and HVDC transmission system model 163

B.1 Comparison between HVAC and HVDC transmission systems 168
B.2 HVDC transmission systems: Indian picture 169
B.3 HVDC transmission systems: World picture 170

Abbreviations

AI	**A**rtificial Intelligence
ANOM	**A**nalysis of Mean
ANOVA	**A**nalysis of Variance
CB	**C**ircuit Breaker
CCC	**C**onstant Current Control
CIGRE	**C**onference Internationale des Grands Reseaux Electriques (International Conference on Large High Voltage Electric Systems)
CSC	**C**urrent Source Control
CT	**C**urrent Transformer
DER	**D**istributed Energy Resources
DG	**D**istributed Generation
EMTDC	**E**lectromagnetic Transients Program for DC
ET	**E**lectromagnetic Transient
ETP	**E**lectromagnetic Transients Program
EV	**E**lectric Vehicle
FACTS	**F**lexible AC Transmission Systems
FDR	**F**alse Discovery Rate
FNR	**F**alse Negative Rate
F-SVM	**F**eature Selected Support Vector Machine
GTO	**G**as Turn-off Thyristor
IEE	**T**he Institution of Electrical Engineers
IEC	**I**nternational Electrotechnical Commission
IEEE	**I**nstitute of Electrical and Electronics Engineers

IGBT	**I**nsulated Gate Commuted Thyristor
LES	**L**east Error Square
MTDC	**M**ultiterminal DC System
OVA	**O**ne Verses Another
OVO	**O**ne Verses One
PDR	**P**ositive Predictive Rate
PES	**P**ower Engineering Society
PLFE	**P**arameter Less Fault Estimation
PMU	**P**hase Measurement Unit
PSCAD	**P**ower System Computer Aided Design
PT	**P**otential transformer
SCR	**S**ilicon Controlled Rectifier
SD	**S**tanderd Deviation
SSTS	**S**olid State Transfer Switch
RTDS	**R**eal-Time Digital Simulator
TACS	**T**ransient Analysis of Control Systems
TPC	**T**ia Power Corporation
TPR	**T**rue Positive Rate
TRV	**T**ransient Recovery Voltage
VSC	**V**oltage Source Converter
TSO	**T**ransmission System Operator
VBV	**V**irtual Branch Voltage
WPPs	**W**ind Power Producers

Symbols

R	Resistance in Ohms
L	Inductance in Henry
C	Capacitance in Micro-Farad
P	Active Power in kilo Watts (kW)
Q	Reactive Power in KvAr
ω	Frequency in radians per second
Q	A statistical measure of PCA
Q_f	Quality factor
μ	Statistical mean
σ^2	Variance
κ	Cohen's Kapppa statistic
χ^2	Statistical chi-square probability distribution
P_R	Receiving end active power
Q_R	Receiving end reactive power
V_S	Sending end voltage
V_R	Receiving end voltage
A	Transmission line parameter
X	Reactance of line
R	Resistance of line
Z	Impedance of line
Y	Line charging admittance of line
I	Current in transmission line
θ	Impedance angle of line

β	Angle part of transmission line parameter B
δ	Phase angle difference between sending and receiving end voltages
α	Angle part of transmission line parameter A
λ	Load multiplication factor
λ_{max}	Maximum loadability factor
l	Maximum number of lines
V_{Sj}	Sending end voltage of j^{th} line
V_{Rj}	Receiving end voltage of j^{th} line
A_j	Transmission line parameter of j^{th} line
β_j	Angle part of transmission line parameter B of j^{th} line
α_j	Angle part of transmission line parameter A of j^{th} line
δ_{SRj}	Phase angle difference between sending and receiving end voltages of j^{th} line
t	tappings of OLTC
R	Resistance of Line
P	Active power
X	Reactance of Line
Q	Reactive power
V_S	Sending end voltage
V_R	Receiving end voltage
μ^F	Fuzzy Membership Function
μ^P	Membership function for real power loss
$Rated\ \ MVA$	Machine-rated MVA; base MVA for impedances
$Rated\ \ kV$	Machine-rated terminal voltage in kV; base kV for impedances
H	Inertia constant in s
D	Machine load damping coefficient
r_a	Armature resistance in p.u.
x_d	Unsaturated d axis synchronous reactance in p.u.
x_q	Unsaturated q axis synchronous reactance in p.u.
$x_d^{'}$	Unsaturated d axis transient reactance in p.u.
$x_q^{'}$	Unsaturated q axis transient reactance in p.u.
$x_d^{''}$	Unsaturated d axis subtransient reactance in p.u.

$x_q^{''}$	Unsaturated q axis subtransient reactance in p.u.
x_l	Leakage or Potier reactance in p.u.
$T_{d0}^{'}$	d axis transient open circuit time constant in s
$T_{q0}^{'}$	q axis transient open circuit time constant in s
$T_{d0}^{''}$	d axis subtransient open circuit time constant in s
$T_{q0}^{''}$	q axis subtransient open circuit time constant in s
$S(1.0)$	Machine saturation at 1.0 p.u. voltage in p.u.
$S(1.2)$	Machine saturation at 1.2 p.u. voltage in p.u.
T_r	Regulator input filter time constant in s
K_a	Regulator gain (continuous acting regulator) in p.u.
T_a	Regulator time constant in s
V_{Rmax}	Maximum regulator output, starting at full load field voltage in p.u.
V_{Rmin}	Minimum regulator output, starting at full load field voltage in p.u.
K_e	Exciter self-excitation at full load field voltage in p.u.
T_e	Exciter time constant in s
K_f	Regulator stabilizing circuit gain in p.u.
T_f	Regulator stabilizing circuit time constant in s
E_1	Field voltage value,1 in p.u.
$SE(E_1)$	Saturation factor at E1
E_2	Field voltage value, 2 in p.u.
$SE(E_2)$	Saturation factor at E2
P_{max}	Maximum turbine output in p.u.
R	Turbine steady-state regulation setting or droop in p.u.
T_1	Control time constant (governor delay) in second
T_2	Hydro reset time constant in s
T_3	Servo time constant in s
T_4	Steam valve bowl time constant in s
T_5	Steam reheat time constant in s
F	Shaft output ahead of reheater in p.u.
$[Z_L]_{abc}$	Total transmission length
$[V_j]_{abc}$	Phase voltage of $j^{th} bus$

$[I_j]_{abc}$	Phase current of $j^{th}bus$
$[Z_L]_{012}$	Total sequence transmission length
$[V_j]_{012}$	Sequence phase voltage of $j^{th}bus$
$[I_j]_{012}$	Sequence phase current of $j^{th}bus$
m	Per unit distance of transmission line
L	Total Line length
L_f	Length of fault location
T_i	Fault inception instant
T_d	Fault detection time
T_r	Response time
$e^{j\delta}$	Synchronization angle
$f(x)$	Hyperplane function
W	Weight function
(x_i, y_i)	Input data-set
δ_i	Loss function
η	Slack variable
$K(x_i, x_j)$	Kernel function
N	Number of sample
k	Sample number
$p(k)$	Power spectral density
†‡	Class function
$\Re$	Real number
$\Im$	Imaginary number
ρ	Correlation coefficient
λ	Threshold value
$J(k)$	Feature correlation within class k

Chapter 1

Introduction

This chapter explains the background, context, and motivation for this work. It also explains the main contributions of this research work and the structure of the thesis.

1.1 Introduction

Electricity has brought a paradigm shift in the quality of life, urbanization, research, national economy, defence and industrial growth. The increasing demand for electricity has enforced the nations to interconnect regional grids together and also integrate renewable energy resources and conventional base resources to the main grids. Thus, modern power systems are enormously large with many complex interconnections and adjoining networks. This interconnection makes system task of greater importance to maintain system security under disturbance condition. In this transmission systems, a bridge between generating source and load has a paramount importance. Thus, fault in this can adversely affect system security and reliability [1]. The transmission systems can experience faults which are caused by storms, lightning, snow, freezing rain, insulation breakdown, short circuits caused by external objects, etc. In the most cases, electrical faults can manifest mechanical damage in the system which must be repaired before returning the line to service. The restoration can be accelerated if the identification of the faulted section, fault location, and classification of faults is either known or can be estimated with reasonable time and accuracy. There are many benefits which can be achieved by using fault estimation method including reducing maintenance time, improving power quality, increasing the power transfer availability, and avoid future misfortunes. This help to identify affected section with their location and type of faults for early repairs to prevent recurrence and

consequent major damages. This is the reason fault detection, location and classification methods are gaining a growing interest in the power systems protection.

The subject of fault estimation has been of considerable interest to electric power utility engineers and researchers for over last two decades. Most of the research done till date, has been aimed at detection, location and classification of transmission line faults. It is mainly because of the impact of transmission lines faults on the power systems and the time required to physically check the faults in transmission lines is much larger than the sub-transmission and distribution systems [2]. On the basis of the literature available for the power system protection, line configuration of transmission systems has been divided into three parts viz high voltage AC, high voltage DC, and hybrid high voltage AC and DC transmission systems.

In this mostly impedance based algorithms [3–9] have been studied to calculate the fault detection, location and classification in high voltage AC transmission lines. However, these methods have limitations due to one or more reasons such as model or system parameter dependency, frequency independent, sophisticated measured data requirement, etc. This leads to the development of several interesting approaches for transmission line fault protection in which the circuit theory based methods [9–12] became the center of attraction for researchers due to their simplicity in understanding and applications. However, the exact determination of fault detection, location and classification is very difficult with the use of frequency dependent transmission lines [13,14]. Nonetheless, these problems have been solved with some popular approaches like, Travelling wave based [15–18] and Knowledge-based [19–23] etc. Although, these approaches has some limitations, as propagation time can be affected by system parameter, network configuration [24] and presence of strong buses [19, 25, 26], these methods do not perform well for faults closer to the relaying point and with small inception angle [27–29], and learning is very time-consuming process [30, 31]. Therefore, each of these developed methods, though are good enough, have faced strong imputation on the fairness of fault estimation process.

A lot of research works are available on fault estimation in the area of power system protection applicable for HVAC transmission systems. However, few research work has been relatively developed in the field of HVDC transmission systems. It is the need to find out whether the methods developed and implemented in the HVAC systems are similarly applicable to HVDC transmission systems or not. Nowadays, primary protection against faults in HVDC transmission lines implement traveling wave-based methods, whereas, for the backup protection uses differential protection methods. One of the first proposals for fault estimation in HVDC transmission system is based on the traveling

wave [32, 33]. Traveling wave-based methods are used for detection and location of the faults, but not for classification of faults. The accuracy of fault detection and location depend on the arrival time and velocity of the traveling wave. To find accurate arrival time of transient wave-front sophisticated instrument is required which makes this technique complicated, costly and computationally burdened [34–36]. To overcome the drawbacks of the above-mentioned methods, several approaches based on artificial intelligent have been developed. Such as artificial neural network (ANN), decision tree, discriminant analysis, and support vector machine (SVM) [37–39], etc. Though, above stated approaches require large training data sets and training time. Thus, limits their applicability for real-time fault estimation without any modification. Since ANN is inspired by biological nervous system process information and has a good pattern recognition capability. This intrigue the researchers to develop several approaches based on derivatives of ANN, such as, radial biased, fuzzy based and back propagation neural network, employed for detection, classification and location of faults [40, 41]. Though, the accuracy of the approaches depends on the selection of hidden layers, which require large training data. To overcome the drawbacks of ANN-based approaches, SVM based approaches are preferred. These are independent of the number of features extracted from the input sample [42]. The major issue in using most of the feature extraction techniques is that, they do not provide an accurate estimation of the fundamental frequency component in the presence of DC offset [43–45]. Further, these techniques have high computational time due to input feature space vector is of high dimension. Therefore, these methods require a supporting method to reduce the dimension of the input feature space vector for the reduction in computational time [45]. Although, each of these developed methods, believed to be fair enough, though faced partial suitability on fault estimation procedure.

Moreover, with increased penetration level of renewable energy resources like wind, solar, tidal energy, etc. are becoming more popular and economical. However, most of these resources are far from the load center. Therefore, integration of renewable energy resources require development of HVDC transmission systems for bulk power transfer with fewer transmission losses. Therefore, the development of hybrid HVAC and HVDC transmission system is increasing day by day. Although, a few approaches that work properly in both HVAC as well as HVDC transmission systems to certain degree of accuracy are already present in the literature [43–45]. However, hybrid transmission systems require an accurate and reliable method that provides fault estimation simultaneously.

The presented work considers several issues related to fault estimation in different transmission system configurations and attempts to resolve these issues with the proposed

methods. The motivation for such issues is discussed in the next subsection.

1.2 Motivation for the Presented Work

Restructuring of the electrical power system has created several new challenges and opportunities for power system producers and distributors in the area of power system protection. Development of different configurations of the transmission systems require their protection as well. Nowadays, the transmission system infrastructure increases rapidly for the fulfillment of the power requirement of the end consumer [2]. Due to this, different new energy resources are developed and the research is still going on. Most of the futuristic energy resources are much far behind the load center. Therefore, the transmission system increases day by day with different configurations as per the requirement. With the increase in transmission lines, the possibility of occurrences of the fault also increases [46]. Thus, a detailed study of power system protection for the Transmission System Operator (TSO) for the fault estimation problem in the right perspective is the need of the attention.

The comprehensive collection of linear and nonlinear fault independent dynamic models for different configurations of power systems are required for validation of the proposed method. The required dynamic models are realistic in nature. Therefore, they became applicable to various types of power systems studies such as fault analysis, protection, dynamic, transient and steady state stability analysis, voltage collapse and contingency analysis etc. From the literature, few of research work take consideration of the frequency dependent transmission systems along with the dynamics of the exciter and governor associated with each generator [47]. Although, the realistic nature of the developed models precisely describe their ability for the system performance under normal and abnormal conditions. The abnormal conditions include faults of transient or permanent types, symmetrical and unsymmetrical types etc.

The predominance of existing fault estimation methods are strictly specific system configuration dependent [48]. However, the fault estimation methods that are independent of system configuration and provide the uniform precise solution for different system configurations is the primary requisite for the TSO. A large number of the researchers have also considered the frequency independent model of transmission lines but practically line parameters are frequency dependent. However, the accuracy of a lot of fault estimation methods is highly influenced by the system parameters [49]. Therefore, it is advisable to develop a fault estimation method independent of system parameters.

The mutual coupling effect of high voltage transmission lines is not get proper attention in the available literature [50]. Since, it reduced the complexity of the transmission system design and system parameter calculation. But, the results obtained may not provide an accurate solution for the real transmission system. Although, the fixed resistive nature of fault impedance has been also considered in the estimation of faults but fault impedance varies from place to place. Also, the effect of weather conditions is also ignored in the existing literature [51].

At present time HVDC transmission system is a favourable choice for transfer bulk power from long distance. Therefore, day by day HVDC transmission system finding place in the system rapidly and with this increase in system line length protection issue also increases. It is observed from existing literature that multi-terminal HVDC system lacks an adequate technique of fault identification, location, and classification [52]. Along with some of the research work for fault estimation for HVDC transmission systems withstand capacity of freewheeling diode which needs attention during complete fault execution has been completely neglected [53]. This may further result in collapsing of the converter system. With the existing infrastructure of HVAC transmission system the development of HVDC transmission system leads to a new area of the hybrid transmission system. Hence, a simultaneous fault estimation method for the hybrid HVAC and HVDC systems which work alike in both transmission systems is essential.

The lots of research works has been focused on the individual evaluation of fault identification, location and classification problems in existing literature. However, for the practical realization of fault identification, location, and classification should be evaluated simultaneously. Since, after identification of faulted section if types of fault and their location are estimated with reasonable accuracy then the system restoration process by the TSO occurs in a minimum time span.

Motivated from these aspects, the research work undertaken in this thesis aims to develop fault estimation methods that provide a precise result on the various transmission systems involving HVAC, HVDC and hybrid HVAC and HVDC transmission systems. Different configurations of transmission systems modelled are taken into consideration. These configurations include frequency dependent modeling and also the mutual coupling between different phases of transmission lines. Proposed methods and developed test transmission systems will be utilized to address the above mentioned mention issues.

1.3 Contributions of the Presented work

The objectives of the research work include the study of power system protection problem for fault estimation in transmission system of different configuration with proposed approaches. The main contributions of this thesis are as follows:

i. PLFE based multi-objective method is proposed for detection, location, and classification of symmetrical, as well as, asymmetrical faults in HVAC transmission systems. This method effectively identifies the faulted sections and precisely pinpoints the fault location without consideration of system parameters. This enables the proposed method to operate with less computational complexity.

ii. Modeling and designing of HVAC transmission test system with consideration of frequency dependent model using PSCAD software. This provides a more realistic environment.

iii. F-SVM based multi-objective method is proposed to precisely recognize the fault detection, location, and classification in HVDC transmission systems. This method employs a feature selection scheme for reduction of computational intensiveness. As a consequence, the fault detection time will be reduced considerably and fault location and classification accuracy will be improved.

iv. The use of F-SVM in the hybrid transmission system to accomplish the multi-objective functions. The proposed F-SVM simultaneously operates for both HVAC, as well as, HVDC transmission systems. This helps the transmission system operator to improve the decision-making process.

v. Modeling and designing of VSC are proposed for HVDC multi-terminals and hybrid transmission system. This will potentially lead to improved power transfer capacity of transmission systems.

vi. Proposed methods and schemes in this thesis are evaluated through a realistic case study.

vii. Finally, the modeling and designing of AC-DC and DC-AC converters are presented for CIGRE (B4.57 and B4.58). In addition, the designing of complete CIGRE (B4.57 and B4.58) system is carried out in PSCAD software environment. This will help the novice researchers working in this area to get better insights about modeling and designing of hybrid transmission systems.

1.4 Organization of the Thesis

Chapter organization is an important part of the thesis that provides a complete overview of the thesis. This thesis consists of six chapters, including an introduction and conclusions. The relationship between different chapters is highlighted in Figure 1.1. The current chapter includes major issue involved in fault estimation in HVAC, HVDC and hybrid transmission systems. It analyses the involved problems in the area that motivated the work, and further contributions of the presented thesis. The rest of the chapters of the thesis are organized as follows.

Chapter-2 provides a comprehensive literature review on issues pertaining to fault estimation in transmission systems, including those of HVAC, HVDC and hybrid transmission lines configuration modelling, rival behavior and imbalance power transfer mechanisms. It offers details on causes, models and solution approaches of the associated issues.

Chapter-3 proposes classical fault estimation strategy for fault detection, location and classification of different types of faults in HVAC transmission systems. The proposed PLFE method is illustrated with three standard transmission test systems. Impact of proposed approaches with three transmission test systems has been discussed.

Chapter-4 presents an efficient method for fault estimation strategy for fault detection, location and classification of different types of faults in HVDC transmission systems. This chapter also describes the modern control strategy and modeling of dynamic systems with the electromagnetic transient program. The proposed method F-SVM using computational approached for fault estimation with half cycle of measured data. All step of the proposed method describes with the mathematical formulation and their applicability shown with two standard HVDC transmission test systems.

Chapter-5 describes the applicability and reliability of the proposed computational method F-SVM in the area of fault estimation in hybrid transmission systems. This chapter also describes the design and control strategy of CIGRE standard dynamic systems with the electromagnetic transient program. The validation of the proposed F-SVM method in the hybrid transmission systems and finding in the area of fault estimation with two test cases are discussed. Besides, the use of hybrid transmission test systems one HVAC test system is also taken for validation of Proposed F-SVM method in all types of the transmission systems configuration.

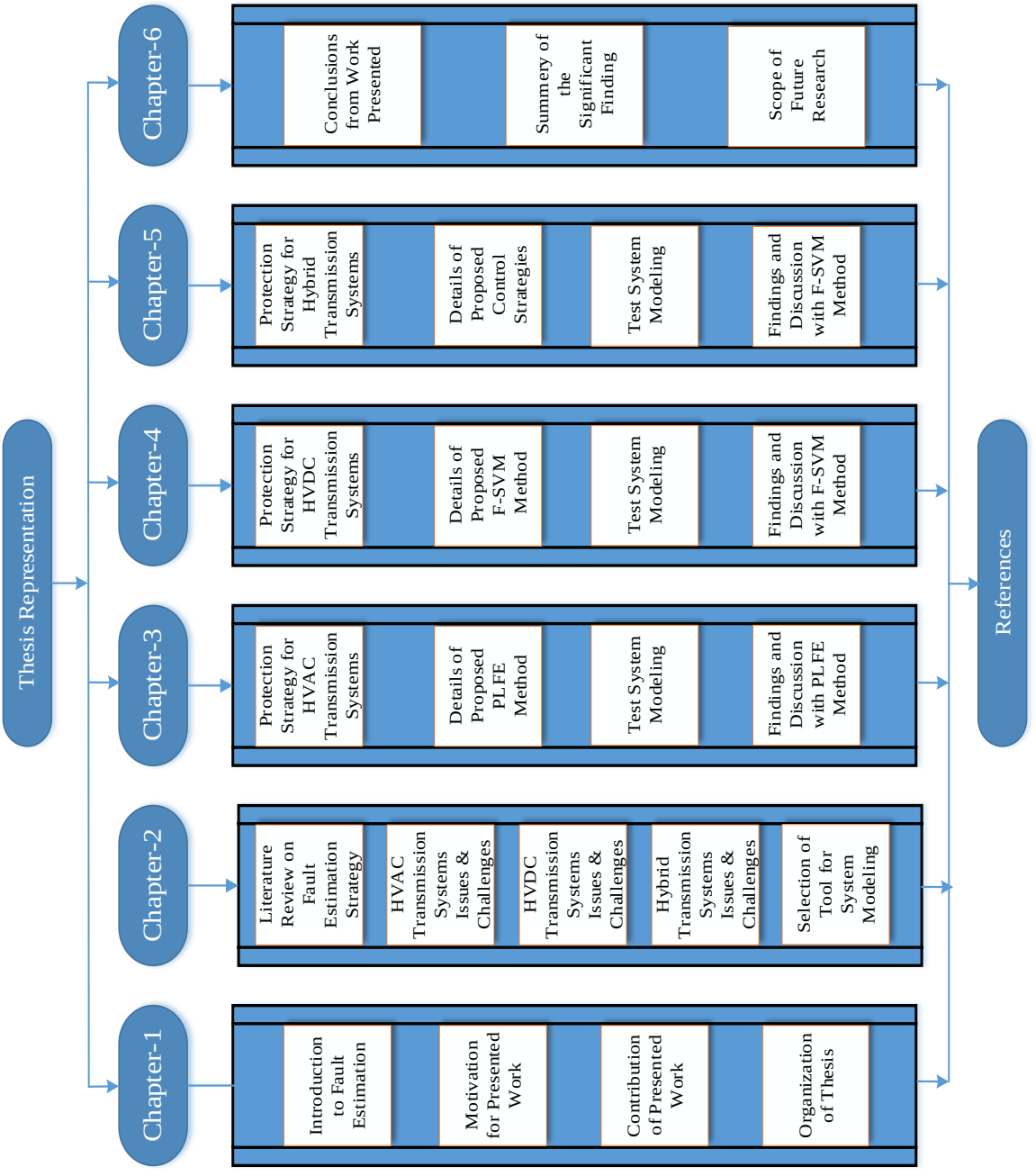

FIGURE 1.1: Thesis structure

Chapter-6 summarized the main findings of the work presented in the thesis and suggests directions for future research in this area.

Finally, Appendix-A provides dynamic data of the IEEE 30-bus, IEEE 39-bus, CIGRE 2-terminal system, CIGRE multi-terminal system, CIGRE 2- terminal hybrid system, CIGRE (B4.57 and B4.58) hybrid system used for validation of proposed methods.

Chapter 2

Literature Review

The chapter deals with the fundamental thought of power system protection highlighting critical issues involved in fault estimation. This chapter further discusses about different fault detection techniques utilized in transmission systems. Further, describe the different software platform for realistic fault scenario generated. Along with application of the electromagnetic transient program to model fault problem and identified research challenges are discussed.

2.1 Introduction

The problem of fault detection, location and classification in the transmission system as well as in distribution systems have been taken into consideration over the last two decades. Transmission lines protection against uncovered deficiency is the most basic protection work in the reliable operation of the power system. With the developments in signal processing techniques, a global positioning system (GPS) and communications have provided to a greater extent of researchers to carry out research with high breadth and depth in that the restrictions of traditional fault protection methods can be modified. Furthermore, the difficulty in data acquisition as well as obtaining the accurate information measure at multiple nodes in the grids with traditional equipment such as a potential transformer, current transformer and remote terminal unit swap with advanced developed intelligent electronic devices (IEDs) [54–56]. The use of phasor measurement units (PMU) has also grown wide attention for monitoring system with synchronized signal data for fault estimation [57]. These technical improvements can provide assurance for a quick and accurate response to faulty situations. The computational ability of computers improved

rapidly. Therefore, high-performance computing solutions such as server clusters are able to complete distributed computing work within a short time span, thus allowing the use of methods with higher computation complexity. Accordance with presently available literature of transmission lines protection, transmission system divided into three types in the power system. On the basis of literature review, some research gaps have been identified and research objectives of the thesis are framed. A brief literature about fault detection, location and classification for HVAC, HVDC and hybrid transmission system is presented in the subsequent section.

2.1.1 Fault Estimation for HVAC Transmission System

The fault estimation was first introduced in transmission systems. Several transmission fault assessment methods employed may be broadly categorized as: Impedance based [58–60], Travelling wave based [15–18] and Knowledge-based [19–23] etc. for different design of transmission system. Fault situation significantly disturbed power transfer capability of a power system, in this faulted period power transfer with another available healthy section due to this system run with reserved capacity and losses are more as compare to the previous system. Therefore, fault assessment becomes an important issue for the system operator for power transfer with minimum loses. Though, true fault assessment methods provide a solution for these losses with system restoration in a minimum time of span, but some very interesting fault assessment methods such as Synchrophasor based [46], Improved Traveling wave based [61–63], and Knowledge-based [64,65] etc. Aforementioned methods have employed different approaches in order to provide an accurate and reliable solution for these fault-related problems. These methods have their own advantages and disadvantages. A brief review of various fault estimation methods is presented here.

Impedance-based methods were first used to fault estimation in transmission lines in the power system. These methods were used by most of the researcher as a solution for fault location problems in previous time but nowadays researchers are using these methods for solving all three problems related to the fault. The motivation of fault location with Impedance based techniques are developed since the 1950 [48]. Impedance-based fault estimation methods are widely used by the utilities and engineers due to their simplicity, low implication cost, low computational burden [58–60, 66]. But, the accuracy of these Impedance based fault estimation methods are adversely affected by fault impedance, lack of fault path information, DC offset and CT saturation, line load flow, system non-linearity, both the remote terminal information [67–70]. Moreover, Impedance

based fault estimation methods require only the accurately measured fundamental voltage and current data. Therefore, as per the requirement of the measured data method is categorized as one-terminal measurement based methods and two-terminal measurement based methods [67, 68]. One-terminal measurement based methods less accurate but their implantation cost is much less as compare to two-terminal measurement based methods. These methods also require signals of pre and post-fault of long duration [69, 70]. With the use of signal filtering for improvement in measured quantity some of the researchers use a different type of transformation techniques such as, Laplace transformation, Discrete Fourier Transformation (DFT), Clark Transformation [67–70]. Although, in recent time due to development of Global Poisoning System (GPS) based measurement such as, Supervisory Control and Data Acquisition (SCADA) and Phasor Measurement Unit (PMU) system provide much accurate, synchronized and real-time measure data of the power system. Due to the advantage of synchronized measure data researcher use it in for providing fault estimation solution with using PMU measurement [50, 70–76]. Impedance-based methods affect the system parameter and system configuration. Therefore, some of the research work tries to overcome this problem with their proposed work that does not use a system parameter for fault estimation [49, 77–80]. These methods have some issue in fault detection and classification also that why some of the hybrid research work reported with some other techniques. Therefore, impedance based methods combine with wavelet transform, weighted least square methods and knowledge base techniques for fault estimation properly. Because these methods are good in fault detection as well as classification problem [15–18, 51, 81–87]. Nevertheless, some of the issues related to these methods are as: effect of shunt reactor and capacitance for long lines [18, 71–73, 77], combined effect of load and fault current [58–60, 66–69], correct fault type identification [58–60, 66, 67] etc. Further, a limited literature [50, 74] is available which addresses the effect of mutual coupling on high voltage transmission lines. Since, it reduced the complexity of the transmission system design and system parameter calculation. But, the results obtained may not provide an accurate solution for the real transmission system. Nowadays, integration of renewable energy resources to the main grid is a common trend to overcome with the load demand. However, this reduces the stability limit. Therefore, the system requires faster fault clearing protection techniques and re-closing schemes [16–18].

Traveling wave based fault estimation methods gain more attention to overcome the drawback of impedance-based methods [27–29, 88, 89]. Because the accuracy of the traveling wave based fault estimation methods depends on the data acquisition system, propagation time, sampling rate and the synchronization time [90]. With the recent day's development in data acquisition and signal processing techniques, traveling wave based fault

estimation methods becoming more attractive where higher accuracy is an important issue [90]. For improving the signal processing Discrete Fourier Transformation, Short-Time Fourier Transform (STFT), Continues Wavelet Transformation, Laplace Transforms, Gabor Transform and Wigner Transform are used for accurately calculating propagation time of wavefront [24, 91–96]. Some of the research work using one terminal data that for estimating fault is less accurate, but simple in implementation as compare with the research work using two terminal data. In fact, methods using one terminal data can estimate fault without using GPS communication and data synchronization [25, 26]. However, these methods have complications in estimating fault near the one terminal and in distinguishing whether the second traveling wave is reflected from fault point or from the remote terminal [26]. Although, for a long transmission line these methods show great advantage regarding technical and economical aspect, due to no need for reactive compensation, large transmission capacity and intermediate switching substation [19,20]. The electromagnetic transient and steady-state characteristics of voltage and currents of half wavelength of transmission line were explored using time reversal properties [21]. Since, these methods do not classify fault type that why using these methods with some classification approaches such as, Artificial Neural Network (ANN), Wavelet Transform, Support Vector Machine (SVM) and Fuzzy Logic [21, 22]. Although, traveling wave based fault estimation methods have many advantages but some issue related to these methods are such as: propagation time can be affected by system parameter, network configuration [24] and presence of strong buses [19, 25, 26], these method does not perform well for fault closer to the relaying point and small inception angle [27–29].

To overcome these drawbacks, combined impedance and traveling- wave-based methods are using knowledge-based methods [23, 97–110]. These methods are commonly used for fault detection as well as classification purpose. knowledge-based methods can be categorized as Artificial intelligence based, statistical analysis based and hybrid methods. There are several artificial intelligence based methods such as Artificial Neural Network (ANN), Fuzzy Logic (FL), Expert System and Genetic algorithms etc. A lot of the knowledge-based methods implement fault estimation models based on statistical learning theory [111]. These methods depend on the extracted feature of measured data for fault estimation. Therefore, researches using some of the statistical approaches with knowledge-based methods such as, Principal Component Analysis (PCA), WMA, IFA, F-score, Modal Transformation, Karrenbauer Transformation and Wavelet Transform and Generate Logic for their objective [23, 97, 98]. ANN and their different configuration are the most popular methods used for fault estimation as: Feed-Forward Artificial Neural Network (FNN),

Radial Basis Function Networks (RBFN), Finite Impulse Response Artificial Neural Network (FIRANN), Adaptive Neuro-Fuzzy Interference System (ANFIS), Chebyshev Neural Network (ChNN), etc [97–104]. Although, ANN is a good method for classification but combined with Wavelet Transform, Discrete Wavelet Transform and Fuzzy Logic etc provide accurate and reliable solution [99–109]. After, ANN popular choice among the researchers is Support Vector Machine (SVM) based fault estimation. With the use of SVM based fault estimation is to find out an optimal hyperplane that maximizes the margin between two class of faults. By the use of non-linear kernel function, SVM classifies a higher dimension of fault class with this non-linearity. SVM is a vector classifier therefore, their accuracy not affected with the use in a different configuration of transmission as well as distribution line such as, single line, double lines, series-compensated lines and shunt-compensated lines [110, 112]. With the SVM researcher using DWT, PCA to reduce the dimension of the wavelet coefficient before using with the SVM fault estimation. Hardware implementation using FPGA and a real-time power simulator was done accurately and result validated. Since, these methods trained with a convex optimization [30,31,113]. As, the use of Wavelet Packet Decomposition (WPD) with Db1 Mother Wavelet extract important feature from only 0.5 cycles of post-fault voltage signal data after noises were eliminated by a filter for fault estimation accurately in small time of duration [114–118]. Although, knowledge-based fault estimation methods have many advantages but some issue related to these methods are such as: appropriate feature extraction is difficult for a particular fault signal, learning is an important step if any case missed or different from training case then fault estimation is difficult, accurate training is a very time-consuming process [30, 31, 113–118].

2.1.2 Fault Estimation for HVDC Transmission System

Numerous research work available on fault estimation in the area of power system protection. These techniques for fault estimation are applicable on high voltage alternating current (HVAC) transmission system. However, limited research work has been carried out in HVDC transmission system. Therefore, their is pressing need to investigate whether the methods adopted in HVAC system can be applicable to HVDC or not. In the present days, the primary protection against fault in HVDC transmission lines uses Traveling wave based methods, whereas for the backup protection uses differential protection methods. One of the first proposals for fault estimation in HVDC transmission system are based on the Traveling wave approach [32,33]. Traveling wave based fault estimation methods found solution on the basic of the time taken to propagate transient wave along the transmission

line from fault point to reference bus [119–121]. Some of the research work available on methods developed with one-terminal measured data [122]. Although, most of the research work available in fault estimation in HVDC require two-terminal measured synchronized data using PMU. The traveling wave based fault estimation methods uses the transients generated due to fault initiation and collect the traveling wave front that continue to bounce back and forth concerning nearest terminal and fault initiation point up to steady state is reached. Therefore, measured data should be synchronized before the traveling wave based fault estimation methods are used. Although, these methods have fast response and are reliable with high accuracy [123–125]. A common issue related to these methods include requirement of high sampling rate for the measured data, which in turn depends on a sophisticated measurement device thus increasing the computational burden. In order to mitigate the above mentioned issues some of the researchers [52, 126–129] employed Fourier Transform and Wavelet Transform with Traveling Wave based fault estimation methods for reliable solution in short time period. Research work is also available with hybrid system that uses intelligence technique with traveling wave based fault estimation methods. Intelligence technique uses with these methods are ANN, SVM, expert solution, etc. These methods using similarity property for fault detection, classification and for fault location traveling wave is used [53, 130–136]. Although, traveling wave based fault estimation methods have many advantages but various issues related to these methods are such as: propagation time can be affected by system parameter, network configuration [33, 119, 122–125] and these method does not perform well for fault closer to the converter station and small inception angle [53, 133–136].

To overcome the drawbacks of the above mentioned methods, several approaches based on artificial intelligent have been developed. Such as artificial neural network (ANN), decision tree, discriminant analysis, and support vector machine (SVM) [37–39]. Above stated approaches require large training data sets and training time, therefore not suitable for real time fault estimation without any modification. Since ANN is inspired by biological nervous systems process information, therefore it has a good pattern recognition capability. So, the researchers have developed several approaches based on derivatives of ANN. Such as, radial biased, fuzzy based and back propagation neural network, is used for detection, classification and location of fault [40, 41]. However, in this technique, the accuracy of the approaches depends on the selection of hidden layers, therefore, training data required is large. And as a result, it increases the computational burden that further delays the execution time of the technique.

To overcome the drawbacks of ANN based approaches SVM based approaches is preferred. SVM is independent of number of features extracted from the input sample [42]. This property is very useful in fault analysis of the transmission line, as measured quantities available with utilities are limited. Different feature extraction techniques such as Discrete Fourier Transform (DFT), Discrete Wavelet Transforms (DWT), Least Error Square (LSE), and Stationary Wavelet Transform (SWT), are implemented with SVM for fault detection and classification [43, 44]. The major issue in using most of the feature extraction techniques is that, it does not provide an accurate estimation of the fundamental frequency component in presence of DC offset [45]. SVM based technique has high computational time, since input feature space vector is of high dimension. If we are able to reduce the dimension of the input feature space vector, the computational time reduces. In literature F-score has been used for identifying the rank of the column in a particular matrix using mean and variance [137]. Although, knowledge-based fault estimation methods have many advantages but some issue related to these methods are such as: appropriate feature extraction is difficult for a particular fault signal [37, 39, 72], learning is an important step if any case missed or different from training case then fault estimation is difficult [41, 43, 50, 75], accurate training is a very time-consuming process [45, 49, 78].

2.2 Critical Review

From the aforementioned literature review, the following research gaps have been identified:

- From the existing literature it is found that much focus has been given on the individual evaluation of fault identification, location and classification problems. However, for practical realization fault identification, location and classification should be evaluated simultaneously.
- The fixed resistive nature of fault impedance has been considered in the estimation of faults but fault impedance varies from place to place. Also, the effect of weather conditions is neglected in the existing literature.
- The mutual coupling effect of high voltage transmission lines is also not given proper attention in most of the available literature.
- Most of the researchers have considered the frequency independent model of transmission lines but practically line parameters are frequency dependent.

- Multi-terminal HVDC system lacks an adequate technique of fault identification, location, and classification.
- A simultaneous fault estimation method for the hybrid HVAC and HVDC systems is the need of the hour.
- A lot of the existing fault estimation methods are strictly specific system configurations dependent.
- The existing fault estimation technique doesn't consider the withstand capacity of freewheeling diode which needs attention during complete fault execution. This may further result in collapsing of the converter system.

2.3 Research Objectives

On the basic of aforementioned critical review, the following research objectives have been framed for the thesis work.

1. To carry out extensive literature survey in the area of fault detection, location, and classification for HVAC, HVDC and Hybrid HVAC & HVDC transmission system.
2. To develop an algorithm for detection, location, and classification of fault in single circuit HVAC transmission lines.
3. To develop an algorithm for detection, location, and classification of fault in Double circuit HVAC transmission lines consider the charging effect.
4. To develop an algorithm for detection, location, and classification of fault in VSC HVDC transmission lines.
5. To develop an algorithms for detection, location, and classification of fault in hybrid HVAC and HVDC transmission lines.

2.4 Selection of Tools for System Modeling

The power system is one of the largest interconnected dynamic systems in recent time. It involves thousands of electrical sources, loads, transmission and distribution lines, power and distribution transformers, relays, circuit breakers etc. Faults in any component of the

power system may cause significant disturbance to the power supply and thus electrical, financial losses and create a disturbance.

In this thesis, their is a collection of linear and non-linear dynamic models for various types of application in the power system. The dynamic models are realistic in nature, which become applicable to various types of power systems studies such as fault analysis, protection, dynamic, transient and steady state stability analysis, voltage collapse and contingency analysis etc. The developed models accomplished with the frequency depended transmission system [13, 14] along with the dynamics of the exciter and governor associated with each generator. Therefore, the realistic nature of the developed models shows their ability to precisely describe the system performance under normal and abnormal conditions. The abnormal conditions include faults of transient or permanent types, symmetrical and unsymmetrical types etc. From the literature of fault estimation in transmission lines comparison of some of the software used for system modeling and analysis are described in Table 2.1. On the basis of objectives, PSCAD is selected for system modeling and MATLAB is used as analysis and validation [138, 139].

TABLE 2.1: Comparison of existing power system software package for fault studies

Software Packages	Stater Transient	Rotor Transient	Sys. Machine Positive Sequence	Sys. Machine Negative Sequence	Sys. Machine Zero Sequence	Time Dependence	Frequency Dependence
	Symmetrical Condition		Unsymmetrical Condition				
PSS/E [140]	No	Yes	Static Ckt.	Static Ckt.	Static Ckt.	No	Yes
Power Factory [141]	No	Yes	Static Ckt.	Static Ckt.	Static Ckt.	No	No
(RMS Model)							
Power Factory [141] EMT Model	Yes	Yes	Static and Rotor Dynamic Included	Static and Rotor Dynamic Included	Static and Rotor Dynamic Included	Yes	Yes
SIMPOW [142] Fundamental freq. Model	No	Yes	Static Ckt.	Static Ckt.	Static Ckt.	No	No
SIMPOW [142] Instantaneous Value Model	Yes	Yes	Static and Rotor Dynamic Included	Static and Rotor Dynamic Included	Static and Rotor Dynamic Included	Yes	No
Simpower system [143] (Specialized Technology)	Yes	Yes	Static and Rotor Dynamic Included	Static and Rotor Dynamic Included	Static and Rotor Dynamic Included	No	No
Simpower system [143] (SimScape Technology)	Yes	Yes	Static and Rotor Dynamic Included	Static and Rotor Dynamic Included	Static and Rotor Dynamic Included	Yes	No
PSCAD/EMTDC [144]	Yes	Yes	Static and Rotor Dynamic Included	Static and Rotor Dynamic Included	Static and Rotor Dynamic Included	Yes	Yes

PSCAD software uses an electromagnetic transient program for solving a differential equation in the time domain for linear and non-linear modes. PSCAD provide a real-time power system environment and synchronized measurement of voltage, current and phasor angle with the help of SCADA or PMU. Since steady-state equations are used to represent the power system for load-flow, protection, stability in power system and that program provide information about fundamental frequency magnitude and phase only. Nevertheless, PSCAD can provide a replica of the response of the power system conditions at all the frequencies with user-defined time step [144].

Chapter 3

Fault Protection Strategies for HVAC Transmission Systems

This chapter presents a efficacious method for fault detection, location, and classification for transmission system. Further, statical analysis is presented to validate proposed method.

3.1 Introduction

Electricity has brought a paradigm shift in the quality of life, urbanization, research, national economy, defence and industrial growth. Ever increasing demand for electricity has forced the nation to interconnect regional grids together and also combine dispatchable and non-dispatchable energy sources to the main grids. Thus, modern power systems are large with many complex interconnections with adjoining networks. This has resulted in a large increase in the number of lines in operation and their total length. Transmission line plays an important role in transferring power from generating station to the distribution centre. These lines experience faults which are caused by storms, lightning, snow, freezing rain, insulation breakdown and, short circuits caused by external objects, etc. In most of the cases, electrical faults manifest in mechanical damage that must be repaired before returning the line to service. The restoration can be expedited if the detection, location, and classification of the fault is either known or can be estimated with reasonable accuracy.

Accurate estimation of fault detection, location, and classification are very important when lines are long and run through inaccessible areas, and weather conditions are highly

unfavorable. The reason being, visual inspection becomes much difficult and highly time-consuming. Fault detection, location and classification provide an estimate for both sustained and transient faults. Normally, transient faults cause minor damage that is not easily visible on inspection. Fault detection, location and classification methods help to identify those locations and type of faults for early repairs to prevent recurrence and consequent major damages.

The subject of fault estimation has been of considerable interest to electric power utility engineers and researchers for over last two decade. Most of the research done at the present time, has been aimed at detection, location, and classification of transmission line faults. This is mainly because of the impact of transmission line faults on the power systems as already discussed above. In brief, the following benefits can be achieved by having a fast and efficient fault estimation scheme:

- Fault estimation methods assist to accelerate the restoration process quickly.
- By specifying the faulted node location and type of fault there is a chance to reduce the losses and isolate the affected areas from the healthy ones by implementing sectionalize switching operations.
- By locating and classifying transient faults it is possible to plan for preventive maintenance tasks and avoid future fault.
- To avoid cascading failures and facilitate safer, secure and reliable power systems.
- To avoid overheating and losses of the line using different paths for the power delivery.

Therefore, the transmission system requires a quick reliable and accurate fault estimation method for the uninterrupted reliable operation of the power systems. Thus, this chapter proposes a novel parameter-less fault estimation method for the HVAC transmission systems. The proposed PLFE method is based upon the principle of Least Error Square and Fourier Transform. For the validation of this proposed method three test systems are considered and investigated under the varying condition of faults. The application results of the proposed method are presented and compared with other established methods.

3.2 Proposed PLFE Fault Estimation Method

Initially, many impedance based methods [3–9] have been studied to calculate the fault detection, location and classification in High voltage AC transmission system, as well. However, these methods have limitation due to one or more reasons such as model dependency or system parameter dependent, frequency dependent, sophisticated measured data requirement, etc. This leads to the development of several interesting approaches for transmission line fault protection in which the circuit theory based methods [9–12] become the center of attraction for researchers due to their simplicity in understanding and application. However, the exact estimation of fault detection, location and classification is impossible with the use of frequency independence transmission line. Therefore, each of these developed methods, thought are good enough, have faced strong imputation on fairness of fault estimation which may be briefly explained in coming subsequent sections.

A new fault detection, location and classification method based upon the two end synchronized/un-synchronized data for high voltage transmission line is proposed which considers arcing faults calculations. In this work, Least Error Square (LES) Principal is used without considering the line parameters. The Least Error Square Principle is used on positive sequence equivalent circuit to calculate the fault distance from the reference bus. This algorithm is simple to understand and simple to implement. Moreover it can be applied to both lumped and distributed transmission lines. However it require less data with non-iterative process. This algorithm provide promising results against the variability in fault resistance on the account of two end data. The two end fault estimation methods work with measured voltage and current data from two end of concerning section bus. In the present scenario, the power system well equipped with modern measurement equipment like Phase Measurement Unit (PMU) and fiber optics communication links that provide synchronized data of voltage and current and also it provide rate of change of frequency.

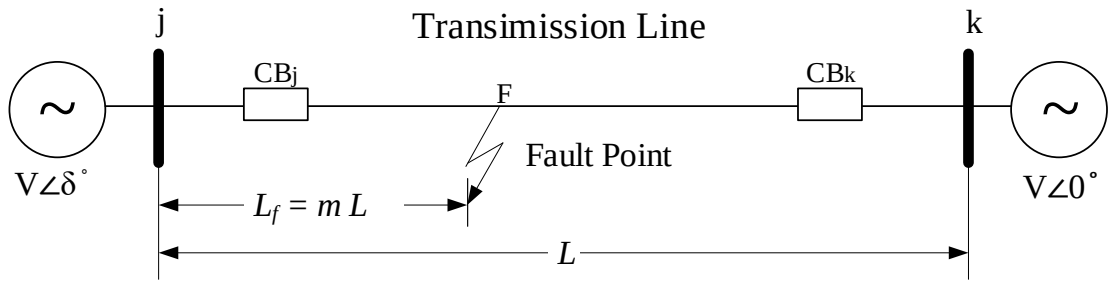

FIGURE 3.1: Schematic diagram of two terminal transmission test system

The proposed PLFE method uses only voltage and current synchronized data if required but if un-synchronized data is available then it's find synchronizing angle and use it for fault assessment.

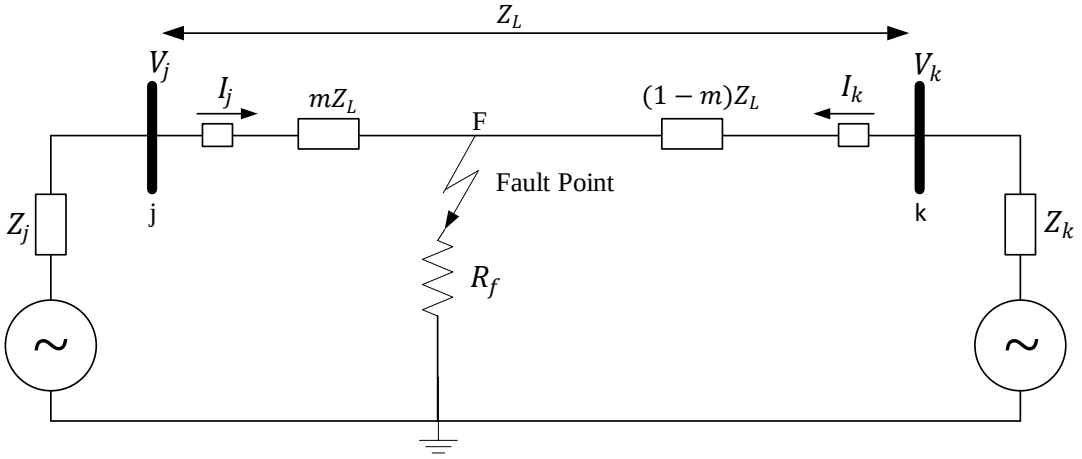

FIGURE 3.2: The equivalent circuit at the time of fault

Let us consider Figure 3.1 and Figure 3.2 which shows the schematic diagram and the equivalent circuit diagram of faulted transmission system. The three-phase voltage to the fault point are computed based on Kirchhoff's Voltage Law from both end are taken and the equations are given as:

$$[V_j]_{abc} = m[Z_L]_{abc}[I_j]_{abc} + ([I_j]_{abc} + [I_k]_{abc})[R_f] \tag{3.1}$$

$$[V_k]_{abc} = (1-m)[Z_L]_{abc}[I_k]_{abc} + ([I_j]_{abc} + [I_k]_{abc})[R_f] \tag{3.2}$$

$$[V_j]_{abc} - [V_k]_{abc} = m[Z_L]_{abc}([I_j]_{abc} + [I_k]_{abc}) - [Z_L]_{abc}[I_k]_{abc} \tag{3.3}$$

where, m is per unit fault distance of transmission line. $[Z_L]_{abc}$ is total transmission line impedance $[I_j]_{abc}$, $[I_k]_{abc}$, $[V_j]_{abc}$, $[V_k]_{abc}$ are the three phase currents and voltage measured at concerning fault section buses as shown in Figure 3.2. If data are not synchronized than synchronized angle of other bus can be calculated with reference bus, here it have been taken as $e^{\jmath\delta}$. It can facilitate estimation of the correct fault location. Now with synchronization angle eq. (3.3) is rewritten for un-synchronized data set as:

$$[V_j]_{abc} - ([V_k]_{abc}e^{\jmath\delta}) = m[Z_L]_{abc}[I_j]_{abc} + ([I_k]_{abc}e^{\jmath\delta}) - [Z_L]_{abc}[I_k]_{abc}e^{\jmath\delta} \tag{3.4}$$

where, $e^{\jmath\delta}$ is written for the synchronization angle. correctly identifying $e^{\jmath\delta}$ with the help of three sample moving window method [145]. Finding accurate angle is much important

because it effect the accuracy of fault location calculation. If finds $e^{\jmath\delta}$ correctly then it easily the solve fault location from eq. (3.4). With using both the eq. (3.3) and (3.4) and rewrite it in the form of eq. (3.5) and (3.6) respectively as:

$$\underbrace{[\triangle V]_{abc}}_{\text{Y}} = m \underbrace{[Z_L]_{abc}([I_j]_{abc} + [I_k]_{abc}) - [Z_L]_{abc}[I_k]_{abc}}_{\text{X}} \tag{3.5}$$

or,

$$\underbrace{[\triangle V]_{abc}}_{\text{Y}} = m \underbrace{[Z_L]_{abc}([I_j]_{abc} + [I_k]_{abc}e^{\jmath\delta}) - [Z_L]_{abc}[I_k]_{abc}e^{\jmath\delta}}_{\text{X}} \tag{3.6}$$

where, $[\triangle V]_{abc} = [V_j]_{abc} - [V_k]_{abc}$ or $[\triangle V]_{abc} = [V_j]_{abc} - ([V_k]_{abc}e^{\jmath\delta})$ for synchronized or un-synchronized data eq. (3.3) or (3.4) respectively.

$$m = [X]^{-1}[Y] \tag{3.7}$$

$$Fault\ Location = m * Length\ of\ Transmission\ Line \tag{3.8}$$

It can be easily computed the fault location of transmission line without knowing line parameter with eq. (3.8).

All derived equations are rewritten using the symmetrical transformation using positive sequence component for further calculation. With generate all possible permanent and transient faults to check the feasibility of the method in fault location. It also take un-synchronized measured data in this section for further calculation. Therefore, It equally applicable for any type of measured voltage and current data of buses. eq. (3.4) can be rewritten for un-synchronized measured data.

$$[V_j]_{012} - ([V_k]_{012}e^{\jmath\delta}) = m[Z_L]_{012}[I_j]_{012} + ([I_k]_{012}e^{\jmath\delta}) - [Z_L]_{012}[I_k]_{012}e^{\jmath\delta} \tag{3.9}$$

where, $[V_j]_{abc} - ([V_k]_{abc}e^{\jmath\delta}) = [T]([V_j]_{012} - ([V_k]_{012}e^{\jmath\delta}))$ and $[T]$ is transformation matrix [145]. eq. (3.5) is rewritten as,

$$[\triangle V]_{012} + [Z_L]_{012}[I_k]_{012} = m[Z_L]_{012}([I_j]_{012} + [I_k]_{012}) \tag{3.10}$$

Now taken the phasor measurement at instant $t = t_1$ then eq. (3.8) is rewritten as,

$$[\triangle V(t_1)]_{012} + [Z_L]_{012}[I(t_1)_k]_{012} = m[Z_L]_{012}([I(t_1)_j]_{012} + [I(t_1)_k]_{012}) \tag{3.11}$$

Now proceed for the N number of sample with constant interval $\triangle t$ eq. (3.11) is rewritten as,

$$\begin{bmatrix} \triangle V(t_1)]_{012} \\ \triangle V(t_2)]_{012} \\ \vdots \\ \vdots \\ \triangle V(t_{N-1})]_{012} \\ \triangle V(t_N)]_{012} \end{bmatrix} = \begin{bmatrix} ([I(t_1)_j]_{012} + [I(t_1)_k]_{012}) & -[I(t_1)_k]_{012} \\ ([I(t_2)_j]_{012} + [I(t_2)_k]_{012}) & -[I(t_2)_k]_{012} \\ \vdots & \vdots \\ \vdots & \vdots \\ ([I(t_{N-1})_j]_{012} + [I(t_{N-1})_k]_{012}) & -[I(t_{N-1})_k]_{012} \\ ([I(t_N)_j]_{012} + [I(t_N)_k]_{012}) & -[I(t_N)_k]_{012} \end{bmatrix} \begin{bmatrix} m[Z_L]_{012} \\ [Z_L]_{012} \end{bmatrix} \tag{3.12}$$

eq. (3.12) can be rewritten as,

$$\Big[V_n\Big] = \Big[I_n\Big] \begin{bmatrix} m[Z_L]_{012} \\ [Z_L]_{012} \end{bmatrix} \tag{3.13}$$

eq. (3.13) should be solve for finding the ratio between unknown variables $m[Z_L]_{012}$ and $[Z_L]_{012}$ rather then computing the value of these variables. Since, this ratio can be enumerated easily for available N number of equations, thus solving eq. (3.13) as,

$$\begin{bmatrix} m[Z_L]_{012} \\ [Z_L]_{012} \end{bmatrix} = \Big[V_n\Big] \Big[I_n\Big]^{-1} \tag{3.14}$$

Then the fault location L_f of line length L is calculated as,

$$L_f = m * L = \frac{m[Z_L]_{012}}{[Z_L]_{012}} \tag{3.15}$$

From eq. (3.15) it can easily found fault location with reasonable accuracy.

For identification of faulted section and faulted running window using quickest change detection approach. In the described approach fourier transform of rate of change of voltage and current phasor of all buses taken as the input function. For normal condition as shown in eq. (3.16)-(3.18). If this condition not satisfied then fault or disturbance present in the system. Therefore, fault are identified in the system with the help of fault detection scheme.

$$\frac{d(V_a)_{k-1}}{dk} = \frac{d(V_a)_k}{dk} = \frac{d(V_a)_{k+1}}{dk} \; or \; \frac{d(i_a)_{k-1}}{dk} = \frac{d(i_a)_k}{dk} = \frac{d(i_a)_{k+1}}{dk} \tag{3.16}$$

$$\frac{d(V_b)_{k-1}}{dk} = \frac{d(V_b)_k}{dk} = \frac{d(V_b)_{k+1}}{dk} \; or \; \frac{d(i_b)_{k-1}}{dk} = \frac{d(i_b)_k}{dk} = \frac{d(i_b)_{k+1}}{dk} \tag{3.17}$$

$$\frac{d(V_c)_{k-1}}{dk} = \frac{d(V_c)_k}{dk} = \frac{d(V_c)_{k+1}}{dk} \; or \; \frac{d(i_c)_{k-1}}{dk} = \frac{d(i_c)_k}{dk} = \frac{d(i_c)_{k+1}}{dk} \tag{3.18}$$

In the literature many methods of quick change detection are described [146, 147]. It can model the change point as a deterministic but unknown positive integer γ. A number of the heuristic method have been developed [148, 149]. In which the log-likelihood based on the current observation is compared with the threshold value to make a decision about the change. In this proposed PLFE method the quick change detection approach is used for fault detection. The basic methodology of this approach is described with preceding basic equation as,

Let X_k is the observation sequence with k=1, 2,...., n. f_0 and f_1 as the pre and post change probability density function. Then Probability measure (expectation) define in eq. (3.19) as,

$$E_\infty \left[logL \left[X \right] \right] = -D(f_0 \,||\, f_1) < 0 \quad and \quad E_1 \left[logL \left[X \right] \right] = D(f_0 \,||\, f_1) > 0 \tag{3.19}$$

where, $L(x) = f_1(x)/f_0(x)$, and E_∞ and E_1 correspond to expectations when $\gamma = \infty$ and $\gamma = 1$, respectively. Thus, after γ, the log likelihood of the observation X is more likely to be above the given threshold value. Although, this method is simple but significant performance gain can be achieved by making use of past observations to make the decision about the change. For the large number of observation, $\sum_{i=\gamma}^{n} logL(X_i)$ grow to ∞. Thus, if $S_n = \sum_{i=1}^{n} logL(X_i)$ is the accumulated log likelihood sum, then before γ, S_n has a positive drift and climbs towards ∞. Therefore, estimated value suggested by the following scheme that detects this change in drift with eq. (3.20) as,

$$\tau_c = inf \left\{ n \geq 1 : (S_n - \min_{1 \leq k \leq n} S_k) \geq b \right\} \tag{3.20}$$

where, τ_c is the change detection time in the observation of the function taken in consideration with $b > 0$. eq. (3.20) is also rewritten with $L(X_i)$ in eq. (3.21) as,

$$\tau_c = inf \left\{ n \geq 1 : W_n \geq b \right\} \tag{3.21}$$

where, $S_n - \min_{1 \leq k \leq n} S_k = \max_{0 \leq k \leq n} \sum_{i=k+1}^{n} \log L(x_i) = \max_{1 \leq k \leq n+1} \sum_{i=k}^{n} \log L(x_i) = W_n$.

For classification proposed PLFE method using some condition that specifies the fault class within prescribe accuracy describe in IEEE standard. There are mostly two types of faults in the electrical power system that is unsymmetrical and symmetrical faults. Unsymmetrical faults are very common but less severe than symmetrical faults. These are mainly three types namely line to ground (L-G), line to line (L-L) and double line to ground (L-L-G) faults. The line to ground fault (L-G) is the most common fault and $(65 - 70)\%$

of faults are of this type. The (L-G) fault causes the conductor to make contact with the earth or ground. Double line to ground (L-L-G) fault causes the two conductors to make contact with the ground, $(15-20)\%$ of faults are (LL-G) fault. The line to line (L-L) faults occurs when two conductors make contact with each other mainly while swinging of lines due to winds. $(5-10)\%$ of the faults are of the line to line fault. Unsymmetrical faults are also called unbalance faults since their occurrence causes unbalance in the system. Unbalance of the system means that impedance values are different in each phase causing unbalance current to flow in the phases. These are more difficult to analyze and are carried out with the help of phase sequence method. Three phase faults are very severe faults and occur rarely in the power systems. These are also called as balanced faults or symmetrical fault. Symmetrical faults are of two types namely line to line to line to ground (L-L-L-G) and line to line to line (L-L-L). Only $(2-5)\%$ of system faults are symmetrical faults. If symmetrical faults occur, the system remains balanced but results in severe damage to the electrical power system equipment. Analysis of these faults is easy and usually carried by per phase basis. In this work only (L-L-L) fault are considered for analysis. For classification of (L-G) faults condition describe in eq. (3.22)-(3.24) are used as,

$$I_b \geq 0 \downarrow, \quad I_c \geq 0 \downarrow, \quad I_c \geq 0 \uparrow, \quad I^1_{a0} = I^1_{a1} = I^1_{a2} \tag{3.22}$$

$$I_a \geq 0 \downarrow, \quad I_c \geq 0 \downarrow, \quad I_b \geq 0 \uparrow, \quad I^1_{a0} = \alpha^2 I^1_{a1} = \alpha I^1_{a2} \tag{3.23}$$

$$I_a \geq 0 \downarrow, \quad I_b \geq 0 \downarrow, \quad I_c \geq 0 \uparrow, \quad I^1_{a0} = \alpha I^1_{a1} = \alpha^2 I^1_{a2} \tag{3.24}$$

For classification of (L-L-G) faults condition describe in eq. (3.25)-(3.27) are used as,

$$I_a \geq 0 \downarrow, \quad I_b = I_c \geq 0 \uparrow, \quad I^1_{a0} + I^1_{a1} + I^1_{a2} = 0 \tag{3.25}$$

$$I_b \geq 0 \downarrow, \quad I_a = I_c \geq 0 \uparrow, \quad I^1_{a0} + \alpha^2 I^1_{a1} + \alpha I^1_{a2} = 0 \tag{3.26}$$

$$I_c \geq 0 \downarrow, \quad I_b = I_c \geq 0 \uparrow, \quad I^1_{a0} + \alpha I^1_{a1} + \alpha^2 I^1_{a2} = 0 \tag{3.27}$$

For classification of (L-L) faults condition describe in eq. (3.28)-(3.30) are used as,

$$I_a \geq 0 \downarrow, \quad I_b = I_c \geq 0 \uparrow, \quad I^1_{a1} + I^1_{a2} = 0 \tag{3.28}$$

$$I_b \geq 0 \downarrow, \quad I_a = I_c \geq 0 \uparrow, \quad \alpha^2 I^1_{a1} + \alpha I^1_{a2} = 0 \tag{3.29}$$

$$I_c \geq 0 \downarrow, \quad I_b = I_a \geq 0 \uparrow, \quad \alpha I^1_{a1} + \alpha^2 I^1_{a2} = 0 \tag{3.30}$$

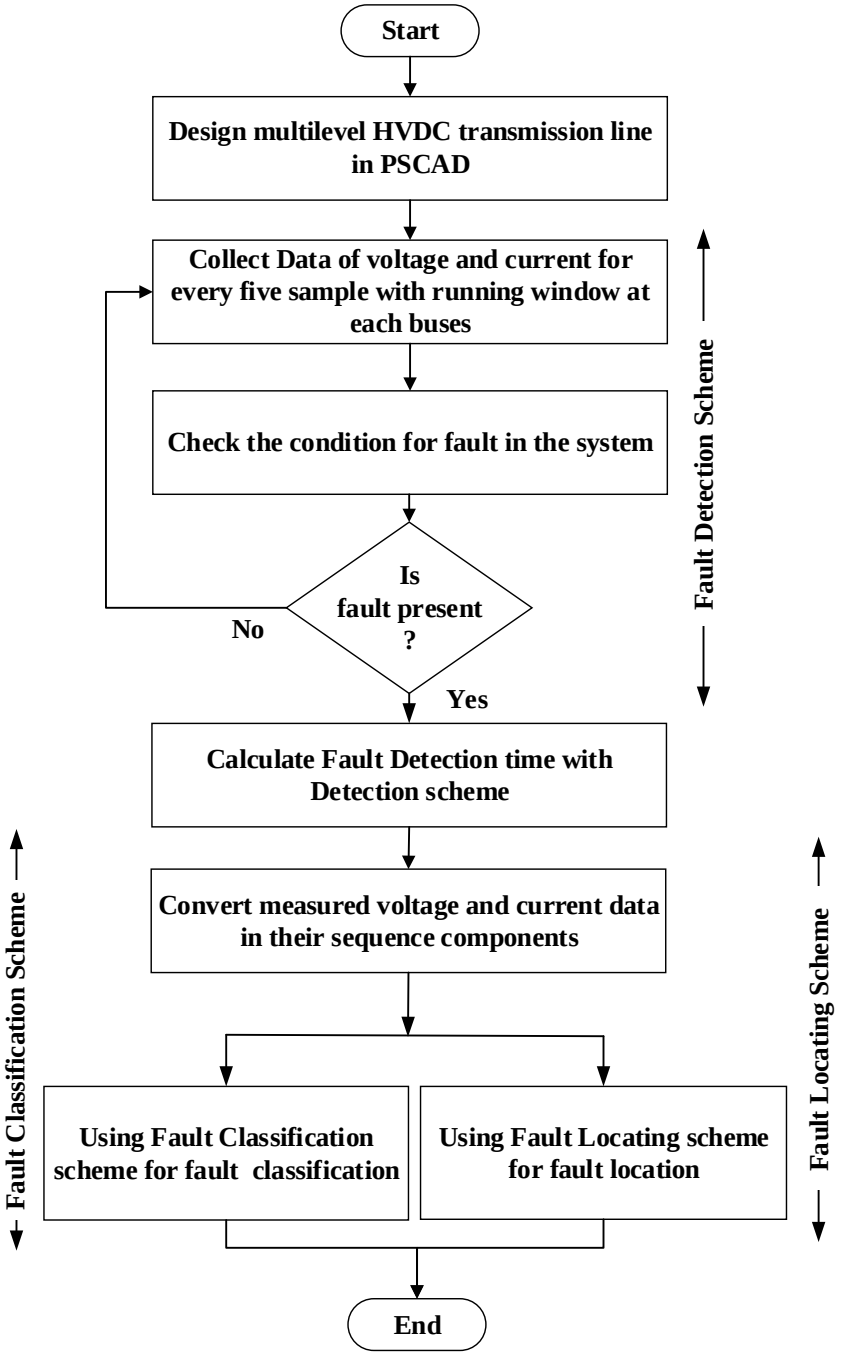

FIGURE 3.3: Flowchart for the proposed PLFE method

For classification of (L-L-L) fault condition describe in eq. (3.31) is used as,

$$\| V_a \| = \| V_b \| = \| V_c \| \geq 0 \downarrow, \quad \| I_a \| = \| I_b \| = \| I_c \| \geq 0 \uparrow \tag{3.31}$$

Further, combining proposed approaches mention in above paragraph according to working step provided in Figure 3.3. Now, with the use of all combined approaches PLFE method provide solution of above three mention objection in simultaneously. Proposed schemes of the three objective describe in next subsections. The overall flowchart is shown in Figure 3.3 provide the working sequence of the proposed method.

3.2.1 PLFE Fault Detection Scheme

Fault detection with parameter-less fault estimation (PLFE) method is based upon the impedance calculation approach with basic classical conditions. It identifies between with and without fault condition from the running time window of every five samples with an increment of one sample. It detects the fault on voltage and current data only. Working steps of this scheme are given below:

- Collect voltage and current signal data at every five sample with increment of one sample.
- Convert rate of change of voltage and current signal in frequency domain with Discrete Fourier Transform (DFT).
- Use rate of change of voltage and current signal data for identification of faulted section.
- Use eq. (3.21) to calculate fault detection time.

3.2.2 PLFE Fault Location Scheme

After fault detection, it is important to locate the fault. In order to locate the fault, the faulted running window used in fault detection scheme is considered. Using eq. (3.15) with measured voltage and current sequence data calculate fault location. Working steps of this scheme are given below:

- Select the faulted section with the help of fault detection scheme.
- Measured voltage and current signal data of both the terminal.
- Convert voltage and current signal data of both the terminal into sequence voltage and current data with sequence transform matrix.

- Use eq. (3.15) for calculation of fault location.

For showing clear variation we take ten test cases for each type of faults which may affect the technique accuracy including fault resistance, line loading and line transposition. The voltage and current data calculated at the sampling frequency at 1.6 MHz. The proposed method based on fundamental phasors, the Recursive Discrete Fourier Technique (DFT) is utilized to find out those phasors. With eq. (3.32) find out the resulted estimated error that shows the accuracy of the fault location scheme.

$$Presentage \;\; Error = \frac{(L_f)_{actual} - (L_f)_{calculated}}{Total\ line\ length} * 100 \tag{3.32}$$

where, $(L_f)_{actual}, (L_f)_{calculated}$ and L are the actual fault location, calculated fault location and transmission line length respectively.

3.2.3 PLFE Fault Classification Scheme

After fault detection, it is also important to classify the fault. In order to classify the fault, faulted section and faulted running window sample voltage and current data is used in fault detection scheme which detects fault is considered. For the classification of fault PLFE based fault classification scheme is used. Eqs. (3.22)-(3.31) show the specific condition for fault classification for of different types. Working steps of this scheme are given below:

- Select considered voltage and current signal data of five sample of running window in which fault detection scheme detect fault.
- Convert consider voltage and current signal data in to their sequence voltage and sequence current data with sequence transform matrix.
- Classify fault type with the help of condition describe in eq. (3.22- 3.31).
- Use PLFE based fault classification scheme for fault classification.

$$True\ Positive\ Rate = \frac{True\ Classification}{\sum (True\ Classification + False\ Classification)} \tag{3.33}$$

$$True\ Negative\ Rate = \frac{False\ Classification}{\sum (True\ Classification + False\ Classification)} \tag{3.34}$$

$$Persantage\ Accuracy = \frac{True\ classification}{Total\ Number\ of\ Cases} \times 100 \tag{3.35}$$

With the help of define eq. (3.33), (3.34), (3.35)) calculate the error variation with fault classification scheme. Overall step of the proposed method is shown in the Figure 3.3.

3.3 Test System for Simulation

To validate the proposed PLFE fault estimation method three HVAC transmission test systems have been taken into consideration which is two terminal, two terminal double circuits and IEEE 39-bus New England system have been used as shown in Figure 3.4, Figure 3.11 and Figure 3.23 respectively. The test transmission system is modelled in PSCAD/ EMTDC with IEEE dynamic data (Appendix-A.2). The transmission line is designed with frequency dependent transmission line modelling [47].

3.3.1 Case-1: Two-terminal HVAC Transmission Test System

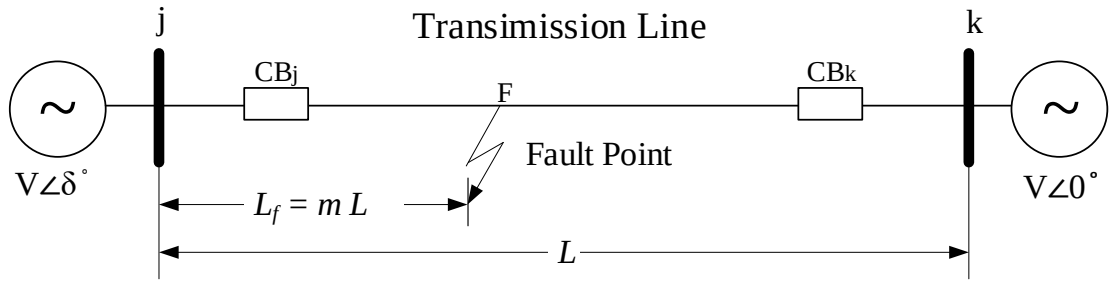

FIGURE 3.4: Schematic diagram of two terminal transmission test system

To validate the proposed PLFE fault estimation method, the single line diagram of 200 km, 230 kV transmission line simulated in the PSCAD transient program illustrated in Figure 3.4. MATLAB software interface is used to implement the algorithm. Thevenin's Equivalent Impedance of voltage sources at bus j and k are given as using mutual coupled R-L circuit as: the positive sequence is $Z_{j1} = 52.9\angle 83$, $Z_{k1} = 52.9\angle 83$ and zero sequence is $Z_{j0} = 52.9\angle 83$, $Z_{k0} = 52.9\angle 83$ respectively.

The fault estimation using low and high resistive faults as well as using arcing faults [145]. This transmission line is represented using frequency- dependent model [47]. Transmission line impedance are given as: the positive sequence is $R_{abc1} = 1.7872404750\Omega$, $L_{abc1} = 25.3881338mH$, $G_{abc1} = 5.0\mu\mho$, $B_{abc1} = 0.163558973m\mho$, and zero sequence is $R_{abc0} = 18.15761005\Omega$, $L_{abc0} = 66.3236615mH$, $G_{abc0} = 5.0\mu\mho$, $B_{abc0} = 033049.1161m\mho$.

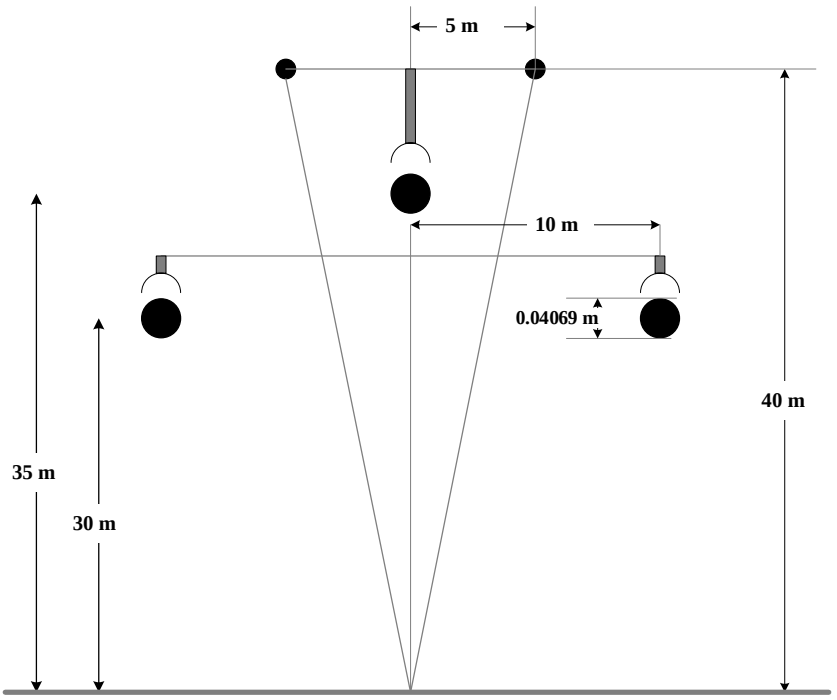

FIGURE 3.5: Tower configuration of two terminal transmission Line

The transmission line configuration is illustrated in Figure 3.5 The phase conductor is Aluminum Conductor Steel Reinforced (ACSR)Cable with DC resistance $0.03206\Omega km$, and radius of the conductor is $0.020345m$. The arrangement of all phase conductor in the form of isosceles triangle with base 10 m and two sides $7.0711m$.The ground wires are solid, its DC resistance is $2.8645\Omega km$, and radius of the ground conductor is $0.0055245m$, height of ground wire above lowest conductor $10m$, Sag of all wire is $10m$. The resistivity of the soil is given as $100\Omega m$.

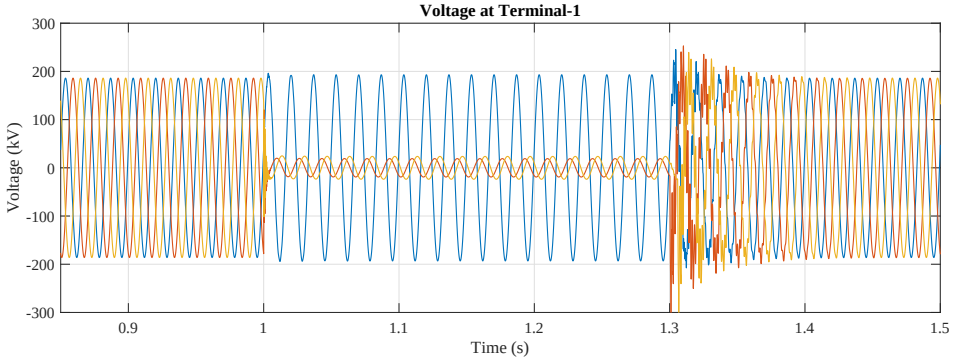

FIGURE 3.6: Voltage at terminal-1 (case-1)

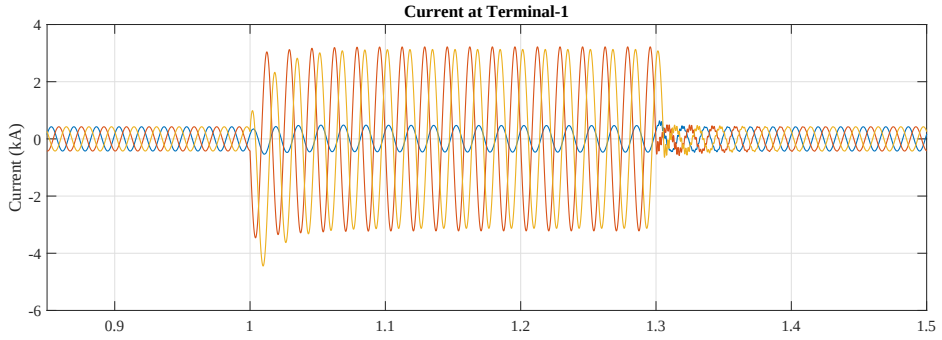

FIGURE 3.7: Current at terminal-1 (case-1)

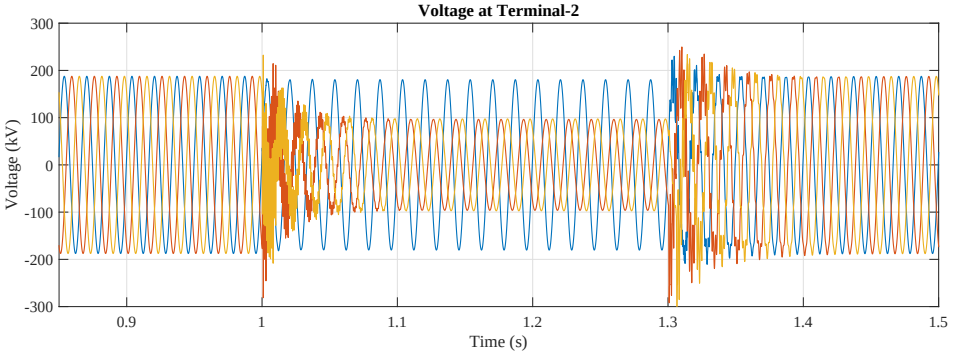

FIGURE 3.8: Voltage at terminal-2 (case-1)

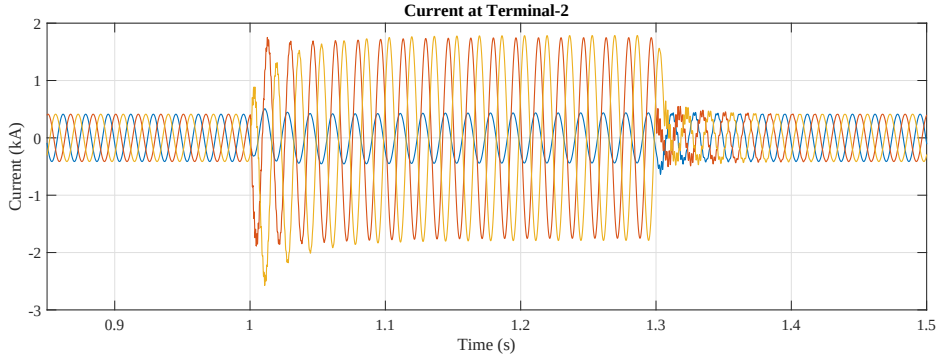

FIGURE 3.9: Current at terminal-2 (case-1)

The length of transmission line is 200 km and the all types of fault is created at every 10 km i.e. at 19 different location at 1s for a duration of 0.3s (approx 10 cycles). The collected data for every sample is having the sampling frequency of 4.8 kHz. Once the transient fault occurs in the system, the line voltage of both end of the line immediately falls. LL-Fault is created in line at connecting terminal (1-2) at 80 km far from terminal-1. Figures 3.6 and 3.7 show the terminal-1 voltage and current and Figures 3.8 & 3.9 show the terminal-2 voltage and current. Both the terminal voltages decreases and current

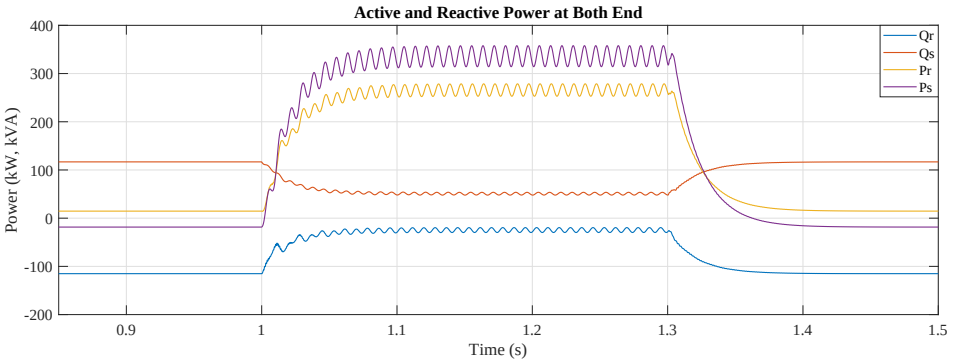

FIGURE 3.10: Active and reactive power at both ends (case-1)

TABLE 3.1: Definition of class with respect to different types of fault

Class-1	Phase A to Ground Fault
Class-2	Phase B to Ground Fault
Class-3	Phase C to Ground Fault
Class-4	Phase A to Phase B Fault
Class-5	Phase A to Phase C Fault
Class-6	Phase B to Phase C Fault
Class-7	Phase A to Phase B to Ground Fault
Class-8	Phase A to Phase C to Ground Fault
Class-9	Phase B to Phase C to Ground Fault
Class-10	Phase A to Phase B to Phase C Fault

increase with respectively. Figure 3.10 shows the active power and reactive power response at the time of fault. It is also observed that current and voltage has harmonic content due to the presence of fault. After fault harmonic content is settled down in few cycle. In this work 10 different faults are simulated which are shown in Table 3.1.

3.3.2 Case-2: Two-terminal Double Circuit HVAC Transmission Test System

For validation of the proposed PLFE fault estimation method, the single line diagram of double 200 km, 230 kV transmission line simulated in the PSCAD transient program illustrated in Figure 4.19. MATLAB software interface is used to implement the algorithm. Thevenin's Equivalent Impedance of voltage sources at bus j and k are given as using mutual coupled R-L circuit as: the positive sequence is $Z_{j1} = 52.9\angle 83$, $Z_{k1} = 52.9\angle 83$ and zero sequence is $Z_{j0} = 52.9\angle 83$, $Z_{k0} = 52.9\angle 83$ respectively.

The transmission line configuration is illustrated in Figure 3.12. The phase conductor is Aluminum Conductor Steel Reinforced (ACSR)Cable with DC resistance $0.03206\Omega km$, and the radius of the conductor is $0.020345m$. The arrangement of all phase conductor

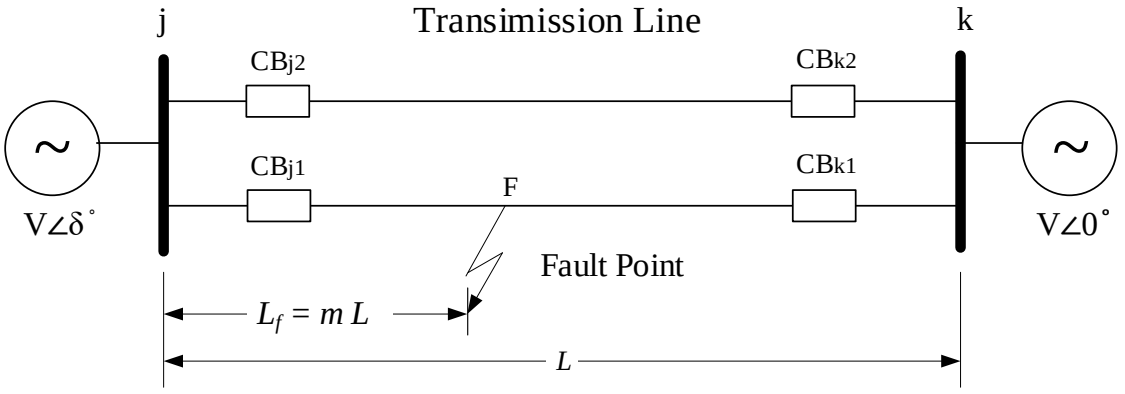

FIGURE 3.11: Schematic diagram of two terminal double circuit transmission test system

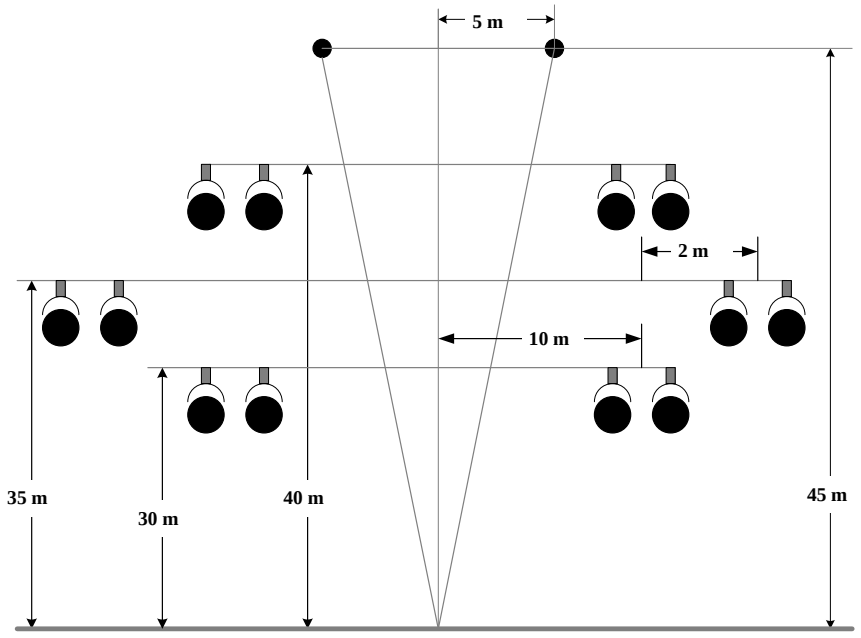

FIGURE 3.12: Tower configuration of double circuit transmission line

in the form of an isosceles triangle with base 10 m and two sides $7.0711m$. The ground wires are solid, its DC resistance is $2.8645\Omega km$, and radius of the ground conductor is $0.0055245m$, the height of ground wire above lowest conductor $10m$, Sag of all wire is $10m$. The resistivity of the soil is given as $100\Omega m$.

The length of the transmission line is 200 km and the all types of fault is created at every 10 km i.e. at 38 different location at 1s for a duration of 0.3s (approx 10 cycles). the collected data for every sample is having the sampling frequency of 4.8 kHz.Once the

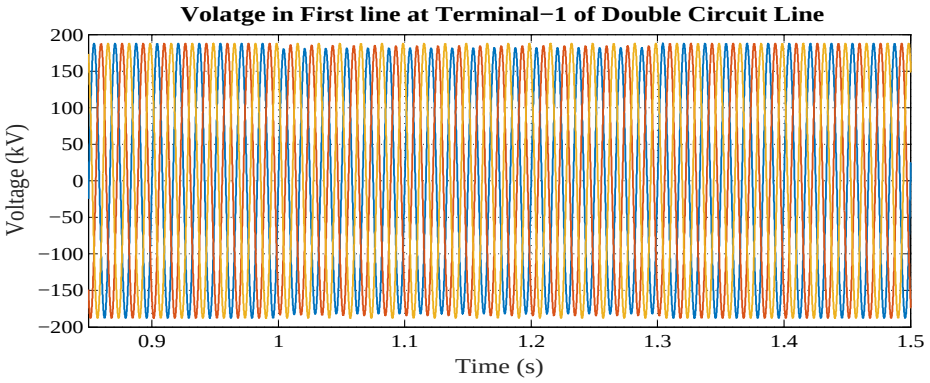

FIGURE 3.13: Voltage at terminal-1 in line-1 (case-2)

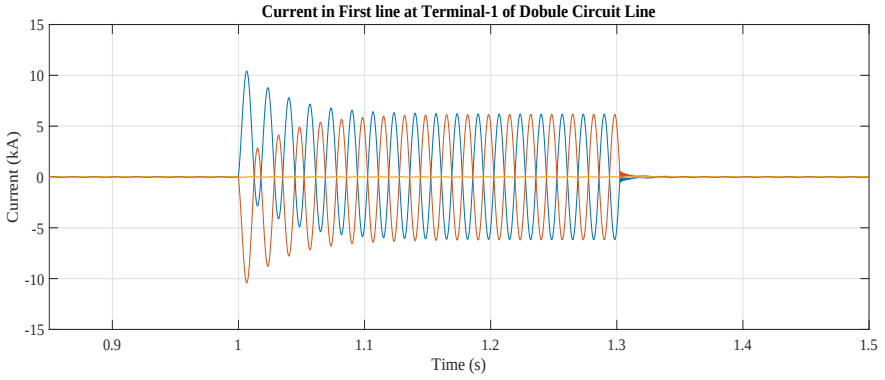

FIGURE 3.14: Current at terminal-1 in line-1 (case-2)

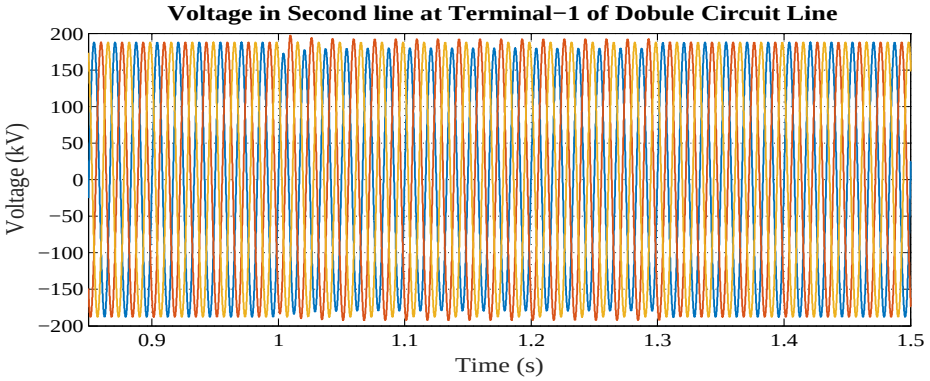

FIGURE 3.15: Voltage at terminal-2 in line-1 (case-2)

transient fault occurs in the system, the line voltage of both terminal end immediately fall.

The fault estimation using low and high resistive faults as well as using arcing faults. This transmission line is represented using frequency-dependent model [47]. Transmission line impedance are given as: the positive sequence is $R_{abc0} = 5.44113181\Omega$, $L_{abc0} =$

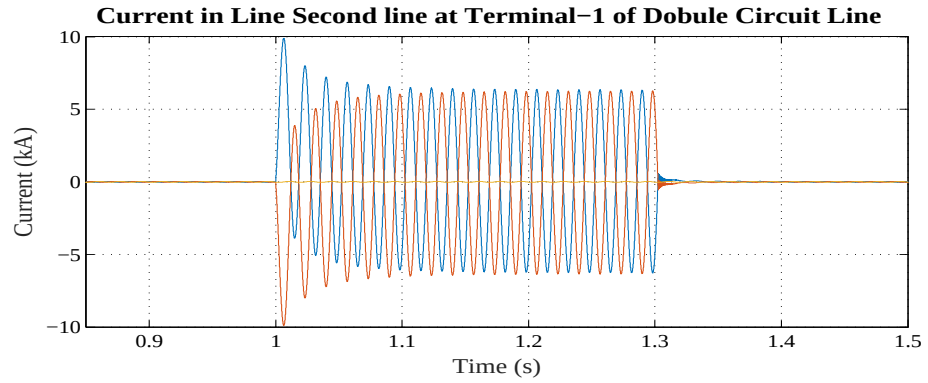

FIGURE 3.16: Current at terminal-2 in line-1 (case-2)

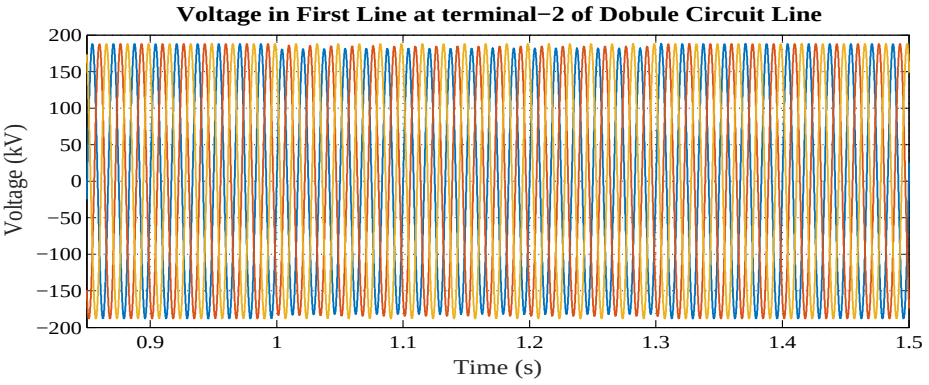

FIGURE 3.17: Voltage at terminal-1 in line-2 (case-2)

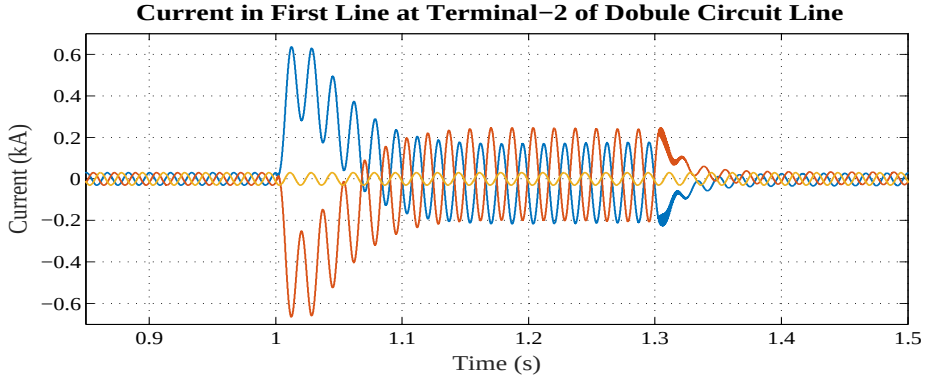

FIGURE 3.18: Current at terminal-1 in line-2 (case-2)

$13.6254007H$, $G_{abc0} = 0.00646001613\mu\mho$, $B_{abc0} = 15.8031843\mu\mho$. and zero sequence is $R_{abc1} = 7.22536499\Omega$, $L_{abc1} = 38.9961302H$, $G_{abc1} = 5.01390641\mu\mho$, $B_{abc1} = 0.147812113m\mho$.

LL-Fault is created in between line at connecting terminal (1-2) at 100 km far from terminal-1. Figures 3.13 and 3.14 show the terminal-1 voltage and current in line-1 similarly Figures 3.15 and 3.16 show the terminal-1 voltage and current in line-2. Figures 3.16

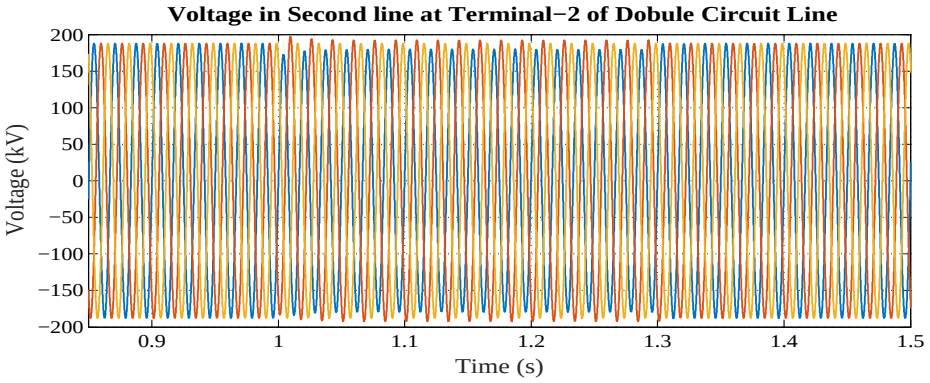

FIGURE 3.19: Voltage at terminal-2 in line-2 (case-2)

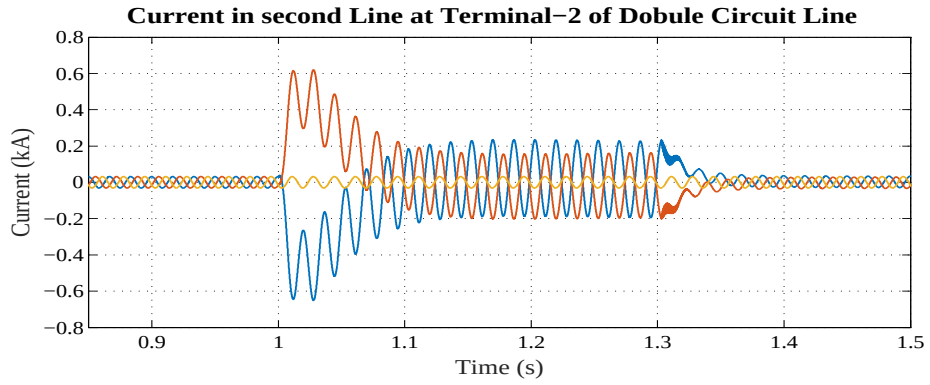

FIGURE 3.20: Current at terminal-2 in line-2 (case-2)

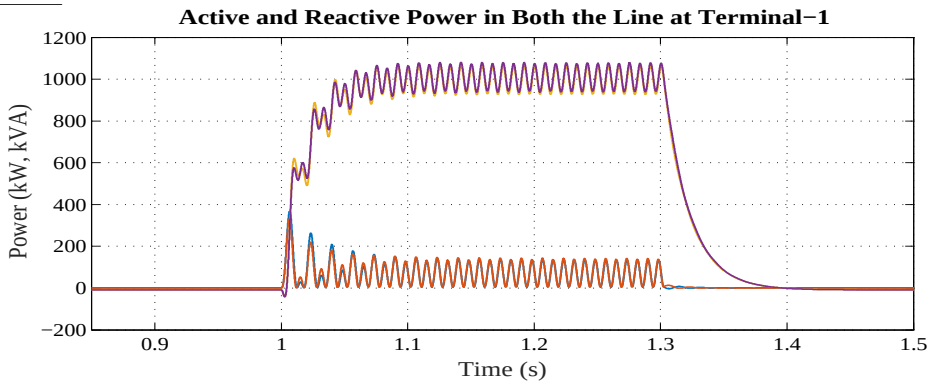

FIGURE 3.21: Active and reactive power at both ends in line-1 (case-2)

and 3.17 and Figure 3.18 show the terminal-2 voltage and current in line-1, Figures 3.19 and 3.20 show the terminal-2 voltage and current in line-2 respectively. Both the terminal voltages decreases and current increase with respectively. Current in both the line at terminal-2 are more harmonic then Terminal-1 currents. Figures 3.21 and 3.22 shows the active power and reactive power response at the time of fault of both the terminal. It is also observed that current and voltage have harmonic content due to the presence

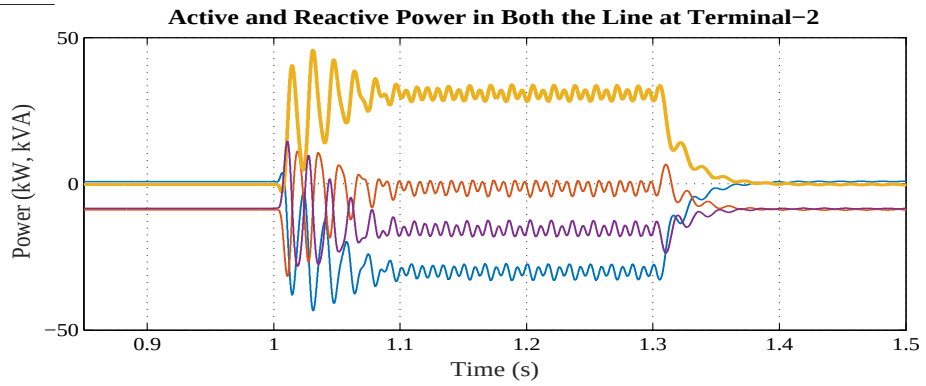

FIGURE 3.22: Active and reactive power at both ends in line-2 (case-2)

of a fault. After fault harmonic content is settled down in a few cycles. In this work, 10 different types of fault are simulated which are shown in the previous section Table 3.1.

3.3.3 Case-3: IEEE 39-Bus New England Transmission Test System

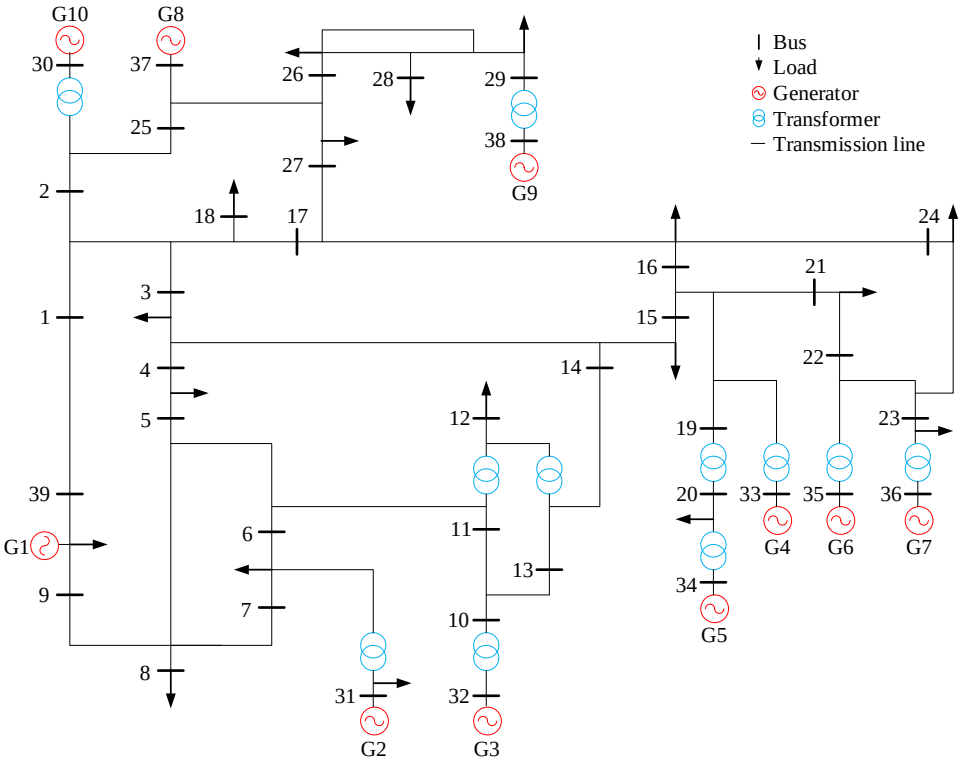

FIGURE 3.23: Schematic diagram of new England 39-bus IEEE dynamic transmission test system

The New England IEEE 39-bus system is used for carrying out the simulation, where the data collected from the Phase Measurement Unit (PMU) installed at different buses in the system. The system has 10 generator bus and rest is load buses. The system also consists of 34 sections of the transmission line of different length. The system is modelled with an electromagnetic transient program available in power system design (PSCAD/ EMTDC) using the IEEE dynamic data. In order to have a realistic system condition, the transmission line is modelled with a frequency dependent model. The schematic line diagram of the system model is shown in Figure 3.23.

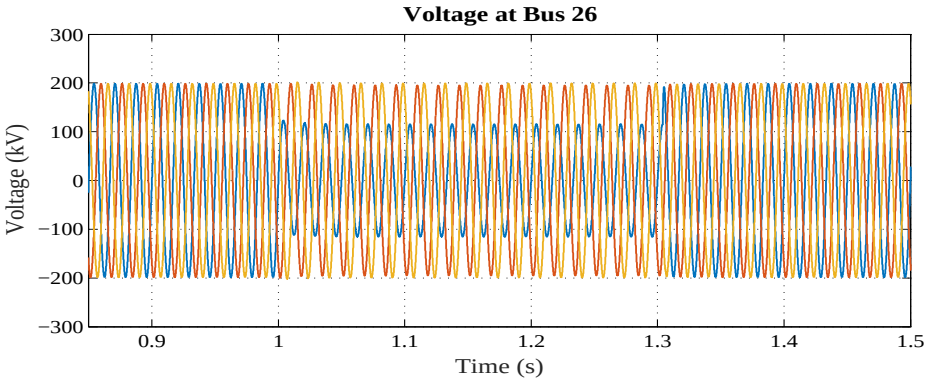

FIGURE 3.24: Voltage at bus-26 (case-3)

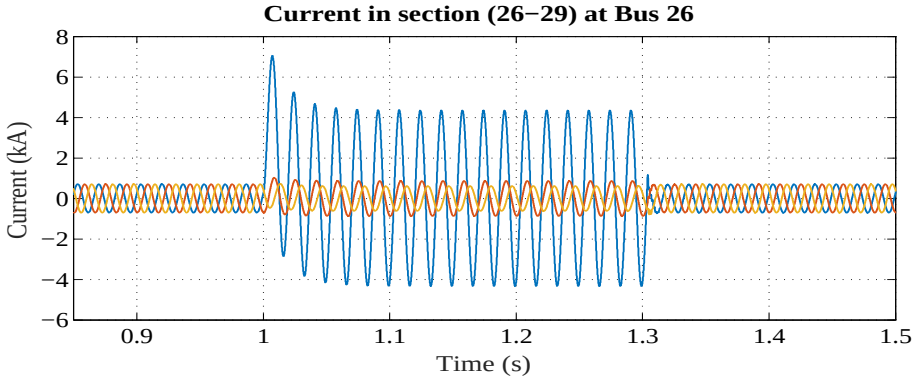

FIGURE 3.25: Current in section (26-29) at bus-26 (case-3)

The total length of the transmission line is 635.7522 km and the ten different types of fault is simulated at every 10 km i.e. at 58 different location, considering that minimum one event in each and every section even if the length is less then 10 km at 1s for a duration of 0.3s (approx 10 cycles). The collected data for every sample is having the sampling frequency of 4.8 kHz. Once the transient fault occurs in the system, the line voltage of both terminal end immediately fall. For a better understanding of the fault situation, one fault case among 10 cases in one of the section in the transmission line is created discuss below.

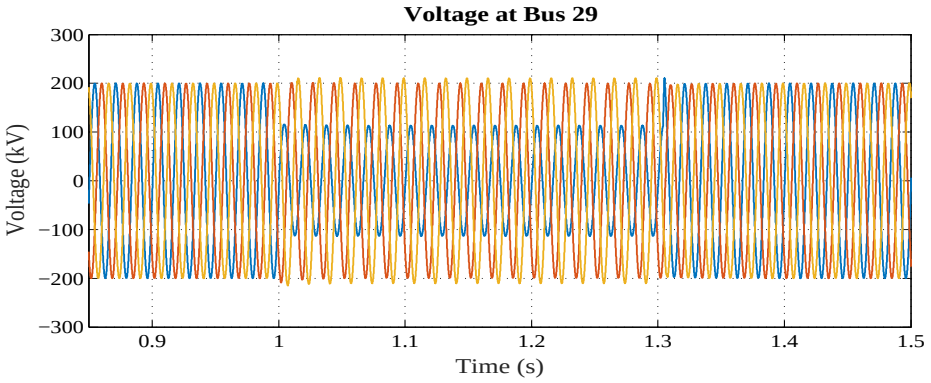

FIGURE 3.26: Voltage at bus-29 (case-3)

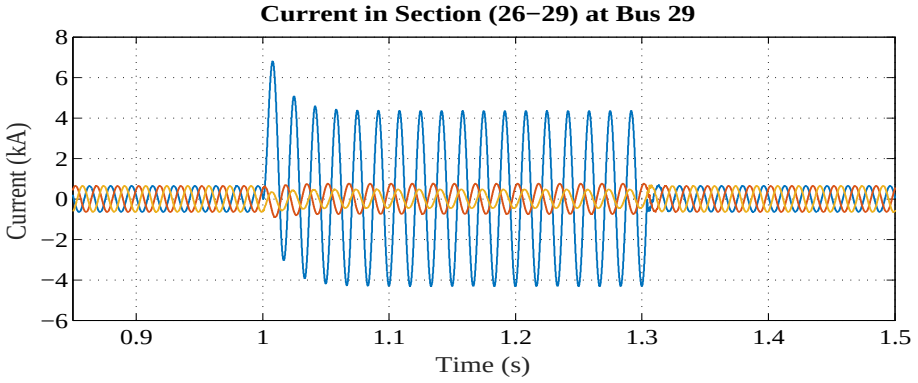

FIGURE 3.27: Current in section (26-29) at bus-29 (case-3)

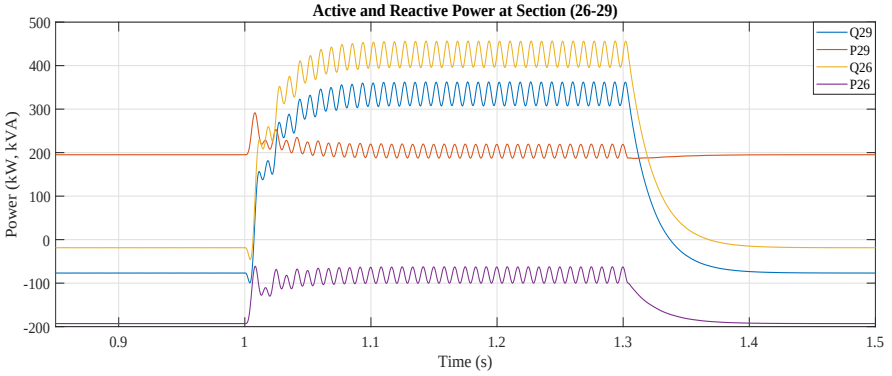

FIGURE 3.28: Active and reactive power flow in section (26-29) (case-3)

LG-Fault is created in line section 26-29 at connecting bus (26-29) at 33 km far from bus 26. Figures 3.24 and 3.25 show the voltage and current at bus 26. Similarly Figures 3.26 and 3.27 show the voltage and current at bus 29. Figure 3.28 shows the active power and reactive power response at bus 26 and bus 29 the time of the fault. It is observed that at the time of phase to ground fault respected phase voltage decreases at both the bus and phase current increases respectively. It is also observed that current and voltage

have harmonic content due to the presence of the fault. After fault harmonic content is settled down in a few cycles. In this work, 10 different types of fault are simulated which are shown in the previous section Table 3.1.

3.4 Results and Discussions

The flowchart is shown in Figure 3.3 provides the working step of the proposed PLFE fault estimation method. The voltage and the current signal is continuously measured and recorded at each bus of the system. The rate of change in voltage and current in frequency and time domain compare with the previous two samples of half cycle running window data with fault detection scheme (3.2.1). Once the fault is detected by the proposed PLFE fault detection scheme. Then, the same half cycle data are used to locate and classify the fault with using PLFE fault location scheme (3.2.2) and PLFE fault classification scheme (3.2.3) respectively.

3.4.1 Case-1: Two-terminal HVAC Transmission Test System

For the test case data generation, 10 different types of fault are simulated in different locations. Taking possible variation in the test case data collection with different fault Inception time. Using the PLFE fault estimation method to find out all the three objects of the fault estimation problem. Obtained result and observations are provided in forthcoming subsections.

3.4.1.1 Outcomes with PLFE Fault Detection Scheme

To test the suitability of this scheme, 10 different types of fault in the overhead transmission line at 50 km, 100 km and 150 km are simulated. The test results of the detection scheme are shown in Table 3.2 with different fault locations and inception instant. First two columns show fault types and fault initiation location. Last three columns show the fault inception instant, detection instant and response time, respectively. From the Table 3.2, it is observed that by using the proposed PLFE fault detection scheme the fault is detected and identified precisely within 4.5 milliseconds with average detection time 2.65 milliseconds, which is well within the allowable time limit as per IEEE standard [137].

TABLE 3.2: Result obtained with PLFE fault detector scheme (case-1)

Fault Type	**Fault Location** (km)	**Fault Inception Instant** $(T_i)s$	**Fault Detection Instant** $(T_d)s$	**Response Time** $(T_r = T_d - T_i)ms$
Class-1	50	0.2	0.2030	3.0
		0.3	0.3032	3.2
		0.4	0.4025	2.5
	100	0.2	0.2033	3.3
		0.3	0.3022	2.2
		0.4	0.4031	3.1
	150	0.2	0.2037	3.7
		0.3	0.3026	2.6
		0.4	0.4037	3.7
Class-4	50	0.2	0.2021	2.1
		0.3	0.3029	2.9
		0.4	0.4031	3.1
	100	0.2	0.2016	1.6
		0.3	0.3031	3.1
		0.4	0.4011	1.1
	150	0.2	0.2032	3.2
		0.3	0.3030	3.0
		0.4	0.4025	2.5
Class-7	50	0.2	0.2024	2.4
		0.3	0.3012	1.2
		0.4	0.4037	3.7
	100	0.2	0.2024	2.4
		0.3	0.3041	4.1
		0.4	0.4029	2.9
	150	0.2	0.2036	3.6
		0.3	0.3031	3.1
		0.4	0.4034	3.4
Class-10	50	0.2	0.2027	2.7
		0.3	0.3024	2.4
		0.4	0.4015	1.5
	100	0.2	0.2012	1.2
		0.3	0.3028	2.8
		0.4	0.4036	3.6
	150	0.2	0.2011	1.1
		0.3	0.3013	1.3
		0.4	0.4021	2.1

3.4.1.2 Outcomes with PLFE Fault Location Scheme

With the use of measured synchronized bus voltage and current running sample data that is provided by the current and voltage sequence transform system in which the PLFE fault detection scheme detects a fault. Results obtain with this scheme are shown in Table 3.3 and percentage error variation shown in Figure 3.29. For the similarity in obtained results taken one class of three phase to ground fault and phase to phase fault showing the result for simplicity.

TABLE 3.3: Result obtained with PLFE fault location scheme using synchronized bus voltage and current data (case-1)

Fault Type	**Actual FL** (km)	**Calculated FL** (km)	**Error in FL** (km)	**Error in FL** %
Class-1	20	19.8782	-0.1218	-0.0609
	40	39.7754	-0.2246	-0.1123
	60	60.1699	0.1699	0.0849
	80	80.1884	0.1884	0.0942
	100	100.0046	0.0046	0.0023
	120	120.0474	0.0474	0.0237
	140	140.8562	0.4562	0.2281
	160	160.1378	0.1378	0.0689
	180	180.1256	0.1256	0.0628
Class-4	20	19.8244	-0.1756	-0.0878
	40	39.7878	-0.2122	-0.1061
	60	59.2544	0.2544	0.1272
	80	80.1926	0.1926	0.0963
	100	100.0068	0.0068	0.0034
	120	120.1026	0.1026	0.0513
	140	139.1286	0.1286	0.0643
	160	160.1244	0.1244	0.0622
	180	180.1053	0.1053	0.0526
Class-7	20	19.8731	-0.1269	-0.0634
	40	39.7916	-0.2084	-0.1042
	60	59.1183	0.1183	0.0592
	80	80.1226	0.1226	0.0613
	100	100.1194	0.1194	0.0597
	120	120.0956	0.0956	0.0442
	140	140.0999	0.0999	0.0499
	160	160.0884	0.0884	0.0442
	180	180.0934	0.0934	0.0467
Class-10	20	19.8162	-0.1838	-0.0119
	40	39.8360	-0.164	-0.0820
	60	59.3718	0.3718	0.1859
	80	80.2004	0.2004	0.1002
	100	100.0728	0.0728	0.0364
	120	120.0112	0.0112	0.0056
	140	139.0536	0.0536	0.0268
	160	160.0886	0.0886	0.0443
	180	180.0563	0.0563	0.0282

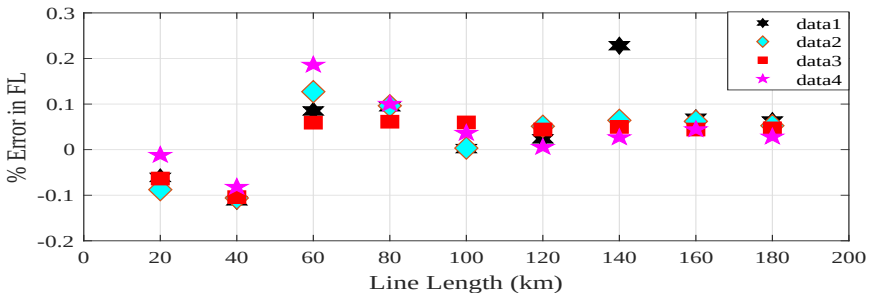

FIGURE 3.29: Performance of PLFE fault location scheme with synchronized bus data (case-1)

With the use of measured un-synchronized bus voltage and current data that is provided by current and voltage transformer with phase measurement system. Results obtain with this scheme are shown in Table 3.4 and percentage error variation shown in Figure 3.30. Figure 3.30 it can be noted that PLFE fault estimation method provides fault location with the maximum percentage error 0.1330 that is equal to in length 0.2660 km or 266.0

TABLE 3.4: Result obtained with PLFE fault location scheme using un-synchronized bus voltage and current data (case-1)

Fault Type	Actual FL (km)	Calculated FL (km)	Error in FL (km)	Error in FL %
Class-1	20	19.7467	-0.2533	-0.1266
	40	39.8289	-0.1711	-0.0855
	60	60.0845	0.0845	0.0422
	80	80.1966	0.1966	0.0983
	100	100.2511	0.2511	0.1256
	120	120.0474	0.1818	0.0909
	140	140.2004	0.2004	0.1002
	160	160.1455	0.1455	0.0727
	180	180.1361	0.1361	0.0680
Class-4	20	19.8012	-0.1988	-0.0994
	40	39.6892	-0.3108	-0.1554
	60	60.1943	0.1943	0.0971
	80	80.2630	0.2630	0.1315
	100	100.0759	0.0759	0.0379
	120	120.0540	0.0540	0.0270
	140	140.0835	0.0835	0.0417
	160	160.1656	0.1656	0.0828
	180	180.1299	0.1299	0.0649
Class-7	20	19.7740	-0.2260	-0.1130
	40	39.8541	-0.1459	-0.0729
	60	60.0922	0.0922	0.0461
	80	80.2630	0.2630	0.1315
	100	100.2290	0.2290	0.1145
	120	120.0838	0.0838	0.0419
	140	140.0898	0.898	0.0449
	160	160.1524	0.1524	0.0762
	180	180.1361	0.1361	0.0680
Class-10	20	19.8721	-0.1279	-0.0639
	40	39.7340	-0.2660	-0.1330
	60	60.1566	0.1566	0.0783
	80	80.2399	0.2399	0.1199
	100	100.1233	0.1233	0.0616
	120	120.0497	0.0497	0.0248
	140	140.1122	0.1122	0.0561
	160	160.0965	0.0965	0.0482
	180	180.1320	0.1320	0.0660

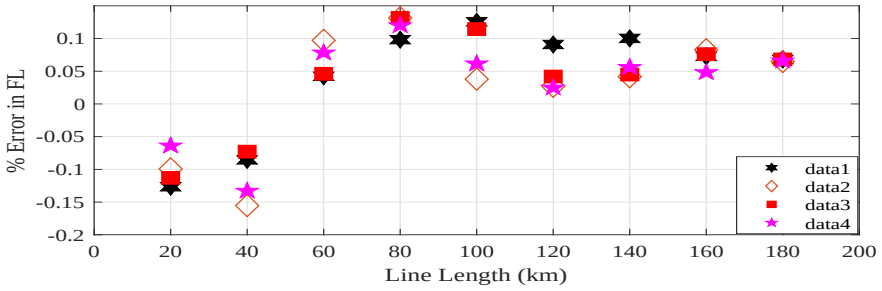

FIGURE 3.30: Performance of PLFE fault location scheme with un-synchronized bus data (case-1)

m that is within the permissible limit provided in IEEE standards [150]. It can also be observed that when the fault location within 40 km the percentage error is negative but above this length percentage error is positive with respect to the terminal-1. This PLFE fault location scheme requires less than one cycle data to providing the location of fault that accelerate the restoration process by reducing the search area and increased transfer

capability of the transmission line in the specific time. It can be observed from Table 3.14 that the error in fault location is least with the proposed scheme which validates the accuracy.

3.4.1.3 Outcomes with PLFE Fault Classification Scheme

TABLE 3.5: Result obtained with PLFE fault classification scheme in sample wise (case-1)

True Class \ Predicted Class	Class-1	Class-2	Class-3	Class-4	Class-5	Class-6	Class-7	Class-8	Class-9	Class-10
Class-1	19									
Class-2		18							1	
Class-3			17			1			1	
Class-4				19						
Class-5					19					
Class-6						18				1
Class-7							19			
Class-8	1		1					17		
Class-9			1						18	
Class-10										19

TABLE 3.6: Result obtained with PLFE fault classification scheme in % wise (case-1)

True Class \ Predicted Class	Class-1	Class-2	Class-3	Class-4	Class-5	Class-6	Class-7	Class-8	Class-9	Class-10	True Positive Rate	False Negative Rate
Class-1	100%										100%	0%
Class-2		94.7%							5.3%		94.7%	5.3%
Class-3			89.5%			5.3%			5.3%		89.5%	10.5%
Class-4				100%							100%	0%
Class-5					100%						100%	0%
Class-6						94.7%				5.3%	94.7%	5.3%
Class-7							100%				100%	0%
Class-8	5.3%		5.3%					89.5%			89.5%	10.5%
Class-9			5.3%						94.7%		94.7%	5.3%
Class-10										100%	100%	0%

The results obtained with this PLFE fault classification scheme are shown in Table 3.5, and Table 3.6. The diagonal elements in Table 3.5 shows the correct classified sample, whereas non-diagonal elements shows false classified samples. Table 3.6 shows the correct classified percentage considering True Positive Rate (TPR) whereas the non-diagonal elements show false classified percentage considering False Negative Rate (FNR) using the

basic equation behind design of confusion matrix are shown in eq. (3.33), eq. (3.34) and eq. (3.35). The classification accuracy of this scheme is 96.31% as shown in Table 3.6.

3.4.2 Case-2: Two-terminal HVAC Double Circuit Transmission Test System

For the validation of the proposed PLFE fault estimation method 10 different types of fault are simulated in a different location with a varying fault condition. Taking possible variation in the different test case data collection with different fault inception time and fault types. Using the PLFE fault estimation method to find out all the three objectives of the fault estimation problem. Obtained result and observations are provided in upcoming sections.

TABLE 3.7: Result obtained with PLFE fault detector scheme (case-2)

Fault Type	**Fault Location** (km)	**Fault Inception Instant** $(T_i)s$	**Fault Detection Instant** $(T_d)s$	**Response Time** $(T_r = T_d - T_i)ms$
Class-1	50	0.2	0.2022	2.2
		0.3	0.3035	3.5
		0.4	0.4031	3.1
	100	0.2	0.2012	1.2
		0.3	0.3022	2.2
		0.4	0.4026	2.6
	150	0.2	0.2023	2.3
		0.3	0.3030	3.0
		0.4	0.4029	2.9
Class-4	50	0.2	0.2019	1.9
		0.3	0.3023	2.3
		0.4	0.4010	1.0
	100	0.2	0.2040	4.0
		0.3	0.3015	1.5
		0.4	0.4013	1.3
	150	0.2	0.2021	2.1
		0.3	0.3016	1.6
		0.4	0.4025	2.5
Class-7	50	0.2	0.2020	2.0
		0.3	0.3039	3.9
		0.4	0.4038	3.8
	100	0.2	0.2012	1.2
		0.3	0.3032	3.2
		0.4	0.4018	1.8
	150	0.2	0.2023	2.3
		0.3	0.3026	2.6
		0.4	0.4038	3.8
Class-10	50	0.2	0.2023	2.3
		0.3	0.3039	3.9
		0.4	0.4019	1.9
	100	0.2	0.2031	3.1
		0.3	0.3029	3.0
		0.4	0.4026	2.6
	150	0.2	0.2031	3.1
		0.3	0.3011	1.1
		0.4	0.4015	1.5

3.4.2.1 Outcomes with PLFE Fault Detection Scheme

To test the suitability of the proposed PLFE fault detection scheme, 10 different types of fault in the overhead transmission line at 50 km, 100 km and 150 km are simulated. The test results of the PLFE fault detection scheme are shown in Table 3.7 for different fault locations and variation in inception instant. First two columns show fault types and fault initiation location. And the last three columns show the fault inception instant, detection instant and response time, respectively. From the Table 3.7, it is observed by using the proposed PLFE fault detection scheme the fault is detected and identified precisely within 4 milliseconds with average detection time is 2.45 milliseconds, which is well within the allowable time limit as per the IEEE standard [150].

3.4.2.2 Outcomes with PLFE Fault Location Scheme

Table 3.8 and Figure 3.31 show the estimated fault location values and percentage error variation in line-1 of double circuit line. Table 3.9 and Figure 3.32 show the estimated fault location values and percentage error variation in line-2 of double circuit line. For the similarity in obtained results, it is taken one class of fault which is three phase to ground fault and phase to phase fault for simplicity.

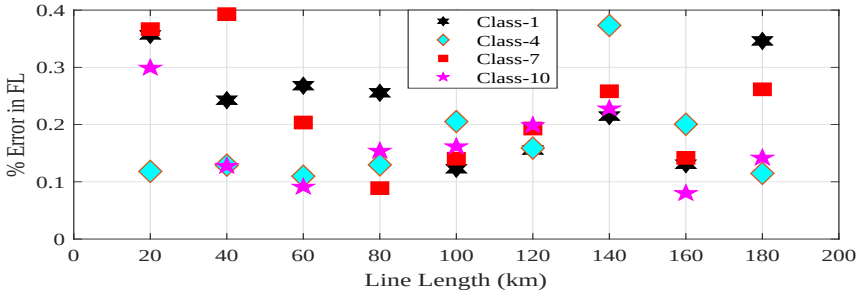

FIGURE 3.31: Performance of PLFE fault location scheme in line-1 (case-2)

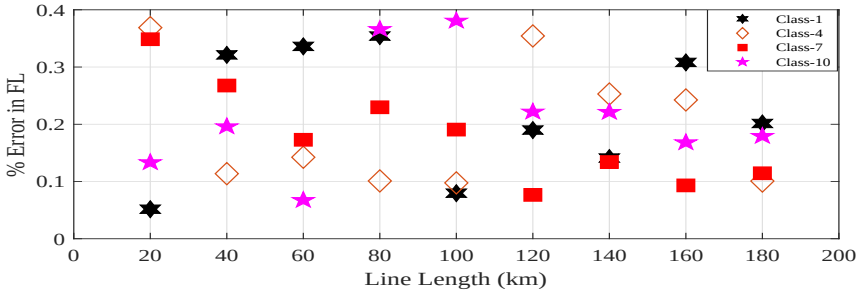

FIGURE 3.32: Performance of PLFE fault location scheme in line-2 (case-2)

TABLE 3.8: Result obtained with PLFE fault location scheme in line-1 (case-2)

Fault Type	**Actual FL** (km)	**Calculated FL** (km)	**Error in FL** (km)	**Error in FL** %
Class-1	20	20.7132	0.7132	0.3566
	40	40.4851	0.4851	0.2426
	60	60.5357	0.5357	0.2679
	80	80.5109	0.5109	0.2555
	100	100.2454	0.2454	0.1227
	120	120.3109	0.3109	0.1555
	140	140.4296	0.4296	0.2148
	160	160.2613	0.2613	0.1307
	180	180.6921	0.6921	0.3461
Class-4	20	20.2363	0.2363	0.1182
	40	40.2581	0.2581	0.1291
	60	60.2195	0.2195	0.1098
	80	80.2594	0.2594	0.1297
	100	100.4105	0.4105	0.2053
	120	120.3178	0.3178	0.1589
	140	140.7464	0.7464	0.3732
	160	160.4011	0.4011	0.2006
	180	180.2294	0.2294	0.1147
Class-7	20	20.7334	0.7334	0.3667
	40	40.7858	0.7858	0.3929
	60	60.4072	0.4072	0.2036
	80	80.1778	0.1778	0.0889
	100	100.2806	0.2806	0.1403
	120	120.3861	0.3861	0.1931
	140	140.5164	0.5164	0.2582
	160	160.2835	0.2835	0.1418
	180	180.5232	0.5232	0.2616
Class-10	20	20.5979	0.5979	0.2990
	40	40.2552	0.2552	0.1276
	60	60.1822	0.1822	0.0911
	80	80.3077	0.3077	0.1539
	100	100.3231	0.3231	0.1616
	120	120.3969	0.3969	0.1985
	140	140.4555	0.4555	0.2278
	160	160.1599	0.1599	0.0800
	180	180.2837	0.2837	0.1419

Table 3.8 and Table 3.9 shows the actual fault location values and the respective estimated fault location values. The percentage error in the estimated fault location with the actual location is calculated using eq. (3.35). From the Table 3.8 and Figure 3.31 it is observed that PLFE fault location scheme provide fault location with the maximum percentage error 0.3929 that is equal to in length 0.7858 km or 785.80 m. And from the Table 3.9 and Figure 3.32 it is noticed that PLFE fault scheme provides fault location with the maximum percentage error 0.3688 that is equal in length 0.7375 km or 737.50 m that is within the permissible limit provided in IEEE standards [150]. It also observed that when the estimated fault location within 40 km, the percentage error is negative but above this length percentage error is positive with respect to the terminal-1. This PLFE fault location scheme requires 1/2 cycle data to providing the location of fault that accelerate the restoration process by reducing the search area and increased transfer capability of the transmission line in 5 milliseconds. It can be observed from Table 3.14 that the error in

TABLE 3.9: Result obtained with PLFE fault location scheme in line-2 (case-2)

Fault Type	**Actual FL** (km)	**Calculated FL** (km)	**Error in FL** (km)	**Error in FL** %
Class-1	20	20.1032	0.1032	0.0516
	40	40.6424	0.6424	0.3212
	60	60.6721	0.6721	0.3361
	80	80.7081	0.7081	0.3541
	100	100.1591	0.1591	0.0796
	120	120.3798	0.3798	0.1899
	140	140.2819	0.2819	0.1410
	160	160.6161	0.6161	0.3081
	180	180.4027	0.4027	0.2014
Class-4	20	20.7375	0.7375	0.3688
	40	40.2273	0.2273	0.1137
	60	60.2847	0.2847	0.1424
	80	80.2019	0.2019	0.1010
	100	100.1952	0.1952	0.0976
	120	120.7085	0.7085	0.3543
	140	140.5058	0.5058	0.2529
	160	160.4849	0.4849	0.2425
	180	180.2015	0.2015	0.1008
Class-7	20	20.6971	0.6971	0.3486
	40	40.5354	0.5354	0.2677
	60	60.3457	0.3457	0.1729
	80	80.4593	0.4593	0.2297
	100	100.3813	0.3813	0.1907
	120	120.1532	0.1532	0.0766
	140	140.2679	0.2679	0.1340
	160	160.1863	0.1863	0.0932
	180	180.2287	0.2287	0.1144
Class-10	20	20.2668	0.2668	0.1334
	40	40.3921	0.3921	0.1961
	60	60.1348	0.1348	0.0674
	80	80.7319	0.7319	0.3660
	100	100.7614	0.7614	0.3807
	120	120.4436	0.4436	0.2218
	140	140.4425	0.4425	0.2213
	160	160.3364	0.3364	0.1682
	180	180.3585	0.3585	0.1793

fault location is least with the proposed PLFE fault location scheme which validates the accuracy.

3.4.2.3 Outcomes with PLFE Fault Classification Scheme

The results obtained with proposed PLFE fault classification scheme are shown in Table 3.10, and Table 3.11. The diagonal elements in Table 3.10 shows the correct classified sample, whereas non-diagonal elements shows false classified samples. Table 3.11 shows the correct classified percentage considering True Positive Rate (TPR) whereas the non-diagonal elements show false classified percentage considering False Negative Rate (FNR) using the basic equation behind design of confusion matrix are shown in eq. (3.33), eq. (3.34) and eq. (3.35). The classification accuracy of this scheme is 94.98% as shown in Table 3.11.

TABLE 3.10: Result obtained with PLFE fault classification scheme in sample wise (case-2)

True Class \ Predicted Class	Class-1	Class-2	Class-3	Class-4	Class-5	Class-6	Class-7	Class-8	Class-9	Class-10
Class-1	36						1		1	
Class-2		35			1		1		1	
Class-3			36		1			1		
Class-4				37			1			
Class-5					38					
Class-6						38				
Class-7	1	1					36			
Class-8	1			1				36		
Class-9		1			1				36	
Class-10				2	1	1				34

TABLE 3.11: Result obtained with PLFE fault classification scheme in % wise (case-2)

True Class \ Predicted Class	Class-1	Class-2	Class-3	Class-4	Class-5	Class-6	Class-7	Class-8	Class-9	Class-10	True Positive Rate	False Negative Rate
Class-1	94.7%						2.6%		2.6%		94.7%	5.3%
Class-2		92.1%			2.6%		2.6%		2.6%		92.1%	7.9%
Class-3			94.7%		2.6%			2.6%			94.7%	5.3%
Class-4				97.4%							94.7%	5.3%
Class-5					100%						100%	0%
Class-6						100%					100%	0%
Class-7	2.6%	2.6%					94.7%				94.7%	5.3%
Class-8								94.7%			94.7%	5.3%
Class-9	2.6%			2.6%					94.7%		94.7%	5.3%
Class-10				5.3%	2.6%	2.6%				89.5%	89.5%	10.5%

3.4.3 Case-3: New England IEEE 39-Bus Transmission Test System

For validating the proposed fault estimation method 10 different types of fault are simulated in a different location with varying fault conditions. Also, taking possible variation in the test fault scenario data collected with different fault inception time. For result validation proposed PLFE fault estimation method taking section (26-29) as a test section for fault detection as well as fault location and classification using 60 test location. Using the PLFE fault estimation method to find out all the three objectives of the problem simultaneously. Obtained results and observations are provided in upcoming sections.

3.4.3.1 Outcomes with PLFE Fault Detection Scheme

TABLE 3.12: Result obtained with PLFE fault detector scheme (case-3)

Fault Type	**Fault Location** (km)	**Fault Inception Instant** $(T_i)s$	**Fault Detection Instant** $(T_d)s$	**Response Time** $(T_r = T_d - T_i)ms$
Class-1	20	0.2	0.2027	2.7
		0.3	0.3036	3.6
		0.4	0.4030	3.0
	40	0.2	0.2016	1.6
		0.3	0.3021	2.1
		0.4	0.4024	2.4
	60	0.2	0.2039	3.9
		0.3	0.3042	4.2
		0.4	0.4036	3.6
Class-7	20	0.2	0.2029	2.9
		0.3	0.3021	2.1
		0.4	0.4016	1.6
	40	0.2	0.2023	2.3
		0.3	0.3042	2.4
		0.4	0.4014	1.4
	60	0.2	0.2028	2.8
		0.3	0.3017	1.7
		0.4	0.4022	2.2
Class-1	20	0.2	0.2027	2.7
		0.3	0.3018	1.8
		0.4	0.4019	1.9
	40	0.2	0.2029	2.9
		0.3	0.3018	1.8
		0.4	0.4035	3.5
	60	0.2	0.2039	3.9
		0.3	0.3042	3.2
		0.4	0.4020	4.2
Class-10	20	0.2	0.2028	2.8
		0.3	0.3013	1.3
		0.4	0.4037	3.7
	40	0.2	0.2036	3.6
		0.3	0.3034	3.5
		0.4	0.4018	1.8
	60	0.2	0.2028	2.8
		0.3	0.3011	1.1
		0.4	0.4023	2.3

To test the suitability of this fault detection scheme, different types of fault in the overhead transmission line at 20 km, 40 km and 60 km are simulated. The test results of the detection scheme are shown in Table 3.12 for different fault locations and inception instant. First two columns show fault types and fault initiation location. Along with the last three columns show the fault inception instant, detection instant and response time, respectively. From the Table 3.12, it is observed that by using the proposed scheme the fault is detected and identified precisely within 4.5 milliseconds with an average time of

detection is 2.65 milliseconds, which is well within the allowable time limit as per IEEE standard [137].

3.4.3.2 Outcomes with PLFE Fault Location Scheme

TABLE 3.13: Result obtained with PLFE fault location scheme (case-3)

Fault Type	**Actual FL** (km)	**Calculated FL** (km)	**Error in FL** (km)	**Error in FL** %
Class-1	5	5.2692	0.2692	0.0423
	10	10.3827	0.3827	0.0602
	15	15.1675	0.1675	0.0263
	20	20.1924	0.1924	0.0303
	25	25.7594	0.7594	0.1194
	30	30.7693	0.7693	0.1210
	35	35.5026	0.5026	0.0791
	40	40.1418	0.1418	0.0223
	45	45.2643	0.2643	0.0416
	50	50.3472	0.3472	0.0546
	55	55.6748	0.6748	0.1061
Class-4	5	5.1108	0.1108	0.0174
	10	10.1301	0.1301	0.0205
	15	15.2183	0.2183	0.0343
	20	20.5544	0.5544	0.0872
	25	25.6122	0.6122	0.0963
	30	30.5534	0.5534	0.0870
	35	35.4156	0.4156	0.0654
	40	40.4829	0.4829	0.0760
	45	45.3074	0.3074	0.0484
	50	50.6213	0.6213	0.0977
	55	55.2323	0.2323	0.0365
Class-7	5	5.5807	0.5807	0.0913
	10	10.2285	0.2285	0.0359
	15	15.3579	0.3579	0.0563
	20	20.5379	0.5379	0.0846
	25	25.6462	0.6462	0.1016
	30	30.1568	0.1568	0.0247
	35	35.7506	0.7506	0.1181
	40	40.643	0.6430	0.1011
	45	45.4408	0.4408	0.0693
	50	50.4051	0.4051	0.0637
	55	55.4127	0.4127	0.0649
Class-10	5	5.3144	0.3144	0.0495
	10	10.456	0.4560	0.0717
	15	15.4575	0.4575	0.0720
	20	20.6723	0.6723	0.1057
	25	25.6564	0.6564	0.1032
	30	30.551	0.5510	0.0867
	35	35.365	0.3650	0.0574
	40	40.6681	0.6681	0.1051
	45	45.4173	0.4173	0.0656
	50	50.3455	0.3455	0.0543
	55	55.7573	0.7573	0.1191

For the validation of the proposed PLFE fault location scheme 10 different types of fault is simulated in section (26-29) of IEEE 30-bus dynamic test transmission system. Table 3.13 and Figure 3.33 show the estimated fault location values and percentage error variation in line section (26-29) of New England IEEE 39-bus transmission line. Table 3.13

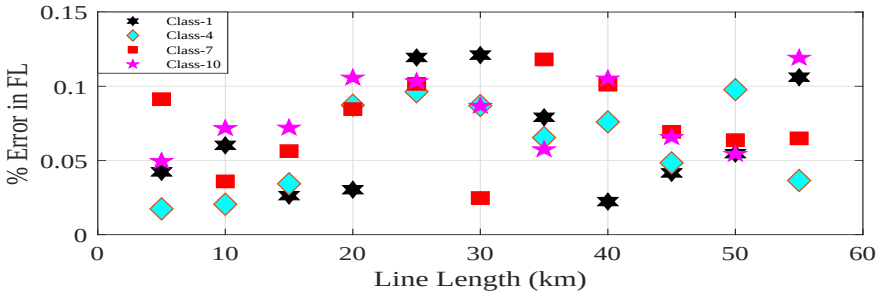

FIGURE 3.33: Performance of PLFE fault location scheme (case-3)

and Figure 3.33 show the estimated fault location values and percentage error variation in Section (26-29) of transmission line. For the similarity in obtained results, it is taken one class of fault which is in consideration three Phase to ground fault and Phase to phase fault for simplicity.

Table 3.13 shows the actual fault location values and the respective estimated fault location values using PLFE fault location scheme. The percentage error in predicted of fault location with the actual location is calculated using eq. (3.35). From the Table 3.13 and Figure 3.33 it is observed that PLFE fault estimation method provide fault location with the maximum percentage error 0.1210 that is equal to in length 0.7693 km or 769.30 m that is within the permissible limit provided in IEEE standards [150]. This proposed fault estimation scheme requires 0.5 cycles of data to providing the location of fault that accelerate the restoration process by reducing the search area and increased transfer capability of transmission line in within 4 milliseconds. Further, it can be observed from Table 3.14 that the error in fault location is least with the proposed PLFE fault location scheme which validates the accuracy.

TABLE 3.14: PLFE fault location scheme comparison with some existing methods

Ref. No.	Basic Approach Used	System Used	Error (%)
[58]	Least square WLS Method	9-bus, 22-bus	0.051, 0.073
[59]	Wide area measurement System	118-bus	1.892
[60]	Impedance based method	2- Terminal double circuit	0.487
[67]	Impedance based method	Two terminal	0.186
[19]	Traveling wave	Two terminal	0.211
[20]	Traveling wave	Two terminal	0.501
[105]	ANN based method	Two terminal	0.224
[45]	ANN based & wavelet	Two terminal	0.012
	PLFE method	**Two-terminal**	**0.074**
Proposed	**PLFE method**	**2-Terminal double circuit**	**0.201**
	PLFE method	**IEEE 39-bus system**	**0.069**

3.4.3.3 Outcomes with PLFE Fault Classification Scheme

TABLE 3.15: Result obtained with PLFE fault classification scheme in sample wise (case-3)

True Class \ Predicted Class	Class-1	Class-2	Class-3	Class-4	Class-5	Class-6	Class-7	Class-8	Class-9	Class-10
Class-1	56				1		1			
Class-2		54		1	2				1	
Class-3			58							
Class-4				57				1		
Class-5					58					
Class-6		1				56			1	
Class-7	1		1		1		53		1	1
Class-8								58		
Class-9		1			1	1			55	
Class-10	2					2	1	1		52

TABLE 3.16: Result obtained with PLFE fault classification scheme in % wise (case-3)

True Class \ Predicted Class	Class-1	Class-2	Class-3	Class-4	Class-5	Class-6	Class-7	Class-8	Class-9	Class-10	True Positive Rate	False Negative Rate
Class-1	96.55%				1.72%			1.72%			96.55%	3.45%
Class-2		93.10%		1.72%	3.45%			1.72%			93.10%	6.89%
Class-3			100%								100%	0.00%
Class-4				98.27%				1.72%			98.27%	1.72%
Class-5					100%						100%	0%
Class-6		1.72%				96.56%			1.72%		96.56%	3.45%
Class-7	1.72%		1.72%		1.72%		91.30%		1.72%	1.72%	91.30%	8.62%
Class-8								100%			100%	0.00%
Class-9				1.72%	1.72%				94.82%		94.10%	5.17%
Class-10	3.45%					3.45%	1.72%	1.72%		89.65%	89.65%	13.79%

The results obtained with proposed PLFE fault classification scheme are shown in Table 3.15, and Table 3.16. The diagonal elements in Table 3.15 shows the correct classified sample, whereas non-diagonal elements shows false classified samples. The diagonal element of Table 3.16 shows the classified percentage considering True Positive Rate (TPR) whereas the non-diagonal elements show false classified percentage considering False Negative Rate (FNR) using the basic equation behind design of confusion matrix are shown in eq. (3.33), eq. (3.34) and eq. (3.35). The classification accuracy of this scheme is 94.98% as shown in Table 3.16.

The results observed in the above subsection with PLFE fault estimation method describe in respected table and figures with acceptable accuracy. From the describe three test cases average total execution time of the proposed PLFE fault estimation method are observed as 9.21 milliseconds, 8.67 milliseconds and 10.83 milliseconds respectively. Further, it is also observed that time of execution of PLFE fault estimation method within one cycle and input requirement of measured voltage and current post-fault data of 0.5 cycle only for all the three test transmission systems. Therefore, the proposed PLFE fault estimation method show their applicability in fault estimation for the transmission system with acceptable accuracy and time [150].

3.5 Summary of the Chapter

This chapter proposes fault detection, location and classification schemes with a single use of PLFE fault estimation method for the HVAC transmission systems. PLFE algorithm takes half cycle data for providing results after fault initiation in few seconds with acceptable accuracy. The proposed PLFE fault estimation method is simple, non-iterative and effective for HVAC transmission systems. This method provides flexibility to the transmission operator to accelerate the restoration process in minimum time of span with less effort.

In this chapter, three test case are modeled with the help of frequency dependent modeling. These three test cases are developed with the help of IEEE standard dynamic data in PSCAD software that provides a similar environment to the real-time system.

As in the resent time researchers and engineers became aware to develop clean and carbon-less energy resources to mitigate not only their peak demand but also base load demand. Therefore, consequently there arises the need to increase renewable energy integration into the main grid. The secure, reliable and economical option is to connect these renewable sources to the main grid via HVDC transmission system.

Chapter 4

Fault Protection Strategies for HVDC Transmission Systems

This chapter presents an effective method for fault detection, location, and classification in HVDC transmission systems. In addition, the transmission line test system model has been developed using standard CIGRE dynamic data. Further, the adaptability of the proposed method is validated and confirmed by statistical analysis.

4.1 Introduction

Electrical energy has become an integral part of human life and its use is increasing globally by leaps and bounds to improve the living standard [151]. The ever-increasing load demand and insufficient supply of electric power have attracted the attention of power engineers/researchers to evolve the methods for effective utilization of electrical energy. For fulfilling the increasing load requirement, conventional as well as renewable energy resources are utilized in depth. Since, the generation of electricity from conventional energy resources using fossil fuels is an important contributor to CO_2 emissions, and are increasingly being replaced by renewables. Throughout the world, the growing awareness concerning environmental footprint of the human species is noticed. The greenhouse gases are considered as the main cause of global warming. In view of this, India has been a strong advocate of the development of renewables for electricity generation, publishing directive to increase energy production using renewables [152]. Also, the contribution of renewables in the energy supply is foreseen, with binding targets of 27% of energy generation from renewable energy sources by 2030 [153].

The different possible renewable sources for electricity generation are solar, geothermal, hydro, tidal, wave, biomass, and wind energy. The use of geothermal, tidal, and wave energy strongly depends on the location. This leaves biomass, solar, and wind energy as the main choices to increase the use of renewable energy sources in India in the short term. As a result, the main increase in electricity generation from renewables in India is coming from wind and solar energy. In India most of the renewable resources are very far from the load centre. This results in transmitting the power over very long distances. Since, the power generated from renewables is mostly DC in nature. Further, it is found that HVDC transmission system becomes economical for a length above 500 km due to recent advancement in power electronics. HVDC in comparison to HVAC transmission system has rapid and flexible control, improved stability along with improved power handling, reduction in transmission losses and overall cost [154, 155]. With an improvement in the efficiency of AC-DC/DC-AC converters, the efficiency of the entire HVDC transmission system has improved significantly. However, the protection of HVDC system is a challenging task.

The problem of fault detection, location, and classification is a challenging task in the transmission systems. However, the problem becomes even more complicated for HVDC transmission system, due to limited known approaches. In the electrical power system, the transmission line plays an important role to transmit power from the generation end to the distribution end (i.e. consumer end). So, the performance of transmission line affects the performance of the whole power system. HVDC system is facing protection issues against false tripping of the circuit breaker for the high rate of rising of current in an inductor, voltage surge, short-circuit, and insulator breakdown etc. Further, at the time of fault the series inductance of the DC line is less compared to the AC line [156]. Therefore, HVDC system is more prone to fault and it becomes necessary to clear the same in minimum possible time. In this concern, the protection scheme of HVDC transmission system must be very efficient to have a reliable operation [157]. This chapter proposes a machine learning based multi-objective fault estimation method that addresses the above-mentioned issues. This proposed F-SVM fault estimation method provides secure, reliable and uninterrupted power supply in power systems. For the validation of the proposed method two test systems are considered and investigated under the varying condition of faults. The application results of the proposed method is presented and compared with other established methods.

4.2 Proposed F-SVM Fault Estimation Method

In literature, several impedance based methods are used for fault estimation. Impedance based methods use voltage and current phasor data to calculate impedance for fault location and classification [158, 159]. However, it is dependent on transmission line model and fundamental frequency phasor [160]. If system experience transients, the faulted signal have to be filtered out for obtaining fundamental frequency phasor. To overcome the drawbacks in the impedance based technique, utilities have been using traveling wave-based techniques in the recent past [161, 162]. Traveling wave-based methods are used for detection and location of the faults, but not for classification of faults. The accuracy of fault detection and location depend on the arrival time and velocity of the traveling wave. To find accurate arrival time of transient wave-front sophisticated instrument is required that makes the techniques complicated, costly and increases computational burden [34]. Traveling wave based methods find the arrival time of traveling transient wave front without taking consideration of respective different frequency components of traveling transient wave having different arrival time [35, 36].

To overcome the drawbacks of the above mentioned methods, several approaches based on artificial intelligent have been developed. Such as Artificial Neural Network (ANN), Decision Tree, Discriminant Analysis, and Support Vector Machine (SVM) [37–39]. Above stated approaches require large training data sets and training time, therefore not suitable for real time fault estimation without any modification. Since ANN is inspired by biological nervous systems process information, therefore it has a good pattern recognition capability. So, the researchers have developed several approaches based on derivatives of ANN. Such as, radial biased, fuzzy based and back propagation neural network, is used for detection, classification and location of fault [40, 41]. Since, the accuracy of the approaches depends on the selection of hidden layers therefore, training data required is large.

To overcome the drawbacks of ANN based approaches SVM based approaches is preferred. SVM is independent of number of features extracted from the input sample [42]. This property is very useful in fault analysis of the transmission line, as measured quantities available with utilities are limited. Different feature extraction techniques such as Discrete Fourier Transform (DFT), Discrete Wavelet Transforms (DWT), Least Error Square (LSE), and stationary wavelet transform (SWT), are implemented with SVM for fault detection and classification [43, 44]. The major issue in using most of the feature extraction techniques is that, it does not provide an accurate estimation of the fundamental frequency component in presence of DC offset [45]. SVM based technique has high

computational time, since input feature space vector is of high dimension. If we are able to reduce the dimension of the input feature space vector, the computational time reduces. In literature F-score has been used for identifying the rank of the column in a particular matrix using mean and variance [137].

In the present work, F-Score based SVM is used for detection, location and classification of different types of the fault in HVDC transmission system. In this method F-score has been modified, and used for the first time as per the best knowledge of author, to reduce the dimension of feature space vector matrix according to dominating feature. It is well known that SVM does not depend on a number of features. However, it depends on dominating features only. Features selection based F-SVM fault estimation method requires a half cycle of data for detection, classification, and location of the different type of faults. It provides an accurate result with the variation of sampling frequency because, its feature vector removes the standard deviation of data in time and frequency domain. Working step of the proposed method is shown in Figure 4.1.

SVM is a binary classifier in nature, but with some modification, SVM can work properly with multi-class classification. Further, SVM is a linear classifier, however can be used for non-linear data with kernel trick. SVM estimates an optimal hyperplane suitable for the dataset to separate their respective classes, as shown in Figure 4.2. Basic equations with some modification of SVM is given in preceding subsections.

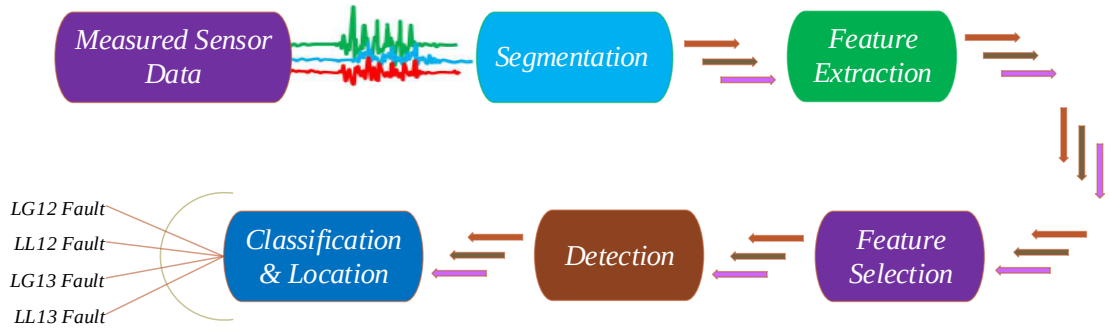

FIGURE 4.1: Working steps for proposed F-SVM method

4.2.1 SVM as Binary Classifier

The training data consist of N pairs of data (x_i, y_i) where $x_i \in \Re^n$ and $y_i \in \{1, -1\}$, $i = 1, 2, 3, ...N$, which define a hyperplane represented by eq. (4.1).

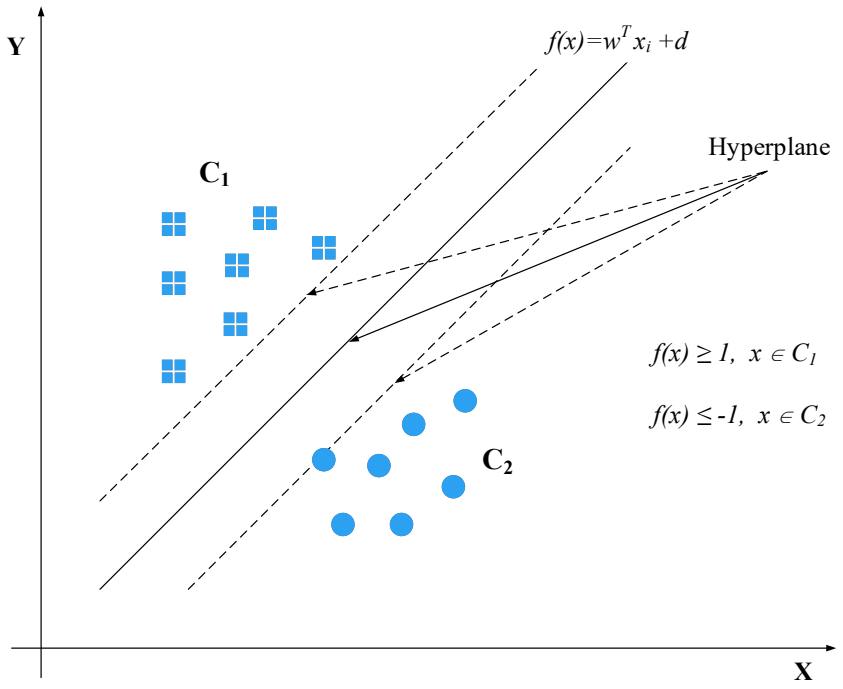

FIGURE 4.2: SVM classification

$$f(x) = w^T x_i + d = 0 \tag{4.1}$$

Where, d is a unit vector $\|d\| = 1$, a classification rule induced by $f(x)$ is as

$$f(x) = sign(w^T x_i + d) \tag{4.2}$$

Where $f(x)$ in eq. (4.1), denotes signed distance between point x and hyperplane $f(x) = w^T x_i + d = 0$. The classes are idiosyncratic, hyperplane function can be defined as $f(x) = w^T x_i + d = 0$ with $y_i f(x_i) > 0 \ \forall_i$. Hence, the hyperplane obtained has a high margin between training points of class 1 & -1 as shown in Figure 4.2

$$\max l \quad \text{for} \quad y_i(w^T x_i + d) \geq l, i = 1, 2, ...N \tag{4.3}$$

The bandwidth in the Figure 4.2 is l units away from the hyperplane on either side as calculated from eq. (4.3). Further, $2l$ units wide margin bandwidth can be more conveniently rephrased as eq. (4.4),

$$\min |d| \quad \text{for} \quad y_i(w^T x_i + d) \geq 1 \tag{4.4}$$

4.2.2 SVM as Multi-class Classifier

The approach commonly used to build multi-class classifier is one-versus-rest, also called as Oone-Versus-All (OVA). OVA technique chooses the class data sample accurately with high margin. However, with low margin data the accuracy of classification is not in the desirable limit. Another scheme which can be used for the modification of SVM for multi-class application is One-Versus-One (OVO). This involves building $|c|(|c|-1)/2$ classes, which reduces the time for training with the use of much smaller training dataset [163]. However, the accuracy of the above-mentioned scheme is quite poor for problem solving with multi-class SVM. To overcome this problem OVA is used for the construction of multi-class SVM by selecting less number of input data-set.

Function $f(x)$ which has the largest margin of ε from the hyperplane y_i for all the given training data. $y_i \in \{1, -1\}$ is optimal hyperplane, then standard form of multi-class SVM is given by eq. (4.5-4.8).

$$\min \frac{1}{2} w^T w + c \sum_{i=1}^{n} \delta_i(\eta_i) + c \sum_{i=1}^{n} \delta_i(\eta_i^*) \tag{4.5}$$

$$[w^T \phi(x_i) + d - y_i] \leq \varepsilon + \delta_i(\eta_i) \tag{4.6}$$

$$\left[y_i - w^T \phi(x_i) - d\right] \leq \varepsilon + \delta_i(\eta_i^*) \tag{4.7}$$

$$\delta_i(\eta_i), \delta_i(\eta_i^*) \geq 0, i = 1, 2, 3, ..N \tag{4.8}$$

Where, c is a predefined value, δ_i is loss function, η is slack variable, $\eta = 2sin(w\Delta t)$ and $\alpha = 2cos(w\Delta t)$ with respect to sinusoidal wave-form at the time of fault at specific frequency and sampling rate ($\frac{\eta^2 \alpha}{2}$). This problem can be reconstructed by finding an optimal solution to the following nonlinear quadratic equation based on eq. (4.2) and eq. (4.5) as,

$$\min f(w, b, \eta, \eta^*) \; = \; \frac{1}{2} w^T w + c \sum_{i=1}^{n} (\delta_i(\eta_i) + \delta_i(\eta_i^*))(w\phi(x)) + b - y_i \; \leq \; \eta_i + \varepsilon \tag{4.9}$$

Eq. (4.9) can be easily solved by introducing two variables α_i, and α_i^*. A function is constructed by considering both the variable and the corresponding constraints. The

constructed function is given by eq. (4.10)

$$max\ f(\alpha,\alpha^*,\eta,\eta^*) = -\eta_i\frac{\partial\delta_i(\eta_i)}{\partial\eta_i} - \eta_i^*\frac{\partial\delta_i(\eta_i^*)}{\partial\eta_i^*} + \sum_{i=1}^{n}(\alpha_i^* - \alpha_i)y_i - \varepsilon\sum_{i=1}^{n}(\alpha_i - \alpha_i^*) + c\sum_{i=1}^{n}(\delta_i(\eta_i) + \delta_i(\eta_i^*)) + \frac{1}{2}\sum_{i,j=1}^{n}(\alpha_i - \alpha_i^*)(\alpha_j - \alpha_j^*)(\phi(x_i),\phi(x_j)) \quad (4.10)$$

The performance of multi-class SVM depends upon the setting of parameters i.e. c, ε and kernel function. Since, the optimal solution of the function depends on all the three parameters mentioned above. The selection of optimal parameter is a complex problem itself. The mapping between input space vector and output space vector is nonlinear. Selection of kernel function usually depends upon the knowledge of application and distribution of input training data. Some commonly used kernel function are polynomial, gaussian Radial Basis Function (RBF), and sigmoid function [164]. The Gaussian RBF is given by eq. (4.11). Among the above given three functions, gaussian RBF with two variable i.e. c and γ has been used in this work using 10-fold cross validation. Gamma parameter decides closeness of training data. Misclassification of training data against the complexity of decision surface is dependent on parameter c. The low value of parameter c makes smooth decision surface and leads to poor accuracy, while a high value of c classifies correctly by selecting more no of samples as support vectors [165].

$$K(x_i,x_j) = e^{-(\frac{\|x_i - x_j\|^2}{\gamma})} \quad (4.11)$$

Eq. (4.12) is obtained using eq. (4.10 and 4.11). Eq. (4.12) is modified function for finding the optimal value of c and γ with reduced complexity.

$$\max f(\alpha,\alpha^*) = \frac{1}{2}\sum_{i,j=1}^{n}(\alpha_i - \alpha_i^*)(\alpha_j - \alpha_j^*)K(x_i,x_j) + \sum_{i=1}^{n}(\alpha_i^* - \alpha_i)y_i - \frac{1}{2c}\sum_{i=1}^{n}(\alpha_i^2 - \alpha_i^{*2}) \quad (4.12)$$

4.2.3 Feature Extraction Scheme

In this work, the features are extracted from the measured voltage and current signal. Measured signal is segmented in half cycle running window with an increment of one sample. For collection of features, time and frequency domain signal are used. DFT is used for frequency domain analysis. At the time of fault, signals appears as sinusoidal. The defined function as mean, median, mode, co-variance, correlation coefficient, skewness, kurtosis, sparseness, irregularity factor, waveform length ratio, root squared zero-order moment,

root squared fourth and eight order moment are used for extraction of features. First eight features are calculated with the help of basic measured signal and last six are calculated by power spectrum. Using these defined function 28-features is properly extracted from running window samples. Feature collected with current window is multiplied with the previous n^{th} window as shown in Figure 4.3. If the features of previous window and current window are from the same class then the correlation value will be enhanced.

For this transform measured signal in power spectral density entire odd moments are considered zero. Moment m of the n^{th} order of the power spectral density is described as $m_n = \sum_k^{N-1}(k^n P[k])$. Where, N is total number of sample, k is sample number, $P[k]$ is power spectral density. Fourier transform is used as time differentiation property for non-zero values of N samples in all feature calculation. Definition of some of the feature is defined as,

- Correlation Coefficient: It provides the measure of linear dependency for the running window sample.
- Skewness: It provides the measure of the asymmetry of the probability distribution of a real-valued random sample around the running window sample mean. The negative value of skewness indicates the sample is in far left from the running window sample mean and the positive value indicates the sample is in far right from the running window sample mean and zero value indicates samples are symmetrically distributed.
- Kurtosis: It provides the measure of how the running window sample distribution outlier-tendency. Its normal distribution is three, more than or less than three shows that the respected distributions that are less outlier-tendency or more outlier-tendency.
- Sparseness: It provides the measure of how much energy of a phasor is packed into a few samples. It is observed that its value should be more than zero.
- Irregularity Factor: It provide the reverse fraction of a number of the peaks to the number of rising zero crossings.
- Waveform Length Ratio: It is the ratio of the first derivative to the second derivative of the waveform length of the running window signal.
- Root Squared Zero-Order Moment:in the frequency domain, it shows the presence of the total power.

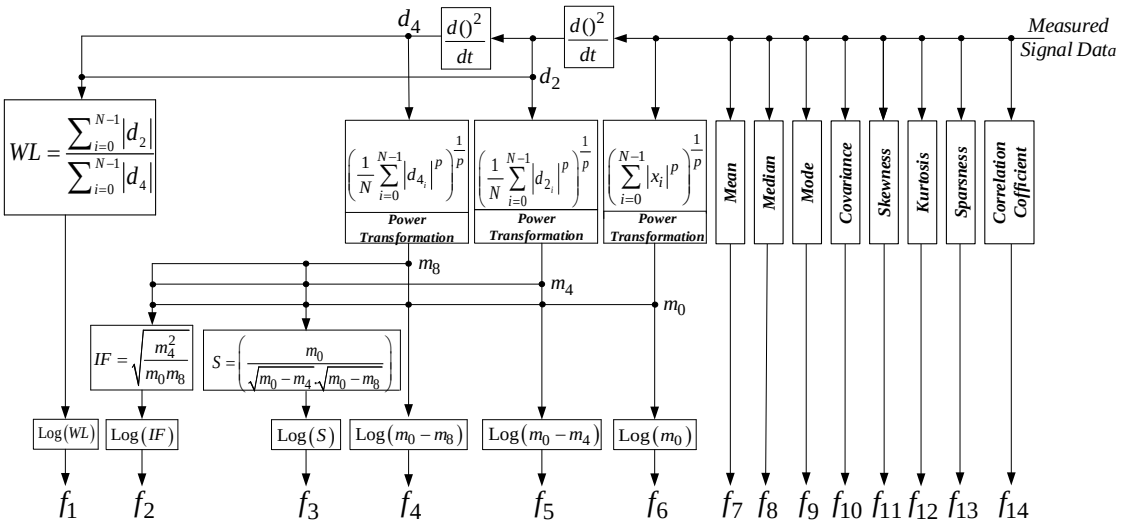

FIGURE 4.3: Flowchart for feature extraction approach

Using these defined functions 14-features are properly extracted from running window samples. Feature collected with current window samples multiplied with the previous n^{th} window samples as shown in Figure 4.4. If the features of the previous window samples are from the same class then the correlation value will be enhanced. All these features samples are extracted with the time domain signal. Therefore, it is called Time Domain Descriptors (TDD) [42].

4.2.4 Feature Selection with Modified F-Score

Proposed F-SVM fault estimation method using a supervised machine learning approach technique to achieve their objectives. It is obvious that with a high dimension of input feature sample vector require much time for detection and classification of sampled data. So, achieving the objectives of the fault estimation problem in the limited time of span much requires a feature sample reduction technique the reduce the dimension of input of feature space vector. It is a well-known fact that SVM is not dependent on a large number of feature samples but depend on dominating features. Therefore, the feature selection scheme is an important tool for SVM based methods. F-Score based feature selection scheme converts high dimension data to lower one with equivalent information content. The useful feature subset is preserved and the redundant features are discarded. The F-Score based feature selection scheme reduces the complexity of the problem. Therefore, increases the accuracy and reduces computational time. It provides a ranking of different

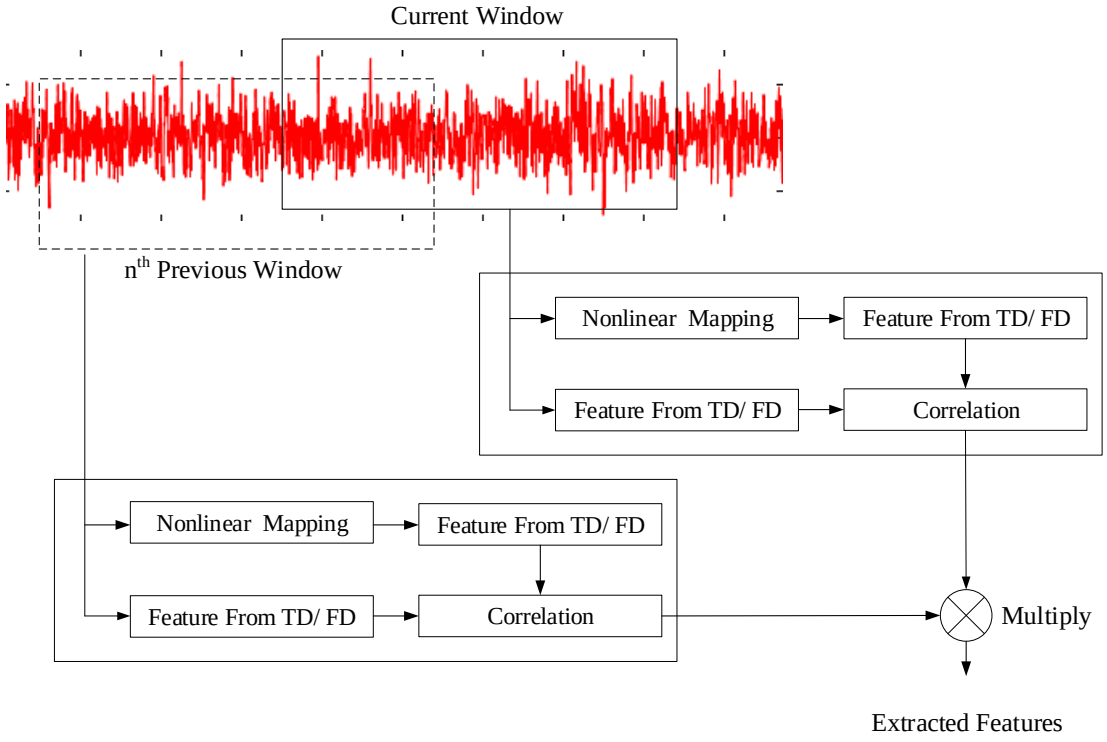

FIGURE 4.4: Feature extraction using time and frequency domain descriptors

features from the feature vector constructed with feature extraction scheme [165]. In this work F-score based features selection scheme is proposed for the multi-objective problem.

For better understanding of this proposed feature selection scheme, let define feature data set $D = (X_n, Y_n)_{n=1}^{N} \in X \times Y$. Where, $X \in \Re^M$ is full data set of input feature matrix, $Y = 1, 2, 3, ..., C$ is the class matrix, and M is the feature dimension. It separate the two classes with symbols (†) and (‡) if $C = 2$. The most discriminative subset of features $S_{opt} \subseteq X$ under some predefined criteria J for $S_{opt} \in \Re^m$. Where, m is the feature dimensionality after feature selection $m < M$. The evaluation criterion of feature ranking is define as,

$$R_j = \frac{\mu_j(\dagger) - \mu_j(\ddagger)}{\sigma_j(\dagger) + \sigma_j(\ddagger)} \tag{4.13}$$

Where, subscripts j denote feature $j = 1, 2, \ldots M$. μ_j and σ_j are the mean and standard deviation j for the observation of the class(†) and class(‡). The large positive value of R_j shows mean strong correlation with class(†) and the large negative value of R_j shows mean strong correlation with class(‡) [166]. The ranking guideline for all the features is calculated as $(\rho_j)^2$, and the correlation coefficient vector ρ is define as,

$$\rho = r^{-1}\mu(\dagger) - \mu(\ddagger) \tag{4.14}$$

Where, $\mu(\dagger)$ and $\mu(\ddagger)$ are the mean vector over the training data sets of class($\dagger$) and class($\ddagger$). The form of within class scatter matrix is denoted by r. Now, r is calculated as $r = \sum_{x \in X(\dagger)} (x - \mu(\dagger))(x - \mu(\dagger))^T + \sum_{x \in X(\ddagger)} (x - \mu(\ddagger))(x - \mu(\ddagger))^T$. Where, $X(\ddagger)$ and $X(\ddagger)$ are the represent the training data set of class($\dagger$) and class($\ddagger$) respectively. The expression for j^{th} feature of F-score is given in eq. (4.15) as,

$$R_j = \frac{(\overline{X}_j^{\dagger} - \overline{X}_j)^2 + (\overline{X}_j^{\dagger} - \overline{X}_j)^2}{\frac{1}{n_{\dagger}-1}\sum_{k=1}^{n_{\dagger}}(x_{k,j}^{+} - \overline{X}_j^{\dagger})^2 + \frac{1}{n_{\ddagger}-1}\sum_{k=1}^{n_{\ddagger}}(x_{k,j}^{\ddagger} - \overline{X}_j^{\ddagger})^2} \tag{4.15}$$

Where, $\overline{X}_j^{\dagger}$ and $\overline{X}_j^{\ddagger}$ are the mean of the j^{th} feature of the total data set. $x_{k,j}^{\dagger}$, and $x_{k,j}^{\ddagger}$ is the j^{th} feature of the ($\dagger$) and ($\ddagger$) class. In eq. (4.15) the numerator represent the classification between ($\dagger$) and ($\ddagger$) class. The denominator describes the one within each of the two class. Large value of R_j will easily reduce the feature vector with input feature matrix. The F- score of each feature is calculated, if the calculated value is greater than the threshold value the feature is selected.

F-score is simple but works only for two class vector. It also does not provide mutual information among the features. In order to work with multi-class, it is necessary to modify and take care of mutual information also. Therefore, modify the F-score scheme from feature pre-processing step and obtained the feature subset for proposed F-SVM fault estimation method in this work. Further, the scheme developed for multiclass and also take care of mutual information among the feature vector. From eq. (4.15), the between-class distance of individual class is calculated between that class to a centre position of all classes. Which calculates the average distance between the centre point of class for feature X_k, and is defined by eq. (4.16) as,

$$N(X_k) = \sum_{1 \le ii < jj \le C} \left(\frac{n_{ii} + n_{jj}}{N}\right)(\overline{x_{ii}^k} - \overline{x_{jj}^k}) \tag{4.16}$$

Where, subscripts ii and jj denote type of class. ii & $jj = 1, 2, 3, ...N$ is the total number of data sample, n_{ii} and n_{jj} denote the number of sample in respective class ii and jj. For feature X_k, the mean of class ii and jj represented with symbol x_{ii}^k and x_{jj}^k. In eq. (4.16) all possible combination of pair of class ii and jj from a total number of classes has been considered and average distance of each class with the center point has been calculated.

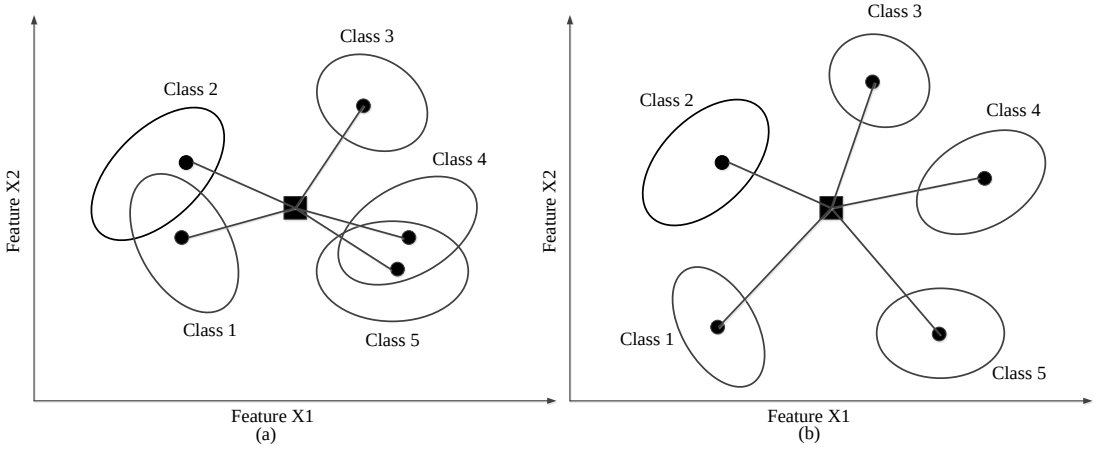

FIGURE 4.5: Different class distribution in feature space (a) Uneven distribution of features (b) Even distribution of features

Variance is calculated for the same data obtained from eq. (4.15) and eq. (4.16) and is shown in Figure 4.5(a) and 4.5(b). In Figure 4.5(a) the distance is smaller and uneven than Figure 4.5(b). Relative distance provided by eq. (4.16) reflect the equal distribution, but in eq. (4.15) it is not properly disturbed within class distance calculated from eq. (4.15) is absolute distance. Further, modified to within class scatter function for feature X_k. Calculation of the relative distance within the range of variance is given by eq. (4.17) as,

$$D(X_k) = \frac{\frac{1}{n_{jj}} \sum_{l=1}^{n_{jj}} ((x_{jj}^k)^l - (\overline{x_{jj}^k}))^2 - \min\limits_{1 \le l \le n_{jj}} ((x_{jj}^k)^l - (\overline{x_{jj}^k}))^2}{\max\limits_{1 \le l \le n_{jj}} ((x_{jj}^k)^l - (\overline{x_{jj}^k}))^2 - \min\limits_{1 \le l \le n_{jj}} ((x_{jj}^k)^l - (\overline{x_{jj}^k}))^2} \tag{4.17}$$

Where, $D(X_k)$ describe the degree of tightness within the classes, small value indicates strong tightness. Ranking for feature selection is provided by eq. (4.18) as,

$$J(k) = \frac{\sum_{jj=1}^{C} N(X_k)}{\sum_{jj=1}^{C} D(X_k)} \tag{4.18}$$

Where, $J(k)$ shows the feature correlation within the class (k), large value shows that strong correlation within the class. This scheme is easily applicable with large number of features and at the same time it is used for training and testing purpose of F-SVM based algorithm.

This selection scheme provides a better result for the purposed algorithm due to reduction in complexity of the problem. This scheme also feedback of the classification accuracy

in search for dominating fracture vector. The threshold value of λ is selected as per problem complexity and feature ranking criterion $J(k)$. For the convenience of calculation λ in this work is selected as 0.0001.

Further, combining proposed approaches mention in subsection (4.2.2 -4.2.4) according to working step provided in Figure 4.1. Now, with the use of all combined approaches F-SVM fault estimation method provide solution of above three mention objective simultaneously. Proposed schemes of the three objectives describe in next subsections. The overall flowchart of the proposed F-SVM fault estimation method shown in Figure 4.6 which describes the working sequence of this method.

4.2.5 F-SVM Fault Detection Scheme

Fault detection with F-SVM fault detection scheme is same as binary classification with two class i.e. with fault and without fault. It classifies between with and without fault, from the running window dominant feature vector of every half cycle. It detects the fault on the basic of their training memory. Working steps of this F-SVM fault detection scheme is given below:

- Collect voltage and current signal data at every half cycle
- Extract specific feature from time and frequency domain signal data.
- Select dominant features with the modified F-score based scheme.
- Use the F-SVM fault detection scheme for fault detection.

4.2.6 F-SVM Fault Location Scheme

After fault detection, it is important to locate the fault with F-SVM fault location scheme. In order to locate the fault, the dominant feature vector used in fault detection scheme is considered. It is observed that the optimal value of c and γ from eq. (4.10) are the same for a particular class of fault. However, the optimal samples for a particular class of fault changes with a change in fault location. Therefore, in order to locate fault accurately, the ratio of voltage and current is evaluated for the optimal sample corresponding to the optimal value of parameters (c and γ) at every half cycle. The parameters c and γ from eq. (4.10) are optimized using Taguchi optimization [167, 168]. The value of $\in$ is taken as 0.001 for optimization. Working steps of this F-SVM fault location scheme is given below:

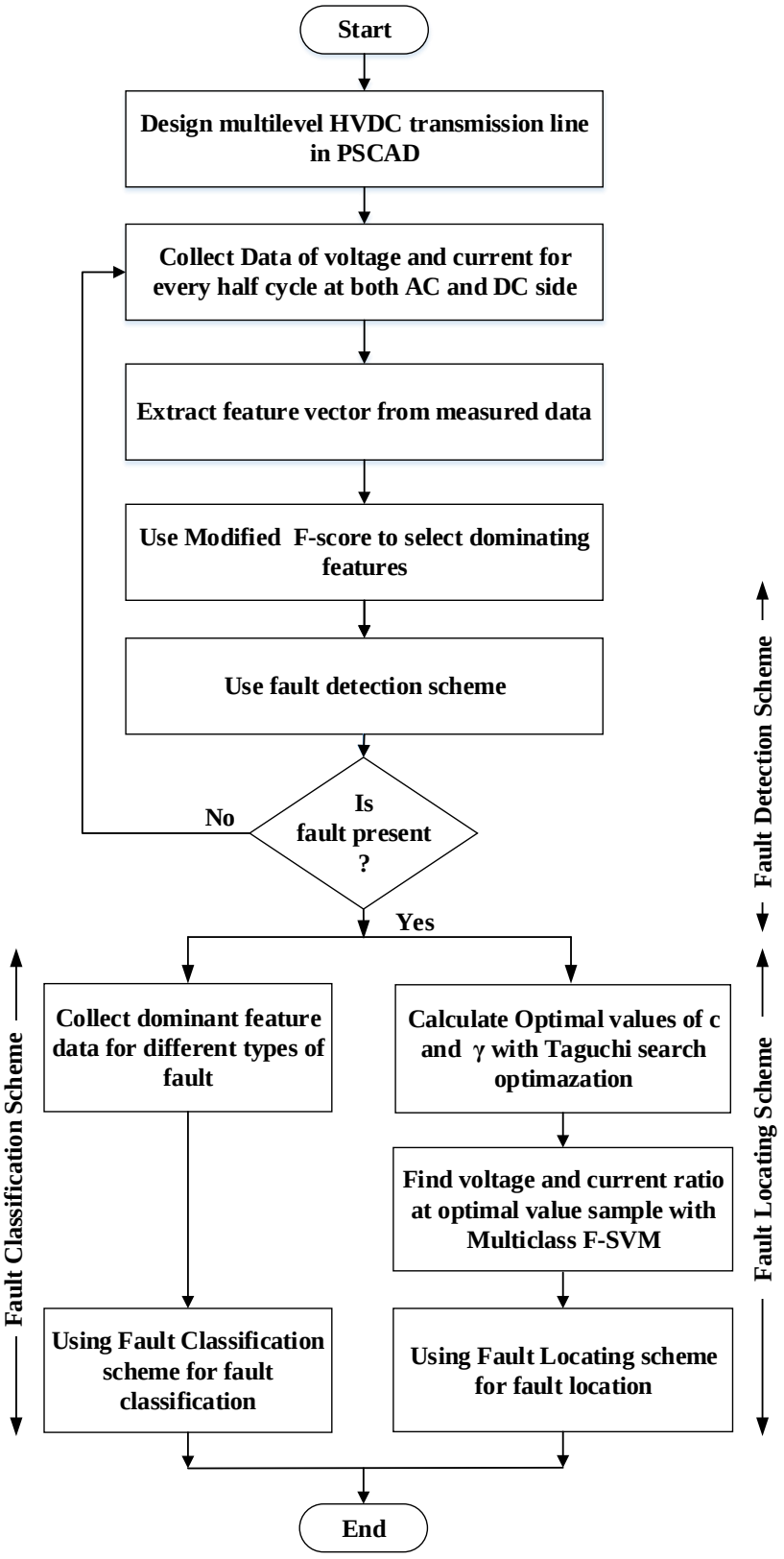

FIGURE 4.6: Flowchart for the proposed F-SVM method

- Select dominant feature vector data of half cycle in which, fault detection scheme detect fault.
- Optimize parameters c and γ, with Taguchi optimization using eq. (4.10).
- For the same, sample that provides the optimal value of c and γ, find voltage and current ratio in the time domain.
- The ratio signifies the fault location of a specific class of fault as given by eq. (4.19).
- Variation in actual and predicated fault location is calculated by eq. (4.20).

$$\frac{v}{i} = r = \frac{\sigma l}{a}; \Rightarrow l = \frac{v}{i} * \frac{a}{\sigma} \tag{4.19}$$

Where, v and i are measured voltage and current at the specific sample. The parameter a and σ denotes the area and resistivity of the transmission line conductor that fixed quantity for a particular design.

$$\%\ Error = \frac{L_{actual\ fault} - L_{predected\ fault}}{L_{total}} \tag{4.20}$$

Where, $(L_f)_{actual}, (L_f)_{calculated}$ and L are the actual fault location, calculated fault location and transmission line length respectively. With eq. (4.20) find out the resulted estimated error that shows the accuracy of the fault location scheme.

4.2.7 F-SVM Classification Scheme

After fault detection, it is also important to classify the fault with F-SVM fault classification scheme. In order to classify the fault, the dominant feature vector used in fault detection scheme which detect fault is considered. For classification multi-class F-SVM algorithm is trained with different types of faults. Further, with trained F-SVM algorithm, it provides classification of fault from the considered running window dominant feature vector of half cycle data. Working steps of this F-SVM fault classification scheme is given below:

- Select dominant feature vector data of half cycle in which fault detection scheme detect fault.
- Use F-SVM fault classification scheme for fault classification.
- Compare classification outcomes with classical eq. (4.21), (4.22), and (4.23).

4.3 Test System for Simulation

To validate the proposed F-SVM fault estimation method two HVDC transmission test system have been taken into consideration that is two terminal HVDC transmission test system and multi-terminal HVDC transmission test system. The CIGRE benchmark transmission model available with PSCAD/EMTDC module is originally a model for mono-polar two-terminal. It is modified into bipolar two and multi-terminal transmission line with VSC control. From the literature [169–171], it found that voltage source converter (VSC) is preferred for controlling the power flow in the HVDC transmission line due to better controllability. Some of the advantage of VSC over the conventional converter as,

- VSC–HVDC provides independent control of both active and reactive power by using PWM technique. The voltage of the AC network is controlled by an AC voltage controller keeping the flow of active power as constant. Source of reactive power compensation i.e. capacitor banks can also be used for voltage profile control [171].
- VSC-HVDC helps to mitigate disturbances in power quality. VSC HVDC has the ability to control the reactive power and voltage of the AC network thereby accord to enhance the power quality. Further, IGBT based converters are capable of working on higher switching frequency, as a result system gives a faster response which offers better controllability in case of flicker and harmonics [172].
- Risk of commutation failure is less. In the case of conventional thyristor-based HVDC system, disturbances of AC system generally leads to commutation failure. VSC HVDC is IGBT based which is a self-commutating semiconductor switch. As a result risk of commutation failure is reduced significantly and likewise improves the overall stability of the system.
- No need for communication. Control system of both converters of both the ends i.e. rectifier and inverter operates independently, as they are not dependent on telecommunication. Which results in better reliability of the converters and improves the speed of response as well.

Multi-terminal DC grid is mostly based on VSC HVDC. Multi-terminal DC grids are best suited for connecting asynchronous systems and offshore power plants like wind power plants and nuclear power plants etc. VSC control uses IGBTs and PWM technique to build converter valves for creating the desired waveform. It is possible to create a waveform

within the preset range of magnitude, phase angle, and frequency using PWM. The VSC control is basically a controlled source of voltage by means of PWM. VSC-HVDC acts as a synchronous source that can control both active and reactive power. Schematic diagram of HVDC-VSC is shown in Figure 4.7.

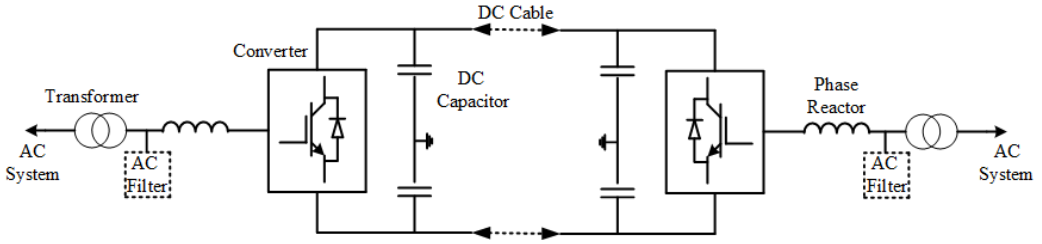

FIGURE 4.7: A VSC-HVDC system controller

VSC can be built for both back-to-back and cable transmission scheme as per the requirements. The AC side arrangements are the same as that of the thyristor scheme. In VSC no reactor on DC side is needed but the AC side reactor is needed due to the generation of high frequencies. Since, VSC can control both active and reactive power. Therefore, there is no need for reactive power compensation and only harmonics filters are needed on the AC side. To reduce voltage ripple on the DC side, a large capacitor is installed which also provide a low inductive path for turn-off the current.

4.3.1 Case-1: Two-terminal HVDC Transmission Test System

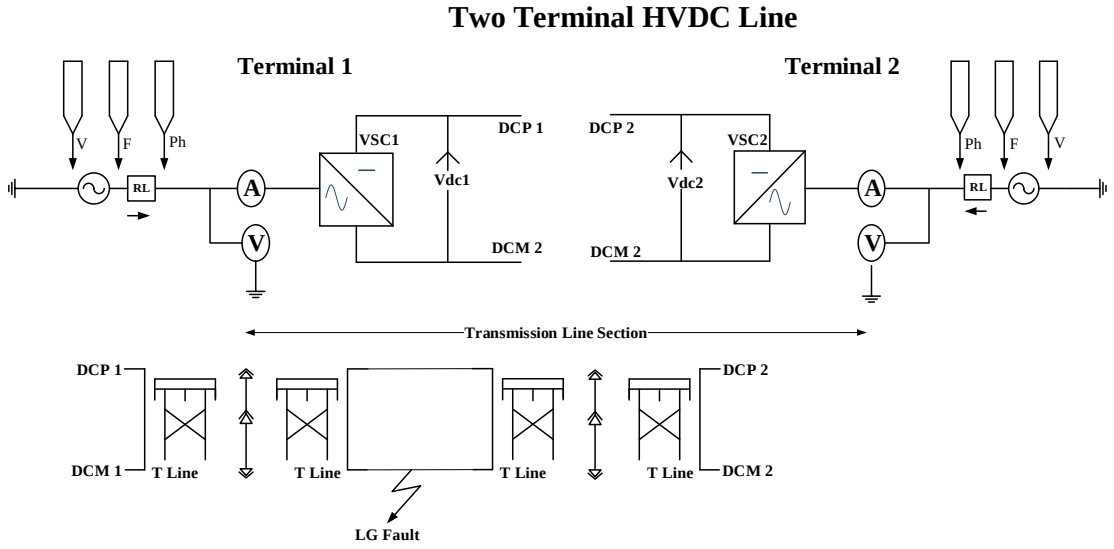

FIGURE 4.8: Schematic diagram of two-terminal HVDC transmission test system

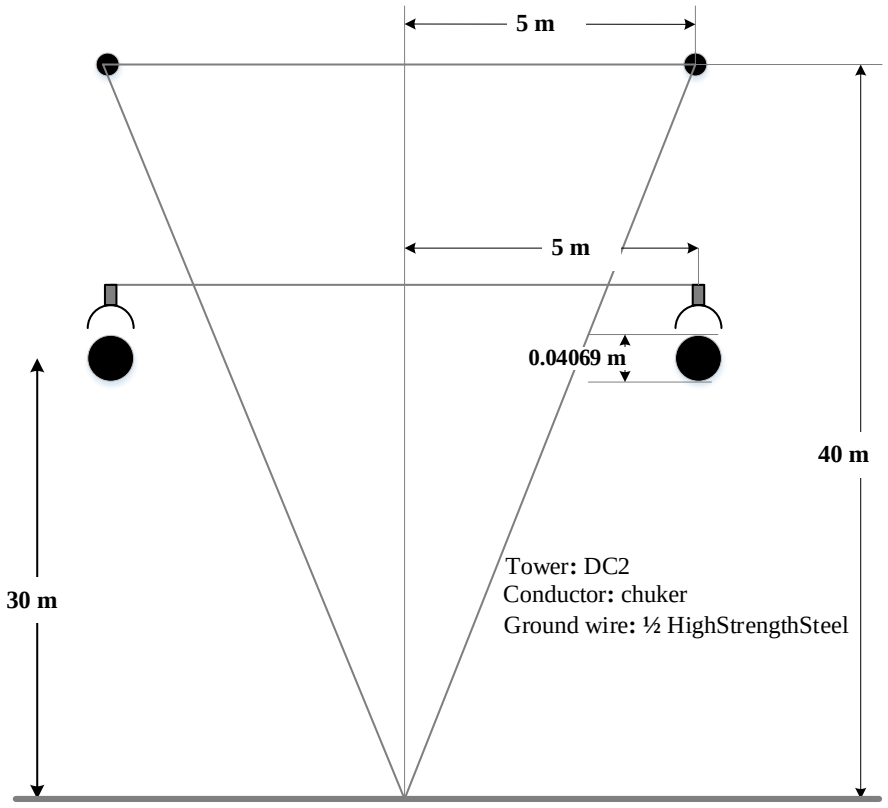

FIGURE 4.9: Tower configuration of HVDC transmission line

To validate the proposed F-SVM fault estimation method, a two-terminal HVDC transmission test system has been used as shown in Figure 4.8. The two-terminal are connected with an overhead transmission line having a length of 600 km. Four types of faults with fault resistance of 5Ω at every $10km$ is simulated in the entire line. With this condition, the data-set is prepared for training and testing purpose for the proposed F-SVM fault estimation method. The transmission line structure along with their configuration is shown in Figure 4.9.

Performance of VSC based HVDC system has been simulated under these circuit specification. The voltage source connected at terminal-1 is terminal voltage 13.8kV, active power 100MVA, and frequency 60Hz. Terminal-1 consists of PWM controlled IGBT based rectifier/inverter having specification as, the terminal voltage 230kV, on-resistance 0.005Ω, off-resistance $100M\Omega$, breakdown voltage 100MV, reverse withstand voltage 100MVA with PWM control. The transformer used at terminal-1 is a 13.8/62.5kV ($\Delta - Y$), Y-side solid grounded at 100MVA. RC Damped Capacitor connected at terminal-1 as capacitance

$1000\mu F$ and resistance 0.5Ω. The specification of the voltage source connected at terminal-2 is terminal voltage 420kV, active power 100MVA, and frequency 60Hz. Terminal-2 consist of PWM controlled IGBT based rectifier/inverter having specification as, the terminal voltage 230kV, on-resistance 0.005Ω, off-resistance $100M\Omega$, breakdown voltage 100MV, reverse withstand voltage 100MVA with PWM control. The transformer used at terminal-2 is a 115kV/62.5kV $(Y-\Delta)$ Y-side solid grounded at 100MVA. Smoothing capacitance $2\mu F$ is connected at terminal-2. Transmission cable connects a terminal (1-2) with specification as voltage rating 169kV and current withstand capacity 0.5kA.

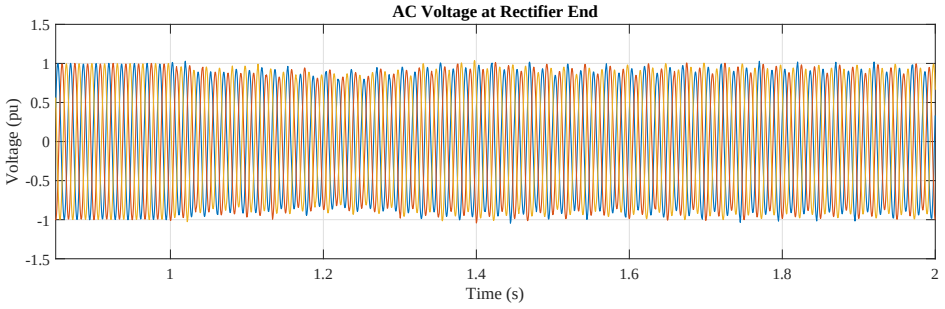

FIGURE 4.10: AC voltage at rectifier end (case-1)

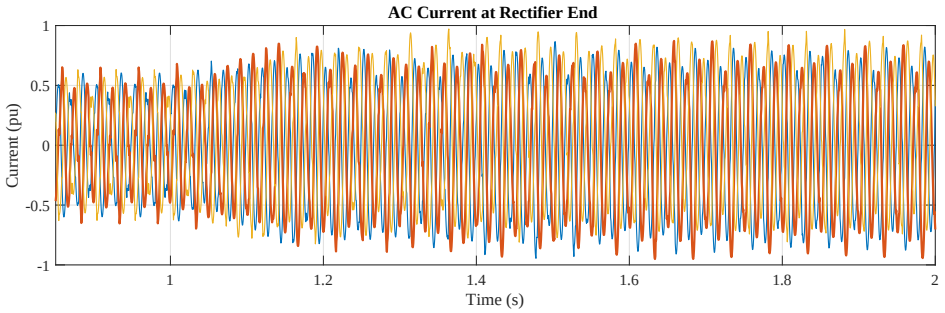

FIGURE 4.11: AC current at rectifier end (case-1)

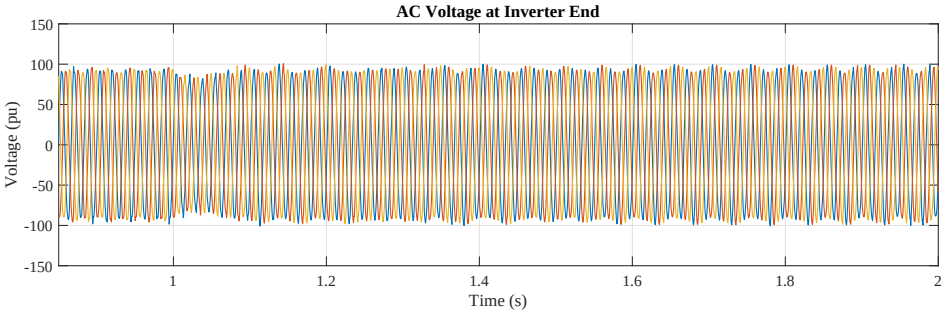

FIGURE 4.12: AC voltage at inverter end (case-1)

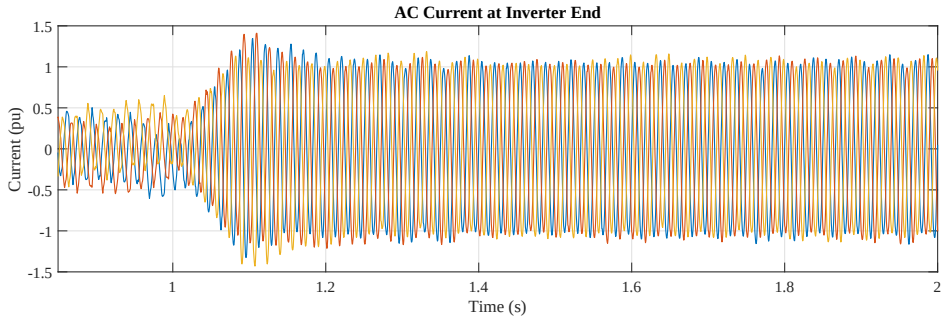

FIGURE 4.13: AC current at inverter end (case-1)

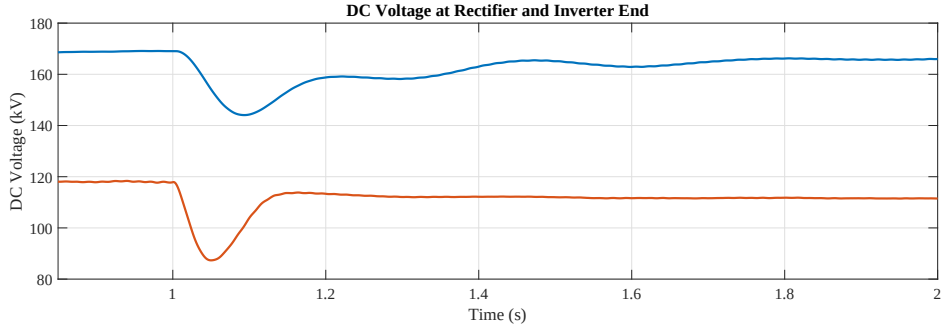

FIGURE 4.14: DC voltage at rectifier and inverter end (case-1)

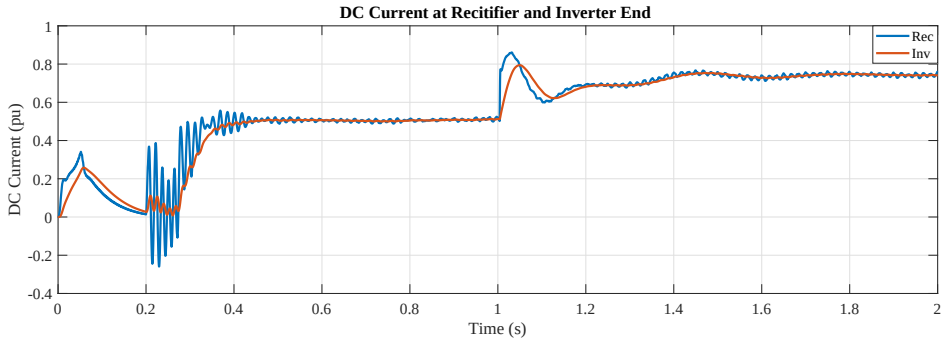

FIGURE 4.15: DC current at rectifier and inverter end (case-1)

The length of transmission line is 600 km and four types of fault are created at every 10 km i.e. at 59 different location at 1 second for a duration of 0.3 seconds (approx 10 cycles). The collected data for every sample is having the sampling frequency of 4.8 kHz. Once the transient fault occurs in the system, the line voltage immediately falls, whereas inverter side DC current falls and rectifier side DC current rise. Therefore, in order to maintain these current is at some predefined level, a control circuit is required. The per-defined value is selected in accordance with the DC voltage. During the fault event, this DC voltage will tend to reduce to a lower value to its threshold value. Therefore, this will bring down the line current to a lower value. It is advisable to limit this current to positive

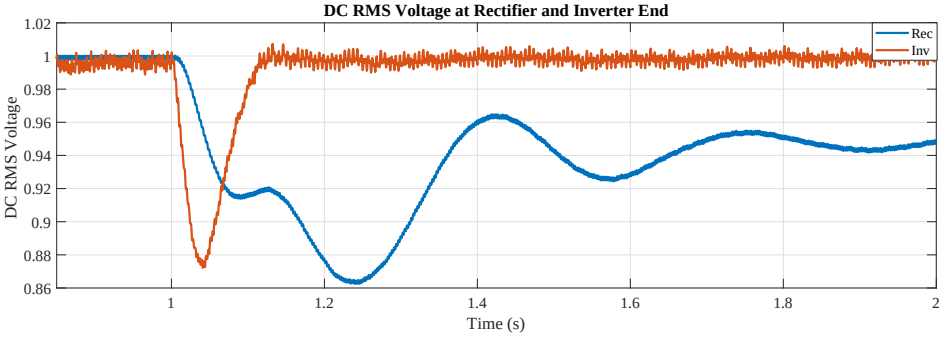

FIGURE 4.16: DC RMS voltage at rectifier and inverter end (case-1)

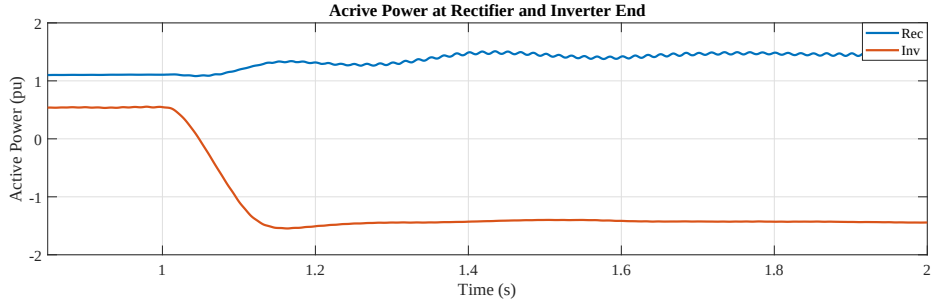

FIGURE 4.17: DC current at rectifier and inverter end (case-1)

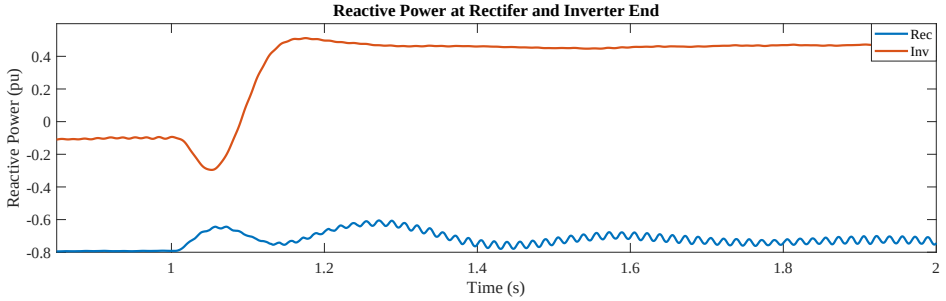

FIGURE 4.18: DC RMS voltage at rectifier and inverter end (case-1)

non-zero value. If it goes beyond this value the reactive power demand on AC part of the system reduces, thereby it will prevent the system to restore [150].

LL-fault is created in DC line at connecting terminal (1-2) at 530 km far from terminal-1. Figures 4.10 and 4.11 show the generator side AC voltage and current at terminal-1 (rectifier end). Line voltage decreases by 20% and line current increase by 60% at terminal-1 as shown in Figures 4.10 and 4.11 respectively at the time of fault. Figures 4.12 and 4.13 shown the generator side AC voltage and current at terminal-2 (inverter end). Line voltage decreases with 25% and line current increase 160% at terminal-2 as shows in Figures 4.12 and 4.13 respectively at the time of fault. Figures 4.14 and 4.15 shows the DC voltage and current of terminal-1 and terminal-2. DC voltage at terminal-1 decrease with 16% and DC

voltage at terminal-2 decrease 27% as shown in Figure 4.14. DC current at terminal-1 and at terminal-2 increase by 70% shown in Figure 4.15. Figure 4.16 shows DC RMS voltage variation in both the terminal. Figures 4.17 and 4.18 shows the active reactive power variation at terminal-1 and terminal-2 respectively at the time of fault. It is observed that rectifier end DC voltage and current has more harmonic content as compare to inverter end DC voltage and current. In this work, different faults are classified as a different class which are the class-1, class-2, class-3 and class-4 stand for positive line to ground fault, negative line to ground fault, line to line fault, line to line ground fault respectively.

4.3.2 Case-2: Multi-terminal HVDC Transmission Test System

To validate the proposed F-SVM fault estimation method, a multi-terminal HVDC transmission test system has been used as shown in Figure 4.19. The three-terminal are connected with transmission cable having a length of 900 km and 600 km. Four types of faults with fault resistance of 5Ω at every 10 km is simulated in both the cables. With this condition, the data-set is prepared for training and testing purpose for the proposed F-SVM fault estimation method. The cable structure along with their configuration is given in Figure 4.20.

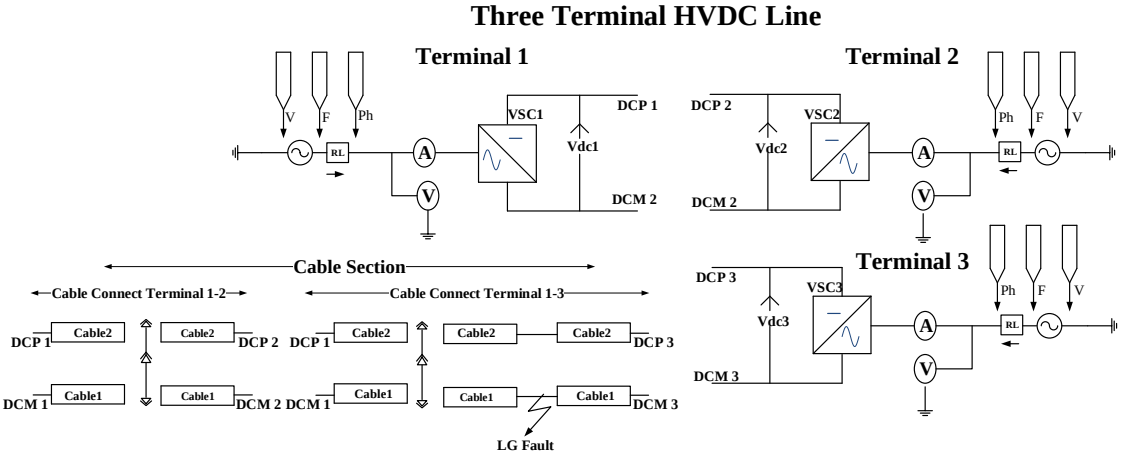

FIGURE 4.19: Schematic diagram of multi-terminal HVDC transmission test system

The performance of VSC based multi-terminal HVDC system has been simulated under these circuit specification. A voltage source connected at terminal-1 is with terminal voltage 420kV, rated power 100MVA, and frequency 60Hz. Terminal-1 consist of PWM controlled IGBT based rectifier/inverter having specification as, the terminal voltage 230kV, on-resistance 0.005Ω, off-resistance $100M\Omega$, breakdown voltage 100MV, reverse withstand

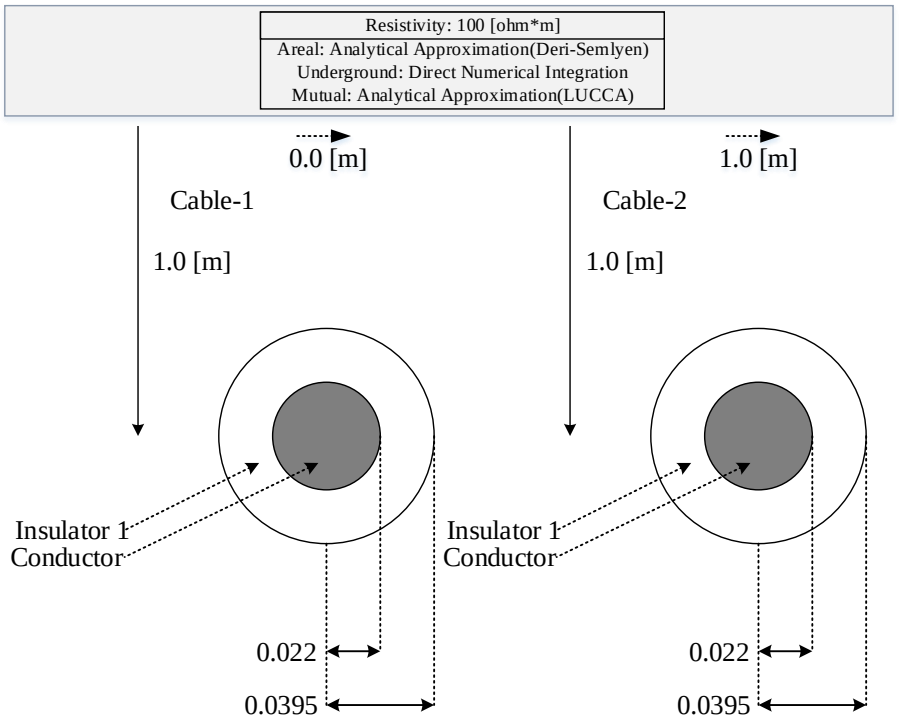

FIGURE 4.20: Tower configuration of HVDC transmission cable

voltage 100MVA with PWM control. The transformer used at terminal-1 is of winding ratio 420kV/230kV (Y-Y) with solidly grounded in primary side and secondary side grounded with the resistance of $1M\Omega$, at 1500MVA. At terminal-1 high pass filter used with resistance 1Ω, inductance $0.1H$, capacitance $5\mu F$ and smoothing reactor in series $0.0724H$. A voltage source connected at terminal-2 is with terminal voltage 420kV, rated power 100MVA, frequency 50Hz. Terminal-2 consist of PWM controlled IGBT based rectifier/inverter having specification as, the terminal voltage 230kV, on-resistance 0.005Ω, off-resistance $100M\Omega$, breakdown voltage 100MV, reverse withstand voltage 100MVA with PWM control. The transformer used at terminal-2 is of winding ratio 420kV/230kV (Y-Y) with solidly grounded in primary side and secondary side grounded with the resistance of $1M\Omega$, at 1500MVA. At terminal-2 high pass filter used with resistance 1Ω, inductance $0.1H$, capacitance $5\mu F$ and smoothing reactor in series $0.0724H$. A voltage source connected at terminal-2 is with terminal voltage 500kV, rated power 100MVA, frequency 50Hz. Terminal-3 consist of PWM controlled IGBT based rectifier/inverter having specification as, the terminal voltage 230kV, on-resistance 0.005Ω, off-resistance $100M\Omega$, breakdown voltage 100MV, reverse withstand voltage 100MVA with PWM control. The transformer used at terminal-3 is of winding ratio 500kV/230kV (Y-Y) with solidly grounded in primary side and secondary side grounded with the resistance of $1M\Omega$, at 1500MVA. At

terminal-3 high pass filter used with resistance 1Ω, inductance $0.1H$, capacitance $5\mu F$ and smoothing reactor in series $0.0724H$. Transmission cable connects terminal (1-2) and terminal (1-3) with DC terminal voltage 500kV, 900km in length and DC terminal voltage 500kV, 600km in length respectively.

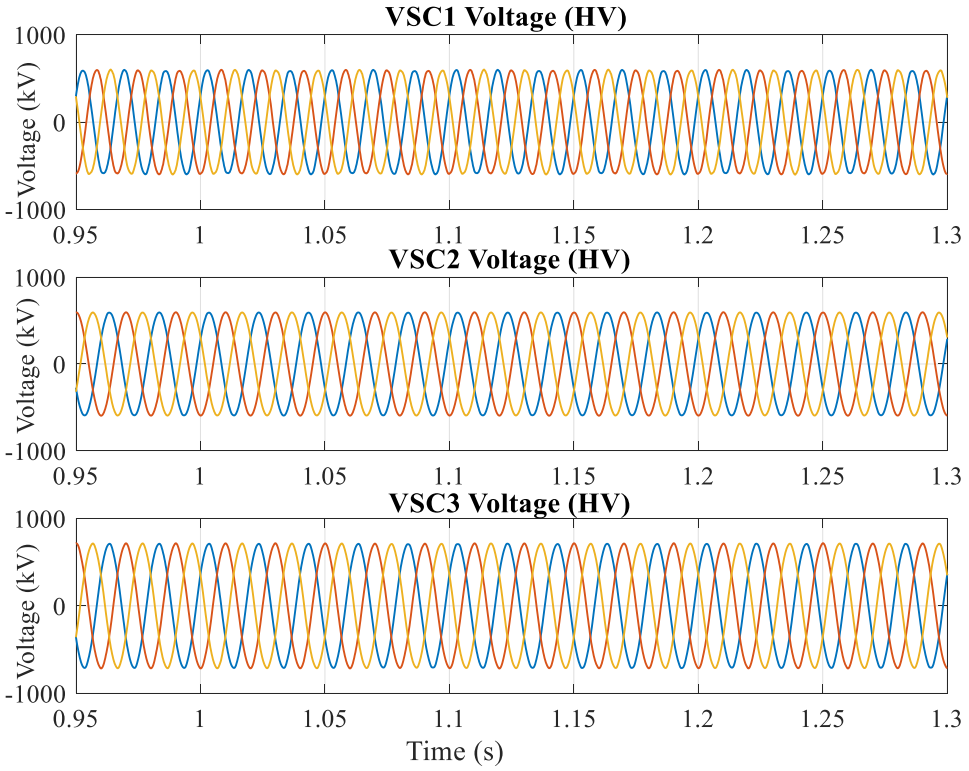

FIGURE 4.21: Zoomed signal of voltage in AC side at the time of fault (case-2)

The first transmission line i.e. cable connecting a terminal (1-2) is 600 km in length. So, at 59 different location four types of faults were created in this first transmission line and 59 different types of sample data-set were collected. The second transmission line i.e cable connecting a terminal (1-3) is 900 km in length. Therefore, at 89 different location four types of fault were created in the second transmission line and 89 types of sample data-set were collected. In this present work, it is assumed that different types of short circuit fault have arisen in the system. All types of fault are initiated at 1 second and exist for 0.1 seconds (approx. 4 cycles). The collected data for every sample is having a sampling frequency of 4.8 kHz. Once the fault occurs in the system, the line voltage will immediately fall, whereas inverter side DC current fall and rectifier side DC current rises. Therefore, in order to maintain these currents at some predefined level, a control circuit is required. The predefined value is selected in accordance with the DC voltage. During

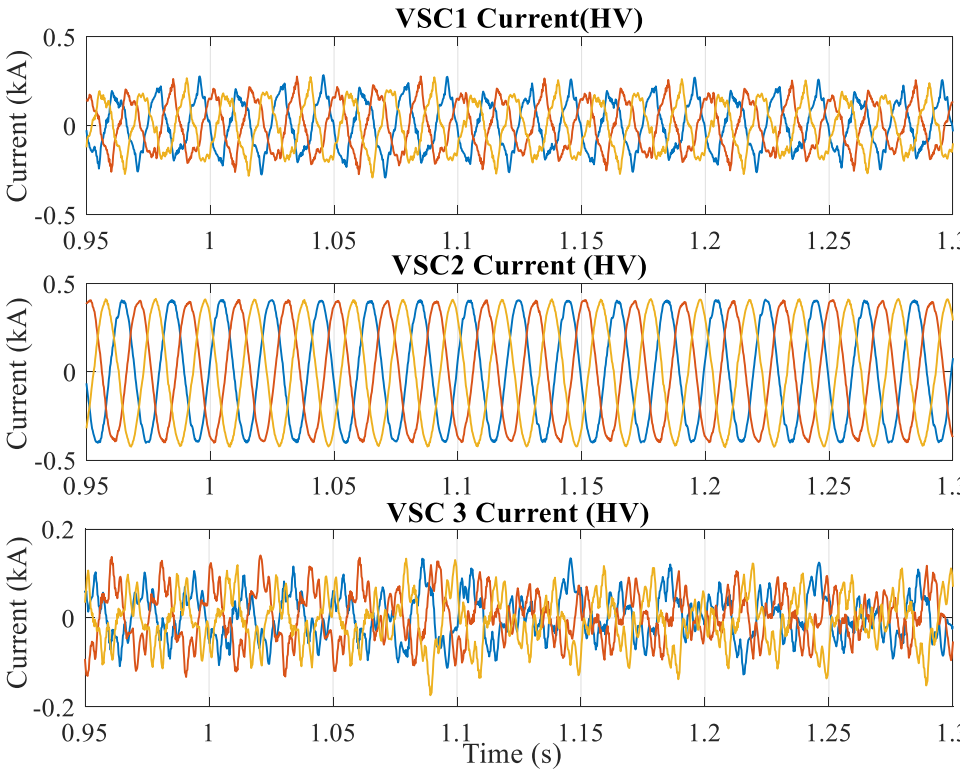

FIGURE 4.22: Zoomed signal of current in AC side at the time of fault (case-2)

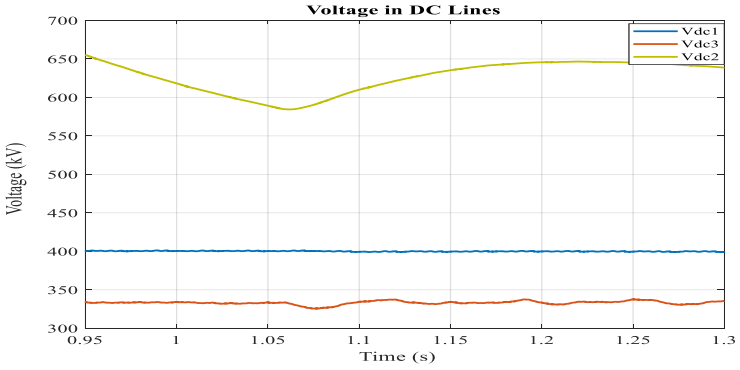

FIGURE 4.23: Zoomed signal of DC side voltage at the time of fault (case-2)

the fault event, this DC voltage will tend to reduce to a lower value to its threshold value. Therefore, this will bring down the line current to a lower value. It is advisable to limit this current to $+ve$ non-zero value. If it goes beyond this value the reactive power demand on the AC part of the system goes down the limit, thereby it will prevent the system to restore [150].

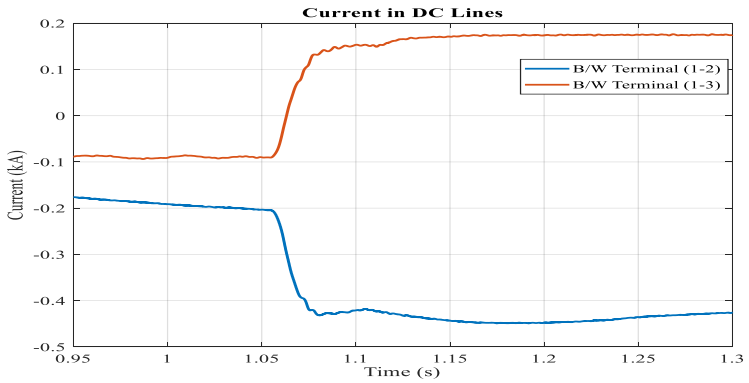

FIGURE 4.24: Zoomed signal of DC side current at the time of fault (case-2)

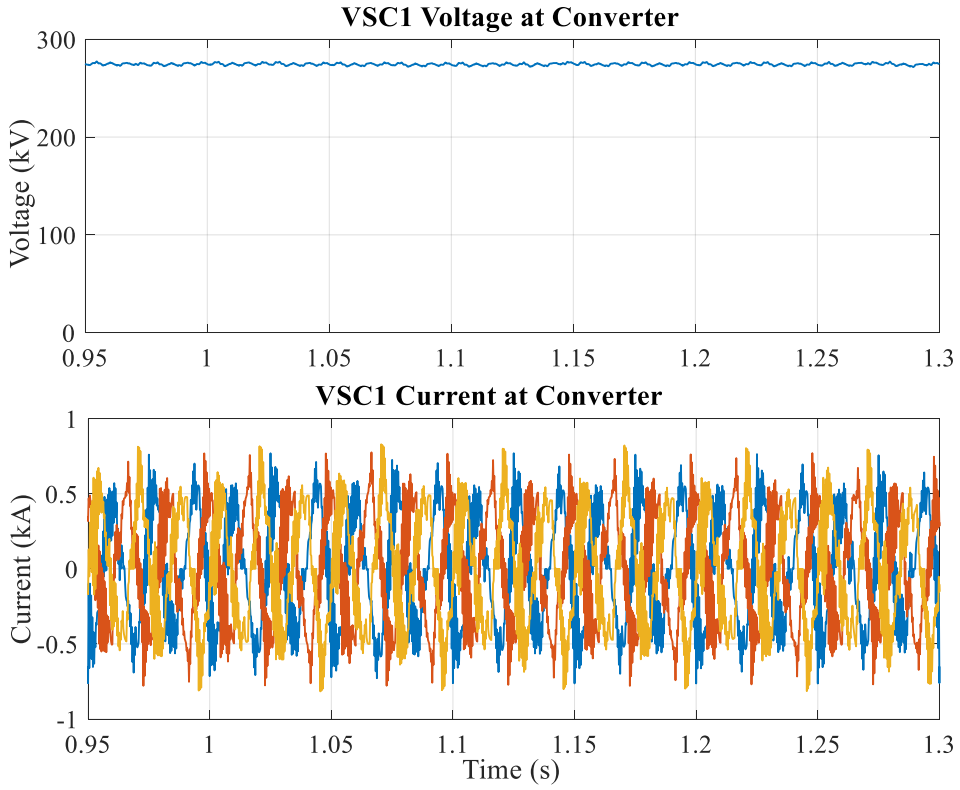

FIGURE 4.25: Zoomed signal of Rms voltage and current at terminal-1 (case-2)

LL-Fault is created in DC line at connecting terminal (1-3) at 530 km far from terminal-1. Figures 4.21, and 4.22 show the generator side AC voltage and current at all the three terminal at same time. Line voltage in AC side of all the three terminal is not much affected due to VSC control strategies shown in Figure4.21. Line current present in section-1 at terminal-1 has harmonic content, in section-1 at terminal-2 has no harmonic distortion, and in section-2 at terminal-2 has more harmonic content due to fault present, and is shown in Figure 4.22. Figures 4.23 and 4.24 show the DC side voltage and current in all

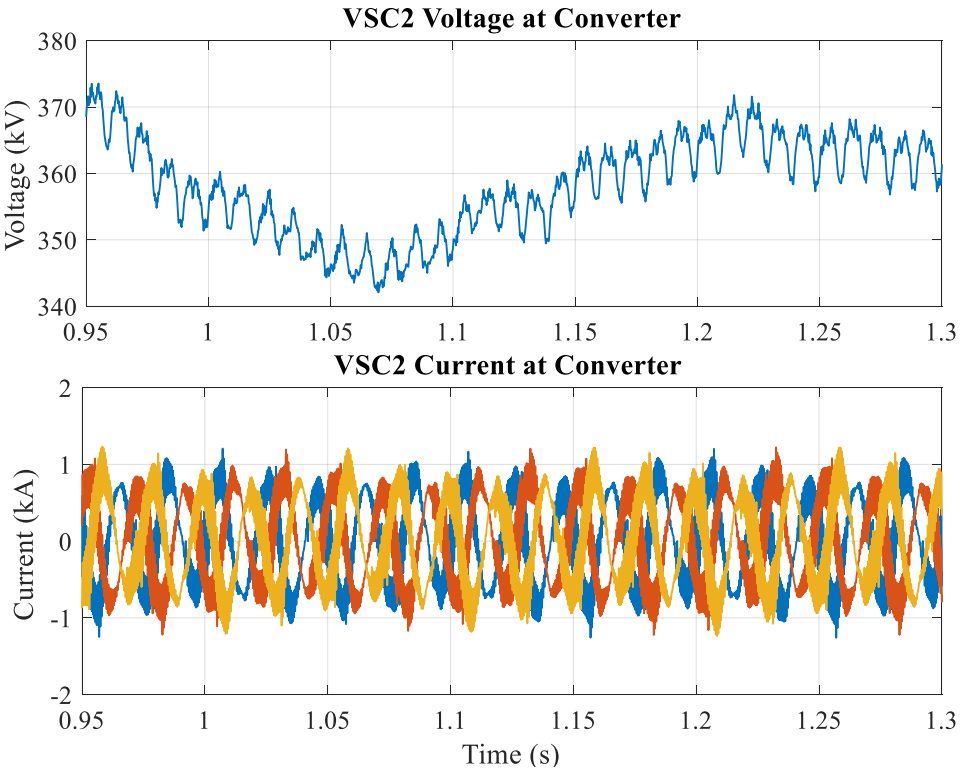

FIGURE 4.26: Zoomed signal of Rms voltage and current at terminal-2 (case-2)

the section. Due to fault present in the system, DC line current is more disturbed but DC terminal voltage is not affected much. The terminal voltage at terminal-1 fall at a maximum of 5% as shown in Figure 4.23. The terminal voltage at terminal-2 fall at a maximum of 0.5% as shown in Figure 4.24. The terminal voltage at terminal-3 fall at a maximum 2% as shown in Figure4.23. The current of the line connecting terminal (1-2) rise at maximum 87% due to inverter action and a line connecting a terminal (1-3) fall 300% due to rectifier action as shown in Figure 4.24. Figures 4.25, 4.26 and 4.27 shows the AC RMS voltage and current of each terminal near the converter end. Voltage and current variation in terminal-2 and terminal-3 are higher as compared to terminal-1 as shown in Figures 4.25, 4.26 and 4.27 respectively. It is also observed that current and voltage has harmonic content due to the presence of a fault. Due to the VSC technique, the voltage of the DC side is maintained constant. In this paper different faults are classified as a different class which are class-1, class-2, class-3, class-4. Class-1 stand for a line to ground fault connecting to the terminal (1-2). Class-2 stand for a line to ground fault connecting a terminal (1-3). Class-3 stand for a line to line fault connecting terminal (1-2). Class-4 stand for a line to line fault connecting a terminal (1-3).

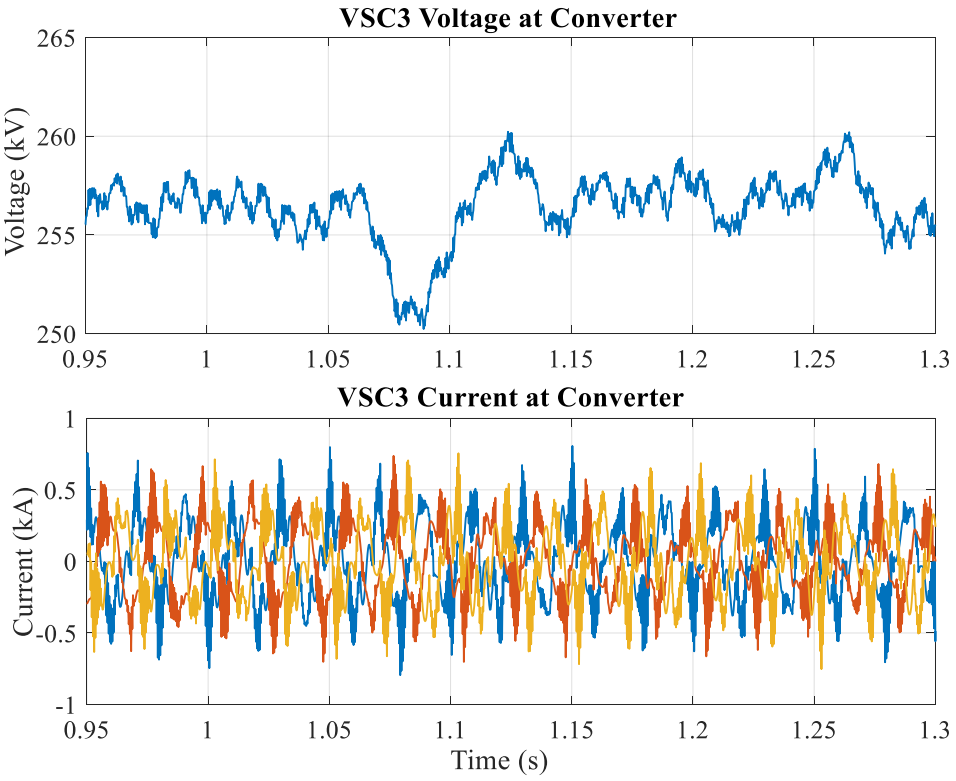

FIGURE 4.27: Zoomed signal of Rms voltage and current at terminal-2 (case-2)

4.4 Results and Discussions

The flowchart is shown in Figure 4.6 provides the working step of the proposed F-SVM fault estimation method. The voltage and current signal of the AC and DC side is continuously measured and recorded at the converter station of the system. The feature vector is extracted and the dominant feature is selected with the help of modified F-score scheme for every half cycle measured data of the running window. These dominant features are observed continuously to detect the presence of a fault. Once the fault is detected by F-SVM fault detection scheme 4.2.5. The same half cycle data are used to locate and classify the fault with the help of F-SVM fault location scheme 4.2.6 and F-SVM fault classification scheme 4.2.7 respectively.

4.4.1 Case-1: Two-terminal HVDC Transmission Test System

For the training purpose of F-SVM fault estimation method four types of faults are simulated in the transmission line at every 10 km of the transmission line and the data is

measured. The data contain 59 instant samples of four different classes, and 392 features vectors are extracted. From all these extracted features 246 dominating features are selected with a modified F-score scheme. 10-fold cross-validation RBF kernel function with 70% data used for training and 30% for testing purpose of the F-SVM fault estimation method.

4.4.1.1 Outcomes with F-SVM Fault Detection Scheme

To test the suitability of the F-SVM fault detection scheme, different types of fault in the overhead transmission line at 50 km, 300 km and 500 km are created. The test results of the fault detection scheme are shown in Table 4.1 for different fault locations and inception instant. First two columns show fault types and fault initiation location. Last three columns show the fault inception instant, detection instant and response time, respectively. From the Table 4.1, it is observed that by using the proposed scheme the fault is detected and identified precisely within 4 milliseconds and average detection time 2.68 milliseconds, which is well within the allowable time limit as per IEEE standard. In order to show the time taken for fault detection with this scheme one sample of class-1

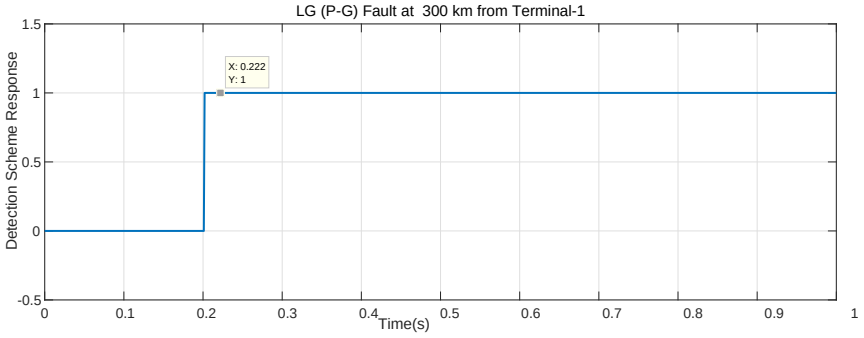

(a) Fault in terminal (1-2) at 300 km from terminal-1

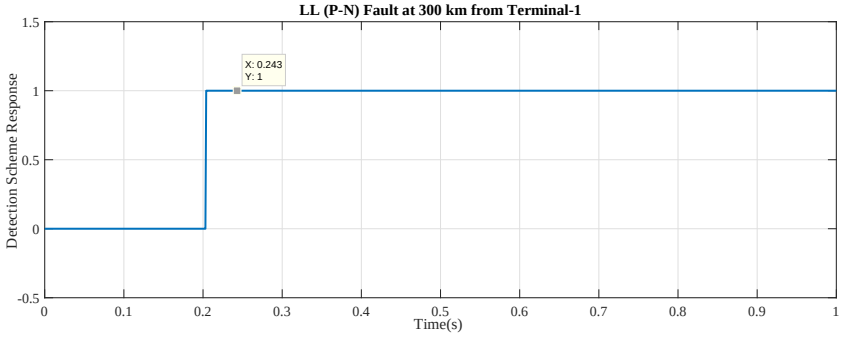

(b) Fault in terminal (1-3) at 300 km from terminal-1

FIGURE 4.28: Response signal of fault detection scheme (case-1)

TABLE 4.1: Result obtained with F-SVM fault detector scheme (case-1)

Fault Type	**Fault Location** (km)	**Fault Inception Instant** $(T_i)s$	**Fault Detection Instant** $(T_d)s$	**Response Time** $(T_r = T_d - T_i)ms$
LG (P-G) (Class 1)	50	0.2	0.2031	3.1
		0.3	0.3011	1.1
		0.4	0.4023	2.3
	300	0.2	0.2022	2.2
		0.3	0.3034	3.4
		0.4	0.4021	2.1
	500	0.2	0.2034	3.4
		0.3	0.3016	1.6
		0.4	0.4025	2.5
LG (N-G) (Class 2)	50	0.2	0.2031	3.1
		0.3	0.3031	3.1
		0.4	0.4033	3.3
	300	0.2	0.2016	1.6
		0.3	0.3023	2.3
		0.4	0.4034	3.4
	500	0.2	0.2021	2.1
		0.3	0.3032	3.2
		0.4	0.4023	2.3
LL (P-N) (Class 3)	50	0.2	0.2021	2.1
		0.3	0.3024	2.4
		0.4	0.4032	3.2
	300	0.2	0.2043	4.3
		0.3	0.3033	3.3
		0.4	0.4032	3.2
	500	0.2	0.2031	3.1
		0.3	0.3021	2.1
		0.4	0.4012	1.2
LLG (P-N-G) (Class 4)	50	0.2	0.2032	3.2
		0.3	0.3033	3.3
		0.4	0.4014	1.4
	300	0.2	0.2024	2.4
		0.3	0.3013	1.3
		0.4	0.4032	3.2
	500	0.2	0.2034	3.4
		0.3	0.2043	4.3
		0.4	0.4034	3.4

and class-3 1 second chosen with inception instant 0.2 seconds at fault location 300km is shown in Figure 4.28.

4.4.1.2 Outcomes with F-SVM Fault Location Scheme

Table 4.2 shows the actual fault location values and the respective estimated fault location values with F-SVM fault location scheme. The percentage error in the predicted fault location with the actual location is calculated using eq. (4.20). Figure 4.29 shows the performance of fault location scheme in a different location. The error observed in fault location calculation on the basis of the respective optimum value of c and γ for different types of faults are shown in Table 4.2. Overall accuracy found with the proposed

scheme is 99.94%. It is also observed that accuracy in LL fault is more than LG fault in the respective transmission line. Percentage error variation is shown in Figure 4.29. The comparison results with some others existing research works are shown in Table 4.6. It can be observed from Table 4.6 that the error in fault location is least with the proposed F-SVM fault location scheme which validates their accuracy.

TABLE 4.2: Result obtained with F-SVM fault location scheme (case-1)

Fault Type	**c**	**γ**	**Actual FL** (km)	**Calculated FL** (km)	**Error in FL** (km)	**Error in FL** (%)
Class 1	5246.82	0.0423	50	50.3071	0.3071	0.0511
			100	100.2218	0.2218	0.0369
			200	200.2750	0.2750	0.0458
			300	300.1983	0.1983	0.0330
			400	400.2255	0.2255	0.0375
			500	500.4080	0.4080	0.0680
Class 2	9346.63	0.03462	50	50.3366	0.3366	0.0561
			100	100.2758	0.2758	0.0459
			200	200.5154	0.5154	0.0859
			300	300.3926	0.3926	0.0654
			400	400.1656	0.1656	0.0276
			500	500.3749	0.3749	0.0624
Class 3	1480.52	0.01021	50	50.2429	0.2429	0.0404
			100	100.2586	0.2586	0.0431
			200	200.4786	0.4786	0.0797
			300	300.3839	0.3839	0.0639
			400	400.4769	0.4769	0.0794
			500	500.1332	0.1332	0.0222
Class 4	3295.42	0.02451	50	50.3654	0.3654	0.0609
			100	100.4896	0.4896	0.0816
			200	200.1650	0.1650	0.0275
			300	300.3844	0.3844	0.0640
			400	400.1060	0.1060	0.0176
			500	500.1811	0.1811	0.0301

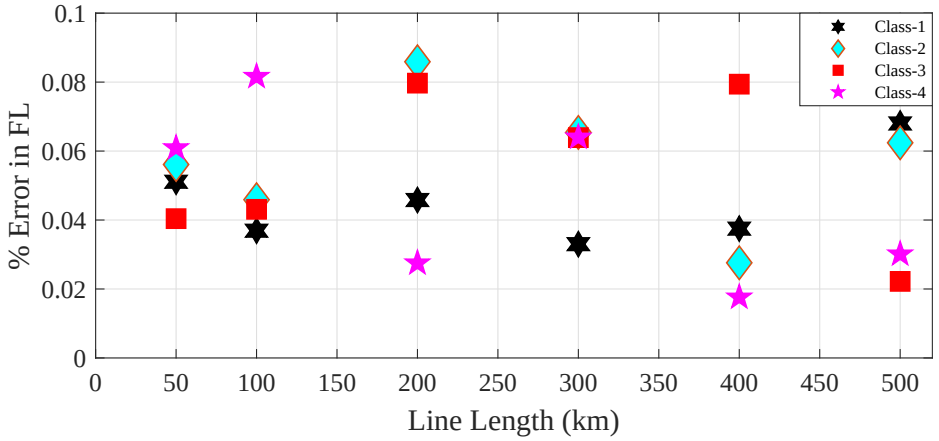

FIGURE 4.29: Performance of F-SVM fault location scheme (case-1)

4.4.1.3 Outcomes with F-SVM Classification Scheme

The results obtained with the F-SVM fault classification scheme are shown in Figures 4.30, and 4.31. The diagonal elements in Figure 4.30(a) shows the correct classified sample, whereas non-diagonal elements shows false classified samples without using the F-score scheme. It shows how many samples in test case classify correctly and how many samples misclassify with a different class. Figure 4.30(b) shows the correct classified percentage considering the True Positive Rate (TPR) whereas the non-diagonal elements show false classified percentage considering False Negative Rate (FNR) without using the F-score scheme. The diagonal elements in Figure 4.30(c) shows the correct classify percentage whereas the non-diagonal elements show false classified percentage with the positive predictive value/ false discovery rate (PPD/FDR) without using the F-score scheme. The classification accuracy without using the F-score is 98.6% with prediction speed of 3400 obs/second and take 1.3747 second for training purpose, as shown in Figure 4.30.

The diagonal elements in Figure 4.31(a) shows the correct classified sample, whereas non-diagonal elements shows false classified samples using the F-score scheme. It shows how many samples in test case classify correctly and how many samples misclassify with a different class. Figure 4.31(b) shows the correct classified percentage considering True Positive Rate whereas the non-diagonal elements show false classified percentage considering False Negative Rate with using the F-score scheme. The diagonal elements in Figure 4.31(c) shows the correct classify percentage whereas the non-diagonal elements show false classified percentage with the positive predictive value/false discovery rate without using the F-score scheme. The classification accuracy with using the F-score with the prediction speed of 3700 obs/second and take 6.362 second for training purpose, as shown in Figure 4.31. The basic equation behind design of confusion matrix are shown in eq. (4.21), eq. (4.22) and eq. (4.23). The comparison result of the F-SVM fault classification scheme with or without using the F-score approach is summarized in Table 4.3 using basic eq. (4.21), eq. (4.22) and eq. (4.23).

$$True \;\; Positive \;\; Rate = \frac{True \;\; Classification}{\sum (True \;\; Classification + False \;\; Classification)} \tag{4.21}$$

$$True \;\; Negative \;\; Rate = \frac{False \;\; Classification}{\sum (True \;\; Classification + False \;\; Classification)} \tag{4.22}$$

$$Persantage \;\; Accuracy = \frac{True \;\; classification}{Total \;\; Number \;\; of \;\; Cases} \times 100 \tag{4.23}$$

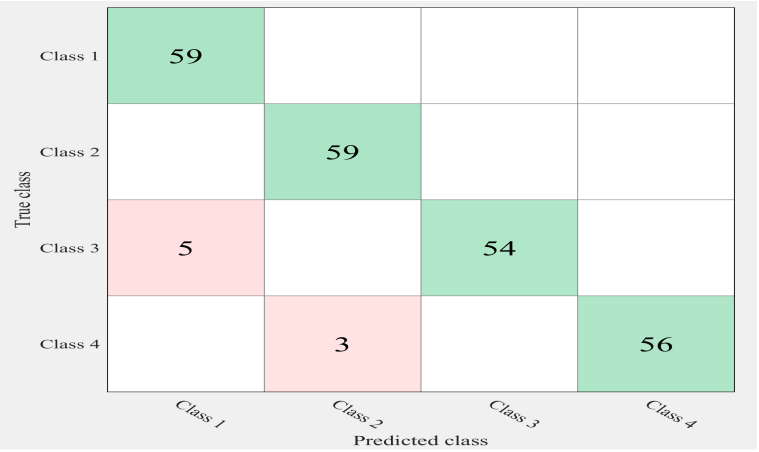

(a) Confusion matrix with number of sample

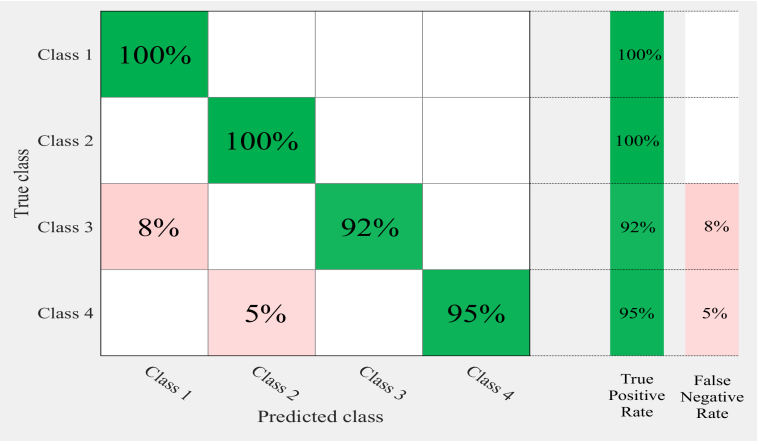

(b) Confusion matrix with TPR/NPR

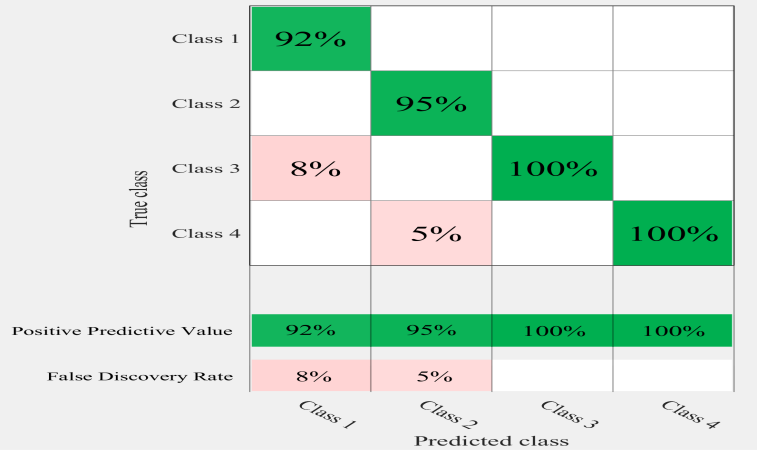

(c) Confusion matrix with PPD/FDR

FIGURE 4.30: Confusion matrix for F-SVM classifier without using F-score (case-1)

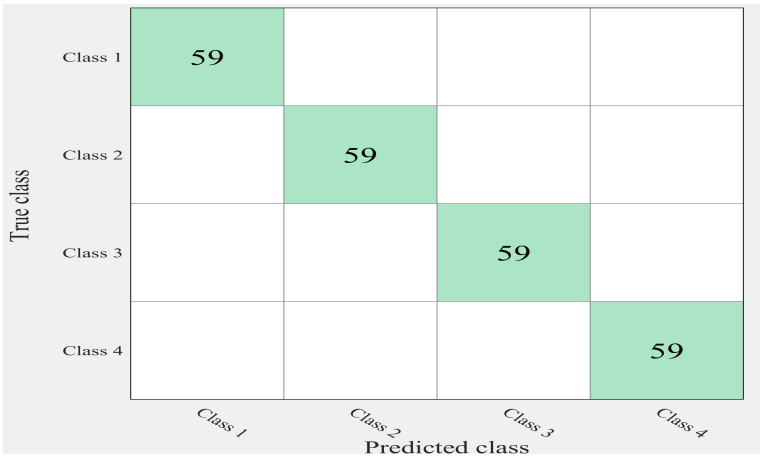

(a) Confusion matrix with number of sample

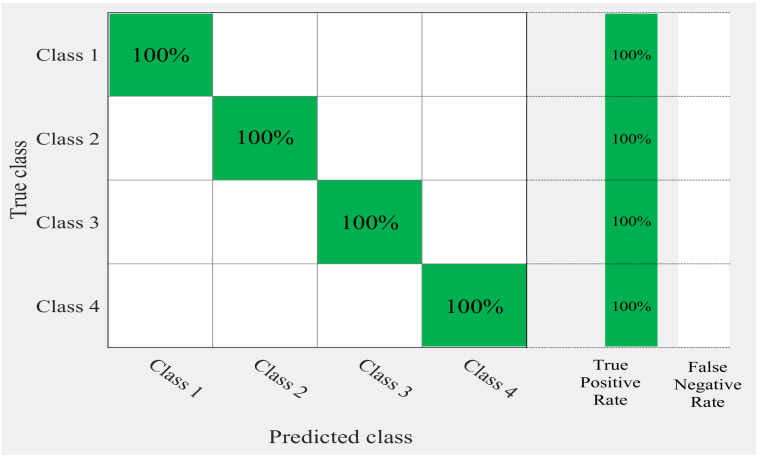

(b) Confusion matrix with TPR/NPR

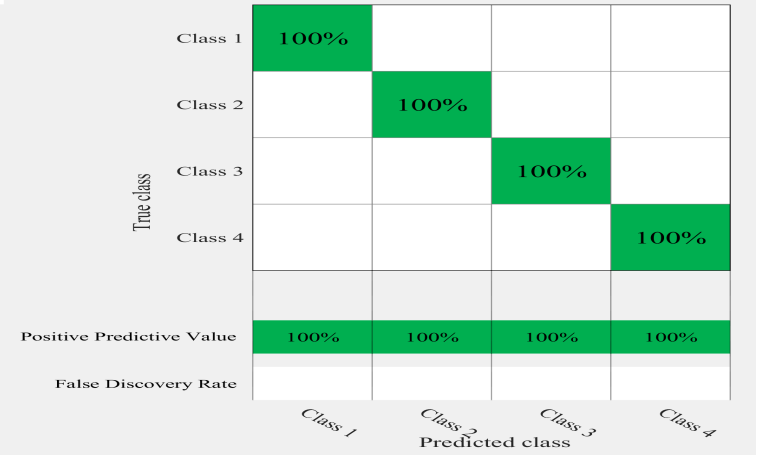

(c) Confusion matrix with PPD/FDR

FIGURE 4.31: Confusion Matrix for F-SVM classifier with using F-score (case-1)

TABLE 4.3: Comparison between with or without using F-score based multi-class F-SVM classifier outcomes (case-1)

	Class	True Positive Rate %	True Negative Rate %	Overall Accuracy %
Without F-Score	Class 1	100	0	96.61
	Class 2	100	0	
	Class 3	91.52	8.47	
	Class 4	94.91	5.08	
With F-Score	Class 1	100	0	100
	Class 2	100	0	
	Class 3	100	0	
	Class 4	100	0	

4.4.2 Case-2: Multi-terminal HVDC Transmission Test System

For the training purpose of F-SVM fault estimation method four types of faults are created in two different sections at every 10 km of the transmission line and the data voltage and current is measured. The data contain 256 instant samples of four different classes, and 21504 features vector is extracted. From all these extracted features 15052 dominating features are selected with a modified F-score scheme. 10-fold cross-validation RBF kernel function with 70% data used for training and 30% for testing purpose of F-SVM fault estimation method.

4.4.2.1 Outcomes with F-SVM Fault Detection Scheme

To test the suitability of this scheme, different types of fault in two different section of the transmission line at 50 km, 300 km and 500 km are created. The test results of the F-SVM fault detection scheme are shown in Table 4.4 for different fault locations and inception instant. First two columns show fault types and fault initiation location. Last three columns show the fault inception instant, detection instant and response time, respectively. From the Table 4.4, it is observed that by using the proposed F-SVM fault detection scheme the fault is detected and identified precisely within 4 milliseconds and average detection time 2.195 milliseconds, which is well within the allowable time limit of IEEE standard. In order to show time taken for fault detection with this fault detection scheme one sample of class-1 and class-3 is chosen with inception, instant 0.2s at fault location 300km is shown in Figure 4.32.

TABLE 4.4: Result obtained with F-SVM fault detector scheme (case-2)

Fault Type	**Fault Location** (km)	**Fault Inception Instant** $(T_i)s$	**Fault Detection Instant** $(T_d)s$	**Response Time** $(T_r = T_d - T_i)ms$
LG12 (Class 1)	50	0.2	0.201	1
		0.3	0.301	1
		0.4	0.403	3
	300	0.2	0.202	2
		0.3	0.301	1
		0.4	0.402	2
	500	0.2	0.201	1
		0.3	0.303	3
		0.4	0.402	2
LG13 (Class 2)	50	0.2	0.203	3
		0.3	0.301	1
		0.4	0.403	3
	300	0.2	0.204	4
		0.3	0.302	2
		0.4	0.402	2
	500	0.2	0.203	3
		0.3	0.303	3
		0.4	0.402	2
LL12 (Class 3)	50	0.2	0.202	2
		0.3	0.302	2
		0.4	0.403	3
	300	0.2	0.204	4
		0.3	0.303	3
		0.4	0.402	2
	500	0.2	0.203	3
		0.3	0.301	1
		0.4	0.402	2
LL13 (Class 4)	50	0.2	0.202	2
		0.3	0.303	3
		0.4	0.401	1
	300	0.2	0.202	2
		0.3	0.301	1
		0.4	0.402	2
	500	0.2	0.202	2
		0.3	0.203	3
		0.4	0.402	2

4.4.2.2 Outcomes with F-SVM Fault Location Scheme

Table 4.5 shows the actual fault location values and the respective estimated fault location values with F-SVM fault estimation method. The percentage error in the predicted fault location with the actual location is calculated using eq. (4.20). Figure 4.33 shows the performance of fault location scheme in a different location. The error observed in fault location calculation on the basis of the respective optimum value of c and γ for different types of faults are shown in Table 4.5. Overall accuracy found with the proposed scheme is 99.958%. It is also observed that accuracy in LL fault is more than LG fault in the respective transmission line. The comparison results with some other existing research works are shown in Table 4.6. It can be observed from Table 4.6 that the error in fault

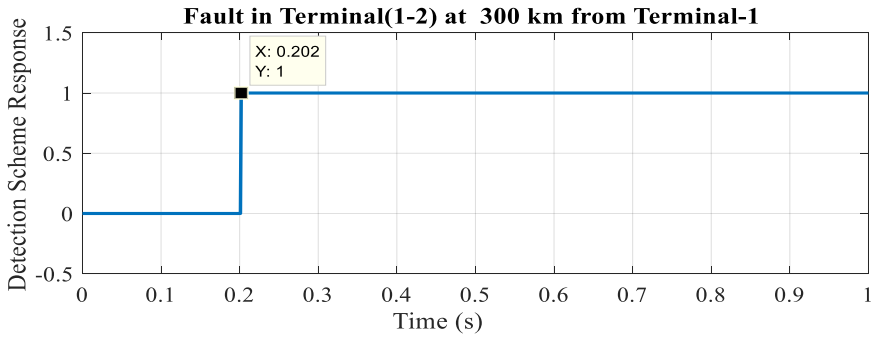

(a) Fault in terminal (1-2) at 300 km from terminal-1

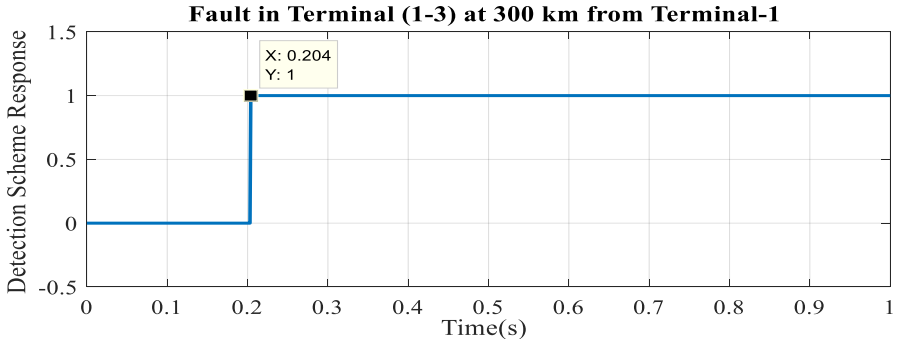

(b) Fault in terminal (1-3) at 300 km from terminal-1

FIGURE 4.32: Response signal of fault detection scheme (case-2)

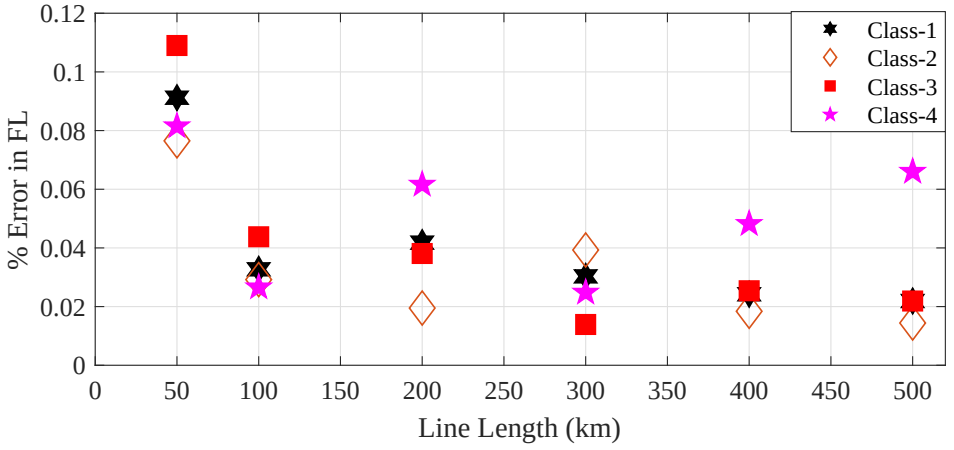

FIGURE 4.33: Performance of F-SVM fault location scheme (case-2)

location is least with the purposed F-SVM fault location scheme which validates their accuracy.

TABLE 4.5: Result obtained with F-SVM fault location scheme (case-2)

Fault Type	**c**	**γ**	**Actual FL** (km)	**Calculated FL** (km)	**Error in FL** (km)	**Error in FL** (%)
LG12	5792.61	0.0625	50	50.5472	0.5472	0.0912
			100	100.1966	0.1966	0.0327
			200	200.2511	0.2511	0.0418
			300	300.0474	0.1818	0.0303
			400	400.1455	0.1455	0.0242
			500	500.1361	0.1361	0.0219
LG13	11585.23	0.04419	50	50.6892	0.6892	0.0765
			100	100.2630	0.2630	0.0292
			200	200.0759	0.1759	0.0195
			300	300.0540	0.3540	0.0393
			400	400.1656	0.1656	0.0184
			500	500.1299	0.1299	0.0144
LL12	23170.47	0.00782	50	50.6541	0.6541	0.1090
			100	100.2630	0.2630	0.0438
			200	200.2290	0.2290	0.0381
			300	300.0838	0.0838	0.0139
			400	400.1524	0.1524	0.0254
			500	500.1361	0.1361	0.0219
LL13	46340.95	0.0069	50	50.7340	0.7340	0.0815
			100	100.2399	0.2399	0.0266
			200	200.1233	0.1233	0.0616
			300	300.0497	0.0497	0.0248
			400	400.0965	0.0965	0.0482
			500	500.1320	0.1320	0.0660

TABLE 4.6: F-SVM fault location scheme comparison with some existing methods

Ref. No.	**Basic Approach Used**	**System Used**	**Error (%)**
[158]	Impedance based method	Three terminal AC System	0.476
[159]	Impedance based method	Two Terminal HVDC	0.196
[162]	Traveling wave	2- Terminal double circuit HVDC	1.233
[36]	Traveling wave	Two terminal HVDC	1.345
[37]	Artificial Neural Network	Two terminal hvdc	2.50
[40]	Radial basis function (ANN)	Two terminal hvdc	0.501
[43]	Support Vector Machine	Multi-terminal VSC HVDC	0.192
[45]	Traveling wave	Multi-terminal VSC HVDC	0.152
Proposed	**Support Vector Machine**	**Two-terminal VSC HVDC**	**0.051**
	Support Vector Machine	**Multi-terminal VSC HVDC**	**0.042**

4.4.2.3 Outcomes with F-SVM Classification Scheme

The results obtained with the F-SVM fault classification scheme are shown in Figure 4.34, and Figure 4.35. The diagonal elements in Figure 4.34(a) show the correct classified sample, whereas non-diagonal elements show false classified samples without using the F-score scheme. It shows how many samples in test case classify correctly and how

TABLE 4.7: Comparison between with or without using F-score based multi-class F-SVM classifier outcomes (case-2)

	Class	True Positive Rate %	True Negative Rate %	Overall Accuracy %
Without F-Score	Class 1	100	0	98.64
	Class 2	97.752	2.247	
	Class 3	96.610	3.508	
	Class 4	100	0	
With F-Score	Class 1	100	0	100
	Class 2	100	0	
	Class 3	100	0	
	Class 4	100	0	

many samples misclassify with a different class. Figure 4.34(b) shows the correct classified percentage considering true positive rate (TPR) whereas the non-diagonal elements show false classified percentage considering false negative rate (FNR) without using the F-score scheme. The diagonal elements in Figure 4.34(c) shows the correct classify percentage whereas the non-diagonal elements show false classified percentage with the positive predictive value/ false discovery rate (PPD/FDR) without using the F-score scheme. The classification accuracy without using the F-score is 98.6% with prediction speed of 3830 obs/second and take 2.8678 second for training purpose, as shown in Figure 4.34.

The diagonal elements in Figure 4.35(a) show the correct classified sample, whereas non-diagonal elements show false classified samples using the F-score scheme. It shows how many samples in test case classify correctly and how many samples misclassify with a different class. Figure 4.35(b) shows the correct classified percentage considering true positive rate whereas the non-diagonal elements show false classified percentage considering false negative rate with using the F-score scheme. The diagonal elements in Figure 4.35(c) shows the correct classify percentage whereas the non-diagonal elements show false classified percentage with the positive predictive value/false discovery rate without using the F-score scheme. The classification accuracy with using the F-score is 100% with the prediction speed 4120 obs/second and take 5.268 second for training purpose, as shown in Figure 4.35. The basic equation behind design of confusion matrix are shown in eq. (4.21), eq. (4.22) and eq. (4.23). The comparison result of the classification scheme with or without using the F-score scheme is summarized in Table 4.7 with using basic eq. (4.21), eq. (4.22) and eq. (4.23). The comparison result of the F-SVM fault classification scheme with or without using modified F-score is summarized in Table 4.7.

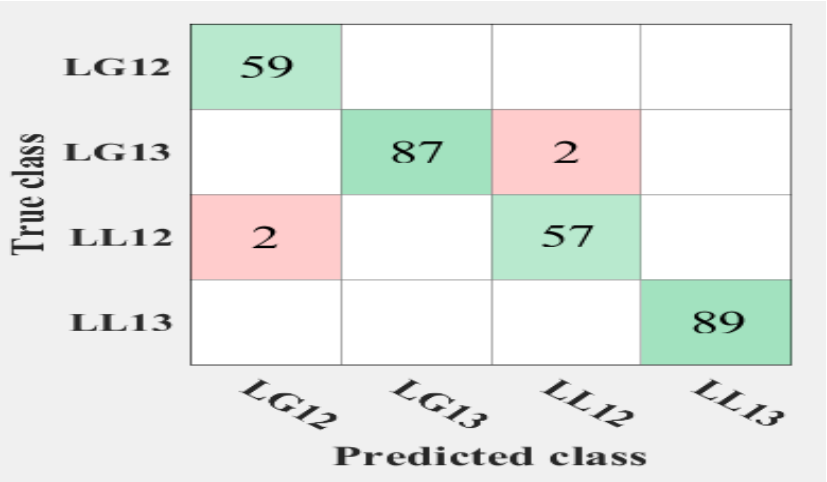

(a) Confusion matrix with number of sample

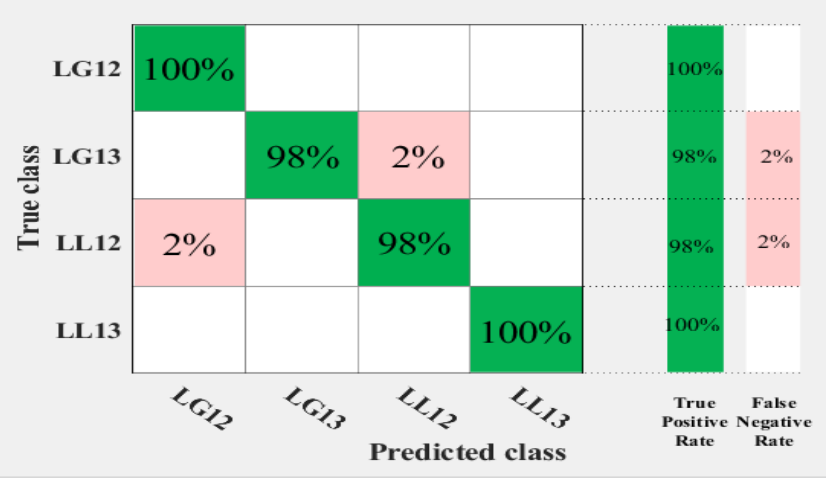

(b) Confusion matrix with TPR/NPR

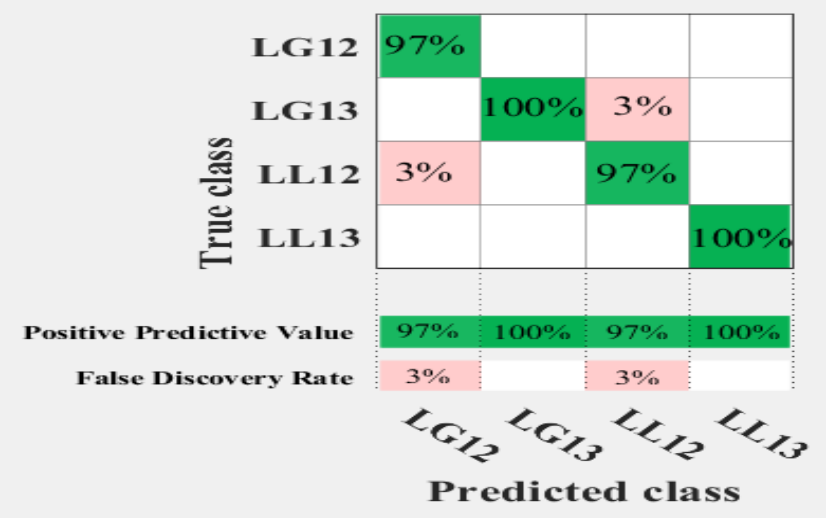

(c) Confusion matrix with PPD/FDR

FIGURE 4.34: Confusion matrix for F-SVM classifier without using F-score (case-2)

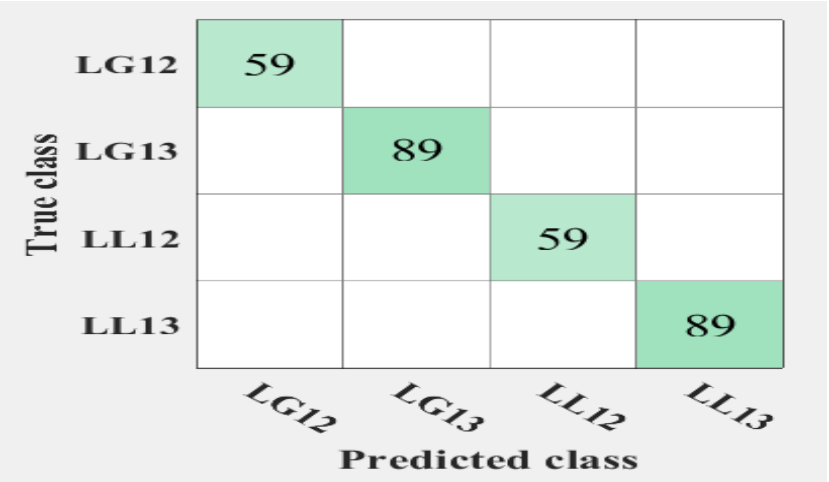

(a) Confusion matrix with number of sample

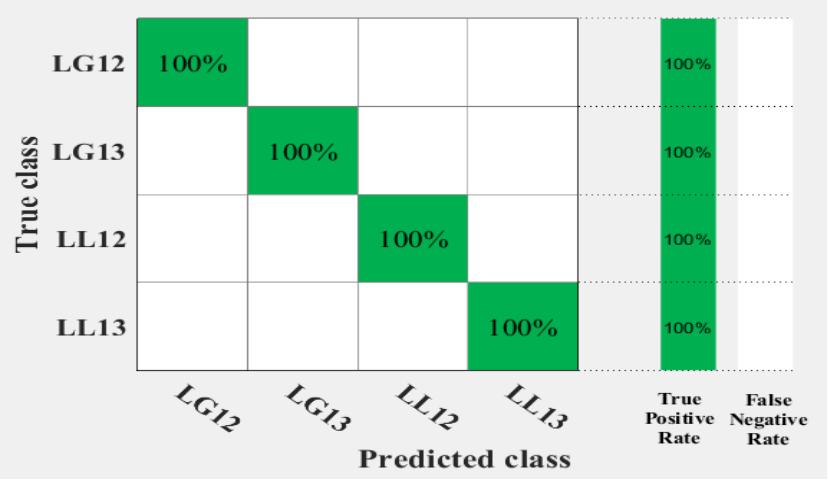

(b) Confusion matrix with TPR/NPR2

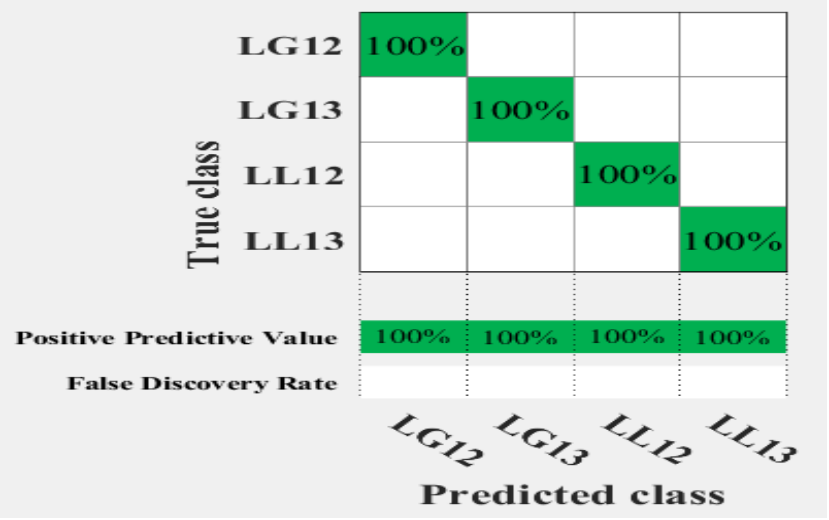

(c) Confusion matrix with PPD/FDR

FIGURE 4.35: Confusion Matrix for F-SVM classifier with using F-score (case-2)

The results observed in the above subsection with F-SVM fault estimation method describe in respected table and figures with acceptable accuracy. From the describe two test cases average total execution time of the proposed F-SVM fault estimation method are observed as 10.03 milliseconds, and 11.54 milliseconds respectively. Further, it is also observed that time of execution of F-SVM fault estimation method within one cycle and input requirement of measured voltage and current post-fault data of 0.5 cycle only for all the two HVDC test transmission systems. Along with, the training time of the proposed F-SVM method takes the extreme of 6.5 seconds before the use of first time after that it does not require further training. Consequently, the suggested F-SVM fault estimation method shows its applicability with reasonable precision and within an acceptable time span for the transmission system [150].

4.5 Summary of the Chapter

This chapter proposes fault detection, location and classification schemes with a single use of F-SVM based method for two and multi-terminal HVDC transmission system. This method provides flexibility to the transmission system operator (TSO) to accelerate the restoration process as quick as possible with minimal effort. The proposed method provides results: for fault detection within 4 milliseconds (average detection time 2.35 milliseconds) by employing fault detection scheme, locating the fault with maximum error 0.1090% (average error 0.0510%) and classifying the fault with 100% accuracy. The total execution time of proposed method with all the three schemes is within 1/2 cycle. The proposed approach is simple, non-iterative and effective for both two and multi-terminal HVDC transmission systems.

In this chapter two test case models are developed with the help of CIGRE HVDC model in PSCAD environment that provides similar results as that of the real time system. The proposed method is designed and tested in MATLAB platform.

Since the existing infrastructure of HVAC system cannot be replaced completely therefore by introducing HVDC system in the existing transmission systems an amalgamation of systems is formed which gives rise to a new hybrid HVAC and HVDC system. The F-SVM method proposed in this chapter is utilized to detect, locate and classify the fault in hybrid HVAC and HVDC system.

Chapter 5

Fault Protection Strategies for Hybrid Transmission Systems

This chapter presents an effective algorithm for fault detection, location and classification for hybrid transmission systems as well as for HVAC transmission systems. Test transmission model is developed with the help of CIGRA dynamic standard data and IEEE dynamic data. Further, statistical analysis are presented to validate proposed algorithm.

5.1 Introduction

In recent times, researchers are much aware of carbon emission due to conventional energy resources. Therefore, renewable energy integration is increasing exponentially to meet the ever-increasing load demand from industrial, commercial and residential customers. HVDC transmission plays an increasingly important role in the field of renewable energy integration and regional power grid interconnection, due to its outstanding advantages in having no commutation failure, flexible control, and superior harmonic performance [173]. High Voltage Direct Current Transmission (HVDC) is considered a better solution for bulk long distance transmissions. The increased use of HVDC is a result of its advantages over the HVAC systems and especially due to its fault stability nature. A better solution is proposed by using a Voltage Source Controlled HVDC. The main advantage of the VSC converter is its flexible power control which enhances the stability of the transmission systems. Nowadays increasing HVDC transmission system introduces a mixed type of transmission system that is hybrid HVDC and HVAC transmission system in order to

defer the investment and make maximum utilization of the existing HVAC system. HVDC system is very much capable to connect all types of synchronous or asynchronous systems to the main grid. The characteristics of the AC and DC transmission system are different from the individual HVAC and HVDC transmission systems. An HVAC transmission system tends to have large inertia and known responses to disturbances. An HVDC transmission system generally has a low endurance to faults and can respond faster. A lot of complex dynamic and transient interactions can occur when the two transmission systems are interconnected. For instance, a single HVAC transmission system fault can lead to concurrent commutation failures in various converter stations. Aiming at maximizing the capacity of existing infrastructure and reducing the need for new transmission corridors, this work investigates the idea of converting existing multi-circuit AC transmission towers to hybrid AC/DC systems. The focus of this work is on the fault estimation related to the fault in the transmission lines of AC and DC corridor.

The Problem of fault detection, location and classification is a challenging task in the HVAC as well as HVDC transmission system as described in previous chapters. However, the problem becomes even more complicated for hybrid transmission systems, due to limited know approaches dealing with their protection and security simultaneously. The transmission line that includes both HVAC and HVDC plays an important role in transferring power across long distances from the generation end to the distribution end. Since, the performance of the transmission line affects the performance of the whole system. Therefore, on occurring a disturbance in the hybrid system both the transmission lines are affected equally, thus it becomes prudent to clear the disturbance in nick of time. In this concern, the protection scheme of an HVDC transmission must be very efficient to have reliable operation. This chapter utilizes the proposed F-SVM method for fault estimation in the hybrid transmission system. For validation of the proposed F-SVM fault estimation method three transmission test cases are considered under varying fault conditions.

5.2 Proposed F-SVM Fault Estimation Method

In this chapter, F-SVM fault estimation method is enhanced with Principal Component Analysis (PCA) approach that is proposed in previous chapter 4 and used for fault estimation of hybrid transmission systems. With using PCA approach feature extraction scheme is improved and used with defined feature functions that is already explained in the previous chapter. Details of PCA approach is describe in this section.

Principal Component Analysis was considered to be a suitable method for extracting feature from the $N \times 2$ dimensional data-set as current and voltage are interconnected quantities. PCA is a linear-algebra based projection technique that maps highly correlated features into a low dimensional space. The resultant feature vectors in this sub-space are non-correlated and orthogonal to each other. Mathematically, it represents an orthonormal basis transformation wherein the input data vectors are projected onto new basis vectors of an m dimensional feature space, where m is the number of features in the original data. The best way to represent a given data-set is to select those features:

- Along which the variance of data points is maximum
- Whose covariance with other features is minimum.

These two conditions also translate into the desired properties of low noise and reduced redundancy. The basic mathematics of PCA can be explained as follows:

Let $X \in R^m$ be a real-valued matrix having n samples or observations where each sample vector is a column. Hence X is arranged as a $m \times n$ data matrix which has to be represented by Y, of same dimension. Let P be a transformation matrix that converts X into a representation matrix Y such that the features of Y follow the two conditions mentioned above. Accordingly, P must be a $m \times m$ matrix that transforms X as in eq. (5.1).

$$PX = Y \tag{5.1}$$

The covariance matrix of Y is given by eq. (5.2) as,

$$Cov(Y) = \frac{1}{n-1} YY^T \tag{5.2}$$

The diagonal elements of $Cov(Y)$ represent the variance of each dimension while the off-diagonal elements are the covariances between different dimensions. To satisfy the two conditions given above, the values of diagonal elements must be high and those of the off-diagonal terms must be least. The best possible way to achieve this is to simply diagonalize this matrix. If P can be represented as collection of row vectors $\begin{bmatrix} p_1 & p_2 ... & p_m \end{bmatrix}^T$ Then,

Y can be expressed as in eq. (5.2).

$$Y = \begin{bmatrix} p_1x_1 & p_1x_2...p_1x_n \\ p_2x_1 & p_2x_2...p_2x_n \\ . & . & . \\ . & . & . \\ p_nx_1 & p_nx_2...p_nx_n \end{bmatrix} \tag{5.3}$$

When, X is a collection of column vectors, $\begin{bmatrix} x_1 & x_2... & x_n \end{bmatrix}$. It is evident from eq. (5.2) that the vectors of X are projected onto the vectors of P which now act as new basis vectors. Since basis vectors of a Euclidean vector space are always orthogonal, they must now be orthonormal so that the projection represents only a rotation, not a stretch or change in length. Therefore, now the task is to find P such that $Cov(Y)$ becomes a diagonal matrix. Also, the essential requirement becomes that P must be a matrix of orthonormal vectors. Using eq. (5.1), eq. (5.2) can be expanded into eq. (5.3) as,

$$\begin{aligned} Cov(Y) &= \frac{1}{n-1} PX(PX)^T \\ Cov(Y) &= \frac{1}{n-1} PXX^TP^T \\ Cov(Y) &= \frac{1}{n-1} PCov(X)P^T \end{aligned} \tag{5.4}$$

To diagonalize $Cov(Y)$, the basic PCA algorithm takes advantage of the fact that Eigen Value Decomposition (EVD) of a symmetric matrix results into orthogonal eigen vectors that can be normalized to unit length. $Cov(X)$ is an $m \times m$ symmetric matrix that can be expressed as in eq. (5.4) based on the standard EVD:

$$Cov(X) = EDE^{-1} \tag{5.5}$$

Here, E is the matrix of eigen vectors of $Cov(X)$ and D is a diagonal matrix of its eigen values. The EVD based PCA suggests the choice of P as $P = E^T$. To make the eigen vectors of $Cov(X)$ orthonormal, the matrix is mean-centered along the dimensions so as to normalize the length to 1. This makes P an orthonormal matrix for whom $P^T = P^{-1}$. Using eq. (5.3), eq. (5.4) can be further expanded to result into eq. (5.5) as,

$$
\begin{aligned}
Cov(Y) &= \frac{1}{n-1} P(EDE^{-1})P^T \\
Cov(Y) &= \frac{1}{n-1} P(EDE^{-1})P^{-1} \\
Cov(Y) &= \frac{1}{n-1} P(P^T DP^{T-1})P^T \\
Cov(Y) &= \frac{1}{n-1} P(P^T DP^{-1-1})P^T \\
Cov(Y) &= \frac{1}{n-1} P(P^T DP)P^T \\
Cov(Y) &= \frac{1}{n-1} (PP^T)D(PP^T) \\
Cov(Y) &= \frac{1}{n-1} (PP^{-1})D(PP^{-1}) \\
Cov(Y) &= \frac{1}{n-1} D
\end{aligned}
\tag{5.6}
$$

Thus the selection of P as E^T made $Cov(Y)$ a diagonal matrix. There is another version of PCA in which the Singular Value Decomposition (SVD) of the input data matrix is used to diagonalize the required matrix. In this approach, the data matrix X is decomposed into two orthogonal and one diagonal matrix as in eq. (5.6).

$$X = U\Gamma V^T \tag{5.7}$$

Here, U is a $n \times m$ matrix with orthonormal columns, V is a $m \times m$ orthonormal matrix and Γ is a $m \times m$ diagonal matrix of singular values. The columns of U are orthonormal eigen vectors of XX^T, columns of V are orthonormal eigenvectors of $X^T X$ and singular values contained in Γ are the square roots of eigen values from U or V in a descending order.

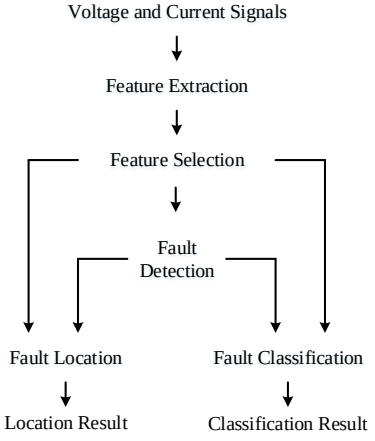

FIGURE 5.1: Working steps of the proposed F-SVM fault estimation method

With the use of PCA approach the proposed F-SVM method enhanced the property of fault estimation for large and complex hybrid transmission systems. Working steps of proposed F-SVM fault estimation method shown in Figure 5.1.

5.3 DC Grid Control Strategies

This chapter uses different control strategies for the hybrid HVAC and HVDC transmission systems. Therefore, this section describes the different control strategies used for the hybrid systems as per the economical and modern trends. The test cases used in this chapter are also designed in accordance with the control strategies.

5.3.1 DC Voltage Control in DC System

DC voltage plays a similar role in DC systems as the frequency in AC systems. VSC converters cannot work with small DC voltage (normally below 0.8–0.9 pu) due to uncontrollable diodes. Due to insulation limits, high DC voltage is strictly forbidden. However, DC voltage changes at different buses due to change in DC power flow. This considerably complicates the creation of the DC voltage regulator and any method for controlling power balancing. DC voltage dynamics in electro-mechanical AC devices are much faster than frequency deviations, whereas, time constants may be even below 10 milliseconds. This shows the consequence of quick converter control, absence of reactive components in DC cable impedances and absence of mechanical inertia. Therefore, the requirement of developing a robust DC voltage controller with wider bandwidth at every VSC terminal is very essential.

5.3.2 Droop Control at VSC Converter

A normal method for exchanging power balancing between all terminals is the DC voltage droop control at VSC converters. This method is created mainly with static curves (P-V, I-V) [174, 175] indicating deviations in DC voltage for load changing circumstances and vice versa. Figure 5.2 shows the line diagram of the VSC converter with DC Voltage droop control method. To regulate the converter current in dq frame, the inner control loop uses a conventional PI controller using decoupling loops. However, to regulate AC voltage or reactive power flow on q-axis and DC voltage or active power flow on d-axis the

outer control loop is used. In every DC grid, only one terminal controls DC voltage and others will regulate active power flow with DC voltage droop feedback ($K_{DCdroopgain}$) [176].

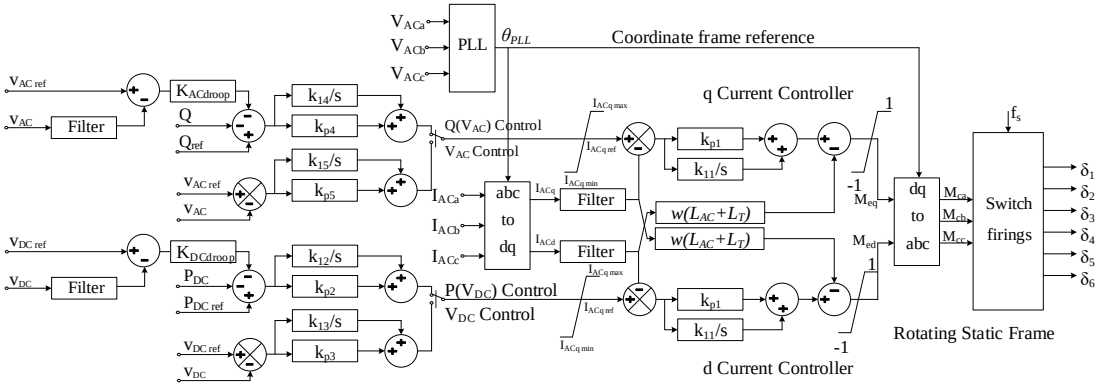

FIGURE 5.2: Schematic diagram of the VSC controller with typical droop DC voltage feedback

5.3.3 3-Level Cascaded Control at VSC Terminal

Cascade control is a renowned control method in the progression industries which split the control problem in two or even more nested control loops [177]. It enhances dynamic performance by regulating intermediate variables and limiting their reference values. It also allows zero error monitoring of variables at each stage, providing essential control without utilizing DC saturation. It will extract power-droop feature from the terminals as it will provide grid stabilization for quick control of DC voltage. Figure 5.3 describes the outer and middle control loops of the suggested 3-LCC on-shore VSC d-axis approach. Even though, the droop control described in Figure 5.2 is same as the inner current control loop.

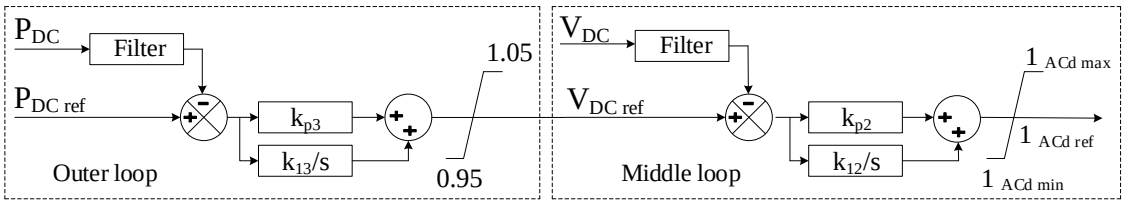

FIGURE 5.3: Schematic diagram of the control structure of 3-LCC for d-axis of VSCs

5.3.4 Dispatcher Center Controller

The dispatcher's duty is to return the power references to each terminal corresponding to the real position in the entire system and the arrangement for power trading. The dispatcher's duty is supposed to be a slow process and can be done manually or automatically as per the requirement. However, the dispatcher should normally be prepared to modify power references to follow the typical variation in load/generation such as variation in wind speed. The construction of the automatic dispatcher controller is shown in Figure 5.4. This is same as that of the DC voltage droop controller. Although, the time constant is less as compared with conventional terminal control droop.

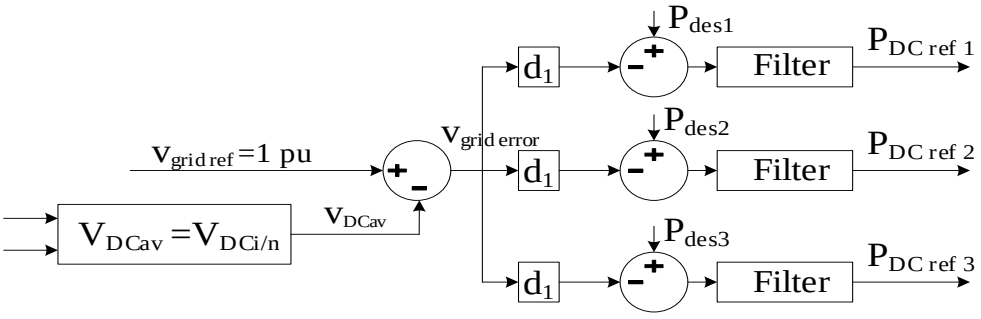

FIGURE 5.4: Schematic diagram of the control structure dispatcher center

5.3.5 DC/DC Converter Control

DC grids are using DC/DC converters [178]. Therefore, same topology is also used in the CIGRE B4 DC grid test system [176, 179]. In this work, as shown in Figure 5.5, a comparable 3-LCC approach is implemented for DC/DC converters. A humble DC chopper is used as the DC/DC topology and the duty ratio D of the control signal.

5.3.6 Wind Farm VSC Converter Control

The VSC converters linked to wind farms are regulated to establish the frequency of the offshore AC systems and keep the equilibrium of power in the offshore grid [176]. These converters restrict the variations associated with the wind power and provide a constant output power supply. Therefore, these converters are considered as constant power sources

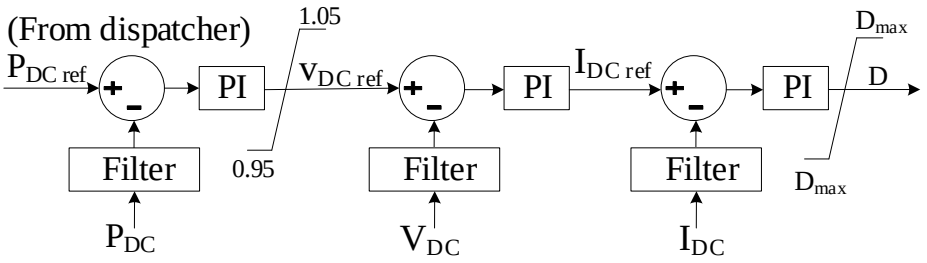

FIGURE 5.5: Schematic diagram of the control structure of the DC/DC converter

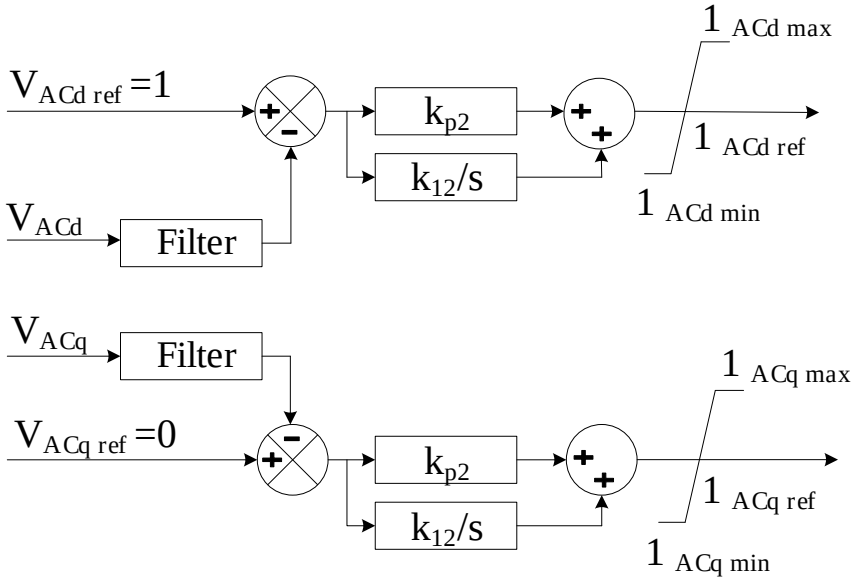

FIGURE 5.6: Schematic diagram of the control structure of the wind farm VSC converter

in the DC grid. Moreover, these converters pose two-level control topology. As shown in Figure 5.6, the outer control loop regulate the respective AC voltage dq-components. And that's how the converter balances offshore island power. Note that, based on future grid connection standards, a DC grid may also have other uncontrollable power converters.

5.4 Test System for Simulation

To validate the proposed method, two hybrid HVAC and HVDC transmission test systems have been taken into consideration that are two terminal hybrid HVAC and HVDC

transmission test system and CIGRE DC grid transmission test system have been used as shown in Figures 5.7 and 5.16 respectively. The CIGRE benchmark transmission model available with PSCAD/ EMTDC module is originally a model for mono-polar two-terminal. It is modified into bipolar two and multi-terminal hybrid transmission test system with VSC control.

From the literature [169–171, 173], it found that Voltage Source Converter (VSC) is preferred for controlling the Power flow in both HVDC as well as hybrid HVAC and HVDC transmission system due to better controllability. Some of the advantages and controlling strategies of VSC control are discussed in section 4.3. The same VSC control is use here for controlling DC line voltage and power flow.

5.4.1 Case-1: Two Terminal Hybrid Transmission Test System

To validate the proposed method, a two-terminal hybrid HVAC and HVDC transmission test system has been used as shown Figure 5.7. The two-terminal is connected with transmission line having the total length of 800 km that is 600km in DC line and 200km in AC line. Four types of faults in DC line and ten types of faults in AC line at every 10 km is simulated in the line. With this condition, the data-set is prepared for training and testing purpose for the proposed algorithm. The transmission line structure along with their configuration is given in Figure 5.8.

Performance of VSC based hybrid HVDC system has been simulated under these circuit specification. The voltage source connected at bus-1 in terminal-1 is terminal voltage of

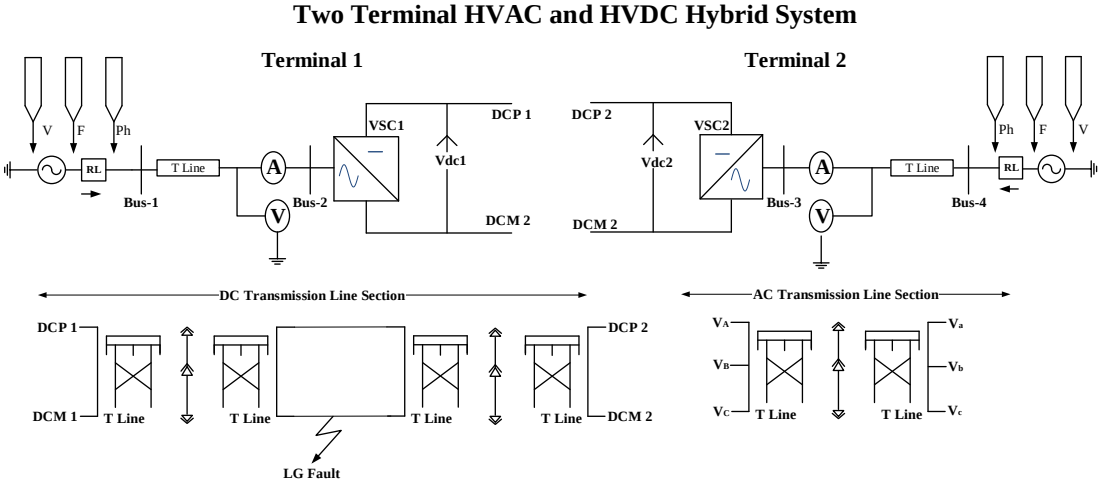

FIGURE 5.7: Schematic diagram of two terminal hybrid transmission test system

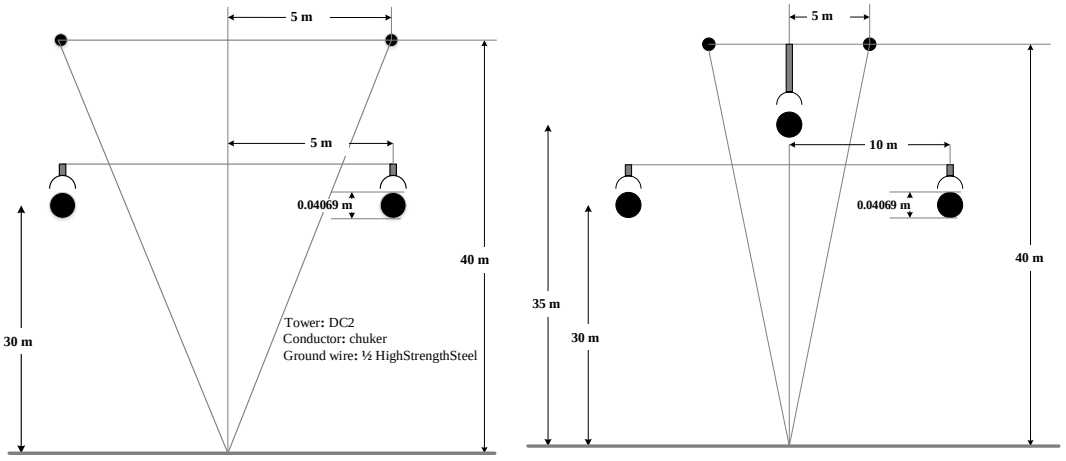

(a) DC Line Cable Configuration (b) AC Line Cable Configuration

FIGURE 5.8: Tower configuration of hybrid transmission Line

13.8kV, active power of 100MVA, and frequency of 60Hz. The AC transmission line of 100km in length is connected between bus-1 and bus-2 at terminal-1. Terminal-1 consist of PWM controlled IGBT based rectifier/inverter having specification as, the terminal voltage 230kV, on-resistance 0.005Ω, off-resistance $100M\Omega$, breakdown voltage 100MV, reverse withstand voltage 100MVA with PWM control. The transformer used at terminal-1 is a 13.8/62.5kV ($\Delta - Y$), Y-side solid grounded at 100MVA. RC Damped Capacitor connected at terminal-1 as capacitance $1000\mu F$ and resistance 0.5Ω. The specification of the voltage source connected at bus-4 in terminal-2 is terminal voltage 420kV, active power 100MVA, and frequency 60Hz. The AC transmission line of 100km in length is connected between bus-3 and bus-4 at terminal-2. Terminal-2 consist of PWM controlled IGBT based

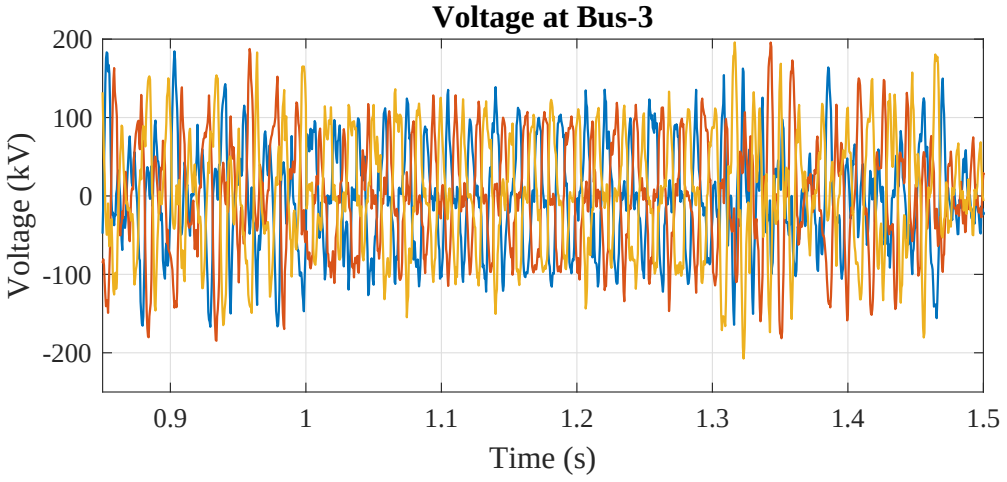

FIGURE 5.9: Voltage at bus-3 at time of fault (case-1)

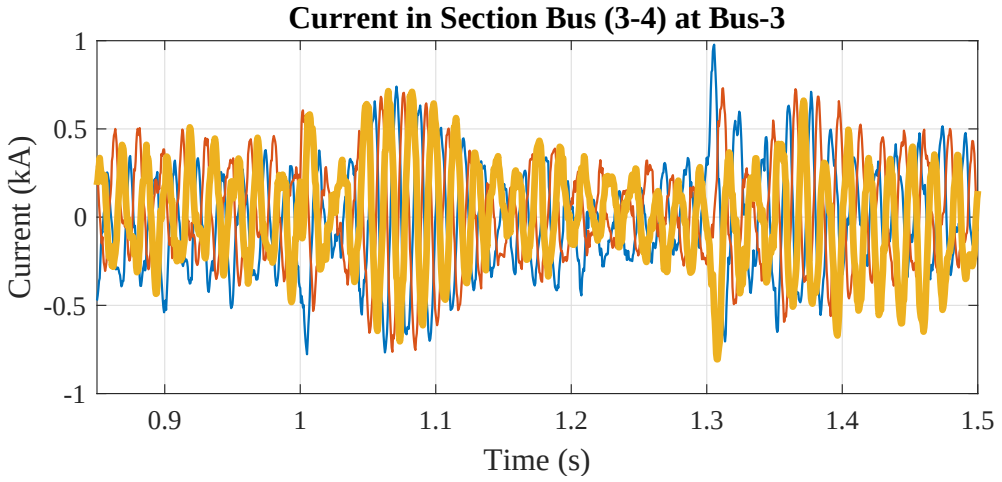

FIGURE 5.10: Current at bus-3 at time of fault (case-1)

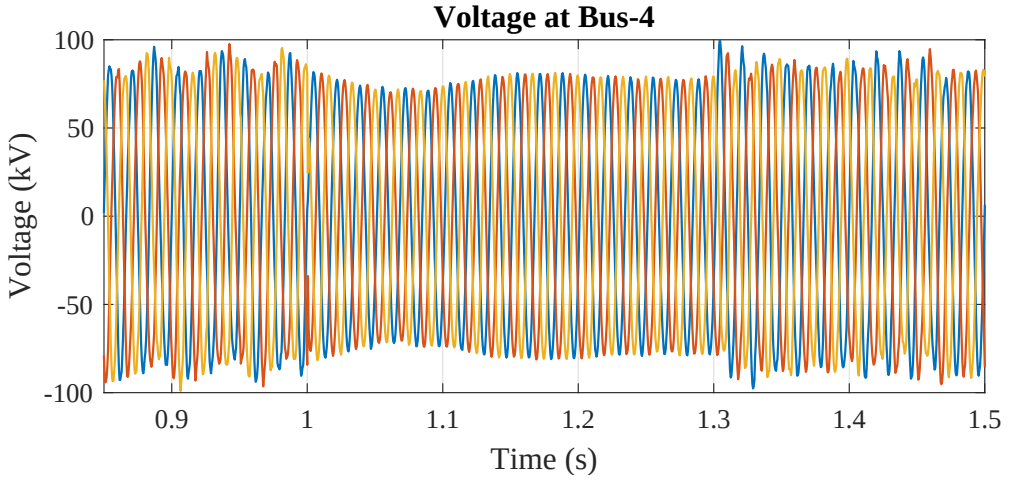

FIGURE 5.11: Voltage at bus-4 at time of fault (case-1)

rectifier/inverter having specification as, the terminal voltage 230kV, on-resistance 0.005Ω, off-resistance $100M\Omega$, breakdown voltage 100MV, reverse withstand voltage 100MVA with PWM control. The transformer used at terminal-2 is a 115kV/62.5kV $(Y - \Delta)$ Y-side solid grounded at 100MVA. Smoothing capacitance of $2\mu F$ is connected at terminal-2. Transmission cable connects a terminal (1-2) with specifications as voltage rating 169kV and current withstand capacity of 0.5kA.

The length of transmission line is 200km in the AC section and 600 km in DC section. Fourteen different types of fault are simulated at every 10 km i.e. at 77 different location at 1s for a duration of 0.3s (approx. 10 cycles). The collected data for every sample is having a sampling frequency of 4.8 kHz. Once the transient fault occurs in the DC section of the system, the line voltage immediately falls, whereas on the inverter side, the DC

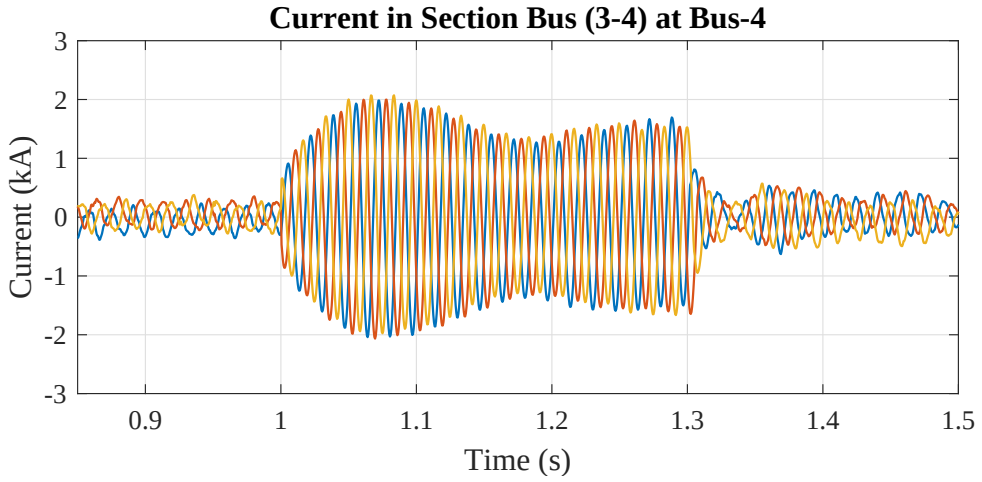

FIGURE 5.12: Current at bus-4 at time of fault (case-1)

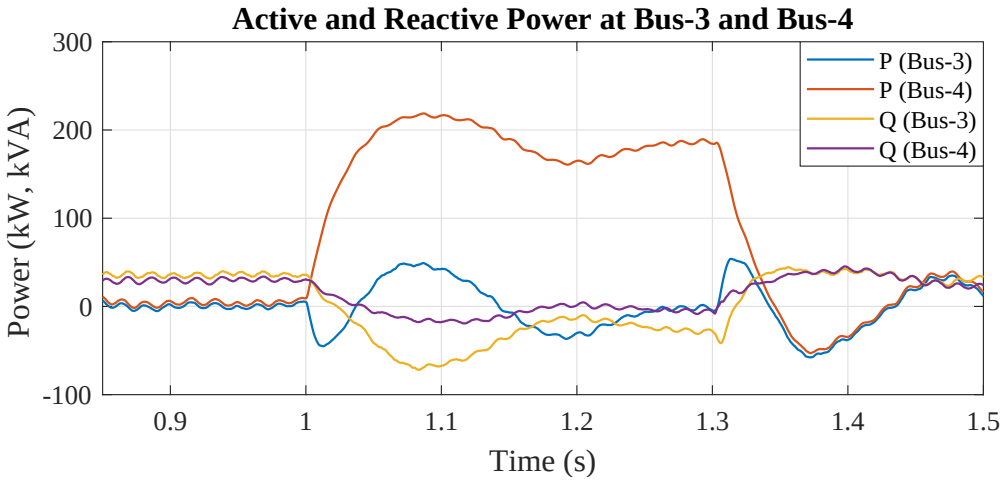

FIGURE 5.13: Active and reactive power at bus-3 and bus-4 at time of fault (case-1)

current falls and on rectifier side DC current rises. Therefore, in order to maintain this current is at some predefined level, a control circuit is required. The pre-defined value is selected in accordance with the DC voltage. During the fault event, this DC voltage will tend to reduce to a lower value to its threshold value. Therefore, this will bring down the line current to a lower value. It is advisable to limit this current to +ve non-zero value. If it goes beyond this value the reactive power demand on the AC part of the system reduces, thereby preventing the system to restore. Once the transient fault occurs in the AC section of the system, the line voltage of the connected bus immediately falls and line current rise. It also effects on the DC section transmission line voltage and current.

LLL-Fault is created in AC line at connecting bus-3 and bus-4 in terminal-2 at 10km far from bus-4 in terminal-2. Figures 5.9 and 5.10 show the AC voltage and current at

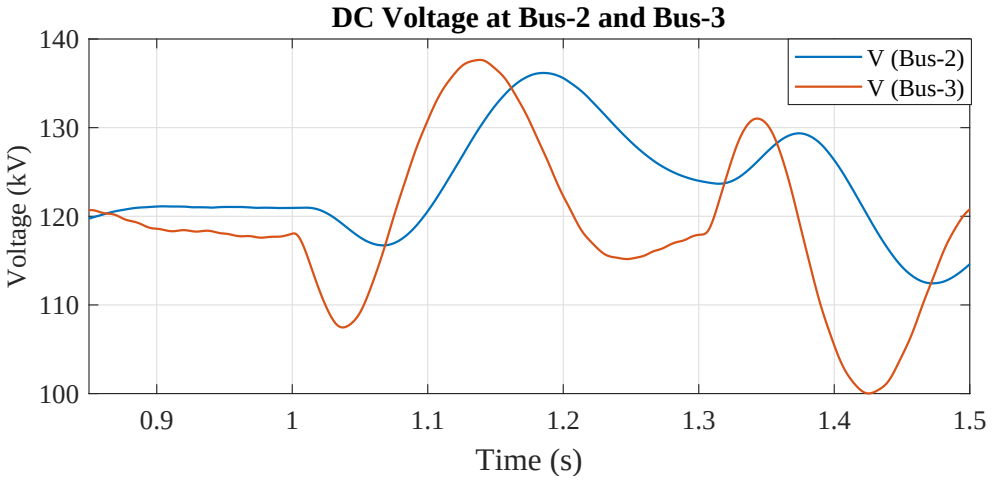

FIGURE 5.14: Dc Voltage at bus-2 and bus-3 at time of fault (case-1)

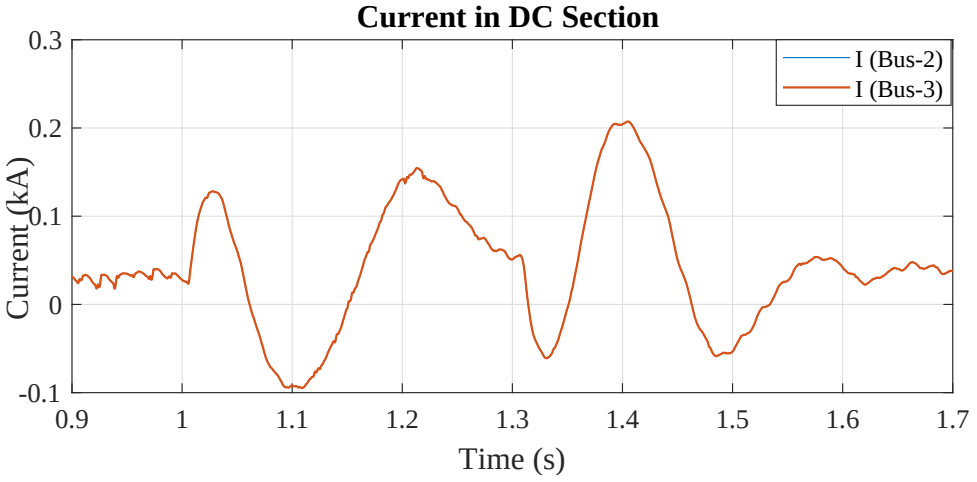

FIGURE 5.15: Current at bus-2 and bus-3 at time of fault (case-1)

bus-3 in terminal-2. Line voltage decreases nearly 24% and line current increases nearly 66% at bus-3 in terminal-2 as shown in Figures 5.9 and 5.10 respectively at the time of fault. Figures 5.11 and 5.12 show the generator side AC voltage and current at bus-4 in terminal-2. Line voltage decreases by 35% and line current increases closely 300% at bus-4 in terminal-2 as shown in Figures 5.11 and 5.12 respectively at the time of fault. Figure 5.13 shows the active reactive power variation at bus-3 and bus-4 in terminal-2 respectively at the time of fault. Active power at bus-3 rise to a maximum of 800% and at bus-4 rise to a maximum of 3000%. Reactive power at bus falls at bus-3 a maximum of 400% and at bus-4 a maximum of 200%. Figures 5.14 and 5.15 show the DC voltage and current at bus-2 and bus-3. DC voltage at bus-2 rises with nearly 7% and DC voltage at bus-3 rise with nearly 17% shown in Figure 5.14. DC current at bus-2 and at bus-3 rise

TABLE 5.1: Definition of class with respect to different types of fault

Class-1	Phase A to Ground Fault in AC Section
Class-2	Phase B to Ground Fault in AC Section
Class-3	Phase C to Ground Fault in AC Section
Class-4	Phase A to Phase B Fault in AC Section
Class-5	Phase A to Phase C Fault in AC Section
Class-6	Phase B to Phase C Fault in AC Section
Class-7	Phase A to Phase B to Ground Fault in AC Section
Class-8	Phase A to Phase C to Ground Fault in AC Section
Class-9	Phase B to Phase C to Ground Fault in AC Section
Class-10	Phase A to Phase B to Phase C Fault in AC Section
Class-11	Positive Phase to Ground Fault in DC Section
Class-12	Negative Phase to Ground Fault in DC Section
Class-13	Positive to Negative Phase Fault in DC Section
Class-14	Positive to Negative Phase to Grounds Fault in DC Section

with nearly 1000% shown in Figure 5.15 respectively. It is observed that DC line current contains more harmonic as compared to AC line current. In this work 14 different faults are simulated which are shown in Table 5.1.

5.4.2 Case-2: CIGRE (B4.57 and B4.58) Hybrid Transmission Test System

To validate the proposed algorithm, the CIGRE (B4.57 and B4.58) hybrid HVAC and HVDC transmission test system has been used as shown in Figure 5.16. Several control strategies and DC grid models presented in section 5.3 are utilized to develop the CIGRE test model. The key attribute of this test system is to provide a dynamically varying system in real time in DC as well as AC section via VSC control mechanism [179,180]. The layout of this test transmission system is shown in Figure 5.16. The following categorization is used for buses and converters: B_a : bus onshore AC (onshore AC bus) B_o : bus offshore AC (offshore AC bus) B_m : bus monopole (DC bus at monopole 400KV system) B_b : bus bipole (DC bus at bipole 800KV DC system) C_m : converter monopole C_b : converter bipole C_d : DC/DC converter

The complete CIGRE hybrid HVAC and HVDC system is developed in PSCAD/EMTDC environment. Two distinct control choices are considered for all onshore and DC/DC converter as 3-LCC control and droop control are shown in Figures 5.3 and 5.2 respectively [173], [181]. In Figure 5.5, the controller gains for DC/DC converters and onshore VSCs (d-axis) of the two control methods are presented. For both these methods, the

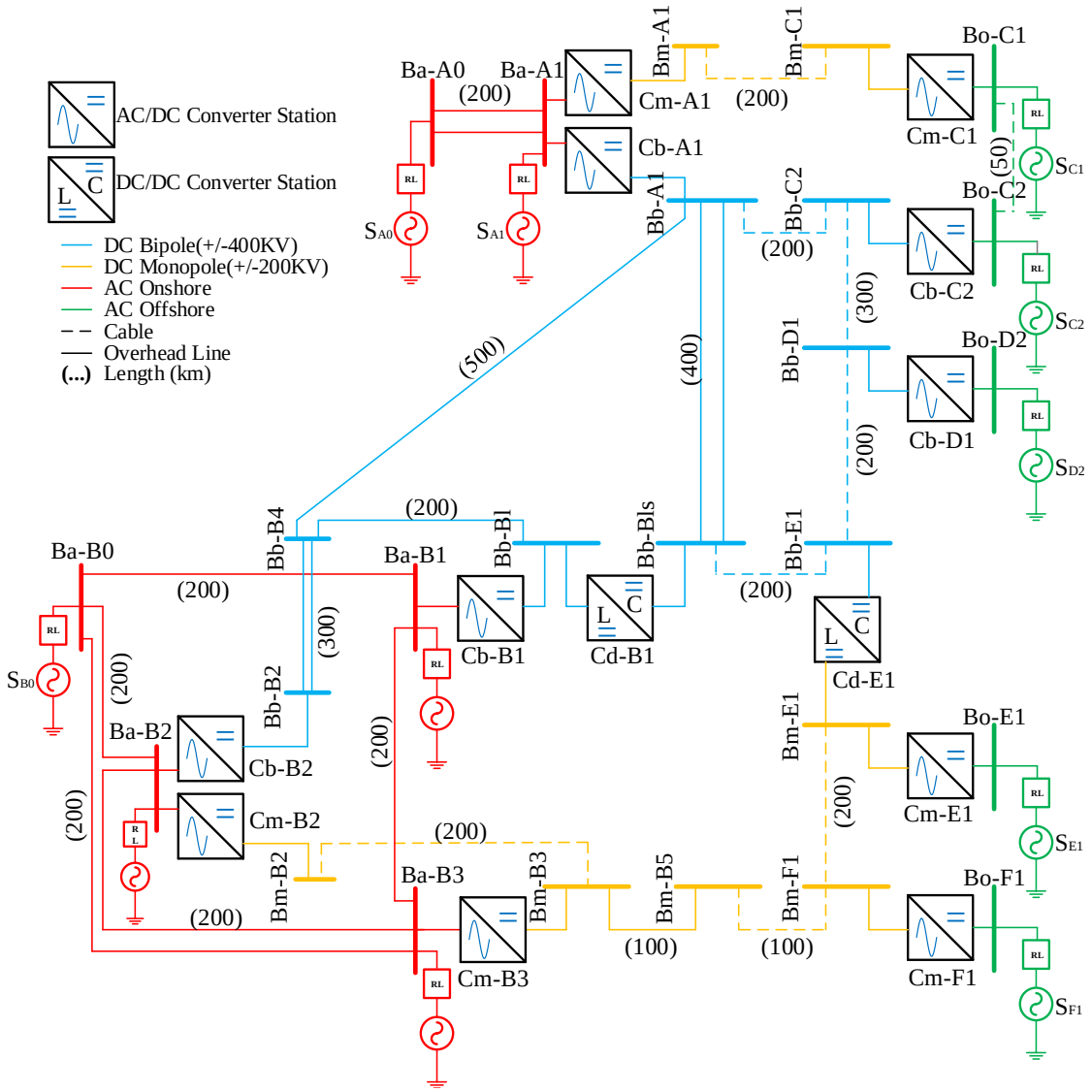

FIGURE 5.16: Schematic diagram of CIGRE (B4.57 and B4.58) hybrid transmission test system

gain for inner current control loops is same and are designed considering a VSC converter control. However, the AC grid is taken as a separate entity. The PI gains for the outer loop of Dc voltage terminal ($C_m - A_1, C_b - A_1, and\ \ C_m - B_3$) in droop control method are $k_p - 0.5$ and $k_i = 10$. All the controller input and output variables are in per unit system.

in order to not interfere with the inner loop dynamics the control is sufficiently slow while the outer control gains are designed to be enabled with droop control. According to the requirement of dynamic responses in the system, the droop gain is varied. With 3-LCC method, a VSC controller is considered for designing the middle loop so as to provide a buffer between AC and DC sections. The gains are increased accordingly to

enable DC voltage control with up-to 20% overshoots. The high value for dispatcher gains ($d_1 = d_2 = ...d_n = 10$) are selected to enable good steady-state control of average DC voltage, while the dispatcher filter time constant is taken as $2s$. The dispatcher droop feedback dynamics are eliminated by this low bandwidth filtering process, which highly influences the dynamics of the DC grid. The hybrid transmission test system details configuration with all data used in the designing of the system is provided in Appendix A.3.

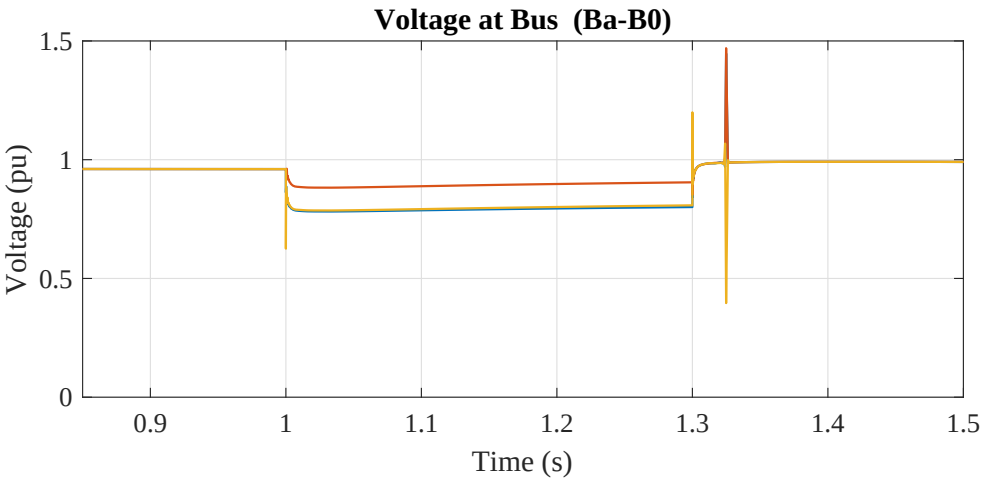

FIGURE 5.17: Voltage at bus (Ba-B0) at the time of fault (case-2)

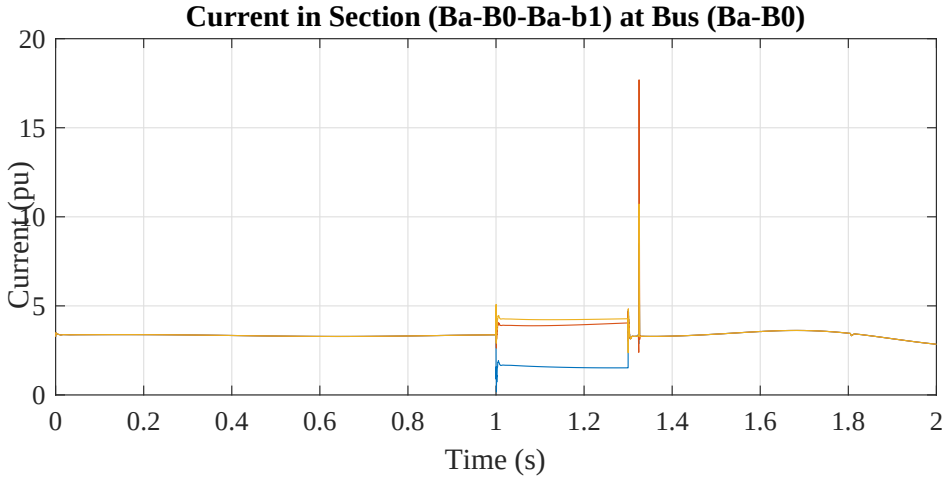

FIGURE 5.18: Current at bus (Ba-B0-Ba-b1) at bus (Ba-B0) at the time of fault (case-2)

The length of the total transmission line is 5250 km and ten types of fault with fault resistance 5Ω in the AC section and four types of fault with fault resistance 5Ω in the DC section are created at 1 second for a duration of 0.3 seconds (approx 10 cycles) at every 10 km i.e. at 525 different location, considering that minimum one event in each and every section even if the length is less then 10km. The collected data for each sample is

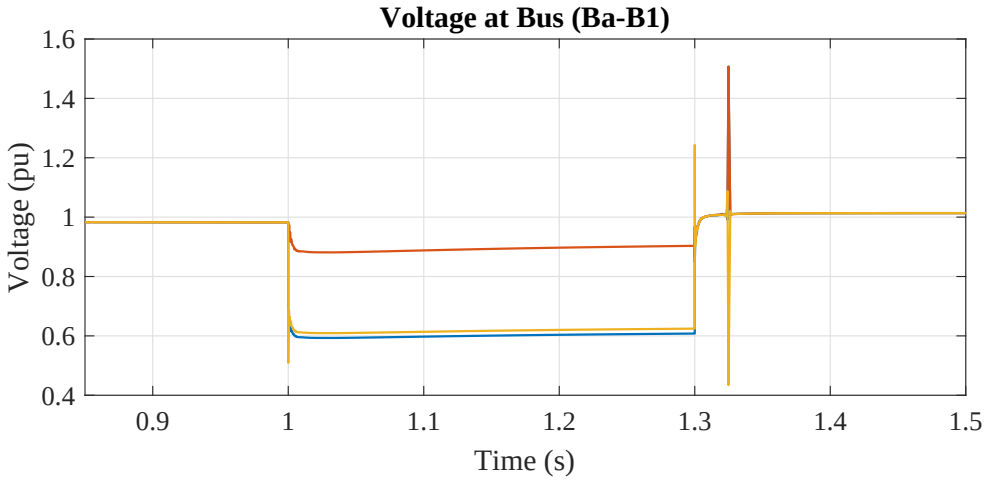

FIGURE 5.19: Voltage at bus (Ba-B1) at the time of fault (case-2)

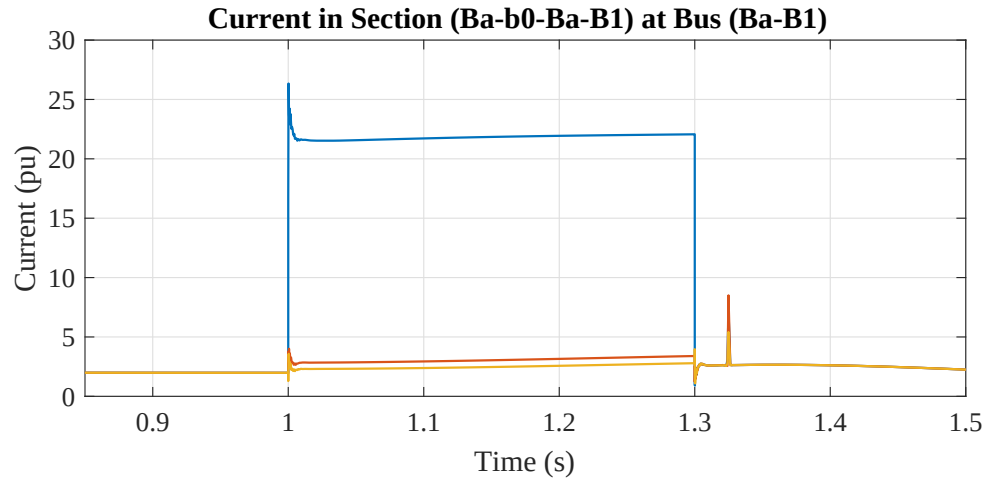

FIGURE 5.20: Current at bus (Ba-b0-Ba-B1) at bus (Ba-B1) at the time of fault (case-2)

having the sampling frequency of 4.8 kHz. Once the transient fault occurs in the system, the line voltage of both terminal ends immediately falls but in this system the effect on other section very less especially in the DC section due to VSC and 3LCC droop control strategies. For a better understanding of the fault situation, one fault case among all cases in one of the AC section in the transmission line is created and discussed below.

LLG-Fault is created in line section $((B_a - B_0) - (B_b - B_4))$ at connecting bus $((B_a - B_0) - (B_b - B_4))$ at 100km far from bus-$(B_a - B_0)$ whereas, the total line length of the section $((B_a - B_0) - (B_b - B_4))$ is 200km. Figures 5.17 and 5.18 show the voltage and current at bus-$(B_a - B_0)$. The voltage of two phases of bus-$(B_a - B_0)$ decreases nearly by 30.20% and one phase decrease nearly by 20.4% are shown in Figure 5.17 at the time of the

fault. Current of two phases in section $((B_a - B_0) - (B_b - B_4))$ at bus-$(B_a - B_0)$ increase nearly 12.64% and one phase decrease nearly by 50.24% are shown in Figure 5.18 due to a LLG fault present in this section. Figures 5.19 and 5.20 show the voltage and current at bus-$(B_b - B_4)$. The voltage of two phases of bus-$B_b - B_4$ decreases nearly by 38.73% and one phase decrease nearly by 10.23% are shown in Figure 5.19 at the time of the fault. Current of in section $((B_a - B_0) - (B_b - B_4))$ at bus-$(B_b - B_4)$ increase nearly by 825%, 20.3% and 40.2% of respected phases as shown in Figure 5.20 due to a LL fault present in this section. It is observed that at the time of LLG fault respected phase voltage decreases at both the bus and phase current increases respectively. It is also observed that current and voltage has harmonic content due to the presence of the fault. Due to fault present in this section it does not effect much in the nearby DC section due to control action of controllers. After clearing of fault harmonic content is settled down in a few cycles. In this work 14 different faults cases are simulated which are shown in Table 5.1.

5.4.3 Case-3: IEEE 30-Bus Transmission Test System

The IEEE 30-bus system is used for carrying out the simulation, where the data collected from the phase measurement unit (PMU) installed at different buses in the system. The system is modelled with an electromagnetic transient program available in power system design (PSCAD/ EMTDC) using the IEEE dynamic data. In order to have a realistic

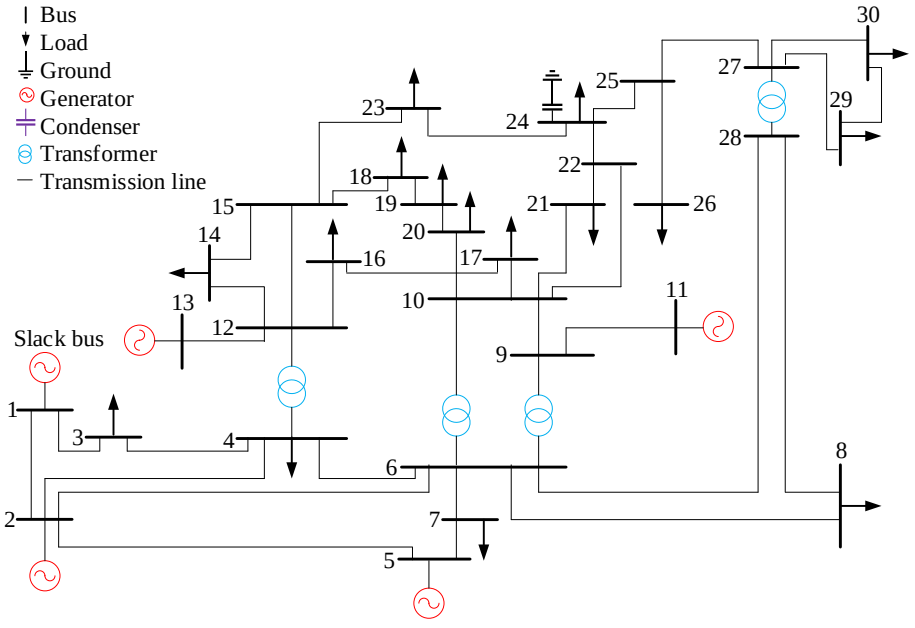

FIGURE 5.21: Schematic diagram of IEEE 30-bus dynamic transmission test system

system condition, the transmission line is modelled with a frequency dependent model. The schematic line diagram of the system model is shown in Figure 5.21. The IEEE-30 bus details configuration with all data used in the designing of the system is provided in Appendix A.1.

The length of total transmission line is 2363.72 km and the ten types of fault is created at every 10 km i.e. at 208 different location, considering that minimum one event in each and every section even if the length is less then 10 km at 1s for a duration of 0.3s (approx 15 cycles). the collected data for every sample is having the sampling frequency of 4.8 kHz. Once the transient fault occurs in the system, the line voltage of both terminal ends immediately fall. For a better understanding of the fault situation, one fault case among 10 cases in one of the section in the transmission line is created discussed below.

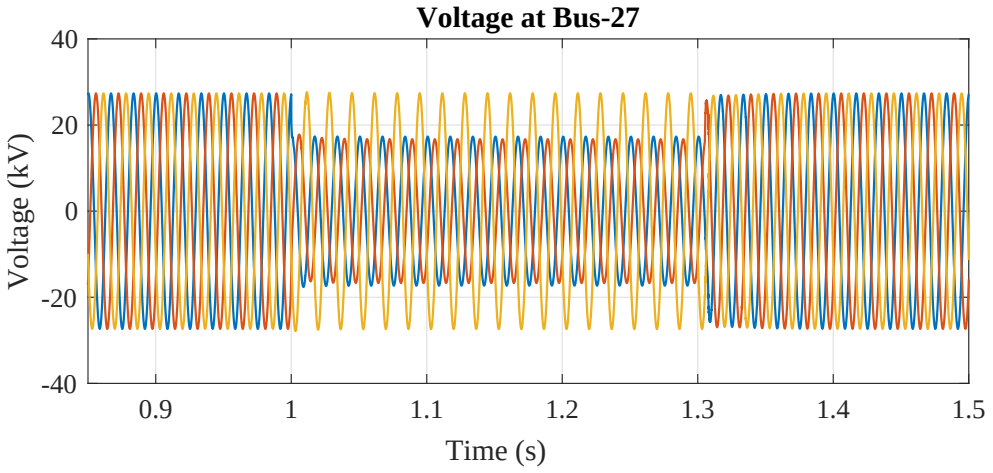

FIGURE 5.22: Voltage at bus-27 at the time of fault (case-3)

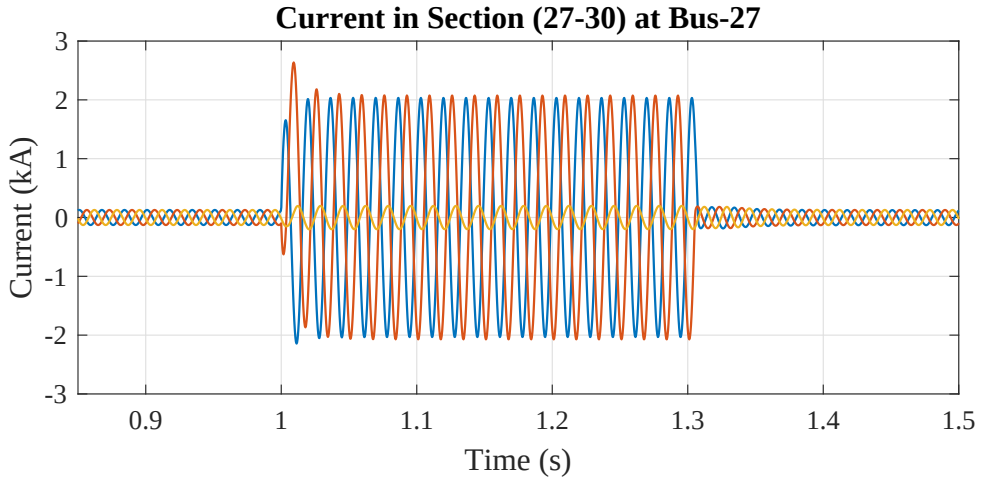

FIGURE 5.23: Current in section(27-30) at bus-27 at time of fault (case-3)

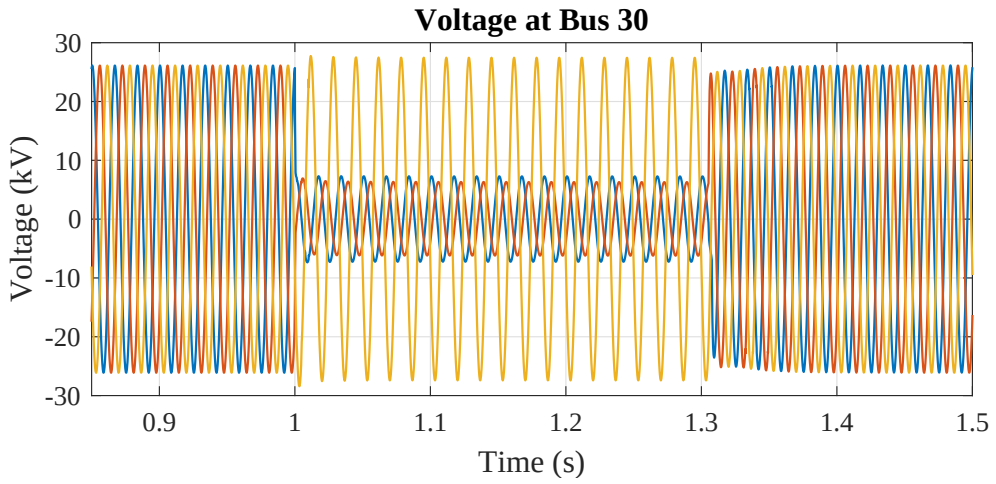

FIGURE 5.24: Voltage at bus-30 at the time of fault (case-3)

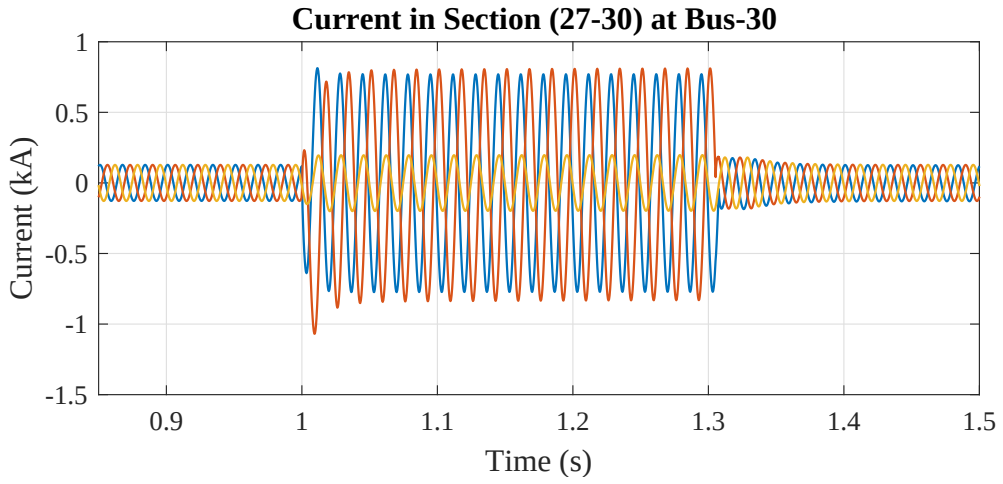

FIGURE 5.25: Current in section(27-30) at bus-30 at time of fault (case-3)

LL-Fault is created in line section (27-30) at connecting bus (27-30) at 100km far from bus 27 whereas, the total line length of the section (27-30) is 210km. Figures 5.22 and 5.23 show the voltage and current at bus-27. The voltage of concerned two phases of bus-27 decreases nearly by 33.34% and current of concerning two phases in section (27-30) at bus-27 increase nearly by 900% and rest phase is not much affected shown in Figures 5.22 and 5.23 due to a LL fault present in this section. Figures 5.24 and 5.25 show the voltage and current at bus-30. The voltage of concerning two phases of bus-27 decreases nearly by 73.23% and current of concerning two phases in section (27-30) at bus-27 increase nearly by 105% and rest phase is not much affected shown in Figures 5.22 and 5.23 due to a LL fault present in this section. Figure 3.28 shows the active power and reactive power response at bus-27 and bus-30 at the time of the fault. Active power at bus-27 increases

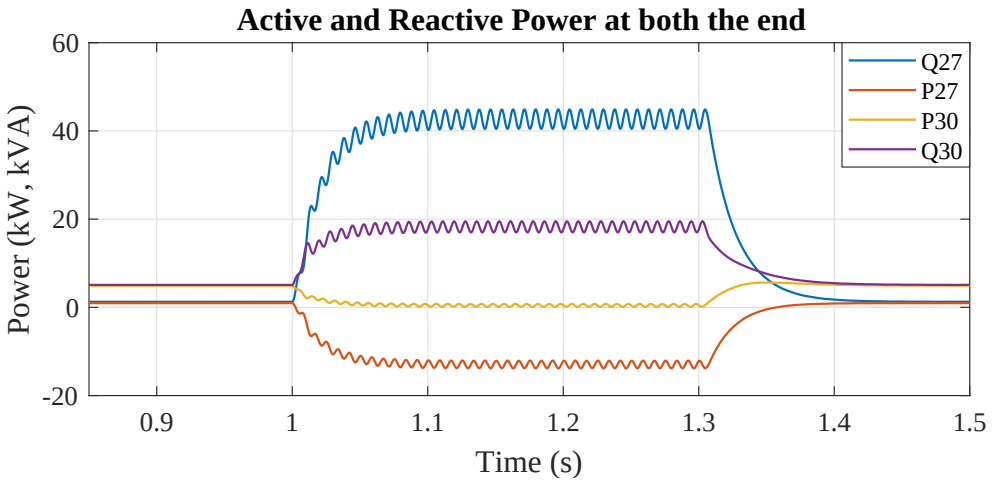

FIGURE 5.26: Power of both the buses at the time of fault (case-3)

nearly by 280% and at bus-30 decrease nearly by 90% shown in Figure 3.28 due to a LL fault present in this section. Reactive power at bus-30 increases nearly by 342% and at bus-30 increases nearly by 1304% shown in Figure 3.28 due to a LL fault present in this section. It is observed that at the time of LL fault respective phase voltage decreases at both the bus and phase current increases respectively. Along with, it is also observed that current and voltage has harmonic content due to the presence of the fault. After clearing of fault harmonic content is settled down in a few cycles. In this work 10 different faults cases are simulated which are shown in Table 5.1.

5.5 Results and Discussions

The flowchart shown in Figure 5.1 provides working steps of the proposed F-SVM fault estimation method. The voltage and current signal of AC and DC side is continuously measured and recorded at the converter station of the system. The feature vector is extracted and dominant feature is selected with the help of modified F-score scheme for every half cycle measured data of the running window. These dominant features are observed continuously to detect the presence of a fault. Once the fault is detected by F-SVM fault detection scheme4.2.5. The same half cycle data are used to locate and classify the fault with the help of F-SVM fault location (4.2.6) and F-SVM classification scheme (4.2.7) respectively.

5.5.1 Case-1: Two-terminal Hybrid Transmission Test System

For the training purpose of F-the SVM fault estimation method four types of faults in DC section and ten types of faults in AC section are created in the transmission lines at every 10 km of the length, the data is measured and collected. The data contains 77 instant samples of fourteen different classes, and 364 features are extracted. From all these extracted features 205 dominating features are selected with a modified F-score scheme. 10-fold cross-validation RBF kernel function with 70% data used for training and 30% for testing purpose of F-SVM fault estimation method.

5.5.1.1 Outcomes with F-SVM Fault Detection Scheme

TABLE 5.2: Result obtained with F-SVM fault detector scheme in AC section (case-1)

Fault Type	**Fault Location** (km)	**Fault Inception Instant** $(T_i)s$	**Fault Detection Instant** $(T_d)s$	**Response Time** $(T_r = T_d - T_i)ms$
Class-1	25	0.2	0.2028	2.8
		0.3	0.3025	2.5
		0.4	0.4041	4.1
	50	0.2	0.2042	4.2
		0.3	0.3017	1.7
		0.4	0.4030	3.0
	75	0.2	0.2028	2.8
		0.3	0.3036	3.6
		0.4	0.4038	3.8
Class-4	25	0.2	0.2021	2.1
		0.3	0.3037	3.7
		0.4	0.4040	4.0
	50	0.2	0.2017	1.7
		0.3	0.3015	1.5
		0.4	0.4030	3.0
	75	0.2	0.2048	4.8
		0.3	0.3024	2.4
		0.4	0.4033	3.3
Class-7	25	0.2	0.2040	4.0
		0.3	0.3020	2.0
		0.4	0.4030	3.0
	50	0.2	0.2038	3.8
		0.3	0.3046	4.6
		0.4	0.4048	4.8
	75	0.2	0.2032	3.2
		0.3	0.3016	1.6
		0.4	0.4016	1.6
Class-10	25	0.2	0.2044	4.4
		0.3	0.3020	2.0
		0.4	0.4043	4.3
	50	0.2	0.2020	2.0
		0.3	0.3047	4.7
		0.4	0.4022	2.2
	75	0.2	0.2018	1.8
		0.3	0.3020	2.0
		0.4	0.4035	3.5

To test the suitability of the F-SVM fault detection scheme, different types of fault in the overhead transmission line of AC section near terminal-1 at 25 km, 50 km, 75 km and in DC section 50 km, 300 km, 500 km are created. The test results of the detection

TABLE 5.3: Result obtained with F-SVM fault detector scheme in DC section (case-1)

Fault Type	**Fault Location** (km)	**Fault Inception Instant** $(T_i)s$	**Fault Detection Instant** $(T_d)s$	**Response Time** $(T_r = T_d - T_i)ms$
Class-11	50	0.2	0.2024	2.4
		0.3	0.3043	4.3
		0.4	0.4033	3.3
	300	0.2	0.2032	3.2
		0.3	0.3047	4.7
		0.4	0.4021	2.1
	500	0.2	0.2040	4.0
		0.3	0.3040	4.0
		0.4	0.4025	2.5
Class-12	50	0.2	0.2013	1.3
		0.3	0.3012	1.2
		0.4	0.4031	3.1
	300	0.2	0.2041	4.1
		0.3	0.3047	4.7
		0.4	0.4016	1.6
	500	0.2	0.2033	3.3
		0.3	0.3029	2.9
		0.4	0.4010	1.0
Class-13	50	0.2	0.2016	1.6
		0.3	0.3042	4.2
		0.4	0.4022	2.2
	300	0.2	0.2031	3.1
		0.3	0.3017	1.7
		0.4	0.4034	3.4
	500	0.2	0.2040	4.0
		0.3	0.3036	3.6
		0.4	0.4038	3.8
Class-14	50	0.2	0.2028	2.8
		0.3	0.3013	1.3
		0.4	0.4019	1.9
	300	0.2	0.2047	4.7
		0.3	0.3028	2.8
		0.4	0.4043	4.3
	500	0.2	0.2032	3.2
		0.3	0.3050	5.0
		0.4	0.4013	1.3

scheme in AC section and in DC section are shown in Table 5.2 and Table 5.3 for different fault locations and inception instant. First two columns of both the tables show fault types and fault initiation location. Last three columns show the fault inception instant, detection instant and response time, respectively. Table 5.2 shows the result obtained with the fault detection scheme in the AC section of the transmission line. It is observed that by using the proposed scheme the fault is detected and identified precisely within 5 milliseconds and average detection time 3.125 milliseconds in the AC section shown in Table 5.2. Along with, it is also observed that the fault detection scheme take less than average detection time 3.125 milliseconds as compared to other class of fault in the AC section of the transmission line. Table 5.3 show the result obtain with the fault detection scheme in the DC section the transmission line. Further, it is observed that by using the

proposed scheme the fault is detected and identified precisely within 4.5 milliseconds and average detection time 3.01675 milliseconds in the DC section shown in Table 5.3. Along with, it is also observed that the F-SVM fault detection scheme take less average detection time 3.016755 milliseconds as compared to other class of faults in the AC section of the transmission line.

5.5.1.2 Outcomes with F-SVM Fault Location Scheme

TABLE 5.4: Result obtained with F-SVM fault location scheme in AC section (case-1)

Fault Type	**c**	γ	**Actual FL** (km)	**Calculated FL** (km)	**Error in FL** (km)	**Error in FL** (%)
Class-1	6040.42	0.0944	10	10.3122	0.3122	0.1561
			20	20.3976	0.3976	0.1988
			30	30.4301	0.4301	0.2151
			40	40.2942	0.2942	0.1471
			50	50.4619	0.4619	0.2310
			60	60.3439	0.3439	0.1720
			70	70.3471	0.3471	0.1736
			80	80.4438	0.4438	0.2219
			90	90.4222	0.4222	0.2111
Class-4	8321.73	0.0768	10	10.3307	0.3307	0.1654
			20	20.1732	0.1732	0.0866
			30	30.1936	0.1936	0.0968
			40	40.4546	0.4546	0.2273
			50	50.1115	0.1115	0.0558
			60	60.2936	0.2936	0.1468
			70	70.1672	0.1672	0.0836
			80	80.4915	0.4915	0.2458
			90	90.3851	0.3851	0.1926
Class-7	12632.35	0.0444	10	10.3002	0.3002	0.1501
			20	20.2884	0.2884	0.1442
			30	30.1238	0.1238	0.0619
			40	40.3728	0.3728	0.1864
			50	50.1157	0.1157	0.0579
			60	60.1286	0.1286	0.0643
			70	70.3087	0.3087	0.1544
			80	80.1387	0.1387	0.0694
			90	90.4273	0.4273	0.2137
Class-10	15533.91	0.0355	10	10.4237	0.4237	0.2119
			20	20.3829	0.3829	0.1915
			30	30.1599	0.1599	0.0800
			40	40.3638	0.3638	0.1819
			50	50.3074	0.3074	0.1537
			60	60.4892	0.4892	0.2446
			70	70.3596	0.3596	0.1798
			80	80.4201	0.4201	0.2101
			90	90.2815	0.2815	0.1408

Table 5.4 and Table 5.5 show the actual fault location values and the respective estimated fault location values using F-SVM fault location scheme. Percentage error in estimated fault location with the actual location is calculated using eq. (4.20). Table 5.4

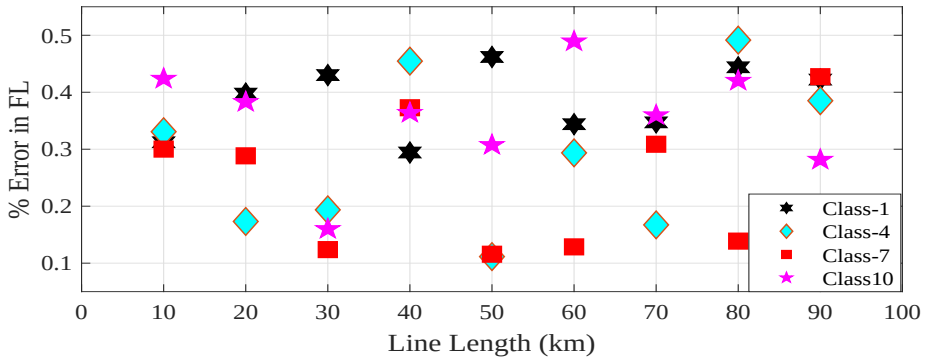

FIGURE 5.27: Performance of F-SVM fault location scheme in AC section (case-1)

TABLE 5.5: Result obtained with F-SVM fault location scheme in DC section (case-1)

Fault Type	**c**	**γ**	**Actual FL** (km)	**Calculated FL** (km)	**Error in FL** (km)	**Error in FL** $(\%)$
Class-11	5437.34	0.0524	60	60.1694	0.1694	0.0282
			120	120.2564	0.2564	0.0427
			180	180.4326	0.4326	0.0721
			240	240.4213	0.4213	0.0702
			300	300.1242	0.1242	0.0207
			360	360.2597	0.2597	0.0433
			420	420.3108	0.3108	0.0518
			480	480.2667	0.2667	0.0445
			540	540.3627	0.3627	0.0605
Class-12	7364.63	0.0372	60	60.3512	0.3512	0.0585
			120	120.2168	0.2168	0.0361
			180	180.2727	0.2727	0.0455
			240	240.1062	0.1062	0.0177
			300	300.4936	0.4936	0.0823
			360	360.1669	0.1669	0.0278
			420	420.1425	0.1425	0.0238
			480	480.2491	0.2491	0.0415
			540	540.1792	0.1792	0.0299
Class-13	10527.26	0.0212	60	60.2959	0.2959	0.0493
			120	120.2358	0.2358	0.0393
			180	180.4807	0.4807	0.0801
			240	240.4681	0.4681	0.0780
			300	300.1211	0.1211	0.0202
			360	360.3951	0.3951	0.0659
			420	420.2076	0.2076	0.0346
			480	480.2691	0.2691	0.0449
			540	540.3191	0.3191	0.0532
Class-14	13762.02	0.0092	60	60.4771	0.4771	0.0795
			120	120.2671	0.2671	0.0445
			180	180.4932	0.4932	0.0822
			240	240.2206	0.2206	0.0368
			300	300.3804	0.3804	0.0634
			360	360.3665	0.3665	0.0611
			420	420.3157	0.3157	0.0526
			480	480.3792	0.3792	0.0632
			540	540.3666	0.3666	0.0611

shows estimated fault location values and variation with actual value in AC section. Figure 5.27 shows the performance of fault location scheme in different location in AC section.

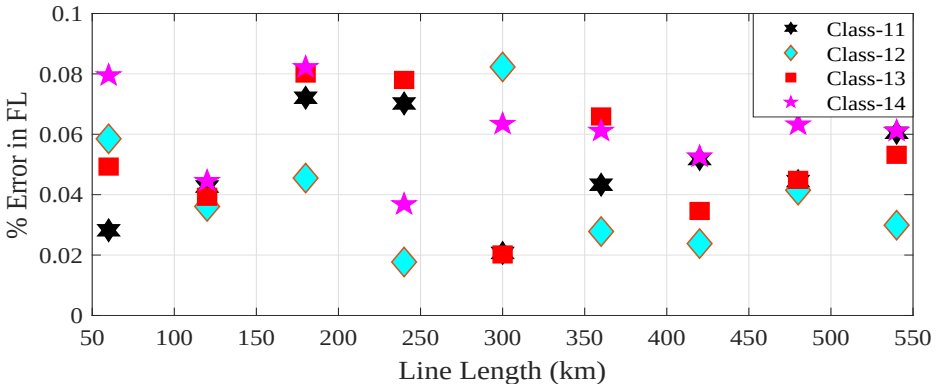

FIGURE 5.28: Performance of F-SVM fault location scheme in DC section (case-1)

The error observed in fault location calculations on the basis of the respective optimum value of c and γ for different types of faults in the AC section are shown in Table 5.4. Overall accuracy found with the proposed scheme is 99.13%. It is also observed that average accuracy in LLG fault is more as compared to other class of fault in the AC section of the transmission line shown in Figure 5.27. Table 5.5 shows estimated fault location values and variation with actual value in DC section. Figure 5.28 shows the performance of fault location scheme in different location in DC section. The error observed in fault location calculation on the basis of the respective optimum value of c and γ for different types of faults in the DC section are shown in Table 5.5. Overall accuracy found with the proposed scheme is 99.94%. It is also observed that average accuracy in negative phase to ground fault is more as compare to other class of fault in the DC section of the transmission line shown in Figure 5.28. The comparison results with some other existing research papers are shown in Table 5.14. It can be observed from Table 5.14 that the error in fault location is least with the proposed F-SVM fault location scheme which validates the accuracy.

5.5.1.3 Outcomes with F-SVM Fault Classification Scheme

The results obtained with the F-SVM fault classification scheme are shown in Figure 5.29, and Figure 5.30. The diagonal elements in Figure 5.29(a) shows the correct classified sample, whereas non-diagonal elements show false classified samples without using the F-score scheme. It show how many samples in test case classify correctly and how many samples misclassify with a different class. Figure 5.29(b) shows the correct classified

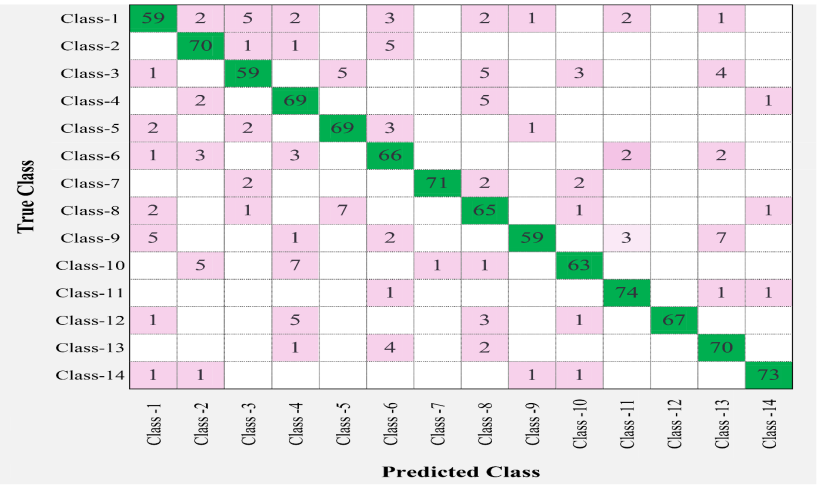

(a) Confusion matrix with number of sample

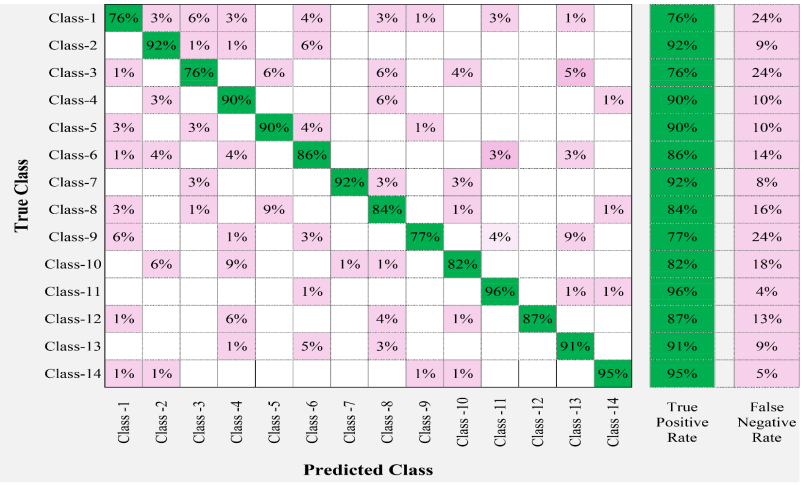

(b) Confusion matrix with TPR/NPR

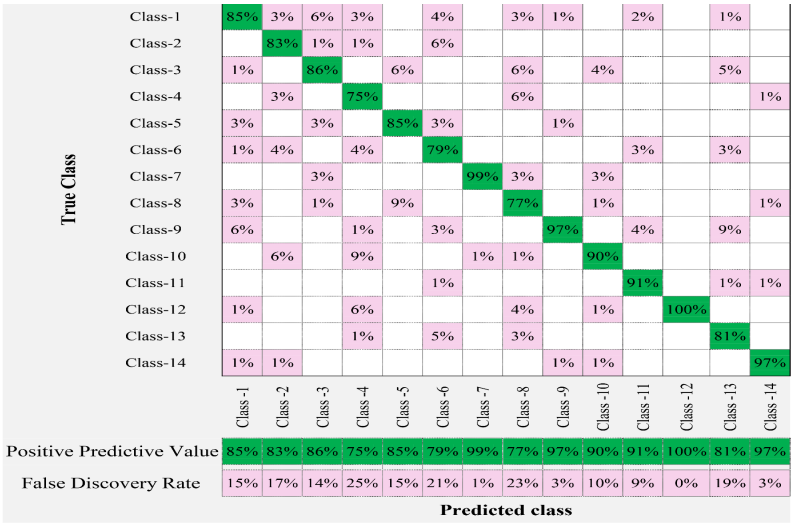

(c) Confusion matrix with PPD/FDR

FIGURE 5.29: Confusion matrix for F-SVM classifier without using F-score (Case-1)

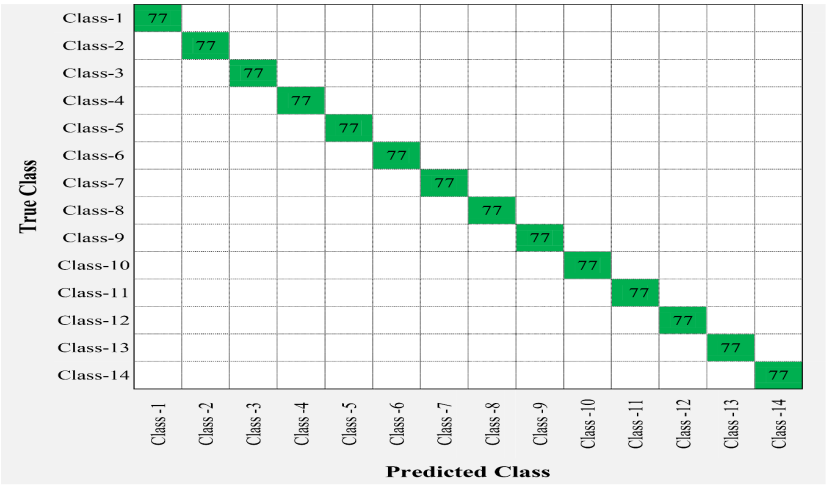

(a) Confusion matrix with number of sample

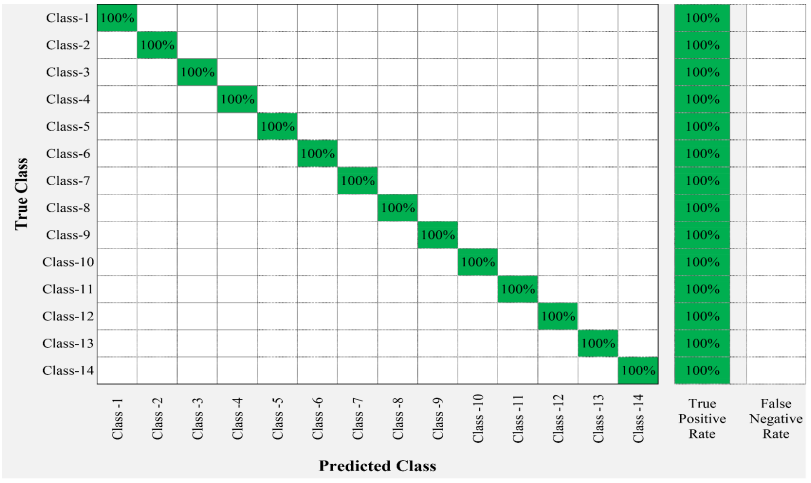

(b) Confusion matrix with TPR/NPR2

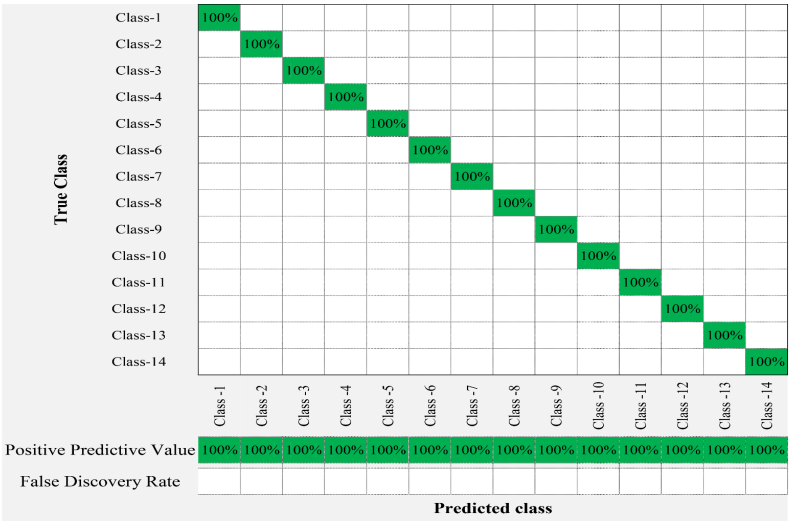

(c) Confusion matrix with PPD/FDR

FIGURE 5.30: Confusion matrix for F-SVM classifier with using F-score (Case-1)

percentage considering True Positive Rate (TPR) whereas the non-diagonal elements show false classified percentage considering False Negative Rate (FNR) without using the F-score scheme. The diagonal elements in Figure 5.29(c) shows the correct classify percentage whereas the non-diagonal elements show false classified percentage with the positive predictive value/false discovery rate (PPD/FDR) without using the F-score scheme. The classification accuracy without using the F-score is 86.64% with prediction speed of 3572 obs/second and take 9.432 seconds for training purpose, as shown in Figure 4.34.

TABLE 5.6: Comparison between with or without using F-score based multi-class F-SVM classifier outcomes (case-1)

	Class	**True Positive Rate %**	**True Negative Rate %**	**Overall Accuracy %**
Without F-Score	Class 1	76.62	23.38	86.64
	Class 2	90.91	9.09	
	Class 3	76.62	23.38	
	Class 4	89.61	10.39	
	Class 5	89.61	10.39	
	Class 6	85.71	14.29	
	Class 7	92.21	7.79	
	Class 8	84.42	15.58	
	Class 9	76.62	23.38	
	Class 10	81.82	18.18	
	Class 11	96.10	3.90	
	Class 12	87.01	12.99	
	Class 13	90.91	9.09	
	Class 14	94.81	5.19	
With F-Score	Class 1	100.00	0.00	100
	Class 2	100.00	0.00	
	Class 3	100.00	0.00	
	Class 4	100.00	0.00	
	Class 5	100.00	0.00	
	Class 6	100.00	0.00	
	Class 7	100.00	0.00	
	Class 8	100.00	0.00	
	Class 9	100.00	0.00	
	Class 10	100.00	0.00	
	Class 11	100.00	0.00	
	Class 12	100.00	0.00	
	Class 13	100.00	0.00	
	Class 14	100.00	0.00	

The diagonal elements in Figure 5.30(a) shows the correct classified sample, whereas non-diagonal elements show false classified samples using the F-score scheme. It shows how many samples in test case classify correctly and how many samples misclassify with a different class. Figure 5.30(b) shows the correct classified percentage considering true positive rate (TPR) whereas the non-diagonal elements show false classified percentage considering false negative rate (FNR) using F-score scheme. The diagonal elements in Figure 5.30(c) shows the correct classify percentage whereas the non-diagonal elements show false classified percentage with the positive predictive value/false discovery rate

(PPD/FDR) without using the F-score scheme. The classification accuracy with using the F-score is 100% with the prediction speed 3712 obs/second and take 8.562 seconds for training purpose, as shown in Figure 5.30. The basic equation behind design of confusion matrix are shown in eq. (4.21), eq. (4.22) and eq. (4.23). The comparison result of the classification scheme with or without using the F-score scheme is summarized in Table 5.6 with using basic eq. (4.21), eq. (4.22) and eq. (4.23).

5.5.2 Case-2: CIGRE (B4.57 and B4.58) Hybrid Transmission Test System

For the training purpose of F-SVM fault estimation method four types of faults in DC section and ten types of faults in AC are created in the transmission line at every 10 km of the transmission line and the data is measured. The data contain 77 instant samples of fourteen different classes, and 364 features are extracted. From all these extracted features 208 dominating features are selected with a modified F-score scheme. 10-fold cross-validation RBF kernel function with 70% data used for training and 30% for testing purpose of F-SVM method.

5.5.2.1 Outcomes with F-SVM Fault Detection Scheme

To test the suitability of the F-SVM fault detection scheme, different types of fault in the overhead transmission line of AC section $((B_a - B_0) - (B_a - B_1))$ with reference bus-$(B_a - B_0)$ at 50 km, 100 km, 150 km and in DC section $((B_b - B_4) - (B_b - A_1))$ at 50 km, 200 km, 400 km are simulated. The test results of the detection scheme in AC section$((B_a - B_0) - (B_a - B_1))$ and in DC section$((B_b - B_4) - (B_b - A_1))$ are shown in Table 5.7 and Table 5.8 for different fault locations and inception instant. First two columns of both the table show fault types and fault initiation location. Last three columns show the fault inception instant, detection instant and response time, respectively. Table 5.7 show the result obtained with the fault detection scheme in the AC section$((B_a - B_0) - (B_a - B_1))$ the transmission line. It is observed that by using the proposed scheme the fault is detected and identified precisely within 5 milliseconds and average detection time 3.34 milliseconds in the AC section$((B_a - B_0) - (B_a - B_1))$ shown in Table 5.2. It is also observed that the fault detection scheme take less average detection time 3.34 milliseconds as compared to other class of fault in the AC section $((B_a - B_0) - (B_a - B_1))$ of the transmission line. Table 5.8 show the result obtained with the fault detection scheme in the DC section$((B_b - B_4) - (B_b - A_1))$ of the transmission line. It is also observed that by using the proposed

TABLE 5.7: Result obtained with F-SVM fault detector scheme in AC section for (case-2)

Fault Type	**Fault Location** (km)	**Fault Inception Instant** $(T_i)s$	**Fault Detection Instant** $(T_d)s$	**Response Time** $(T_r = T_d - T_i)ms$
Class-1	50	0.2	0.2049	4.9
		0.3	0.3029	2.9
		0.4	0.4022	2.2
	100	0.2	0.2030	3.0
		0.3	0.3015	1.5
		0.4	0.4017	1.7
	150	0.2	0.2057	5.7
		0.3	0.3058	5.8
		0.4	0.4039	3.9
Class-4	50	0.2	0.2022	2.2
		0.3	0.3028	2.8
		0.4	0.4051	5.1
	100	0.2	0.2011	1.1
		0.3	0.3012	1.2
		0.4	0.4018	1.8
	150	0.2	0.2042	4.2
		0.3	0.3047	4.7
		0.4	0.4042	4.2
Class-7	50	0.2	0.2037	3.7
		0.3	0.3025	2.5
		0.4	0.4047	4.7
	100	0.2	0.2019	1.9
		0.3	0.3044	4.4
		0.4	0.4019	1.9
	150	0.2	0.2028	2.8
		0.3	0.3041	4.1
		0.4	0.4049	4.9
Class-10	50	0.2	0.2056	5.6
		0.3	0.3049	4.9
		0.4	0.4034	3.4
	100	0.2	0.2032	3.2
		0.3	0.3032	3.2
		0.4	0.4025	2.5
	150	0.2	0.2035	3.5
		0.3	0.3036	3.6
		0.4	0.4051	5.1

scheme the fault is detected and identified precisely within 6 milliseconds and average detection time 3.32 milliseconds in the DC section $((B_b - B_4) - (B_b - A_1))$ shown in Table 5.8. Along with it is also observed that the fault detection scheme take less average detection time 3.32 milliseconds as compared to other class of faults in the AC section of the transmission line.

TABLE 5.8: Result obtained with F-SVM fault detector scheme in DC section for (case-2)

Fault Type	**Fault Location** (km)	**Fault Inception Instant** $(T_i)s$	**Fault Detection Instant** $(T_d)s$	**Response Time** $(T_r = T_d - T_i)ms$
Class-11	50	0.2	0.2042	4.2
		0.3	0.3029	2.9
		0.4	0.4054	5.4
	200	0.2	0.2037	3.7
		0.3	0.3028	2.8
		0.4	0.4057	5.7
	400	0.2	0.2055	5.5
		0.3	0.3038	3.8
		0.4	0.4041	4.1
Class-12	50	0.2	0.2020	2.0
		0.3	0.3025	2.5
		0.4	0.4034	3.4
	200	0.2	0.2022	2.2
		0.3	0.3052	5.2
		0.4	0.4020	2.0
	400	0.2	0.2021	2.1
		0.3	0.3019	1.9
		0.4	0.4021	2.1
Class-13	50	0.2	0.2026	2.6
		0.3	0.3056	5.6
		0.4	0.4032	3.2
	200	0.2	0.2019	1.9
		0.3	0.3055	5.5
		0.4	0.4059	5.9
	400	0.2	0.2032	3.2
		0.3	0.3016	1.6
		0.4	0.4023	2.3
Class-14	50	0.2	0.2040	4.0
		0.3	0.3023	2.3
		0.4	0.4040	4.0
	200	0.2	0.2046	4.6
		0.3	0.3021	2.1
		0.4	0.4016	1.6
	400	0.2	0.2025	2.5
		0.3	0.3026	2.6
		0.4	0.4031	3.1

5.5.2.2 Outcomes with F-SVM Fault Location Scheme

Table 5.9 and Table 5.10 shows the actual fault location values and the respective estimated fault location values using F-SVM fault location scheme. Percentage error in estimated fault location with the actual location is calculated using eq. (4.20). Table 5.9 shows the estimated fault location values and variation with actual value in AC section. Figure 5.31 shows the performance of fault location scheme in different locations in AC section. The error observed in fault location calculation on the basis of the respective optimum value of c and γ for different

TABLE 5.9: Result obtained with F-SVM fault location scheme in AC section (case-2)

Fault Type	**c**	**γ**	**Actual FL** (*km*)	**Calculated FL** (*km*)	**Error in FL** (*km*)	**Error in FL** (%)
Class-1	4383.29	0.0843	20	20.2705	0.2705	0.1353
			40	40.2173	0.2173	0.1087
			60	60.0976	0.0976	0.0488
			80	80.1423	0.1423	0.0712
			100	100.1652	0.1652	0.0826
			120	120.2954	0.2954	0.1477
			140	140.0891	0.0891	0.0446
			160	160.2639	0.2639	0.1320
			180	180.2112	0.2112	0.1056
Class-4	7318.38	0.06194	20	0.1441	0.1441	0.0721
			40	40.0978	0.0978	0.0489
			60	60.1571	0.1571	0.0786
			80	80.1903	0.1903	0.0952
			100	100.0802	0.0802	0.0401
			120	120.1974	0.1974	0.0987
			140	140.1066	0.1066	0.0533
			160	160.1462	0.1462	0.0731
			180	180.1958	0.1958	0.0979
Class-7	8359.27	0.0418	20	20.113	0.113	0.0565
			40	40.1226	0.1226	0.0613
			60	60.2043	0.2043	0.1022
			80	80.1163	0.1163	0.0582
			100	100.2561	0.2561	0.1281
			120	120.2957	0.2957	0.1479
			140	140.2326	0.2326	0.1163
			160	160.136	0.136	0.0680
			180	180.1966	0.1966	0.0983
Class-10	10037.12	0.03742	20	20.077	0.077	0.0385
			40	40.2766	0.2766	0.1383
			60	60.2699	0.2699	0.1350
			80	80.2545	0.2545	0.1273
			100	100.1152	0.1152	0.0576
			120	120.1986	0.1986	0.0993
			140	140.0557	0.0557	0.0279
			160	160.1563	0.1563	0.0782
			180	180.1282	0.1282	0.0641

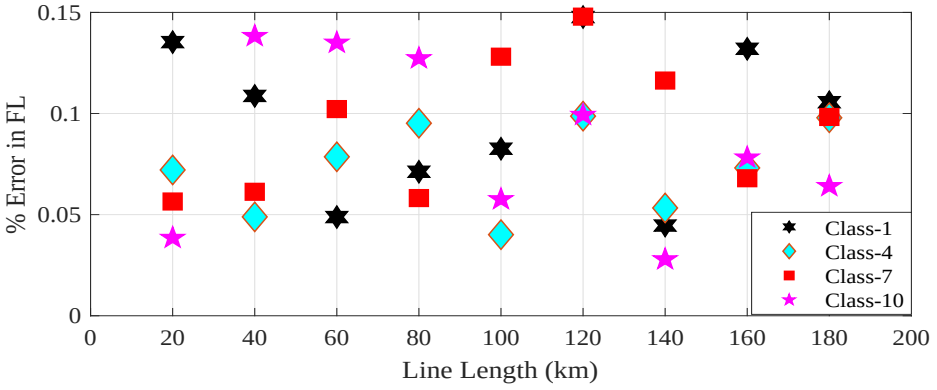

FIGURE 5.31: Performance of F-SVM fault location scheme in AC section (case-2)

TABLE 5.10: Result obtained with F-SVM fault location scheme in DC section (case-2)

Fault Type	**c**	**γ**	**Actual FL** (km)	**Calculated FL** (km)	**Error in FL** (km)	**Error in FL** (%)
Class-11	3825.62	0.08263	50	50.5409	0.5409	0.1082
			100	100.4346	0.4346	0.0869
			150	150.1952	0.1952	0.0390
			200	200.2845	0.2845	0.0569
			250	250.3304	0.3304	0.0661
			300	300.5908	0.5908	0.1182
			350	350.1782	0.1782	0.0356
			400	400.5278	0.5278	0.1056
			450	450.4224	0.4224	0.0845
Class-12	4621.45	0.06142	50	50.2881	0.2881	0.0576
			100	100.1955	0.1955	0.0391
			150	150.3141	0.3141	0.0628
			200	200.3806	0.3806	0.0761
			250	250.1603	0.1603	0.0321
			300	300.3948	0.3948	0.0790
			350	350.2131	0.2131	0.0426
			400	400.2923	0.2923	0.0585
			450	450.3915	0.3915	0.0783
Class-13	6714.58	0.04692	50	50.2259	0.2259	0.0452
			100	100.2452	0.2452	0.0490
			150	150.4085	0.4085	0.0817
			200	200.2326	0.2326	0.0465
			250	250.5122	0.5122	0.1024
			300	300.5913	0.5913	0.1183
			350	350.4651	0.4651	0.0930
			400	400.2719	0.2719	0.0544
			450	450.3932	0.3932	0.0786
Class-14	9526.19	0.02572	50	50.1539	0.1539	0.0308
			100	100.5532	0.5532	0.1106
			150	150.5398	0.5398	0.1080
			200	200.5089	0.5089	0.1018
			250	250.2304	0.2304	0.0461
			300	300.3972	0.3972	0.0794
			350	350.1113	0.1113	0.0223
			400	400.3126	0.3126	0.0625
			450	450.2564	0.2564	0.0513

types of faults in the AC section are shown in Table 5.9. Overall accuracy found with the proposed scheme is 99.91%. It is also observed that average accuracy in LL fault is more as compared to other class of faults in the AC section of the transmission line shown in Figure 5.31. Table 5.10 show the estimated fault location values and variation with actual value in DC section. Figure 5.32 shows the performance of fault location scheme in different location in DC section. The error observed in fault location calculation on the basis of the respective optimum value of c and γ for different types of faults in the DC section are shown in Table 5.10. Overall accuracy found with the proposed scheme is 99.93%. Although, it is also observed that average accuracy in negative phase to ground

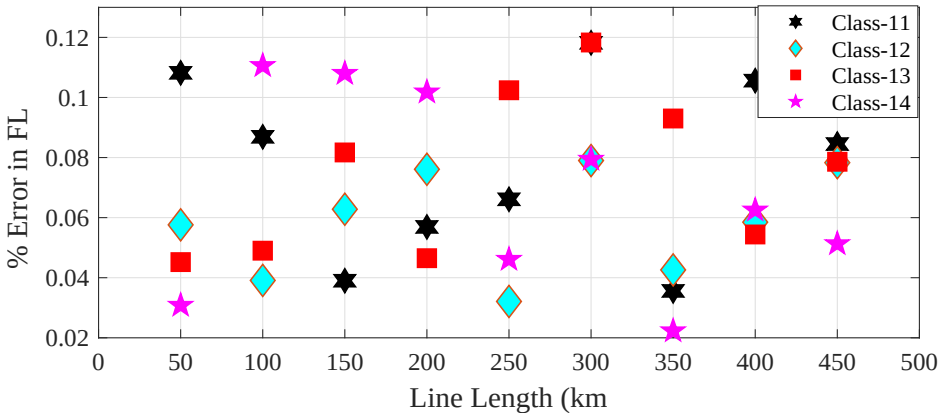

FIGURE 5.32: Performance of F-SVM fault location scheme in DC section (Case-2)

fault is more as compared to other class of faults in the DC section of the transmission line shown in Figure 5.32. The comparison results with some other existing research works are shown in Table 5.14. It can be observed from Table 5.14 that the error in fault location is least with the proposed F-SVM fault location scheme which validates the accuracy.

5.5.2.3 Outcomes with F-SVM Fault Classification Scheme

The results obtained with the F-SVM fault classification scheme are shown in Figures 5.33, and 5.34. The diagonal elements in Figure 5.33(a) show the correct classified sample, whereas non-diagonal elements show false classified samples without using the F-score scheme. It shows how many samples in test case classify correctly and how many samples misclassify with a different class. Figure 5.33(b) shows the correct classified percentage considering True Positive Rate (TPR) whereas the non-diagonal elements show false classified percentage considering False Negative Rate (FNR) without using the F-score scheme. The diagonal elements in Figure 5.33(c) shows the correct classify percentage whereas the non-diagonal elements show false classified percentage with the positive predictive value/ false discovery rate (PPD/FDR) without using the F-score scheme. The classification accuracy without using the F-score is 95.95% with prediction speed of 959 obs/second and take 10.502 seconds for training purpose, as shown in Figure 4.34.

The diagonal elements in Figure 5.34(a) show the correct classified sample, whereas non-diagonal elements show false classified samples using the F-score scheme. It shows how many samples in test case classify correctly and how many samples misclassify with a different class. Figure 5.34(b) shows the correct classified percentage considering true positive rate (TPR) whereas the non-diagonal elements show false classified percentage

considering false negative rate (FNR) using the F-score scheme. The diagonal elements in Figure 5.34(c) shows the correct classify percentage whereas the non-diagonal elements show false classified percentage with the positive predictive value/false discovery rate (PPD/FDR) without using the F-score scheme. The classification accuracy using the F-score is 100% with the prediction speed 1027 obs/second and take 8.290 seconds for training purpose, as shown in Figure 5.34. The basic equation to design the confusion matrix are shown in eq. (4.21), eq. (4.22) and eq. (4.23). The comparison result of the classification scheme with or without using the F-score scheme is summarized in Table 5.11 with using basic eq. (4.21), eq. (4.22) and eq. (4.23).

TABLE 5.11: Comparison between with or without using F-score based multi-class F-SVM classifier outcomes (case-2)

	Class	**True Positive Rate %**	**True Negative Rate %**	**Overall Accuracy %**
Without F-Score	Class 1	93.33	6.67	95.95
	Class 2	95.62	4.38	
	Class 3	95.05	4.95	
	Class 4	97.71	2.29	
	Class 5	96.57	3.43	
	Class 6	93.90	6.10	
	Class 7	95.62	4.38	
	Class 8	94.67	5.33	
	Class 9	92.38	7.62	
	Class 10	95.81	4.19	
	Class 11	98.86	1.14	
	Class 12	97.52	2.48	
	Class 13	98.67	1.33	
	Class 14	97.52	2.48	
With F-Score	Class 1	100.00	0.00	100
	Class 2	100.00	0.00	
	Class 3	100.00	0.00	
	Class 4	100.00	0.00	
	Class 5	100.00	0.00	
	Class 6	100.00	0.00	
	Class 7	100.00	0.00	
	Class 8	100.00	0.00	
	Class 9	100.00	0.00	
	Class 10	100.00	0.00	
	Class 11	100.00	0.00	
	Class 12	100.00	0.00	
	Class 13	100.00	0.00	
	Class 14	100.00	0.00	

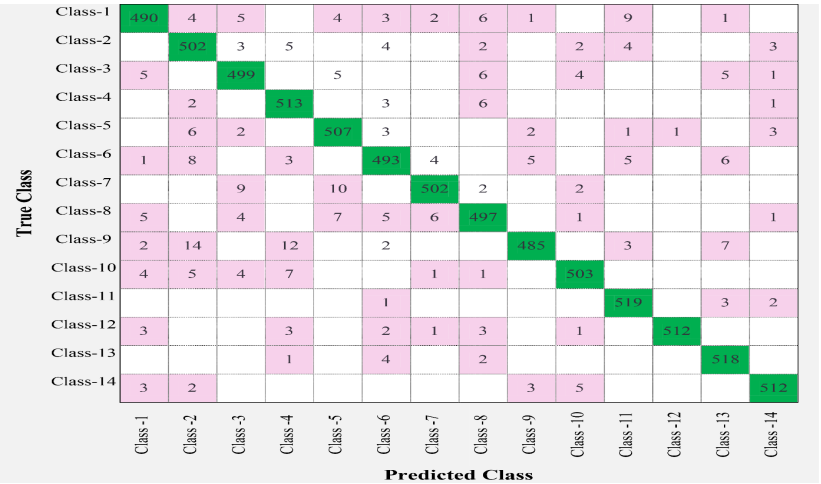

(a) Confusion matrix with number of sample

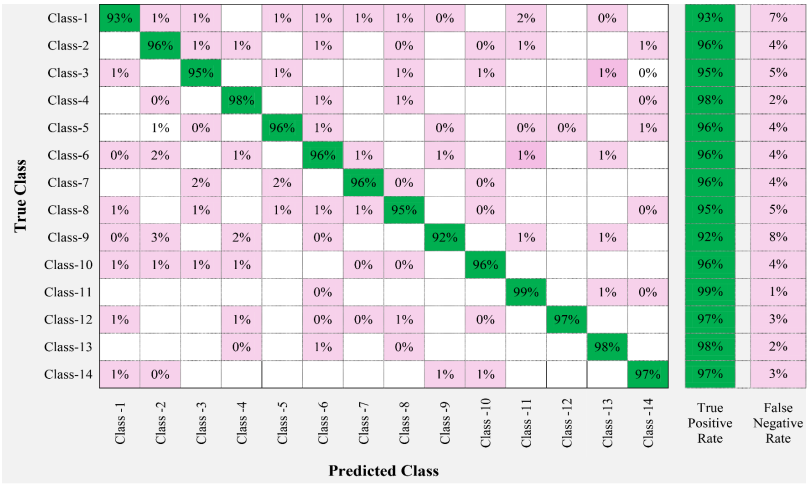

(b) Confusion matrix with TPR/NPR

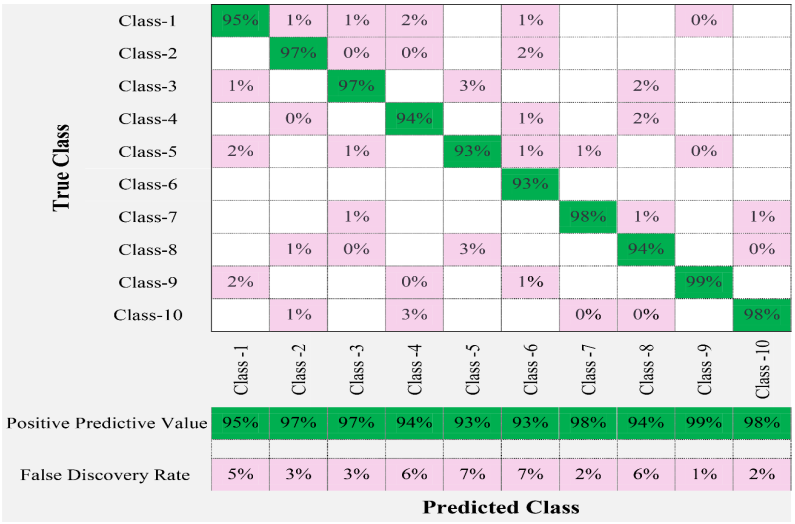

(c) Confusion matrix with PPD/FDR

FIGURE 5.33: Confusion matrix for F-SVM classifier without using F-score (Case-2)

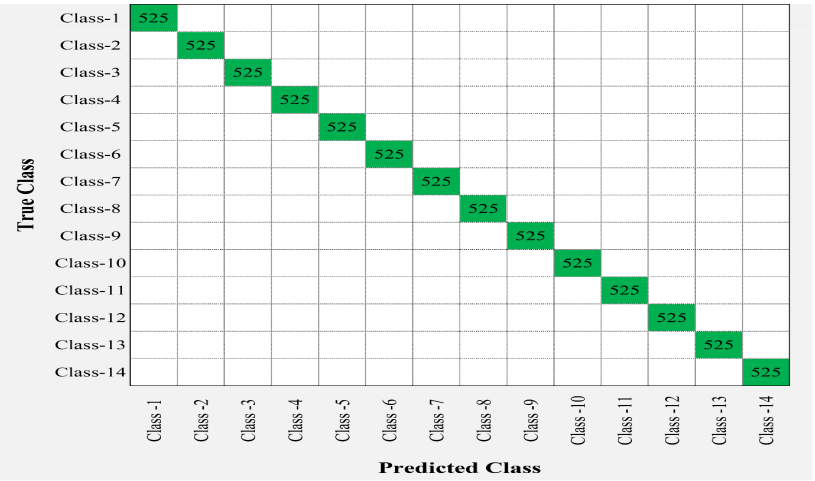

(a) Confusion matrix with number of sample

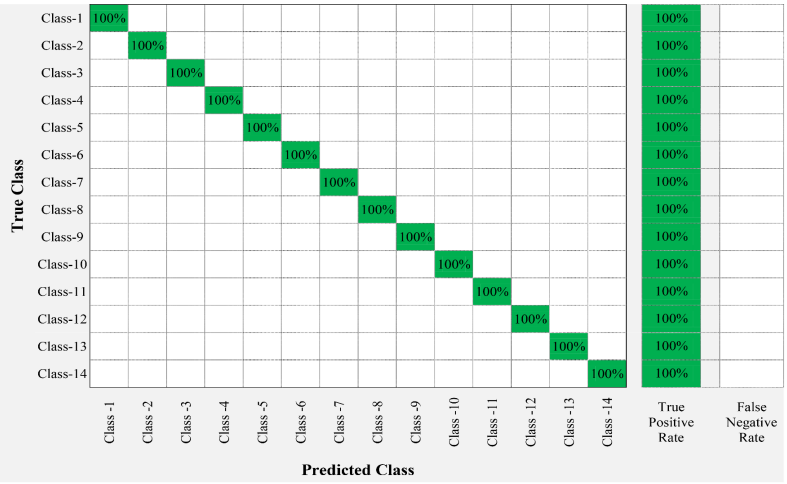

(b) Confusion matrix with TPR/NPR2

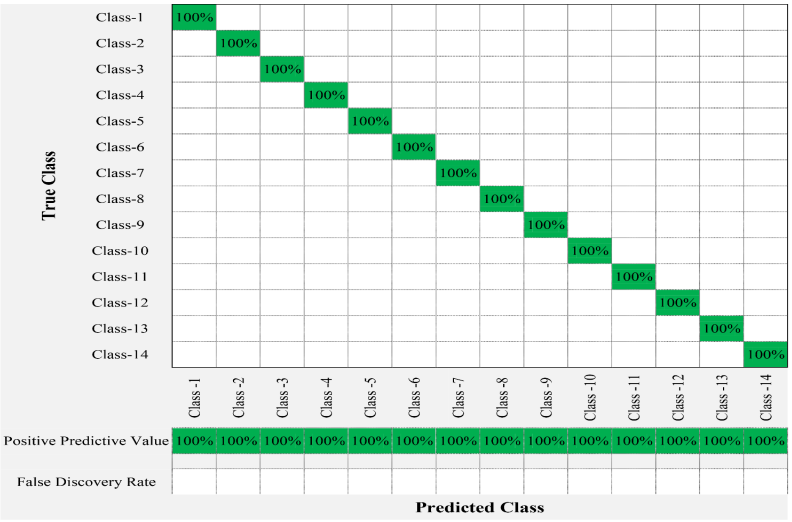

(c) Confusion matrix with PPD/FDR

FIGURE 5.34: Confusion matrix for F-SVM classifier with using F-score (Case-2)

5.5.3 Case-3: IEEE 30-Bus HVAC Transmission Test System

For the training purpose of F-SVM fault estimation method ten types of faults are created in each sections at every 10 km of the transmission line and the data is measured. The data contains 236 instant samples of ten different classes, and 448 features vector are extracted. From all these extracted features 290 dominating features are selected with a modified F-score scheme. 10-fold cross-validation RBF kernel function with 70% data used for training and 30% for testing purpose of F-SVM fault estimation method.

TABLE 5.12: Result obtained with F-SVM fault detector scheme (case-3)

Fault Type	**Fault Location** (km)	**Fault Inception Instant** $(T_i)s$	**Fault Detection Instant** $(T_d)s$	**Response Time** $(T_r = T_d - T_i)ms$
Class-1	50	0.2	0.2014	1.4
		0.3	0.3023	2.3
		0.4	0.4050	5.0
	100	0.2	0.2011	1.1
		0.3	0.3056	5.6
		0.4	0.4047	4.7
	150	0.2	0.2034	3.4
		0.3	0.3039	3.9
		0.4	0.4022	2.2
Class-4	50	0.2	0.2058	5.8
		0.3	0.3037	3.7
		0.4	0.4036	3.6
	100	0.2	0.2022	2.2
		0.3	0.3034	3.4
		0.4	0.4041	4.1
	150	0.2	0.2044	4.4
		0.3	0.3030	3.0
		0.4	0.4028	2.8
Class-7	50	0.2	0.2012	1.2
		0.3	0.3054	5.4
		0.4	0.4056	5.6
	100	0.2	0.2050	5.0
		0.3	0.3015	1.5
		0.4	0.4023	2.3
	150	0.2	0.2027	2.7
		0.3	0.3044	4.4
		0.4	0.4017	1.7
Class-10	50	0.2	0.2015	1.5
		0.3	0.3043	4.3
		0.4	0.4035	3.5
	100	0.2	0.2049	4.9
		0.3	0.3046	4.6
		0.4	0.4055	5.5
	150	0.2	0.2055	5.5
		0.3	0.3027	2.7
		0.4	0.4045	4.5

5.5.3.1 Outcomes with F-SVM Fault Detection Scheme

To test the suitability of the F-SVM fault detection scheme, different types of faults in the overhead transmission line of section (27-30) near bus-27 at 50 km, 100 km, 150 km are simulated. The test results of the detection scheme in section (27-30) are shown in Table 5.12 for different fault locations and inception instant. First two columns of both the table shows fault types and fault initiation location. Last three columns show the fault inception instant, detection instant and response time, respectively. Table 5.12 shows the result obtained with the fault detection scheme in the section (27-30) of the transmission line. It is observed that by using the proposed scheme the fault is detected and identified precisely within 6 milliseconds and average time of detection 3.59 milliseconds in the section (27-30) shown in Table 5.12.

5.5.3.2 Outcomes with F-SVM Fault Location Scheme

Table 5.13 shows the actual fault location values and the respective estimated fault location values using F-SVM fault location scheme. Percentage error in estimated fault location with the actual location is calculated using eq. (4.20). Table 5.13 shows the estimated fault location values and variation with actual value in section (27-30) of the transmission line. Figure 5.35 shows the performance of fault location scheme in a different location in section (27-30) of the transmission line. The error observed in fault location calculation on the basis of the respective optimum value of c and γ for different types of faults in the section (27-30) are shown in Table 5.13. Overall accuracy found with the proposed scheme is 99.83%. It is also observed that average accuracy in LLG fault is more

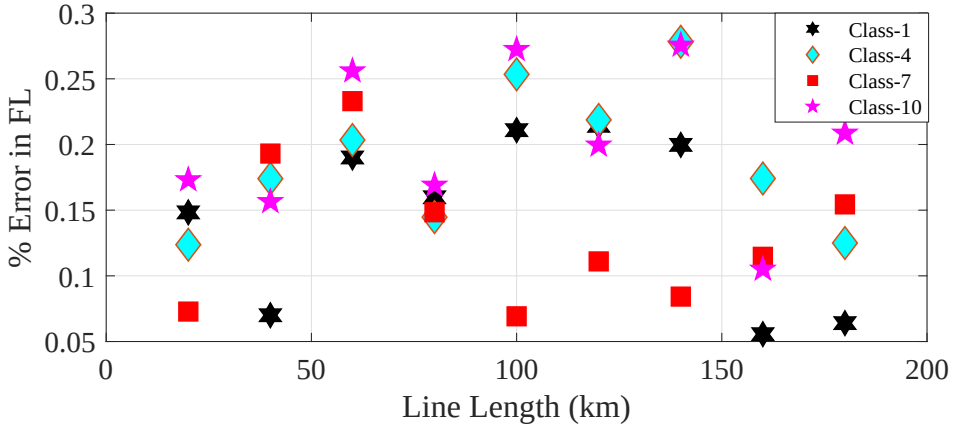

FIGURE 5.35: Performance of F-SVM fault location scheme (Case-3)

TABLE 5.13: Result obtained with F-SVM fault location scheme (case-3)

Fault Type	**c**	**γ**	**Actual FL** (km)	**Calculated FL** (km)	**Error in FL** (km)	**Error in FL** (%)
Class-1	4278.22	0.09246	20	20.3114	0.3114	0.1483
			40	40.1471	0.1471	0.0700
			60	60.3993	0.3993	0.1901
			80	80.3355	0.3355	0.1598
			100	100.4428	0.4428	0.2109
			120	120.4499	0.4499	0.2142
			140	140.4193	0.4193	0.1997
			160	160.1168	0.1168	0.0556
			180	180.1344	0.1344	0.0640
Class-4	62541.51	0.08542	20	20.2598	0.2598	0.1237
			40	40.3654	0.3654	0.1740
			60	60.4272	0.4272	0.2034
			80	80.3038	0.3038	0.1447
			100	100.5321	0.5321	0.2534
			120	120.4592	0.4592	0.2187
			140	140.5843	0.5843	0.2782
			160	160.3657	0.3657	0.1741
			180	180.2626	0.2626	0.1250
Class-7	8235.13	0.06248	20	20.1528	0.1528	0.0728
			40	40.4055	0.4055	0.1931
			60	60.4894	0.4894	0.2330
			80	80.3117	0.3117	0.1484
			100	100.1454	0.1454	0.0692
			120	120.2332	0.2332	0.1110
			140	140.1768	0.1768	0.0842
			160	160.2405	0.2405	0.1145
			180	180.3242	0.3242	0.1544
Class-10	1183.34	0.03943	20	20.3636	0.3636	0.1731
			40	40.3287	0.3287	0.1565
			60	60.5377	0.5377	0.2560
			80	80.3549	0.3549	0.1690
			100	100.5718	0.5718	0.2723
			120	120.4189	0.4189	0.1995
			140	140.5788	0.5788	0.2756
			160	160.2204	0.2204	0.1050
			180	180.4381	0.4381	0.2086

as compare to other class of fault in the section (27-30) of the transmission line shown in Figure 5.35. The comparison results with some other existing research papers are shown in Table 5.14. It can be observed from Table 5.14 that the error in fault location is least with the proposed F-SVM fault location scheme which validates the accuracy.

5.5.3.3 Outcomes with F-SVM Fault Classification Scheme

The results obtained with the F-SVM fault classification scheme are shown in Figures 5.36, and 5.37. The diagonal elements in Figure 5.36(a) shows the correct classified sample, whereas non-diagonal elements show false classified samples without using the F-score scheme. It shows how many samples in the test case classify correctly and how

TABLE 5.14: F-SVM fault location scheme comparison with some existing methods

Ref. No.	Basic Approach Used	System Used	Error (%)
[158]	Impedance Based Method	Three Terminal AC System	0.476
[159]	Impedance Based Method	Two Terminal HVDC	0.196
[162]	Traveling Wave Based	2 Terminal Double Circuit HVDC	1.233
[36]	Traveling Wave Based	Two Terminal HVDC	1.345
[37]	Artificial Neural Network	Two Terminal HVDC	2.50
[40]	Radial Basis Function (ANN)	Two Terminal HVDC	0.501
[43]	Support Vector Machine	Multi-terminal VSC HVDC	0.092
[45]	Traveling Wave Based	Multi-terminal VSC HVDC	0.152
	Support Vector Machine	**Two-Terminal VSC HVDC**	**0.051**
	Support Vector Machine	**Multi-terminal VSC HVDC**	**0.042**
Proposed	**Support Vector Machine**	**Two Terminal Hybrid System**	**0.048**
	Support Vector Machine	**CIGRE Hybrid System**	**0.078**
	Support Vector Machine	**IEEE Bus-30 HVAC System**	**0.166**

many samples misclassify with a different class. Figure 5.36(b) shows the correct classified percentage considering True Positive Rate (TPR) whereas the non-diagonal elements show false classification percentage considering False Negative Rate (FNR) without using the F-score scheme. The diagonal elements in Figure 5.36(c) shows the correct classification percentage whereas the non-diagonal elements show false classification percentage with the positive predictive value/false discovery rate (PPD/FDR) without using the F-score scheme. The classification accuracy without using the F-score is 95.10% with prediction speed of 893 obs/second and take 8.602 seconds for training purpose, as shown in Figure 5.36.

The diagonal elements in Figure 5.37(a) show the correct classified sample, whereas non-diagonal elements show false classified samples using the F-score scheme. It shows how many samples in test case classify correctly and how many samples misclassify with a different class. Figure 5.37(b) shows the correct classified percentage considering True Positive Rate (TPR) whereas the non-diagonal elements show false classified percentage considering False Negative Rate (FNR) with using the F-score scheme. The diagonal elements in Figure 5.37(c) shows the correct classification percentage whereas the non-diagonal elements show false classification percentage with the positive predictive value/false discovery rate (PPD/FDR) with using the F-score scheme. The classification accuracy using the F-score is 100% with the prediction speed 984 obs/second and take 6.992 seconds for training purpose, as shown in Figure 5.37. The basic equations for designing of confusion matrix are shown in eq. (4.21), eq. (4.22) and eq. (4.23). The comparison result of the classification scheme with or without using the F-score scheme is summarized in Table 5.15 using basic eq. (4.21), eq. (4.22) and eq. (4.23).

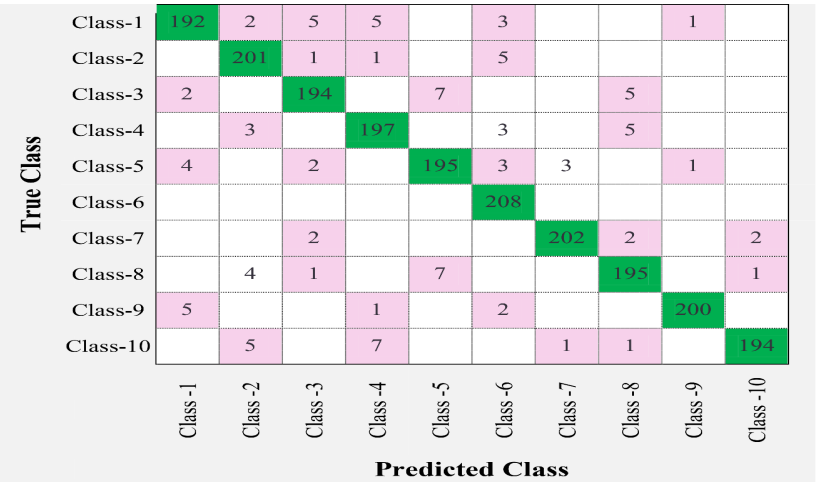

(a) Confusion matrix with munber of sample

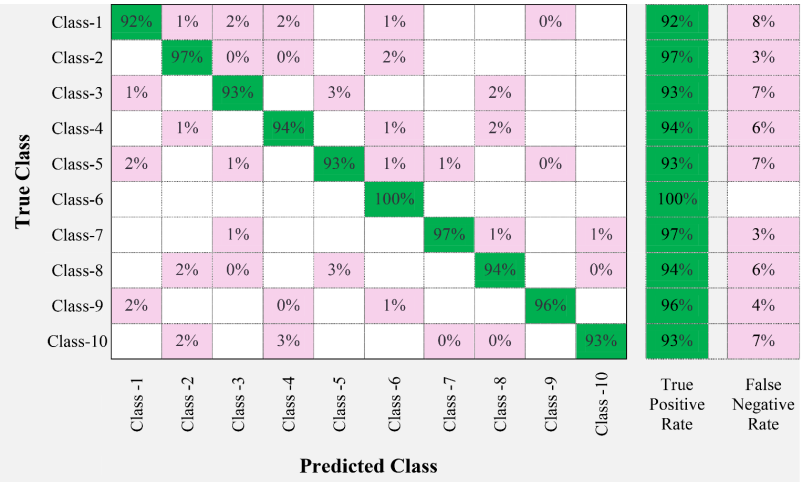

(b) Confusion matrix with TPR/NPR

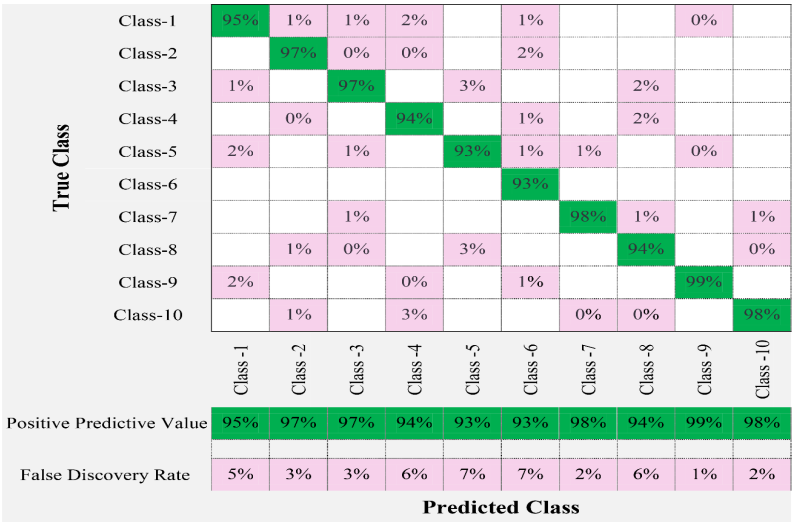

(c) Confusion matrix with PPD/FDR

FIGURE 5.36: Confusion matrix for F-SVM classifier without using F-score (Case-3)

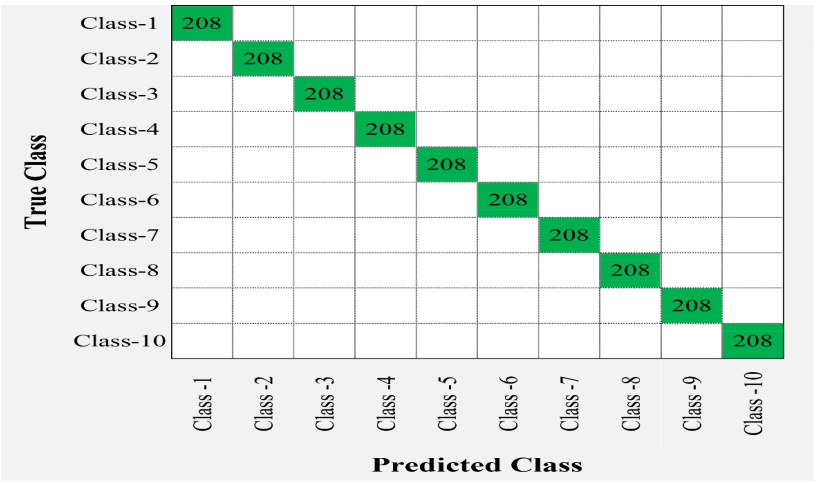

(a) Confusion matrix with number of sample

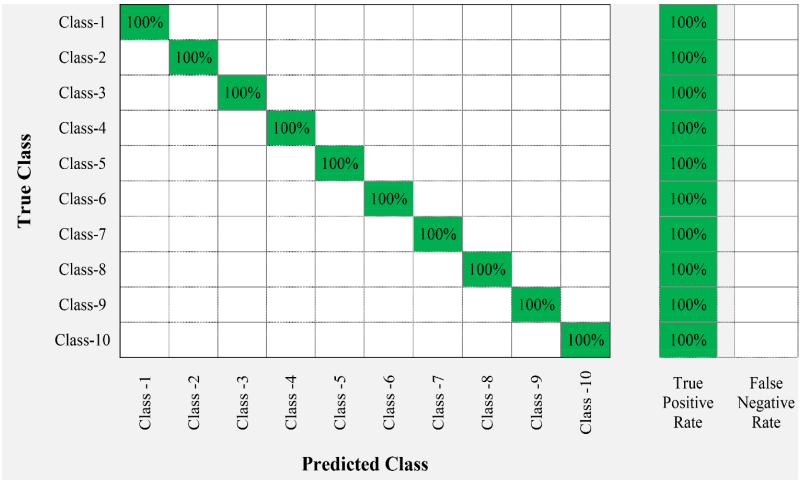

(b) Confusion matrix with TPR/NPR2

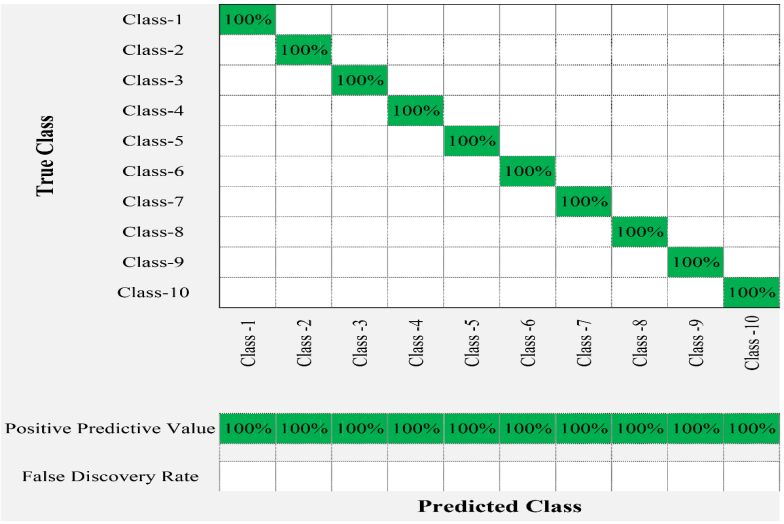

(c) Confusion matrix with PPD/FDR

FIGURE 5.37: Confusion Matrix for F-SVM classifier with using F-score (Case-3)

TABLE 5.15: Comparison between with or without using F-score based multi-class F-SVM classifier outcomes (case-3)

	Class	True Positive Rate %	True Negative Rate %	Overall Accuracy %
Without F-Score	Class 1	92.31	7.69	95.10
	Class 2	96.63	3.37	
	Class 3	93.27	6.73	
	Class 4	94.71	5.29	
	Class 5	93.75	6.25	
	Class 6	100.00	0.00	
	Class 7	97.12	2.88	
	Class 8	93.75	6.25	
	Class 9	96.15	3.85	
	Class 10	93.27	6.73	
With F-Score	Class 1	100.00	0.00	100
	Class 2	100.00	0.00	
	Class 3	100.00	0.00	
	Class 4	100.00	0.00	
	Class 5	100.00	0.00	
	Class 6	100.00	0.00	
	Class 7	100.00	0.00	
	Class 8	100.00	0.00	
	Class 9	100.00	0.00	
	Class 10	100.00	0.00	

The results observed in the above subsection with F-SVM fault estimation method describe in respected table and figures with acceptable accuracy. From the describe three test cases average total execution time with the proposed F-SVM fault estimation method are observed as 10.79 milliseconds, and 13.62 milliseconds and 12.07 milliseconds respectively. Further, it is also observed that time of execution of F-SVM fault estimation method within one cycle and input requirement of measured voltage and current post-fault data of 0.5 cycle only for all the two HVDC test transmission systems. Along with, the training time of the proposed F-SVM method takes the extreme of 14 seconds before the use of first time after that it does not require further training. Consequently, the suggested F-SVM fault estimation method shows its applicability with reasonable precision and within an acceptable time span for the transmission system [150].

5.6 Summary of the Chapter

This chapter estimates fault detection, location and classification by implementing F-SVM based method, already proposed in chapter 4, for hybrid HVAC and HVDC transmission systems as well as HVAC transmission system. In this method, there is an increased flexibility provided to the TSO for acceleration of the rest rotation process as quickly as possible through limited efforts. This method provides results within three cycles after

fault initiation with good accuracy. The proposed approach is simple but effective and non-iterative for all types of transmission systems.

In this chapter, three transmission test models are designed with the help of CIGRE DC grid model and dynamic model of IEEE-30 bus in PSCAD environment that provides similar environment as provided by the real time system.

Chapter 6

Conclusions and Future Scope

This chapter summarizes the thesis by outlining the major contributions and findings from the research. It further proposes some future works that can be done to improve power system protection strategies with these proposed methods.

6.1 General

Fault estimation methods is of prime importance to maintain the quality of power and security in a complex interconnected power system. It even becomes a greater issues in transmission systems which is an important pillar between generating sources and consumers. Moreover, the occurrence of faults on transmission systems is a common problem. Thus, fault estimation methods are important tools for TSO for expediting repairs after the occurrence of a fault on a transmission systems. This work propose and explain details of two methods based on importance and machine learning for protection of transmission systems.

This research attempts to develop strategies for different configuration of transmission systems considering the variation in faults conditions and system configuration limits. This addresses multiple concerns associated with fault estimation strategies such as detection, location, classification, feature extraction, feature selection, network constrain and different types of fault imbalance conditions. Developed methods and approaches have been illustrated through realistic case studies. The proposed work is relevant to various types of available transmission systems configurations worldwide, including HVAC, HVDC and hybrid transmission systems. It is observed that TSO can minimize their restoration

time and losses which results in minimum maintenance cost of transmission system using the proposed fault estimation strategies. For the validation of proposed methods different transmission systems configurations developed in PSCAD environment with inherent features of realistic environment. This thesis work also includes all the variation in transmission system configuration along with integration of renewable energy resources and their related issues. The outcomes of the proposed methods are within the range describe by IEEE standard [150] and compared with existing available in literature.

A summery of main findings of the research work carried out in this theses and future scope in this area are presented in subsequent section.

6.2 Summary of the Significant Findings

The research work undertaken in this thesis is initiated by developing an understanding of fault detection, location, and classification problem in a different configuration of transmission systems. A reasonable fault estimation strategy has been proposed for HVAC, HVDC and hybrid transmission system under a variety of the fault condition. Different configuration of the transmission system is modelled with dynamic real-time test system data in PSCAD environment. Different fault scenario is simulated in PSCAD environment and validate proposed methods of fault estimation in MATLAB environment.

The obtained results show that applicability of the PLFE method in the HVAC transmission system. This proposes fault detection, location and classification schemes with a single use of PLFE method for the HVAC transmission system. PLFE algorithm takes half cycle data for providing results after fault initiation in few seconds with acceptable accuracy. The proposed approach is simple, non-iterative and effective for HVAC transmission system. This method provides flexibility to the transmission operator to accelerate the rest-rotation process as quick as possible with less effort and effectively identifies the faulted sections and precise pinpoints the fault location without consideration of system parameters.

This work proposes fault detection, location and classification schemes with a single use of F-SVM based method for two and multi-terminal HVDC transmission system. It is also system parameters independent similar to PFLE with quick response, but superior classification of faults than PFLE. And its suitability on HVDC and hybrid as well as on HVAC transmission systems shows its effectiveness and robustness. The proposed

approach is simple, non-iterative. The obtained results show that applicability of the F-SVM method in the HVDC transmission system.

This work contributes a machine learning based multi-objective approach for fault estimation in the transmission system. For this a features extraction and selection approach is proposed due to dependency of F-SVM on dominating features than all features. In this features extraction extracts important features from the voltage and current signals and feature selection is used to select the dominating features to reduce high dimensionality. This overall reduce computational burden. This work is further extended using the hybrid transmission test systems. In this work, the proposed F-SVM method shows its applicability for fault estimation in not only HVDC, HVAC but also in hybrid HVAC and HVDC transmission systems. In this method, there is increased flexibility provided to the TSO for the acceleration of the rest rotation process as quickly as possible through limited efforts. This method provides results within three cycles after fault initiation with good accuracy. This works also contribute to the modeling and designing of AC-DC and DC-AC converters are presented for CIGRE (B4.57 and B4.58). In addition, the designing of complete CIGRE (B4.57 and B4.58) system is carried out in PSCAD software environment. This will help the novice researchers working in this area to get better insights about modeling and designing of hybrid transmission systems.

Finally, this thesis contributes by validating the proposed methods with precise accuracy and reliability for the transmission systems. The present work provides an understanding of fault analysis, their effects on the transmission system, and its associated issue such as power losses, voltage dip, high current in the lines, etc. This issues handled in this would continue to attract research interest.

6.3 Future Scope for Research

Research and development is a continuous process. Each step of research work opens many avenues for future research. As a consequence of the investigations carried out, a variety of issues pertaining to fault estimation for different configurations of the transmission systems have been sorted out. Though, there are several inter-related issues to be resolved, some require urgent attention due to their wide implications. Following are some of the aspects, identified as a promising area for future research work in the realm of study:

i. The presented fault estimation methods could be used in the same manner in distribution systems for fault analysis.

ii. The proposed work can be extended to detection, location and classification for cascaded as well as time-dependent faults.

iii. The proposed methods could also be used for all types of disturbances present in the power systems for example: lighting, transient fault, over-voltage, and under-voltage etc.

iv. The proposed F-SVM method can be used for detection of islanding problem in power systems. Although, it can also be used for detection of change in frequency oscillations.

v. The presented fault estimation methods could be further improved by using advanced data management methods and incorporating information about different disturbing events that appear in the transmission systems.

vi. Proposed methods can also be used to detection weak points of power system due to transients, insulation breakdown, and spark caused by switching etc.

vii. Proposed methods could be further illustrated by real-time practical case studies in transmission as well as distribution systems.

viii. Other signal processing and machine learning methods can be explored for better performance of fault detection, location, and classification schemes.

Apart from these issues for future research, fault estimation for different configurations of transmission systems pose several unique operation and protection challenges for power producers as well as for system operators. These challenges create ample opportunities for researchers in this area.

Publications

Based on the research carried out, following papers have been published/accepted/communicated for publication in various journal and conference out of this thesis work:

International Journals

1. J. P. Keshri & H. P. Tiwari, "Fault Detection, Classification in Multi-terminal HVDC Transmission System with MC-SVM," *Journal of Intelligent & Fuzzy Systems*, vol. pre-press, pp. 1-11, 2018, DOI: 10.3233/JIFS-169782, Publisher: IOS Press [SCI Indexed; Impact Factor 1.426].

2. J. P. Keshri, and H. P. Tiwari, "Fault Location in Overhead Transmission Line without using Line Parameters," *International Journal of Electrical, Electronics and Data Communication*, Volume-5, Issue-5, May-2017, ISSN: 2320-2084, Publisher: IRAJ Press [Impact Factor 3.46].

3. J. P. Keshri & H. P. Tiwari, "Fault Location Methods in HVDC Transmission System-A Review," *In Intelligent Computing Techniques for Smart Energy Systems*, pp. 411-419. Springer, Singapore, 2020, Publisher: Springer [Scopus Indexed; Impact Factor 0.69].

4. J. P. Keshri & H. P. Tiwari, "F-SVM based Fault Detection, Location, and Classification in Multi-terminal HVDC Transmission System," *IEEE Transaction on Power Delivery*, 2019, Publisher: IEEE Xplore. (Under Review)

5. J. P. Keshri & H. P. Tiwari, "PLFE Based Complete Protection of Fault in Transmission Systems," *Special Issue on Artificial Intelligence in Renewable Energy Systems*, 2019, Publisher: ELSEVIER. (Under Review)

6. J. P. Keshri & H. P. Tiwari, "Real Time Security Assessment of Hybrid AC/DC Transmission System using Supervised Machine Learning Approach," *Special Section*

on Hybrid AC/DC Transmission Grids-TPWRD & TPWRS, 2019, Publisher:IEEE Xplore. (Under Review)

7. Jay Prakash Keshri, & Dr. Harpal Tiwari, "Quality of Power Enhancement of Distribution Network System Using DSTATCOM in Simulink Tool of MATLAB," *Electric Power Systems Research*, Publisher: EPSR. (*Communicated in EPSR*)

8. Jay Prakash Keshri, & Dr. Harpal Tiwari,"Frequency Regulation for Securing Microgrid Stability using V2G Technology," *Turkish Journal of Electrical Engineering & Computer Sciences*, Publisher: Scientific and Technological Research Council of Turkey. (*Communicated in EPCS*)

International Conferences

1. Jay Prakash Keshri, & Dr. Harpal Tiwari, 'Fault Classification in VSC-HVDC Transmission System using Machine Learning Approach," 8^{th} *International Conference on Power Systems (ICPS), 2019.*

2. J. P. Keshri & H. P. Tiwari, "Detection and Classification of Transmission Line Faults using Modified F-SVM," 18^{th} *IEEE International Conference on Environment and Electrical Engineering (IEEE-EEEIC18) &* 2^{nd} *IEEE Industrial and Commercial Power System Conference Europe (I&CPS Europe)*, 12-15 June, In Palermo, Italy, 2018.

3. J. P. Keshri & H. P. Tiwari, "Fault Location in Overhead Transmission Line without using Line Parameters," 4^{th} *International Conference on Science, Engineering & Technology (ICSET)*, Malaysia 2017.

4. J. P. Keshri & H. P. Tiwari, "Parameter-Less Fault Locator using Synchronized/Un-Synchronized Data for Overhead Transmission Line," *International Conference on Computer, Communications & Electronics (COMPTELIX 2017)*, In Jaipur, India, July, 2017.

Appendix A

Transmission Test Systems

This section describes the collection of the dataset used for the designing and modelling of dynamic transmission test systems used in the different chapters of this thesis.

A.1 Study System–1 (IEEE 30-Bus Data)

The system consists of loads, capacitor banks, transmission lines, and generators. Fig. A.1 depicts part of the PSCAD model of IEEE 30-bus system. Transmission

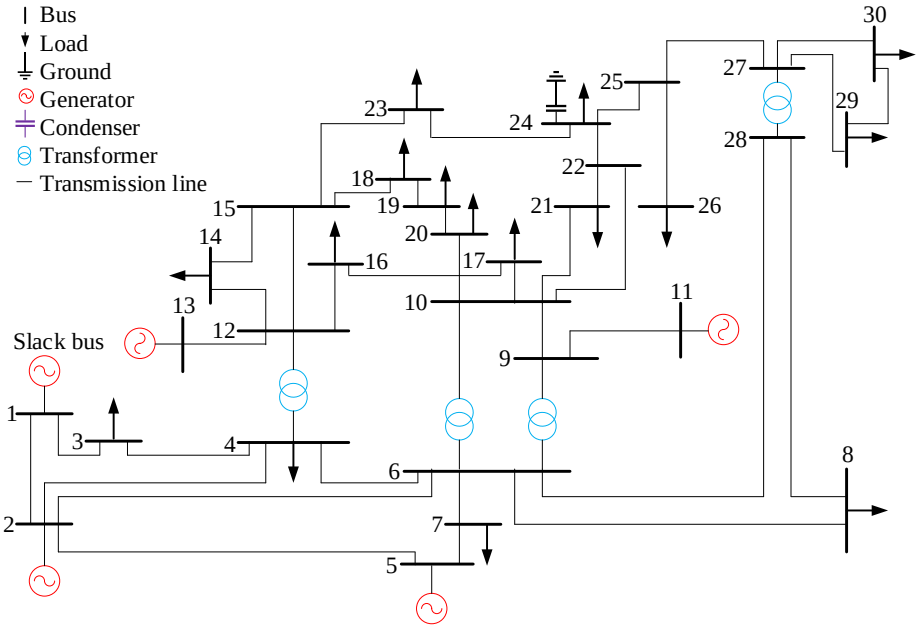

FIGURE A.1: Single line diagram of IEEE-39 Bus transmission system

TABLE A.1: Terminal conditions of IEEE 30-bus system

Bus	V [kV]	δ [deg]	P [pu]	Q [pu]
1	139.92	98.4316	2.6095	-0.1679
2	137.6932	93.0798	0.4	0.5
5	133.452	84.2658	0	0.3685
8	133.32	86.6183	0	0.3714
11	35.706	84.3227	0	0.1617
13	35.343	83.4883	0	0.1062

TABLE A.2: Transmission line characteristics of IEEE 30-bus system

Line		R [pu/m]	X [pu/m]	B [pu/m]
From Bus	To Bus			
1	2	1.92E-07	5.75E-07	5.28E-07
1	3	4.52E-07	1.65E-06	4.08E-07
2	4	5.70E-07	1.74E-06	3.68E-07
2	5	4.72E-07	1.98E-06	4.18E-07
2	6	5.81E-07	1.76E-06	3.74E-07
3	4	1.32E-07	3.79E-07	8.40E-08
4	6	1.19E-07	4.14E-07	9.00E-08
5	7	4.60E-07	1.16E-06	2.04E-07
6	7	2.67E-07	8.20E-07	1.70E-07
6	8	1.20E-07	4.20E-07	9.00E-08
6	28	1.69E-07	5.99E-07	1.30E-07
8	28	6.36E-07	2.00E-06	4.28E-07
9	10	1.00E-09	1.10E-06	1.00E-09
9	11	1.00E-09	2.08E-06	1.00E-09
10	17	3.24E-07	8.45E-07	1.00E-09
10	20	9.36E-07	2.09E-06	1.00E-09
10	21	3.48E-07	7.49E-07	1.00E-09
10	22	7.27E-07	1.50E-06	1.00E-09
12	13	1.00E-09	1.40E-06	1.00E-09
12	14	1.23E-06	2.56E-06	1.00E-09
12	15	6.62E-07	1.30E-06	1.00E-09
12	16	9.45E-07	1.99E-06	1.00E-09
14	15	2.21E-06	2.00E-06	1.00E-09
15	18	1.07E-06	2.19E-06	1.00E-09
15	23	1.00E-06	2.02E-06	1.00E-09
16	17	5.24E-07	1.92E-06	1.00E-09
18	19	6.39E-07	1.29E-06	1.00E-09
19	20	3.40E-07	6.80E-07	1.00E-09
21	22	1.16E-07	2.36E-07	1.00E-09
22	24	1.15E-06	1.79E-06	1.00E-09
23	24	1.32E-06	2.70E-06	1.00E-09
24	25	1.89E-06	3.29E-06	1.00E-09
25	26	2.54E-06	3.80E-06	1.00E-09
25	27	1.09E-06	2.09E-06	1.00E-09
27	29	2.20E-06	4.15E-06	1.00E-09
27	30	3.20E-06	6.03E-06	1.00E-09
29	30	2.40E-06	4.53E-06	1.00E-09

lines are modelled using the Frequency dependent model. Table A.2 shows the transmission line parameters.

TABLE A.3: Approximate line lengths based on typical line reactance values of IEEE 30-bus system

From Bus	To Bus	Total Reactance(Ω)	Approximate length of the line based on typical line reactance values(km)
1	2	10.0188	20.00
1	3	28.7496	57.50
2	4	30.3177	60.60
2	5	34.4995	69.00
2	6	30.6662	61.30
3	4	6.6037	13.20
4	6	7.2135	14.40
5	7	20.2118	40.40
6	7	14.2877	28.60
6	8	7.3181	14.60
6	28	10.4369	20.90
8	28	34.848	69.70
9	10	19.1664	38.30
9	11	36.2419	72.50
10	17	14.7233	29.40
10	20	36.4162	72.80
10	21	13.0506	26.10
10	22	26.136	52.30
12	13	24.3936	48.80
12	14	44.6054	89.20
12	15	22.6512	45.30
12	16	34.6738	69.30
14	15	34.848	69.70
15	18	38.1586	76.30
15	23	35.1965	70.40
16	17	33.4541	66.90
18	19	22.4769	45.00
19	20	11.8483	23.70
21	22	4.1121	8.22
22	24	31.1889	62.40
23	24	47.0448	94.10
24	25	57.3249	115.00
25	26	66.2112	132.00
25	27	36.4162	72.80
27	29	72.3096	145.00
27	30	105.0667	210.00
29	30	78.9307	158.00

The line resistances and reactances are provided in Table A.5 for each line segment of the test system. The Table A.3 lists the approximate line length of each segment, based on typical line data as shows in Table A.5. System loads are modelled as a constant PQ load with parameters as shown in Table A.4.

TABLE A.4: Load characteristics of IEEE 30-bus system

Bus	P [pu]	Q [pu]
2	0.217	0.127
3	0.024	0.012
4	0.076	0.016
5	0.942	0.19
7	0.228	0.109
8	0.3	0.3
10	0.058	0.02
12	0.112	0.075
14	0.062	0.016
15	0.082	0.025
16	0.035	0.018
17	0.09	0.058
18	0.032	0.009
19	0.095	0.034
20	0.022	0.007
21	0.175	0.112
23	0.032	0.016
24	0.087	0.067
26	0.035	0.023
29	0.024	0.009
30	0.106	0.019

TABLE A.5: Typical line reactance values of IEEE 30-bus system

Voltage (kV)	R (Ω/km)	X (Ω/km)
72	0.41	0.5
138	0.14	0.5
230 (single)	0.09	0.5
230 (bundled)	0.04	0.4
345 (bundled)	0.03	0.3
500 (bundled)	0.02	0.3

A.2 Study System–2 (IEEE 39-Bus Data)

The system consists of loads, capacitor banks, transmission lines, and generators. Fig. A.2 depicts part of the PSCAD model of IEEE 39-bus system.

Each machine (generator) is represented as a voltage source where its source impedance is set arbitrarily as 10 Ohms. Table A.6 summarizes the setting for each source, with a base of 100 MVA for per unitizing.

Transmission lines are modelled using the Frequency dependent model. Table A.7 shows the transmission line parameters.

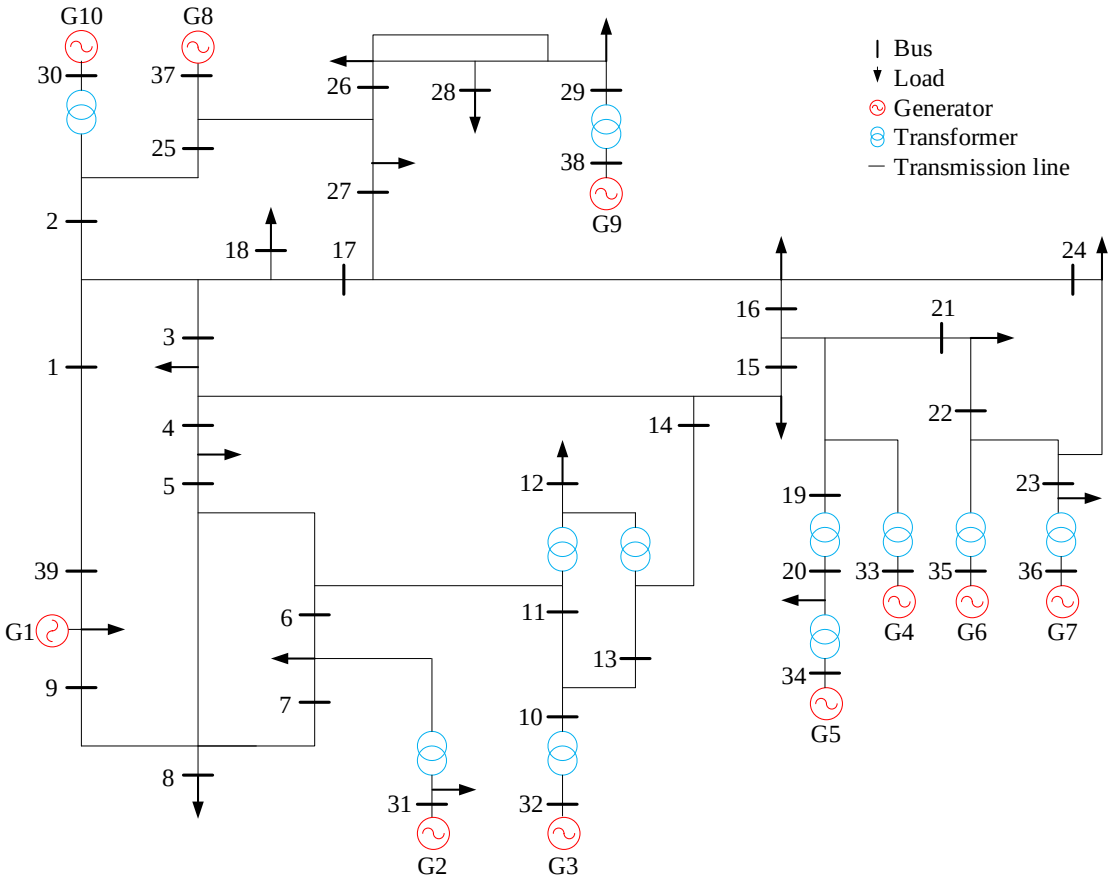

FIGURE A.2: Single line diagram of IEEE-39 Bus transmission system

TABLE A.6: Terminal conditions of IEEE 39-bus system

Bus	V [kV]	δ [deg]	P [pu]	Q [pu]
31	225.86	-1.59	5.713	3.639
30	240.925	-3.73	2.5	0.832
32	226.113	1.79	6.5	0.015
33	229.356	2.87	6.32	0.697
34	232.829	1.46	5.08	1.488
35	241.339	4.78	6.5	1.67
36	244.605	7.46	5.6	0.754
37	236.394	2.05	5.4	-0.353
38	236.095	7.3	8.3	-0.005
39	236.9	-10.06	10	-0.365

TABLE A.7: Transmission line characteristics of IEEE 39-bus system

Line		R [pu/m]	X [pu/m]	B [pu/m]
From Bus	To Bus			
1	2	0.0035	0.0411	0.6987
1	39	0.001	0.025	0.75
2	3	0.0013	0.0151	0.2572
2	25	0.007	0.0086	0.146
3	4	0.0013	0.0213	0.2214
3	18	0.0011	0.0133	0.2138
4	5	0.0008	0.0128	0.1342
4	14	0.0008	0.0129	0.1382
5	6	0.0002	0.0026	0.0434
5	8	0.0008	0.0112	0.1476
6	7	0.0006	0.0092	0.113
6	11	0.0007	0.0082	0.1389
7	8	0.0004	0.0046	0.078
8	9	0.0023	0.0363	0.3804
9	39	0.001	0.025	1.2
10	11	0.0004	0.0043	0.0729
10	13	0.0004	0.0043	0.0729
13	14	0.0009	0.0101	0.1723
14	15	0.0018	0.0217	0.366
15	16	0.0009	0.0094	0.171
16	17	0.0007	0.0089	0.1342
16	19	0.0016	0.0195	0.304
16	21	0.0008	0.0135	0.2548
16	24	0.0003	0.0059	0.068
17	18	0.0007	0.0082	0.1319
17	27	0.0013	0.0173	0.3216
21	22	0.0008	0.014	0.2565
22	23	0.0006	0.0096	0.1846
23	24	0.0022	0.035	0.361
25	26	0.0032	0.0323	0.513
26	27	0.0014	0.0147	0.2396
26	28	0.0043	0.0474	0.7802
26	29	0.0057	0.0625	1.029
28	29	0.0014	0.0151	0.0249

TABLE A.8: Typical line reactance values of IEEE 39-bus system

Voltage (kV)	R (Ω/km)	X (Ω/km)
72	0.41	0.5
138	0.14	0.5
230 (single)	0.09	0.5
230 (bundled)	0.04	0.4
345 (bundled)	0.03	0.3
500 (bundled)	0.02	0.3

The line resistances and reactances are provided in Table A.7 for each line segment of the test system. The following Table A.9 lists the approximate line length of each segment, based on typical line data as shows in Table A.8. System loads are modelled as a constant PQ load with parameters as shown in Table A.10.

TABLE A.9: Approximate line lengths based on typical line reactance values of IEEE 39-bus system

From Bus	To Bus	Total Reactance(Ω)	Approximate length of the line based on typical line reactance values(km)
1	2	21.7419	43.4838
1	39	13.225	26.45
2	3	7.9879	15.9758
2	25	4.5494	9.0988
3	4	11.2677	22.5354
3	18	7.0357	14.0714
4	5	6.7712	13.5424
4	14	6.8241	13.6482
5	6	1.3754	2.7508
5	8	5.9248	11.8496
6	7	4.8668	9.7336
6	11	4.3378	8.6756
7	8	2.4334	4.8668
8	9	19.2027	38.4054
9	39	13.225	26.45
10	11	2.2747	4.5494
10	13	2.2747	4.5494
13	14	5.3429	10.6858
14	15	11.4793	22.9586
15	16	4.9726	9.9452
16	17	4.7081	9.4162
16	19	10.3155	20.631
16	21	7.1415	14.283
16	24	3.1211	6.2422
17	18	4.3378	8.6756
17	27	9.1517	18.3034
21	22	7.406	14.812
22	23	5.0784	10.1568
23	24	18.515	37.03
25	26	17.0867	34.1734
26	27	7.7763	15.5526
26	28	25.0746	50.1492
26	29	33.0625	66.125
28	29	7.9879	15.9758

TABLE A.10: Load characteristics of IEEE 39-bus system

Bus	P [pu]	Q [pu]
3	3.22	0.024
4	5	1.84
7	2.338	0.84
8	5.22	1.76
12	0.075	0.88
15	3.2	1.53
16	3.294	0.323
18	1.58	0.3
20	6.8	1.03
21	2.74	1.15
23	2.475	0.846
24	3.086	-0.922
25	2.24	0.472
26	1.39	0.17
27	2.81	0.755
28	2.06	0.276
29	2.835	0.269
31	0.092	0.046
39	11.04	2.5

A.3 Study System–3 (CIGRE (B4.57 and B4.58) Hybrid Transmission System Data)

The technical notes describe the details of the DC grid. The system consist of loads, capacitor bank, transmission lines, and generator. Fig. A.3 depicts part of the PSCAD model of CIGRE hybrid transmission test system. The complete DC grid test system Basic Configuration is shown as,

- 2 onshore AC systems
  - System A (A0 and A1)
  - System B (B0, B1, B2 and B3)
- 4 offshore AC systems
  - System C (C1 and C2)
  - System D (D1)
  - System E (E1)
  - System F (F1)

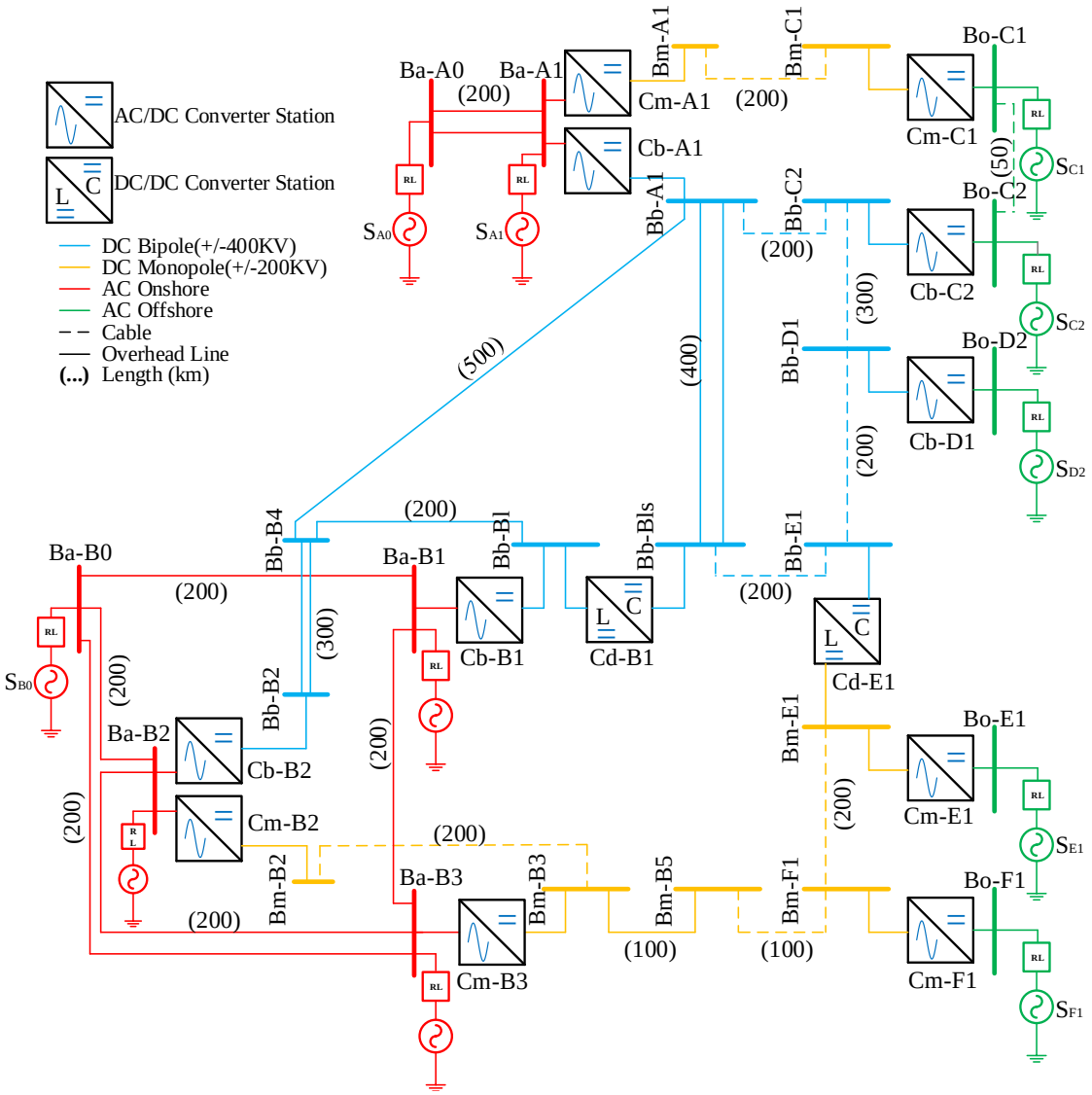

FIGURE A.3: Schematic diagram of CIGRE (B4.57 and B4.58) hybrid HVAC and HVDC transmission system model

- 2 DC nodes, with no connection to AC
  - B4
  - B5
- 3 VSC-DC systems
  - DCS1 (A1 and C1)
  - DCS2 (B2, B3, B5, F1 and E1)
  - DCS3 (A1, C2, D1, E1, B1, B4 and B2)

A.3.1 Basic System Data for DC Grid

Table A.11 gives the voltages of the different subsystems and Table A.12 AC bus data.

Table A.11: System data

System	Voltage [kV]
AC Onshore	380
AC Offshore	145
DC Sym. Monopole	+/-200
DC Bipole	+/-400

Table A.12: AC bus data

Bus	Bus Type	Generation [MW]	Load [MW]
Ba-A0	Slack Bus	...	...
Ba-A1	PQ	-2000	1000
Ba-B0	Slack Bus	...	...
Ba-B1	PQ	-1000	2200
Ba-B2	PQ	-1000	2300
Ba-B3	PQ	-1000	1900
Ba-C1	PQ	-500	0
Ba-C2	PQ	-500	0
Ba-D1	PQ	-1000	0
Ba-E1	PQ	0	100
Ba-F1	PQ	-500	0

Table A.13, Table A.14 and Table A.15 give the data for all the AC-DC converter stations.

Table A.13: DCS1 data

AC-DC Converter Station	Power Rating [MVA]	Operation Mode Setpoints
Cm-A1	800	Q = 0 VDC = 1pu
Cm-C1	800	AC Slack

Table A.14: DCS2 data

AC-DC Converter Station	Power Rating [MVA]	Operation Mode Setpoints	
Cm-B2	800	Q = 0	$V_{DC} = 0.99pu$
Cm-B3	1200	$V_{AC} = 1pu$	P = 800MW
Cm-E1	200	AC Slack	
Cm-F1	800	AC Slack	

Table A.15: DCS3 data

AC-DC Converter Station	Power Rating [MVA]	Operation Mode Setpoints	
Cb-A1	2*1200	VAC = 1pu	VDC = 1.01pu
Cb-B1	2*1200	VAC = 1pu	P = 1500MW
Cb-B2	2*1200	VAC = 1pu	P = 1700MW
Cb-C2	2*400	VAC = 1pu	P = - 600MW
Cb-D1	2*800	AC Slack	

All converters operate on 400kV DC voltage and 220kV AC voltage. The AC voltage at the Point of Common Coupling (PCC) can be either 380kV (onshore) or 145kV (offshore), but this only influences the ratio of the ideal transformer while it does not influence the rest of the converter pole model. Table A.16 shows the DC-DC converter data.

The offshore DC-DC converter at E1 operates at 800kV on the -side and at 400kV on the -side. The onshore DC-DC converter at B1 operates at 800kV on both sides. Table A.17 shows the DC-DC converter data.

Table A.16: AC-DC converter pole data

	pu	E1	C2	A1, B2, C1, D1, F1	A1, B1, B2, B3
S	1	$200MVA$	$400MVA$	$800MVA$	$1200MVA$
L	25.50%	$196mH$	$98mH$	$49mH$	$33mH$
R	1.00%	2.420Ω	1.210Ω	0.605Ω	0.403Ω
G	0.10%	$1.25\mu S$	$2.50\mu S$	$5.00\mu S$	$7.50\mu S$
C	$60ms$	$75\mu F$	$150\mu F$	$300\mu F$	$450\mu F$

Table A.17: DC-DC converter station data

	pu	E1	B1
S	1	$1000MW$	$2000MW$
L	$5ms$	$800mH$	$1600mH$
R	1200%	$1,92\Omega$	$3,84\Omega$
G	$0,025\%$	$0,390625\mu S$	$0,78125\mu S$
C	$5ms$	$7,8125\mu F$	$15,625\mu F$

The test systems contain AC and DC cables and overhead lines. The R-L-G-C parameters needed for average value simulation are given in Table A.18. AC slack busses are modelled as voltage source with R-L impedance. The parameters are given in Table A.19.

The control parameters of all AC-DC converters are given in Table A.20, Table A.21 and Table A.22. The control parameter of DC-DC converter are shown in Table A.23.

TABLE A.18: Line data for average value model simulation

$LineData$	R $[\Omega/km]$	L $[mH/km]$	C $[\mu F/km]$	G $[\mu S/km]$	$Max.current$ $[A]$
$DCOHL+/-400kV$	0.0114	0.9356	0.0123	-	3500
$DCOHL+/-200kV$	0.0133	0.8273	0.0139	-	3000
$DCcable+/-400kV$	0.0095	2.112	0.1906	0.048	2265
$DCcable+/-200kV$	0.0095	2.111	0.2104	0.062	1962
$ACcable145kV$	0.0843	0.2526	0.1837	0.041	715
$ACOHL380kV$	0.02	0.8532	0.0135	-	3555

TABLE A.19: Slack bus data

S	30GVA
X/R	10
T	15s
	15MW/mHz
V	380kV

TABLE A.20: DCS1 control data

AC-DC Converter Station	Control Mode
Cm-A1	Q VDC
Cm-C1	AC Slack

TABLE A.21: DCS2 control data

AC-DC Converter Station	Control Mode	V_{AC} $droop$ $[pu, MVAr/kV]$	V_{DC} $droop$ $[pu; MW/kV]$
Cm-B2	Q(VAC) P(VDC)	$10; 21.053$	$10; 40$
Cm-B3	Q(VAC) P(VDC)	$10; 31.579$	$10; 60$
Cm-E1	AC Slack	-	-
Cm-F1	AC Slack	-	-

TABLE A.22: DCS3 control data

AC-DC Converter Station	Control Mode	V_{AC} $droop$ $[pu; MVAr/kV]$	V_{DC} $droop$ $[pu; MW/kV]$
Cb-A1	$Q(V_{AC})$ $P(V_{DC})$	$10; 63.158$	$10; 60$
Cb-B1	$Q(V_{AC})$ $P(V_{DC})$	$10; 63.158$	$10; 60$
Cb-B2	$Q(V_{AC})$ $P(V_{DC})$	$10; 63.158$	$10; 60$
Cb-C2	V_{AC} P	-	-
Cb-D1	AC Slack	-	-

TABLE A.23: DC-DC converter control data

DC-DC Converter Station	Control Mode	D [%]
Cd-B1	D	99.595
Cd-E1	D	50.28

Appendix B

Commercial and Technical Information

This section describes the importance of the HVDC transmission system in the recent time of the Indian power transmission system. Further, it also shows their comparison with HVAC transmission system with figure and tables.

B.1 Indian Scenario of Power Transmission System

Indian government wants to fulfil the power requirement of all the need their citizen so, it increases our power generation through renewable energy and also increases transmission capacity day by day and try to fulfil power requirement of the consumer in the country. Government initiate the high voltage AC and DC transmission so, that bulk power will be transmitted easily from generation end to consumer end. For this they have developed high voltage transmission corridor and also upgrade their transmission lines to 765 kV line. With the increase in transmission line capacity, it also increases complexity and the problem like interconnection with a different type of transmission systems and faults due to the long system in open and goes through different weather conditions. Along with, the rapid development in HVDC technology due to an increase in renewable energy resources transmission system operator prefer HVDC transmission system for bulk power transfer to the consumer ends. Because, for bulk power transfer for a long distance it is advisable to opt DC transmission system for economical as well as environment-friendly as shown in Fig. B.1. For this region, the Indian government also develop their HVDC transmission

system corridor and plane to increase in future. The Indian government also plan to supply power to long distance place and nearby country with HVDC transmission systems. Some of the example as HVDC transmission systems with extra-long overhead (OH) lines such as the 1728 km Bishwanath-Agra and 1368 km Talcher-Kolar and extra-long underground (UG) cables used in a part of 268km Sri Lanka-India interconnection of HVDC system are commissioned in India.

As per the commitment from the European Union to reduce 80% greenhouse gas emission by 2050. Therefore, the Indian government significant quantities of renewable energies have increasingly been added to the generation mix in the near future. Since, most of the renewable resource is located in remote locations, the concept of a high voltage direct current (HVDC) "Supergrid" has emerged as an interesting possibility in future. There are many projects that have been planned or carried out in the last decade in which several important HVDC installations have been developed around the world as shown in Fig. B.3. As for example: "Tres Amigas SuperStation", which will provide a connection between the three major U.S. transmission network (Eastern, Western and Texas Network). The world longest HVDC link in Brazil, allowing the transmission of the energy generated from the hydroelectric power plant in Rio Madeira to south Brazil carrying 7100MW electricity at 600kV over 2,500 km. In India largest HVDC link between Talcher-Kolar deliver power from the eastern region to southern region carrying 2500 MW electricity at 500 kV, over 1450 km as shown in Fig. B.2. Along with from data of the Table B.2 shows the HVAC and HVDC transmission system increased to approximately double in the last decade. It also describes the installed and planed line length of transmission corridor in India. Along with, Table B.1 describe the present scenario of HVDC transmission corridor in India. Therefore it shows that the Indian government also plan to achieve the power surplus in the country.

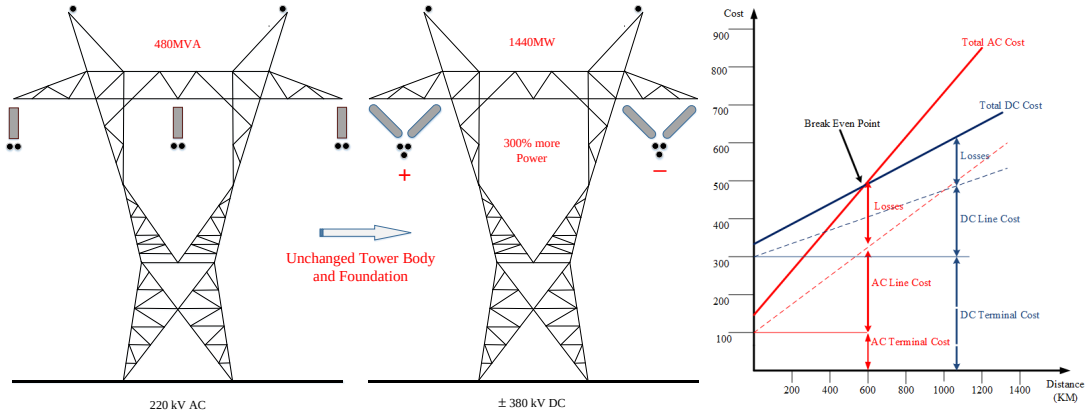

FIGURE B.1: Comparison between HVAC and HVDC transmission systems

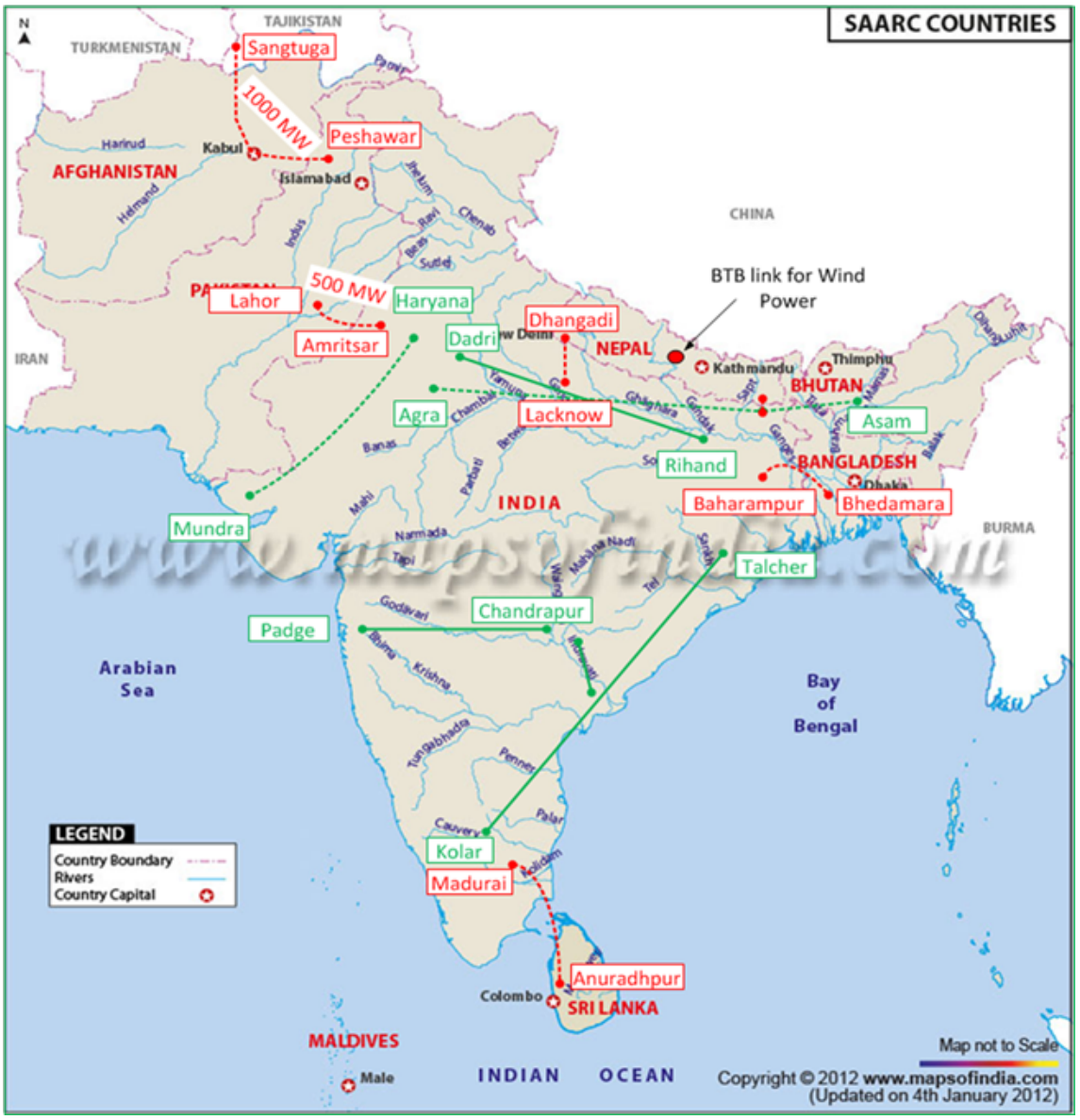

FIGURE B.2: HVDC transmission systems: Indian picture

*(Source: https://www.mapsofindia.com/HVDC-system)

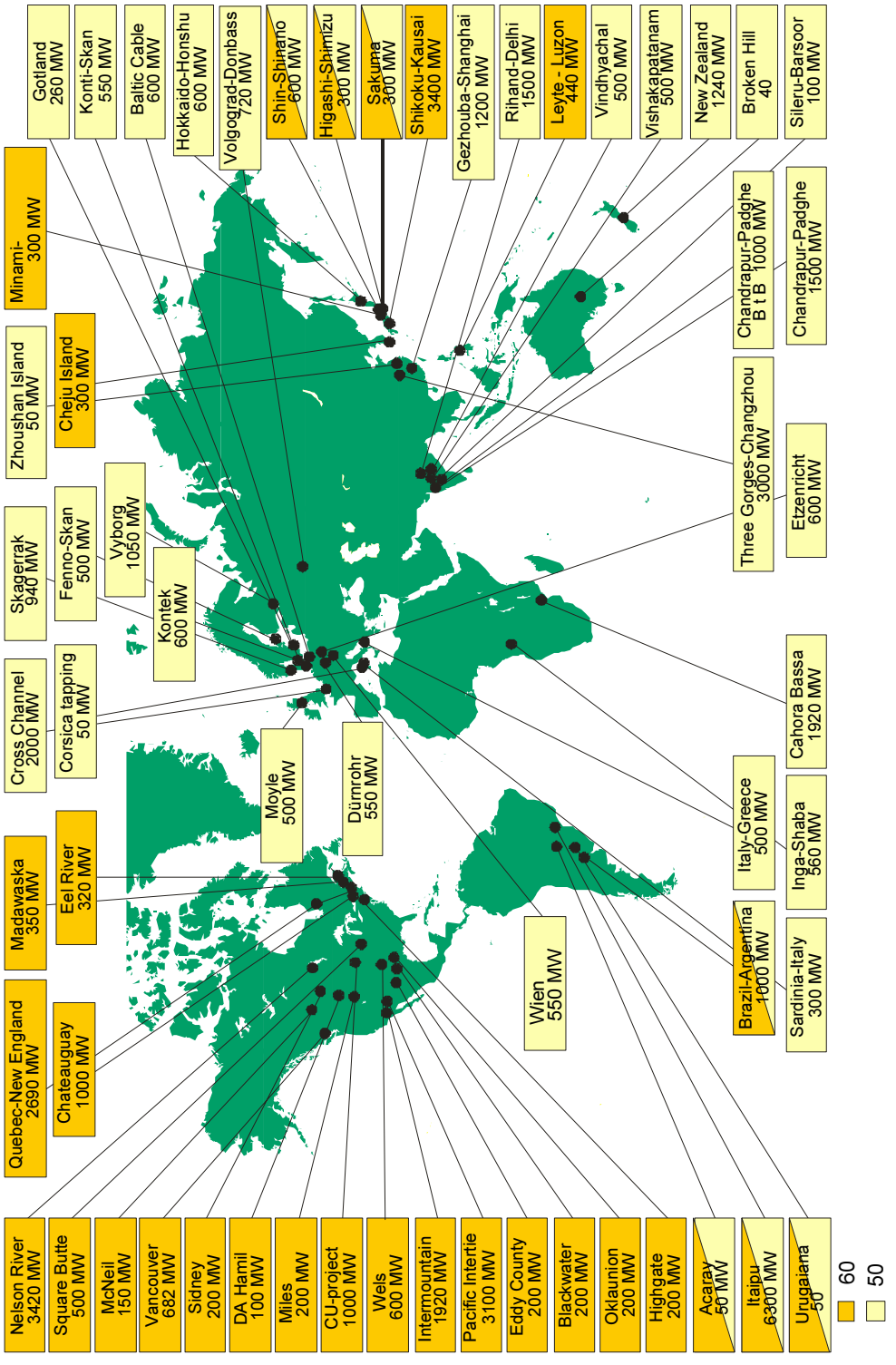

FIGURE B.3: HVDC transmission systems: World picture

*(Source: http://large.stanford.edu/courses/2010/ph240/hamerly1/docs/energyweek00.pdf)

Table B.1: HVDC transmission system: Indian scenario

S. No	Project Name	Connecting region	Commissioned on	Power rating (MW)	AC voltage (kV)	DC voltage (kV)	Mode of operation	No. of Poles/ Blocks	Length of line (km)
				Monopole line					
1	Barsur-Lower Sileru	AP Transco	1989 Decommission 2014	400	200	200	Mono	2	196
				Bipolar line					
2	Rihand-Dadri	ER-WR	Dec-91	1500	400	500	Bipole	2	816
3	Chandrapu-Padghe	CR-WR	1999	1504	400	500	Bipole	2	752
4	Talcher-Kolar	ER-SR	Jun-03	2738	400	500	Bipole	2	1369
5	Ballia- Bhiwadi	ER-NR	Pole1: March 2010 Pole 2: March 2011	2500	400	500	Bipole	2	780
6	Mundra- Mohindergarh	WR-NR	2012	1500	400	500	Bipole	2	986
				Multi-terminal Line					
7	Bishwanath-Agra	NER-ER	2015	6000	400	800	Multi- Terminal	2	1728
				Back to Back connection					
8	Vidhyanchal	WR-NR	Apr-89	2x250	400	70	Back To Back	2	
9	Chandrapur	WR-SR	Dec-97	2x500	400	205	Back To Back	2	
10	Sasaram	ER-SR	Sep-02	1x500	400	205	Back To Back	2	
11	*Gazuwaka*(*VizagI&II*)	ER-SR	1999 March 2005	2x500	400	Block1: 205 Block 2: 176	Back To Back	2	
				International Connections					
12	India - Bangladesh	ER (India)-WR (Bangladesh)	October 2013	1x500	400	400	Bipole	2	125
13	India- Sri Lanka	SE (India)-NW (Sri-Lanka)	2013	Stage1:1x500 Stage2:1x500	400	220	Bipole	2	285

*Source: http://powermin.nic.in/hvdc-system-india/10^{th} *and* $11^{th} - plane - report$

TABLE B.2: Transmission system projection during 12^{th} plan in India

Transmission Line (EHVAC/HVAC/HVDC)					
	At the end of 10th plan	Addition during the first four years of 11th plan (2007-2011)	Expected at the end of 11th plan	Projected addition during the 12th plan (2012-2016)	Expected at the end of 12th Plan
HVDC Bipolar Lines (ckm)	5,872	1,580	9,452	9,440	18,892
765kv	1,704	1,636	4,164	27,000	31,164
400kv	75,722	26,856	1,14,979	38,000	1,52,979
220kv	1,14,629	19,780	1,40,976	35,000	1,75,976
Total transmission line (ckm)	1,97,927	49,852	2,69,571	1,09,440	3,79,011
Substation (HVAC and HVDC)					
Total HVDC terminal capacity MW	8,000	8,500	13,500	13,000	26,500
Total AC substation capacity MVA	2,49,439	96,075	3,72,894	2,70,000	642,894

*Source: https://niti.gov.in/writereaddata/files/$new_initiatives$
*ckm: circuit kilometer

Bibliography

[1] O. I. Elgerd, *Electric Energy Systems Theory: An Introduction.* McGraw-Hill Book Company, New York, NY, 1982.

[2] M. Ilic, F. Galiana, and L. Fink, *Power Systems Restructuring: Engineering and Economics.* Springer Science & Business Media, 2013.

[3] A. T. Johns and S. Jamali, "Accurate fault location technique for power transmission lines," *IEE Proceedings C - Generation, Transmission and Distribution*, vol. 137, no. 6, pp. 395–402, 1990.

[4] A. S. S. Altaie and J. Asumadu, "Fault detection and classification for compensating network using combination relay and ann," in *2015 IEEE International Conference on Electro/Information Technology (EIT)*, 2015, pp. 351–356.

[5] R. N. Mahanty and P. B. D. Gupta, "Application of rbf neural network to fault classification and location in transmission lines," *IEE Proceedings - Generation, Transmission and Distribution*, vol. 151, no. 2, pp. 201–212, March 2004.

[6] M. T. Hagh, K. Razi, and H. Taghizadeh, "Fault classification and location of power transmission lines using artificial neural network," in *2007 International Power Engineering Conference (IPEC 2007)*, 2007, pp. 1109–1114.

[7] K. M. Silva, B. A. Souza, and N. S. D. Brito, "Fault detection and classification in transmission lines based on wavelet transform and ann," *IEEE Transactions on Power Delivery*, vol. 21, no. 4, pp. 2058–2063, 2006.

[8] J. Izykowski, E. Rosolowski, P. Balcerek, M. Fulczyk, and M. M. Saha, "Accurate noniterative fault location algorithm utilizing two-end unsynchronized measurements," *IEEE Transactions on Power Delivery*, vol. 25, no. 1, pp. 72–80, 2010.

[9] M. Davoudi, J. Sadeh, and E. Kamyab, "Parameter-free fault location for transmission lines based on optimisation," *IET Generation, Transmission & Distribution*, vol. 9, no. 11, pp. 1061–1068, 2015.

[10] M. Davoudi, J. Sadeh, and E. Kamyab, "Transient-based fault location on three-terminal and tapped transmission lines not requiring line parameters," *IEEE Transactions on Power Delivery*, vol. 33, no. 1, pp. 179–188, Feb 2018.

[11] C. A. Apostolopoulos and G. N. Korres, "A novel algorithm for locating faults on transposed/untransposed transmission lines without utilizing line parameters," *IEEE Transactions on Power Delivery*, vol. 25, no. 4, pp. 2328–2338, 2010.

[12] Y. Liao and N. Kang, "Fault-location algorithms without utilizing line parameters based on the distributed parameter line model," *IEEE Transactions on Power Delivery*, vol. 24, no. 2, pp. 579–584, 2009.

[13] L. Yang, F. Chen, M. Xue, Y. Li, S. Chen, and L. Zou, "A novel fault location method for hvdc transmission lines," in *2019 IEEE PES GTD Grand International Conference and Exposition Asia (GTD Asia)*, March 2019, pp. 341–346.

[14] S. Saha and M. Aldeen, "Dynamic modeling of power systems experiencing faults in transmission / distribution networks," *IEEE Transactions on Power Systems*, vol. 30, no. 5, pp. 2349–2363, 2014.

[15] A. S. Dobakhshari and A. M. Ranjbar, "A novel method for fault location of transmission lines by wide-area voltage measurements considering measurement errors," *IEEE Transactions on Smart Grid*, vol. 6, no. 2, pp. 874–884, 2014.

[16] M. K. Neyestanaki and A. Ranjbar, "An adaptive pmu-based wide area backup protection scheme for power transmission lines," *IEEE Transactions on Smart Grid*, vol. 6, no. 3, pp. 1550–1559, 2015.

[17] N. Kang, J. Chen, and Y. Liao, "A fault-location algorithm for series-compensated double-circuit transmission lines using the distributed parameter line model," *IEEE Transactions on Power Delivery*, vol. 30, no. 1, pp. 360–367, 2014.

[18] T. G. Bolandi, H. Seyedi, S. M. Hashemi, and P. S. Nezhad, "Impedance-differential protection: A new approach to transmission-line pilot protection," *IEEE Transactions on Power Delivery*, vol. 30, no. 6, pp. 2510–2518, Dec 2015.

[19] H. Manesh, G. Lugrin, R. Razzaghi, C. Romero, M. Paolone, and F. Rachidi, "Anew method to locate faults in power networks based on electromagnetic time reversal," in *2012 IEEE* 13^{th} *International Workshop on Signal Processing Advances in Wireless Communications (SPAWC)*. IEEE, 2012, pp. 469–474.

[20] K. Andanapalli and B. R. Varma, "Travelling wave based fault location for teed circuits using unsynchronised measurements," in *2013 International Conference on Power, Energy and Control (ICPEC)*. IEEE, 2013, pp. 227–232.

[21] P. E. Argyropoulos and H. Lev-Ari, "Wavelet customization for improved fault-location quality in power networks," *IEEE Transactions on Power Delivery*, vol. 30, no. 5, pp. 2215–2223, 2015.

[22] M.-R. Mosavi and A. Tabatabaei, "Traveling-wave fault location techniques in power system based on wavelet analysis and neural network using gps timing," *Wireless Personal Communications*, vol. 86, no. 2, pp. 835–850, 2016.

[23] H. H. Szu, "Automatic fault recognition by image correlation neural network techniques," *IEEE Transactions on Industrial Electronics*, vol. 40, no. 2, pp. 197–208, 1993.

[24] F. Lopes, K. Silva, F. Costa, W. Neves, and D. Fernandes, "Real-time traveling-wave-based fault location using two-terminal unsynchronized data," *IEEE Transactions on Power Delivery*, vol. 30, no. 3, pp. 1067–1076, 2014.

[25] V. Kale, S. Bhide, and P. Bedekar, "Fault location estimation based on wavelet analysis of traveling waves," in *2012 Asia-Pacific Power and Energy Engineering Conference*. IEEE, 2012, pp. 1–5.

[26] A. Megahed, H. Elrefaie, A. M. Moussa, and Y. Marghany, "Wavelet based fault location technique for two and three terminal lines," in *2012 IEEE Power and Energy Society General Meeting*. IEEE, 2012, pp. 1–7.

[27] M. El-Hami, L. Lai, D. Daruvala, and A. Johns, "A new travelling-wave based scheme for fault detection on overhead power distribution feeders," *IEEE Transactions on Power Delivery*, vol. 7, no. 4, pp. 1825–1833, 1992.

[28] M. Vitins, "A correlation method for transmission line protection," *IEEE Transactions on Power Apparatus and Systems*, no. 5, pp. 1607–1617, 1978.

[29] P. F. Gale, J. Stokoe, and P. A. Crossley, "Practical experience with travelling wave fault locators on scottish power's 275 amp; 400 kv transmission system," in *Sixth International Conference on Developments in Power System Protection (Conf. Publ. No. 434)*. IET, March 1997, pp. 192–196.

[30] U. B. Parikh, B. Das, and R. Maheshwari, "Fault classification technique for series compensated transmission line using support vector machine," *International Journal of Electrical Power & Energy Systems*, vol. 32, no. 6, pp. 629–636, 2010.

[31] S. R. Samantaray, P. K. Dash, and G. Panda, "Distance relaying for transmission line using support vector machine and radial basis function neural network," *International Journal of Electrical Power & Energy Systems*, vol. 29, no. 7, pp. 551–556, 2007.

[32] M. Ando, E. Schweitzer, and R. Baker, "Development and field-data evaluation of single-end fault locator for two-thermal hvdc transmission lines part 1: Data collection system and field data," *IEEE Transactions on Power Apparatus and Systems*, no. 12, pp. 3524–3530, 1985.

[33] M. Ando, E. Schweitzer, and et al., "Development and field-data evaluation of single-end fault locator for two-thermal hvdc transmission lines part 2: Data collection system and field data," *IEEE Transactions on Power Apparatus and Systems*, no. 12, pp. 3531–3537, 1985.

[34] Y. Ma, H. Li, G. Wang, and J. Wu, "Fault analysis and traveling-wave-based protection scheme for double-circuit lcc-hvdc transmission lines with shared towers," *IEEE Transactions on Power Delivery*, vol. 33, no. 3, pp. 1479–1488, 2018.

[35] O. K. Nanayakkara, A. D. Rajapakse, and R. Wachal, "Traveling-wave-based line fault location in star-connected multiterminal hvdc systems," *IEEE transactions on power delivery*, vol. 27, no. 4, pp. 2286–2294, 2012.

[36] F. Kong, Z. Hao, and B. Zhang, "A novel traveling-wave-based main protection scheme for ± 800 kv uhvdc bipolar transmission lines," *IEEE Transactions on Power Delivery*, vol. 31, no. 5, pp. 2159–2168, Oct 2016.

[37] A. Mazon, I. Zamora, J. Gracia, K. Sagastabeutia, and J. Saenz, "Selecting ann structures to find transmission faults," *IEEE Computer Applications in Power*, vol. 14, no. 3, pp. 44–48, 2001.

[38] P. D. Achlerkar, S. Samantaray, and M. S. Manikandan, "Variational mode decomposition and decision tree based detection and classification of power quality disturbances in grid-connected distributed generation system," *IEEE Transactions on Smart Grid*, vol. 9, no. 4, pp. 3122–3132, 2018.

[39] E. Koley, S. K. Shukla, S. Ghosh, and D. K. Mohanta, "Protection scheme for power transmission lines based on svm and ann considering the presence of non-linear loads," *IET Generation, Transmission & Distribution*, vol. 11, no. 9, pp. 2333–2341, 2017.

[40] H. Cui and N. Tu, "Hvdc transmission line fault localization base on rbf neural network with wavelet packet decomposition," in *2015 12th International Conference on Service Systems and Service Management (ICSSSM)*. IEEE, 2015, pp. 1–4.

[41] A. Yadav and A. Swetapadma, "Enhancing the performance of transmission line directional relaying, fault classification and fault location schemes using fuzzy inference system," *IET Generation, Transmission & Distribution*, vol. 9, no. 6, pp. 580–591, 2015.

[42] H. Trevor, T. Robert, and F. JH, "The elements of statistical learning: Data mining, inference, and prediction," 2009.

[43] J. M. Johnson and A. Yadav, "Complete protection scheme for fault detection, classification and location estimation in hvdc transmission lines using support vector machines," *IET Science, Measurement & Technology*, vol. 11, no. 3, pp. 279–287, 2016.

[44] A. Yusuff, A. Jimoh, and J. Munda, "Fault location in transmission lines based on stationary wavelet transform, determinant function feature and support vector regression," *Electric Power Systems Research*, vol. 110, pp. 73–83, 2014.

[45] O. K. Nanayakkara, A. D. Rajapakse, and R. Wachal, "Location of dc line faults in conventional hvdc systems with segments of cables and overhead lines using terminal measurements," *IEEE Transactions on Power Delivery*, vol. 27, no. 1, pp. 279–288, 2012.

[46] T. L. Y. Lee, C. Chao and C. Liu, "A synchrophasor-based fault location method for three-terminal hybrid transmission lines with one off-service line branch," *IEEE Transactions on Power Delivery*, vol. 33, no. 6, pp. 3249–3251, Dec 2018.

[47] J. R. Marti, "Accurate modelling of frequency-dependent transmission lines in electromagnetic transient simulations," *IEEE Transactions on Power Apparatus and Systems*, vol. PAS-101, no. 1, pp. 147–157, Jan 1982.

[48] M. M. Saha, J. J. Izykowski, and E. Rosolowski, *Fault location on power networks*. Springer Science & Business Media, 2009.

[49] Y. Liao and N. Kang, "Fault-location algorithms without utilizing line parameters based on the distributed parameter line model," *IEEE Transactions on Power Delivery*, vol. 24, no. 2, pp. 579–584, 2009.

[50] Li Shengfang, Fan Chunju, Yu Weiyong, Cai Huarong, and K. K. Li, "A new phase measurement unit (pmu) based fault location algorithm for double circuit lines," in *2004 Eighth IEE International Conference on Developments in Power System Protection*, vol. 1, April 2004, pp. 188–191 Vol.1.

[51] K. Ramar, H. Low, and E. E. Ngu, "One-end impedance based fault location in double-circuit transmission lines with different configurations," *International Journal of Electrical Power & Energy Systems*, vol. 64, pp. 1159–1165, 2015.

[52] M. Farshad and J. Sadeh, "A novel fault-location method for hvdc transmission lines based on similarity measure of voltage signals," *IEEE Transactions on Power Delivery*, vol. 28, no. 4, pp. 2483–2490, 2013.

[53] S. Azizi, M. Sanaye-Pasand, M. Abedini, and A. Hasani, "A traveling-wave-based methodology for wide-area fault location in multiterminal dc systems," *IEEE Transactions on Power Delivery*, vol. 29, no. 6, pp. 2552–2560, 2014.

[54] M. Kezunovic, "Smart fault location for smart grids," *IEEE Transactions on Smart Grid*, vol. 2, no. 1, pp. 11–22, March 2011.

[55] Y. Ouyang, J. He, J. Hu, and S. X. Wang, "A current sensor based on the giant magnetoresistance effect: Design and potential smart grid applications," *Sensors*, vol. 12, no. 11, pp. 15 520–15 541, 2012.

[56] J. Han, J. Hu, Y. Yang, Z. Wang, S. X. Wang, and J. He, "A nonintrusive power supply design for self-powered sensor networks in the smart grid by scavenging energy from ac power line," *IEEE Transactions on Industrial Electronics*, vol. 62, no. 7, pp. 4398–4407, July 2015.

[57] J. De La Ree, V. Centeno, J. S. Thorp, and A. G. Phadke, "Synchronized phasor measurement applications in power systems," *IEEE Transactions on Smart Grid*, vol. 1, no. 1, pp. 20–27, June 2010.

[58] T. Takagi, Y. Yamakoshi, J. Baba, K. Uemura, and T. Sakaguchi, "A new alogorithm of an accurate fault location for ehv/uhv transmission lines: Part-ii fourier transformation method," *IEEE Transactions on Power Apparatus and Systems*, no. 3, pp. 564–573, 1982.

[59] T. Takagi, Y. Yamakoshi, M. Yamaura, R. Kondow, and T. Matsushima, "Development of a new type fault locator using the one-terminal voltage and current data," *IEEE Transactions on Power apparatus and systems*, no. 8, pp. 2892–2898, 1982.

[60] L. Eriksson, M. M. Saha, and G. Rockefeller, "An accurate fault locator with compensation for apparent reactance in the fault resistance resulting from remote-end infeed," *IEEE Transactions on Power Apparatus and Systems*, no. 2, pp. 423–436, 1985.

[61] Y. Z. J. Ding, X. Wang and L. Li, "Distributed traveling-wave-based fault-location algorithm embedded in multiterminal transmission lines," *IEEE Transactions on Power Delivery*, vol. 33, no. 6, pp. 3045–3054, Dec 2018.

[62] P. Nan, C. Menghan, L. Rui, and F. Zare, "Asynchronous fault location scheme for half-wavelength transmission lines based on propagation characteristics of voltage travelling waves," *IET Generation, Transmission Distribution*, vol. 13, no. 4, pp. 502–510, 2019.

[63] O. Naidu and A. K. Pradhan, "A traveling wave-based fault location method using unsynchronized current measurements," *IEEE Transactions on Power Delivery*, vol. 34, no. 2, pp. 505–513, April 2019.

[64] J. Jiang, C. Chuang, Y. Wang, C. Hung, J. Wang, C. Lee, and Y. Hsiao, "A hybrid framework for fault detection, classification, and location—part i: Concept, structure, and methodology," *IEEE Transactions on Power Delivery*, vol. 26, no. 3, pp. 1988–1998, July 2011.

[65] I. M. Karmacharya and R. Gokaraju, "Fault location in ungrounded photovoltaic system using wavelets and ann," *IEEE Transactions on Power Delivery*, vol. 33, no. 2, pp. 549–559, 2018.

[66] T. Takagi, Y. Yamakoshi, J. Baba, K. Uemura, and T. Sakaguchi, "A new alogorithm of an accurate fault location for ehv/uhv transmission lines: Part-i fourier transformation method," *IEEE Transactions on Power Apparatus and Systems*, no. 3, pp. 1316–1323, 1981.

[67] D. Novosel, D. G. Hart, E. Udren, and J. Garitty, "Unsynchronized two-terminal fault location estimation," *IEEE transactions on Power Delivery*, vol. 11, no. 1, pp. 130–138, 1996.

[68] J.-A. Jiang, J.-Z. Yang, Y.-H. Lin, C.-W. Liu, and J.-C. Ma, "An adaptive pmu based fault detection/location technique for transmission lines-i theory and algorithms," *IEEE Transactions on Power Delivery*, vol. 15, no. 2, pp. 486–493, 2000.

[69] J.-A. Jiang, Y.-H. Lin, J.-Z. Yang, T.-M. Too, and C.-W. Liu, "An adaptive pmu based fault detection/location technique for transmission lines-ii pmu implementation and performance evaluation," *IEEE Transactions on Power Delivery*, vol. 15, no. 4, pp. 1136–1146, 2000.

[70] H. Lin, Ying, C.-W. Liu, and C.-S. Yu, "A new fault locator for three-terminal transmission lines using two-terminal synchronized voltage and current phasors," *IEEE Transactions on Power Delivery*, vol. 17, no. 2, pp. 452–459, 2002.

[71] H. Lin Ying, W. Liu Chih, and et al., "A new pmu-based fault detection/location technique for transmission lines with consideration of arcing fault discrimination-part i: Theory and algorithms," *IEEE Transactions on power Delivery*, vol. 19, no. 4, pp. 1587–1593, 2004.

[72] Y. H. Lin, C. W. Liu, and C. S. Chen, "A new pmu-based fault detection/location technique for transmission lines with consideration of arcing fault discrimination-part ii: Theory and algorithms," *IEEE Transactions on power Delivery*, vol. 19, no. 4, pp. 1594–1601, 2004.

[73] C.-L. Chuang, J.-A. Jiang, Y.-C. Wang, C.-P. Chen, and Y.-T. Hsiao, "An adaptive pmu-based fault location estimation system with a fault-tolerance and load-balancing communication network," in *2007 IEEE Lausanne Power Tech.* IEEE, 2007, pp. 1197–1202.

[74] F. Chunju, D. Xiuhua, L. Shengfang, and Y. Weiyong, "An adaptive fault location technique based on pmu for transmission line," in *2007 IEEE Power Engineering Society General Meeting*. IEEE, 2007, pp. 1–6.

[75] A. Jain, A. Thoke, and R. Patel, "Classification of single line to ground faults on double circuit transmission line using ann," *International Journal of Computer and Electrical Engineering*, vol. 1, no. 2, pp. 197–203, 2009.

[76] M. Fulczyk, P. Balcerek, J. Izykowski, E. Rosolowski, and M. Saha, "Fault locator using two-end unsynchronized measurements for uhv series compensated parallel lines," in *International Conference on High Voltage Engineering and Application*. IEEE, 2008, pp. 88–91.

[77] M. A. Mirzai and A. A. Afzalian, "A novel fault-locator system, algorithm, principle and practical implementation," *IEEE Transactions on Power Delivery*, vol. 25, no. 1, pp. 35–46, 2009.

[78] R. Kavasseri and S. K. Srinivasan, "Joint placement of phasor and conventional power flow measurements for fault observability of power systems," *IET Generation, Transmission & Gistribution*, vol. 5, no. 10, pp. 1019–1024, 2011.

[79] J. Izykowski, E. Rosolowski, P. Balcerek, M. Fulczyk, and M. M. Saha, "Accurate non-iterative fault location algorithm utilizing two-end unsynchronized measurements," *IEEE Transactions on Power Delivery*, vol. 25, no. 1, pp. 72–80, 2010.

[80] J. Izykowski, E. Rosolowski, P. Balcerek, M. Fulczyk, and M. M. Saha, "Fault location on double-circuit series-compensated lines using two-end unsynchronized measurements," *IEEE Transactions on Power Delivery*, vol. 26, no. 4, pp. 2072–2080, Oct 2011.

[81] A. Salehi-Dobakhshari and A. M. Ranjbar, "Application of synchronised phasor measurements to wide-area fault diagnosis and location," *IET Generation, Transmission & Distribution*, vol. 8, no. 4, pp. 716–729, 2013.

[82] A. S. Dobakhshari and A. M. Ranjbar, "A wide-area scheme for power system fault location incorporating bad data detection," *IEEE Transactions on Power Delivery*, vol. 30, no. 2, pp. 800–808, April 2015.

[83] M. Davoudi, J. Sadeh, and E. Kamyab, "Parameter-free fault location for transmission lines based on optimization," *IET Generation, Transmission & Distribution*, vol. 9, no. 11, pp. 1061–1068, 2015.

[84] J. Ma, X. Pei, W. Ma, and Z. Wang, "A new transmission line pilot differential protection principle using virtual impedance of fault component," *Canadian Journal of Electrical and Computer Engineering*, vol. 38, no. 1, pp. 37–44, winter 2015.

[85] J. Ma, Y. Shi, W. Ma, and Z. Wang, "Location method for interline and grounded faults of double-circuit transmission lines based on distributed parameters," *IEEE Transactions on Power Delivery*, vol. 30, no. 3, pp. 1307–1316, 2014.

[86] T. P. S. Baains, M. Zadeh, and R. Dadash, "Enhanced phasor estimation technique for fault location in series-compensated lines," *IEEE Transactions on Power Delivery*, vol. 30, no. 4, pp. 2058–2060, 2015.

[87] T. P. S. Bains and M. R. D. Zadeh, "Supplementary impedance-based fault-location algorithm for series-compensated lines," *IEEE Transactions on Power Delivery*, vol. 31, no. 1, pp. 334–342, Feb 2016.

[88] F. H. Magnago and A. Abur, "A new fault location technique for radial distribution systems based on high frequency signals," in *1999 IEEE Power Engineering Society Summer Meeting. Conference Proceedings (Cat. No. 99CH36364)*, vol. 1. IEEE, 1999, pp. 426–431.

[89] Kit Po Wang and K. Lee, "Visualizing wavelet transformed travelling waves on power transmission line using java," in *2000 International Conference on Advances in Power System Control, Operation and Management, APSCOM-00*, vol. 2, Oct 2000, pp. 349–353 vol.2.

[90] H. Hizman, P. Crossley, P. Gale, and G. Bryson, "Fault section identification and location an a distribution feeder using travelling waves," in *IEEE Power Engineering Society Summer Meeting,*, vol. 3. IEEE, 2002, pp. 1107–1112.

[91] D. W. Thomas, R. J. Carvalho, and E. T. Pereira, "Fault location in distribution systems based on traveling waves," in *2003 IEEE Bologna Power Tech Conference Proceedings,*, vol. 2. IEEE, 2003, pp. 5–pp.

[92] K. Rajesh and N. Yadaiah, "Fault identification using wavelet transform," in *2005 IEEE/PES Transmission & Distribution Conference & Exposition: Asia & Pacific*. IEEE, 2005, pp. 1–6.

[93] T. Ji, Y. Wang, Q. Yuan, and Y. Sun, "Fault location technique of railway automatic blocking and continuous power transmission lines using travelling waves," in *Proceedings of the* 29^{th} *Chinese Control Conference*. IEEE, 2010, pp. 4068–4072.

[94] P. Jafarian and M. Sanaye-Pasand, "A traveling-wave-based protection technique using wavelet/pca analysis," *IEEE Transactions on Power Delivery*, vol. 25, no. 2, pp. 588–599, 2010.

[95] S. M. Tayebi and A. Kazemi, "A novel fault direction discrimination and location technique for three-terminal transmission lines," in *2011 International Conference on Applied Superconductivity and Electromagnetic Devices*. IEEE, 2011, pp. 92–96.

[96] F. Lopes, W. Santos, D. Fernandes, W. Neves, and B. Souza, "An adaptive fault location method for smart distribution and transmission grids," in *2011 IEEE PES Conference on Innovative Smart Grid Technologies Latin America (ISGT LA)*. IEEE, 2011, pp. 1–7.

[97] A. Bernieri, G. Betta, A. Pietrosanto, and C. Sansone, "A neural network approach to instrument fault detection and isolation," in *Conference Proceedings.* 10^{th} *Anniversary. IMTC/94. Advanced Technologies in I & M. 1994 IEEE Instrumentation and Measurement Technology Conference (Cat. No. 94CH3424-9)*. IEEE, 1994, pp. 139–144.

[98] D. Novosel, B. Bachmann, D. Hart, Y. Hu, and M. M. Saha, "Algorithms for locating faults on series compensated lines using neural network and deterministic methods," *IEEE Transactions on Power Delivery*, vol. 11, no. 4, pp. 1728–1736, 1996.

[99] B. Bachmann, D. Novosel, D. Hart, Y. Hu, and M. M. Saha, "Application of artificial neural networks for series compensated line protection," in *Proceedings of International Conference on Intelligent System Application to Power Systems.* IEEE, 1996, pp. 68–73.

[100] A. O. Fernandez and N. K. I. Ghonaim, "A novel approach using a firann for fault detection and direction estimation for high-voltage transmission lines," *ieee Transactions on Power Delivery*, vol. 17, no. 4, pp. 894–900, 2002.

[101] M. J. B. Reddy and D. K. Mohanta, "Performance evaluation of an adaptive-network-based fuzzy inference system approach for location of faults on transmission lines using monte carlo simulation," *IEEE Transactions on Fuzzy Systems*, vol. 16, no. 4, pp. 909–919, 2008.

[102] P. Warlyani, A. Jain, A. Thoke, and R. Patel, "Fault classification and faulty section identification in teed transmission circuits using ann," *International Journal of Computer and Electrical Engineering*, vol. 3, no. 6, pp. 807–811, 2011.

[103] P. Ray, B. Panigrahi, and N. Senroy, "Extreme learning machine based fault classification in a series compensated transmission line," in *2012 IEEE International Conference on Power Electronics, Drives and Energy Systems (PEDES).* IEEE, 2012, pp. 1–6.

[104] P. Ray, B. K. Panigrahi, and N. Senroy, "Hybrid methodology for fault distance estimation in series compensated transmission line," *IET Generation, Transmission & Distribution*, vol. 7, no. 5, pp. 431–439, 2013.

[105] P. Ray and D. Mishra, "Artificial intelligence based fault location in a distribution system," in *2014 International Conference on Information Technology.* IEEE, 2014, pp. 18–23.

[106] A. Yadav, P. Warlyani, and A. Thoke, "Fault classification, distance location and faulty section identification in teed transmission circuits using artificial neural network," *International Journal of Computer Applications*, vol. 47, no. 15, pp. 19–25, 2012.

[107] M. J. B. Reddy, D. V. Rajesh, P. Gopakumar, and D. K. Mohanta, "Smart fault location for smart grid operation using rtus and computational intelligence techniques," *IEEE Systems Journal*, vol. 8, no. 4, pp. 1260–1271, Dec 2014.

[108] P. Gopakumar, M. J. B. Reddy, and D. K. Mohanta, "Adaptive fault identification and classification methodology for smart power grids using synchronous phasor angle measurements," *IET Generation, Transmission & Distribution*, vol. 9, no. 2, pp. 133–145, 2015.

[109] A. Yadav and A. Swetapadma, "Enhancing the performance of transmission line directional relaying, fault classification and fault location schemes using fuzzy inference system," *IET Generation, Transmission & Distribution*, vol. 9, no. 6, pp. 580–591, 2015.

[110] A. Swetapadma and A. Yadav, "A single ended directional fault section identifier and fault locator for double circuit transmission lines using combined wavelet and ann approach," *International Journal of Electrical Power & Energy Systems*, vol. 69, pp. 27–33, 2015.

[111] V. N. Vapnik, "An overview of statistical learning theory," *IEEE Transactions on Neural Networks*, vol. 10, no. 5, pp. 988–999, Sep. 1999.

[112] B. E. Boser, I. M. Guyon, and V. N. Vapnik, "A training algorithm for optimal margin classifiers," in *Proceedings of the Fifth Annual Workshop on Computational Learning Theory*. ACM, 1992, pp. 144–152.

[113] B. Bhalja and R. P. Maheshwari, "Wavelet-based fault classification scheme for a transmission line using a support vector machine," *Electric Power Components and Systems*, vol. 36, no. 10, pp. 1017–1030, 2008.

[114] H. Livani and C. Y. Evrenosoğlu, "A fault classification and localization method for three-terminal circuits using machine learning," *IEEE Transactions on Power Delivery*, vol. 28, no. 4, pp. 2282–2290, 2013.

[115] J. A. Jiang, C. L. Chuang, Y. C. Wang, C. H. Hung, J. Y. Wang, C. H. Lee, and Y. T. Hsiao, "A hybrid framework for fault detection, classification, and location—part i: Concept, structure, and methodology," *IEEE Transactions on Power Delivery*, vol. 26, no. 3, pp. 1988–1998, 2011.

[116] J.-A. Jiang, C.-L. Chuang, Y.-C. Wang, C.-H. Hung, J.-Y. Wang, C.-H. Lee, and Y.-T. Hsiao, "Ahybrid framework for fault detection, classification, and location—part ii: Implementation and test results," *IEEE Transactions on Power Delivery*, vol. 26, no. 3, pp. 1999–2008, 2011.

[117] Z. Moravej, M. Khederzadeh, and M. Pazoki, "New combined method for fault detection, classification, and location in series-compensated transmission line," *Electric Power Components and Systems*, vol. 40, no. 9, pp. 1050–1071, 2012.

[118] M. J. B. Reddy, D. V. Rajesh, P. Gopakumar, and D. K. Mohanta, "Smart fault location for smart grid operation using rtus and computational intelligence techniques," *IEEE Systems Journal*, vol. 8, no. 4, pp. 1260–1271, Dec 2014.

[119] Y. Kwon, S. Kang, D. Lee, and H. Kim, "Fault location algorithm based on cross correlation method for hvdc cable lines," in *2008 IET 9th International Conference on Developments in Power System Protection (DPSP 2008)*, March 2008, pp. 360–364.

[120] K. Nanayakkara, A. Rajapakse, and R. Wachal, "Fault location in extra long hvdc transmission lines using continuous wavelet transform," in *International Conference on Power Systems Transients*, 2011, pp. 14–17.

[121] O. Nanayakkara, A. Rajapakse, R. Wachal, and H. Manitoba, "Fault location in extra long hvdc transmission lines using discrete wavelet transform," in *Conference on Power Systems*, 2010.

[122] G. Song, X. Cai, S. Gao, J. Suonan, and G. Li, "Natural frequency based protection and fault location for vsc-hvdc transmission lines," in *2011 International Conference on Advanced Power System Automation and Protection*, vol. 1. IEEE, 2011, pp. 177–182.

[123] H. Cui and N. Tu, "Hvdctransmission line fault localization base on rbf neural network with wavelet packet decomposition," in *2015 12th International Conference on Service Systems and Service Management (ICSSSM)*. IEEE, 2015, pp. 1–4.

[124] M. Xu, Z. Cai, Y. Liu, and X. Ku, "A novel coordination scheme of wavefront and wave speed for hvdc travelling wave fault location," in *2011 International Conference on Advanced Power System Automation and Protection*, vol. 1. IEEE, 2011, pp. 102–107.

[125] H. Shu, X. Tian, G. Zhang, K. Liu, and S. Sun, "Fault location for 800 kv hvdc transmission lines using natural frequency of single terminal voltage data," *Proceedings of the Chinese Society of Electrical Engineering*.

[126] O. K. Nanayakkara, A. D. Rajapakse, and R. Wachal, "Location of dc line faults in conventional hvdc systems with segments of cables and overhead lines using terminal measurements," *IEEE Transactions on Power Delivery*, vol. 27, no. 1, pp. 279–288, 2012.

[127] M. Shukr, D. W. P. Thomas, and P. Zanchetta, "Vsc-hvdc transmission line faults location using active line impedance estimation," in *2012 IEEE International Energy Conference and Exhibition (ENERGYCON)*, 2012, pp. 244–248.

[128] L. Xie, L. Jin, X. Wang, L. Ning, and T. Wang, "Improved protection method of hvdc transmission line based on the analysis of traveling wave dispersion," in *2014 International Conference on Power System Technology*. IEEE, 2014, pp. 467–473.

[129] Z.-Y. He, K. Liao, X.-P. Li, S. Lin, J.-W. Yang, and R.-K. Mai, "Natural frequency-based line fault location in hvdc lines," *IEEE Transactions on Power delivery*, vol. 29, no. 2, pp. 851–859, 2013.

[130] L. Yuansheng, W. Gang, and L. Haifeng, "Time-domain fault-location method on hvdc transmission lines under unsynchronized two-end measurement and uncertain line parameters," *IEEE Transactions on Power delivery*, vol. 30, no. 3, pp. 1031–1038, 2015.

[131] H. J. Bahirat, H. K. Høidalen, and B. A. Mork, "Thevenin equivalent of voltage-source converters for dc fault studies," *IEEE Transactions on Power Delivery*, vol. 31, no. 2, pp. 503–512, 2015.

[132] S. Luo, X. Dong, S. Shi, and B. Wang, "A directional protection scheme for hvdc transmission lines based on reactive energy," *IEEE Transactions on Power Delivery*, vol. 31, no. 2, pp. 559–567, 2015.

[133] J. P. Triveno, V. P. Dardengo, and M. C. de Almeida, "An approach to fault location in hvdc lines using mathematical morphology," in *2015 IEEE Power & Energy Society General Meeting*. IEEE, 2015, pp. 1–5.

[134] Z. Li, G. Zou, B. Tong, H. Gao, and Q. Feng, "Novel traveling wave protection method for high voltage dc transmission line," in *2015 IEEE Power & Energy Society General Meeting*. IEEE, 2015, pp. 1–5.

[135] M. Ikhide, S. Tennakoon, A. Griffiths, S. Subramanian, and H. Ha, "Fault detection in multi-terminal modular multilevel converter (mmc) based high voltage dc (hvdc) transmission system," in *2015 50^{th} International Universities Power Engineering Conference (UPEC)*. IEEE, 2015, pp. 1–6.

[136] R. Vidal-Albalate, H. Beltran, A. Rolan, E. Belenguer, R. Peña, and R. Blasco-Gimenez, "Analysis of the performance of mmc under fault conditions in hvdc-based offshore wind farms," *IEEE Transactions on Power Delivery*, vol. 31, no. 2, pp. 839–847, 2015.

[137] Q. Song, H. Jiang, and J. Liu, "Feature selection based on fda and f-score for multi-class classification," *Expert Systems with Applications*, vol. 81, pp. 22–27, 2017.

[138] D. Zhang, X. Jin, B. Zhou, H. Su, Y. Chen, and L. Zhu, "A study on hvdc user-defined modeling in pss/e," in *2015 5th International Conference on Electric Utility Deregulation and Restructuring and Power Technologies (DRPT)*, Nov 2015, pp. 386–391.

[139] K. Kaberere, K. Folly, and A. Petroianu, "Assessment of commercially available software tools for transient stability: Experience gained in an academic environment," in *2004 IEEE Africon. 7th Africon Conference in Africa (IEEE Cat. No. 04CH37590)*, vol. 2. IEEE, 2004, pp. 711–716.

[140] M.-S. Lu, C.-L. Chang, W.-J. Lee, and L. Wang, "Combining the wind power generation system with energy storage equipment," *IEEE Transactions on Industry Applications*, vol. 45, no. 6, pp. 2109–2115, 2009.

[141] D. Powerfactory, "Powerfactory user's manual," *DIgSILENT, GmbH*, vol. 14, 2011.

[142] E. Johansson, "Detailed description of synchronous machine models used in simpow," 01 2002.

[143] R. R. Gilbert Sybille, Patrice Brunelle, *SimPower Systems User Guide, R2016b, [user's Guide]*. MathWorks, 2017.

[144] E. U. Guide, "Manitoba hvdc research centre inc," *Winnipeg, MB, Canada*, 2016.

[145] A. G. Phadke and J. S. Thorp, *Computer Relaying for Power Systems*. John Wiley & Sons, 2009.

[146] W. A. Shewhart, "The application of statistics as an aid in maintaining quality of a manufactured product," *Journal of the American Statistical Association*, vol. 20, no. 152, pp. 546–548, 1925.

[147] W. A. Shewhaart, *Economic Control of Quality of Manufactured Product*, ser. Bell Telephone Laboratories series. American Society for Quality Control, 1931.

[148] E. S. Page, "Continuous inspection schemes," *Biometrika*, vol. 41, no. 1/2, pp. 100–115, 1954.

[149] V. V. Veeravalli, "Decentralized quickest change detection," *IEEE Transactions on Information Theory*, vol. 47, no. 4, pp. 1657–1665, 2001.

[150] "Ieee guide for determining fault location on ac transmission and distribution lines," *IEEE Std C37.114-2014 (Revision of IEEE Std C37.114-2004)*, pp. 1–76, Jan 2015.

[151] B. K. Bose, "Energy, environment, and advances in power electronics," *IEEE Transactions on Power Electronics*, vol. 15, no. 4, pp. 688–701, July 2000.

[152] M. of New and R. Energy, "Growth of electricity sector in india from 1947-2017, annual report 2016-2017," 2018.

[153] M. Singh and C. Shekhar, "Growth of electricity sector in india from 1947–2015," *Central Electricity Authority, Goverment of India*, pp. 18–19, 2015.

[154] Y. Guo, H. Gao, Q. Wu, H. Zhao, J. Ø stergaard, and M. Shahidehpour, "Enhanced voltage control of vsc-hvdc-connected offshore wind farms based on model predictive control," *IEEE Transactions on Sustainable Energy*, vol. 9, no. 1, pp. 474–487, 2018.

[155] N. Flourentzou, V. G. Agelidis, and G. D. Demetriades, "Vsc-based hvdc power transmission systems: An overview," *IEEE Transactions on Power Electronics*, vol. 24, no. 3, pp. 592–602, 2009.

[156] Y. Ma, G. Zou, Z. Gao, C. Sun, T. Du, and Y. Liu, "Analytic approximation of fault current contributed by dc capacitors in vsc-hvdc pole-to-pole fault," in *2017 IEEE Electrical Power and Energy Conference (EPEC)*. IEEE, 2017, pp. 1–6.

[157] R. Shah, R. Preece, and M. Barnes, "The impact of voltage regulation of multiinfeed vsc-hvdc on power system stability," *IEEE Transactions on Energy Conversion*, vol. 33, no. 4, pp. 1614–1627, 2018.

[158] B. Mahamedi, M. Sanaye-Pasand, S. Azizi, and J. G. Zhu, "Unsynchronised fault-location technique for three-terminal lines," *IET Generation, Transmission & Distribution*, vol. 9, no. 15, pp. 2099–2107, 2015.

[159] H.-x. Ha, B.-h. Zhang, and Z.-l. Lv, "A novel principle of single-ended fault location technique for ehv transmission lines," *IEEE Transactions on Power Delivery*, vol. 18, no. 4, pp. 1147–1151, 2003.

[160] J. Izykowski, R. Molag, E. Rosolowski, and M. M. Saha, "Accurate location of faults on power transmission lines with use of two-end unsynchronized measurements," *IEEE Transactions on Power Delivery*, vol. 21, no. 2, pp. 627–633, 2006.

[161] R. Krishnathevar, H. Low, and E. Ngu, "One end impedance based fault location in double circuit transmission lines with different configurations," *International Journal of Electrical Power & Energy Systems*, vol. 64, pp. 1159–1165, 01 2015.

[162] F. V. Lopes, B. F. Kusel, and K. M. Silva, "Traveling wave based fault location on half wavelength transmission lines," *IEEE Latin America Transactions*, vol. 14, no. 1, pp. 248–253, 2016.

[163] H. Livani and C. Y. Evrenosoğlu, "A fault classification method in power systems using dwt and svm classifier," in *PES T& D 2012*. IEEE, 2012, pp. 1–5.

[164] V. Cherkassky and Y. Ma, "Practical selection of svm parameters and noise estimation for svm regression," *Neural Networks*, vol. 17, no. 1, pp. 113–126, 2004.

[165] Y.-W. Chen and C.-J. Lin, "Combining svms with various feature selection strategies," in *Feature Extraction*. Springer, 2006, pp. 315–324.

[166] X. W. Chen, "Gene selection for cancer classification using bootstrapped genetic algorithms and support vector machines," in *Computational Systems Bioinformatics. CSB2003. Proceedings of the 2003 IEEE Bioinformatics Conference. CSB2003*, Aug 2003, pp. 504–505.

[167] N. K. Meena, A. Swarnkar, N. Gupta, and K. R. Niazi, "Multi-objective taguchi approach for optimal dg integration in distribution systems," *IET Generation, Transmission & Distribution*, vol. 11, no. 9, pp. 2418–2428, 2017.

[168] N. K. Meena, A. Swarnkar, N. Gupta, and K. Niazi, "A taguchi-based approach for optimal placement of distributed generations for power loss minimization in distribution system," in *2015 IEEE Power & Energy Society General Meeting*. IEEE, 2015, pp. 1–5.

[169] L. Weimers, "New markets need new technology," in *Proc. of 2000 International Conference on Power System Technology*, vol. 2, sep. 2000, pp. 873–877.

[170] R. Rudervall, J. Charpentier, and R. Sharma, "High voltage direct current (hvdc) transmission systems technology review paper," *Energy week, Washington, D.C, USA*, vol. 2000, pp. 1–19, 2000.

[171] L. Weimers, "Hvdc light a new technology for a better environment," *Power Engineering Review, IEEE*, vol. 18, pp. 19–20, 09 1998.

[172] M. Bollen, *Understanding Power Quality Problems: Voltage Sags, Swell , and Interruptions*, ser. IEEE - TP 139-0. Wiley, 2000.

[173] S. Debnath, J. Qin, B. Bahrani, M. Saeedifard, and P. Barbosa, "Operation, control, and applications of the modular multilevel converter: A review," *IEEE Transactions on Power Electronics*, vol. 30, no. 1, pp. 37–53, Jan 2015.

[174] N. R. Chaudhuri and B. Chaudhuri, "Adaptive droop control for effective power sharing in multi-terminal dc (mtdc) grids," *IEEE Transactions on Power Systems*, vol. 28, no. 1, pp. 21–29, Feb 2013.

[175] C. D. Barker and R. Whitehouse, "Autonomous converter control in a multi-terminal hvdc system," in *9th IET International Conference on AC and DC Power Transmission (ACDC 2010)*, Oct 2010, pp. 1–5.

[176] T. Vrana, Y. Yang, D. Jovcic, S. Dennetiere, J. Jardini, and H. Saad, *The CIGRE B4 DC Grid Test System*. Electra, IEEE, 10 2013, no. 270.

[177] M. Skliar, "Process dynamics and control, 2nd edition by dale e. seborg, thomas f. edgar, and duncan a. mellichamp," *AIChE Journal*, vol. 54, no. 11, pp. 3026–3026, 2008.

[178] A. N. Shiryaev, "On optimum methods in quickest detection problems," *Theory of Probability & Its Applications*, vol. 8, no. 1, pp. 22–46, 1963.

[179] T. An, X. Zhou, C. Han, Y. Wu, Z. He, H. Pang, and G. Tang, "A dc grid benchmark model for studies of interconnection of power systems," *CSEE Journal of Power and Energy Systems*, vol. 1, no. 4, pp. 101–109, Dec 2015.

[180] K. Rouzbehi, A. Miranian, J. I. Candela, A. Luna, and P. Rodriguez, "A generalized voltage droop strategy for control of multiterminal dc grids," *IEEE Transactions on Industry Applications*, vol. 51, no. 1, pp. 607–618, Jan 2015.

[181] A. A. Jamshidifar and D. Jovcic, "$3-level$ cascaded voltage source converters controller with dispatcher droop feedback for direct current transmission grids," *IET Generation, Transmission Distribution*, vol. 9, no. 6, pp. 571–579, 2015.

Biography

Author's Brief Biography

Jay Prakash Keshri is currently pursuing Ph.D degree in Electrical Engineering from Malaviya National Institute of Technology Jaipur. He received M. Tech degree in Power Systems from Malaviya National Institute of Technology Jaipur in 2014, B. Tech degree in Electrical Engineering from West Bengal University of Technology in 2010. Mr. Jay Prakash Keshri is member of some professional origination as, IEEE, IET, and CIGRE. He published articles in various journals and conferences in international and national repute. His current research interests are in the field of computational intelligence and Machine Learning applications to Engineering especially in Power System.